GEOCHEMISTRY AND STRUCTURE OF THE ARCHAEAN GRANITOID - SUPRACRUSTAL TERRANE, SOUTHEASTERN TRANSVAAL AND NORTHERN NATAL.

by

RORIC GERARD SMITH

1987

Submitted in partial fulfilment of the requirements
for the degree of Doctor of Philosophy
in the Department of Geology and Mineralogy,

University of Natal, Pietermaritzbug,
South Africa.

I, RORIC GERARD SMITH hereby declare that this thesis

and it's accompanying maps is my own original work,

that all assistance and sources of information

have been acknowledged, and that this work

has not been presented to any other

University for the purpose of a higher degree.

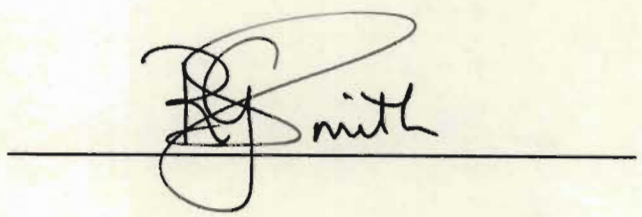

ABSTRACT

Tonalitic and trondhjemitic granitoids pre- and post-date supracrustal, dominantly metavolcanic sequences. Gneisses that are considered on structural grounds to pre-date the Commondale Supracrustal Suite consist of the Layered and Luneburg Gneisses. The bimodal Layered Gneisses comprise tonalitic, trondhjemitic and granodioritic gneisses conformably interlayered with subordinate amphibolite layers and are lithologically similar to the bimodal Gneiss Suite in Swaziland. Highly deformed pre-D_2 amphibolite dykes cross-cut the lithological layering in the Layered Gneisses. These gneisses together with the strongly foliated homogeneous Luneburg Tonalite Gneiss that may represent a stratiform intrusion beneath the Layered Gneisses are interpreted to be of similar age on the basis of similar deformational histories. These rock-types collectively constitute the Gneiss Complex and are inferred to be the primitive sialic crust on which the supracrustal sequences were deposited. The Gneiss Complex has been strongly deformed by thrusts, shears and three phases of folding.

The highly deformed Commondale Supracrustal Suite is characterized by a predominance of amphibolites and mafic and ultramafic schists metamorphosed at amphibolite grade. The aluminum depleted basaltic komatiites and peridotitic komatiites (Al_2O_3/TiO_2 between 8 and 16) are interlayered with subordinate banded iron formations and metaquartzites. The Matshempondo Peridotite Suite, ~ 3.34 Ga old (Sm - Nd), is discordant to these supracrustal rocks and provides a minimum age for the Commondale Supracrustal Suite. The Matshempondo Peridotite Suite comprises a 640m thick sequence of alternating layers of olivine cumulate and spinifex-textured peridotites. Microcyclic olivine spinifex-olivine cumulate layering observed above metre-scale spinifex layers and the extremely high Al_2O_3/TiO_2 ratios of between 60 and 90 have not been documented before in Archaean peridotitic komatiites from other greenstone occurrences. Sm - Nd data are consistent with an origin by sequential partial melting of isotopically inhomogeneous mantle residues.

Post D_1 - pre D_2 emplacement of the Trondhjemite-Tonalite-Granodiorite Suite into the Gneiss Complex and supracrustals represents a period of significant granitoid underplating. Five distinct lithological types constitute this suite. Although contacts between the lithologies are generally poorly exposed, regional scale mapping reveals the cross-cutting and relative age relations of the different granitoids. The Bazane Porphyritic Trondhjemite Suite was intruded at the interface between the Gneiss Complex and the Commondale Supracrustal Suite. The Leucotonalite Gneiss and, subsequently, Hornblende Granodiorite Suite were intruded and cross-cut the tabular Bazane trondhjemites, Layered Gneisses and the supracrustals. The Braunschweig Tonalite Gneiss intruded the Luneburg Tonalite Gneiss, however its age relative to the rest of the Trondhjemite-Tonalite-Granodiorite Suite is uncertain. The Luneburg Tonalite Gneiss is intruded by minor leucotonalitic and granitic rock-types.

The granitoids are of trondhjemitic affinity except the Hornblende Granodiorite Suite that is sub-alkaline. Primordial mantle normalized LILE and HFSE patterns suggest broadly similar sources for the tonalites and trondhjemites. The Rb/Sr and Sr/Ba ratios are consistent with an origin by ten to thirty percent batch melting of amphibolites. Trace element and phase diagram constraints suggest that the granitic and quartz monzonitic components of the Bazane Porphyritic Trondhjemite Suite represent fractionation products of a tronhjemitic liquid. Volumetrically minor leucocratic granites and quartz monzonites derived by partial melting of siliceous crust intrude the tonalitic gneisses.

D_1 is the first recognizable deformation in the Commondale Supracrustal Suite and is characterized by recumbent folds and thrusts in both the supracrustals and Gneiss Complex. Horizontal tectonism and sodic granitoid underplating led to substantial thickening of the crust prior to D_2. Folding about vertical northeasterly trending axial surfaces during the D_2 deformational event and additional homogeneous shortening by at least 60 percent in the Layered Gneisses resulted in substantial vertical extension. The Commondale Supracrustal Suite is preserved as a series of hook-shaped interference folds that collectively represent a complex F_2 sheath-like structure suggesting that the supracrustals deformed more

competently than the structurally lower Gneiss Complex. Mylonites record a dextral sense of shearing during late D_2 at the contact between the Bazane trondhjemites and the Commondale supracrustals, whereas D_3 is characterized by sinistral shearing and faulting in the supracrustal suite. D_4 deformation involved open to tight refolding of pre-existing structures and fabrics about steeply inclined northwesterly trending axial surfaces.

ACKNOWLEDGMENTS

I wish to thank my supervisors Professor D R Hunter and Dr A H Wilson for their support, expert advice and continued interest in this project. In addition their fruitful discussions and suggestions on numerous field trips is acknowledged.

This project forms part of the research undertaken by the Archaean Studies Research Group of the University of Natal, Pietermaritzburg for which funding by the CSIR is gratefully acknowledged.

I wish to thank Dr R Carlson and the Department of Terrestrial Magnetism of the Carnegie Institution of Washington for making the Sm-Nd study possible while Dr A H Wilson was on sabbatical at the Institution. A sabbatical grant to A.H.W. from the CSIR is gratefully acknowledged.

Dr D Strydom is thanked for his help in quantifying D_1 in the Commondale synform and for numerous discussions on structure, especially that of the Commondale Supracrustal Suite.

Professor V von Brunn enlightened the author on Dwyka Formation diamictites in the southeastern Transvaal.

Pat Suthan and Mukesh Seyambu prepared the thin sections. Roy Seyambu and Pat Suthan are thanked for their expert technical assistance.

I wish to thank Dave Sleigh for his company and sense of humour while resident in our abandoned farm-house during mapping of adjacent areas in 1984 and Reimar Hiestermann for permission to use this well located facility.

The farming community in the Luneburg, Commondale and Paulpietersburg area are thanked for their hospitality. In particular Edgar and Dorothy Shütte generously provided accommodation for three months during 1985 and 1986. Others I wish to thank are Alex Puttkamer, Heinz Hinze, Helmut Meyer, Werner Schütte, Reimar Hiestermann, Sieghart Klingenberg and Siegfried Klingenberg.
Numerous people contributed to this project through valuable discussions. Some of them are Professor's D R Hunter, V von Brunn,

and Dr's D Strydom, A H Wilson, J R Krynauw, D Buhmann and Gill Chutter, Gavin Brown, Geoff Grantham, Bruce Groenewald, Pete Mendonidis, Cow Preston and Dave Sleigh.

Freda Richards proficiently drafted the maps and numerous figures.

Linda Morley expertly typed the manuscript and numerous drafts with great patience and to her I owe a great debt.

Barbara Rimbault painstakingly typed most of the tables.

I wish to acknowledge my gratitude to my parents for their continued encouragement and support throughout my career as a student. Finally I wish to thank Gill for her encouragement and support.

ERRATA

No pages are missing between page 253 and 256. The omission of pages 254 and 255 result from reformatting to accommodate late corrections.

CONTENTS

Page

ABSTRACT

ACKNOWLEDGEMENTS

CHAPTER 1 INTRODUCTION 1

General 1

Location and extent of the study area 3

Previous work, Aims and Approach 4

Age and chronostratigraphic relationship of the study area to the early Archaean terrane in eastern Transvaal and Swaziland. 6

CHAPTER 2 GENERAL GEOLOGY 9

PONGOLA SEQUENCE 9

Nsuze Group 9

Mozaan Group 14

USUSHWANA COMPLEX 14

KAROO SEQUENCE 16

Dwyka Formation 16

Ecca Group 17

POST-KAROO DOLERITE SHEETS 17

MAFIC DYKES 18

CHAPTER 3 GRANITOID LITHOSTRATIGRAPHY 19

Granitoid Classification 19

Gneiss Complex 19

Trondhjemite-Tonalite-Granodiorite Suite 29

Unfoliated and Weakly Foliated Granitoids 34

Granitic intrusions in the Luneburg Tonalite Gneiss 34

Leucocratic Granite and Quartz Monzonite 34

CHAPTER 4 PETROGRAPHY OF THE GRANITOIDS 37
GNEISS COMPLEX 37
Layered Gneisses 37
Luneburg Tonalite Gneiss 41
TRONDHJEMITE-TONALITE-GRANODIORITE SUITE 43
Leucotonalite Gneiss 43
Bazane Porphyritic Trondhjemite Suite 44
Braunschweig Tonalite Gneiss 47
Hornblende Granodiorite Suite 48
WEAKLY FOLIATED GRANITOIDS 52
Medium-grained leucotonalite 52
Biotite granite 52
Sodic granite 52
UNFOLIATED GRANITOIDS 53
Leucocratic Granite 53
Equigranular Quartz Monzonite 53

CHAPTER 5 GRANITOID GEOCHEMISTRY AND PETROGENESIS 55
PART 1 : GRANITOID GEOCHEMISTRY 55
GNEISS COMPLEX 55
Layered Gneisses 55
Luneburg Tonalite Gneiss 72
TRONDHJEMITE-TONALITE-GRANODIORITE SUITE 74
Leucotonalite Gneiss 74
Braunschweig Tonalite Gneiss 79
Hornblende Granodiorite Suite 81
Bazane Porphyritic Trondhjemite Suite 83
WEAKLY FOLIATED GRANITOIDS 90
UNFOLIATED GRANITOIDS 94

PART 2 : PETROGENESIS 96

The Origin of Tonalite and Trondhjemite Magmas 96

PETROGENETIC IMPLICATIONS FOR THE ARCHAEAN GRANITOIDS 99

General 99

Rock/Primordial mantle LILE and HFSE patterns 99

A Model for the Tonalitic and Trondhjemitic Gneisses 103

Bazane Porphyritic Trondhjemite Suite : The product of fractionating trondhjemitic magma 108

Weakly Foliated Granitoids 112

Unfoliated Granitoids 114

SUMMARY AND CONCLUSIONS 115

CHAPTER 6 COMMONDALE SUPRACRUSTAL SUITE 117

Introduction 117

Field Relations 118

Geochemistry 120

Summary 130

CHAPTER 7 MATSHEMPONDO PERIDOTITE SUITE 134

INTRODUCTION 134

Archaean komatiites and spinifex-textured rocks 134

Textural terminology 137

PART 1 : FIELD RELATIONS AND PETROGRAPHY 140

FIELD RELATIONS 140

Geological and Structural Setting 140

The Layered Suite 141

1. TYPE 1 COOLING UNIT 143

2. TYPE 2 COOLING UNIT 151

3. TYPE 3 COOLING UNIT 151

Breccia zones and evidence for current action 158

PETROGRAPHY 158
Olivine plate spinifex 160
Pyroxene spinifex 163
Olivine mesocumulates 165
Olivine orthocumulates 165
Mixed spinifex-cumulate rocks 167
Microcyclic spinifex-cumulate units 169
PART 2 : GEOCHEMISTRY 170
Sample Localities 170
MAJOR ELEMENTS 170
Cooling Units 170
Microcyclic Unit 176
Interelement variations 176
TRACE ELEMENTS 180
Cooling Units 180
Microcyclic Unit 182
Interelement variations 184
Effects of alteration on geochemistry 184
High field strength incompatible elements 186
Molecular proportion ratio diagrams 191
Sm-Nd SYSTEMATICS 193
Sm-Nd data 196
Calculated model dates and epsilon 196
CRYSTALLIZATION AND DIFFERENTIATION OF THE MATSHEMPONDO PERIDOTITE SUITE 201
Introduction 201
Liquid compositions 202

Crystallization and differentiation in the cooling units 209

1) Crystallization mechanism for A and B units in TYPE 1, 2 and 3 cooling units 210

2) Crystallization mechanism for microcyclic units 213

COMPARISON OF GEOCHEMISTRY AND SOURCE OF THE MATSHEMPONDO PERIDOTITE SUITE TO KOMATIITES FROM OTHER GREENSTONE BELTS. 215

SUMMARY AND CONCLUSIONS. 218

CHAPTER 8 STRUCTURE 220

INTRODUCTION 220

D_1 223

D_1 in the Gneiss Complex 223

D_1 in the Commondale Supracrustal Suite 227

D_2 236

D_2 in the Gneiss Complex and Commondale Supracrustal Suite 236

D_2 in the Trondhjemite-Tonalite-Granodiorite Suite 243

S-C mylonites and fabric relationships 243

Deformation of competent and incompetent planar elements and determination of the minimum strain ellipsoid 247

Quartzofeldspathic veins as strain markers 247

Amphibolitic dykes as strain markers 257

Summary of strain data 262

D_3 264

D_4 266

D_5 and later events 269

CHAPTER 9 SUMMARY AND CONCLUSIONS 270

SUMMARY 270

CONCLUSIONS 275

1. Inferences from field relationships 275
2. Granitoid geochemistry 276
3. Matshempondo Peridotite Suite 276
4. Structure and tectonics 277

REFERENCES 278

APPENDICES 289

APPENDIX 1 SAMPLE DESCRIPTIONS 290

APPENDIX 2 SAMPLING AND ANALYTICAL TECHNIQUES 301

CHAPTER 1

INTRODUCTION.

General.

Early Archaean granitoids and supracrustal rocks of the Kaapvaal Province crop out in the eastern and southeastern Transvaal, northern Natal and Swaziland, Fig. 1.1. The study area in northern Natal and southeastern Transvaal that is the subject of this thesis forms part of the much larger Archaean granitoid-greenstone terrane in eastern Transvaal and Swaziland (Fig. 1.1). The terrane in Swaziland has been extensively investigated by Hunter (1968, 1970, 1973, 1974, 1979); Jackson and Robertson (1983), Jackson (1984) and others. The Barberton greenstone belt and associated granitoids in the eastern Transvaal have been investigated by Viljoen et. al. (1969a, 1969b); Anhaeusser (1971, 1973, 1980); Anhaeusser and Robb (1980); de Wit (1982), de Wit et. al (1983), Robb (1981), Robb and Anhaeusser (1983) and many others. No geological studies of the study area have been undertaken since the regional reconnaissance survey by Humphrey and Krige (1931).

The present study concerns the early Archaean supracrustal and granitoid rocks north, west and east of Paulpietersburg (MAP 1).

Early Archaean supracrustal rocks account for about 15% of the map area. The largest supracrustal remnant of approximately 100 km^2 is referred to in this study as the Commondale Supracrustal Suite. Small rafts of supracrustal rocks between 1 and 8 km^2 in area are also preserved within the granitoid terrane.

The supracrustal rocks are predominantly mafic and ultramafic metavolcanics with subordinate amounts of massive metaquartzites, banded iron formation (BIF) and meta-argillites. The Commondale supracrustal rocks are preserved in two major synforms separated by a major shear zone, and a number of smaller structures in the Commondale area. Within the southernmost of these major synforms a sequence of

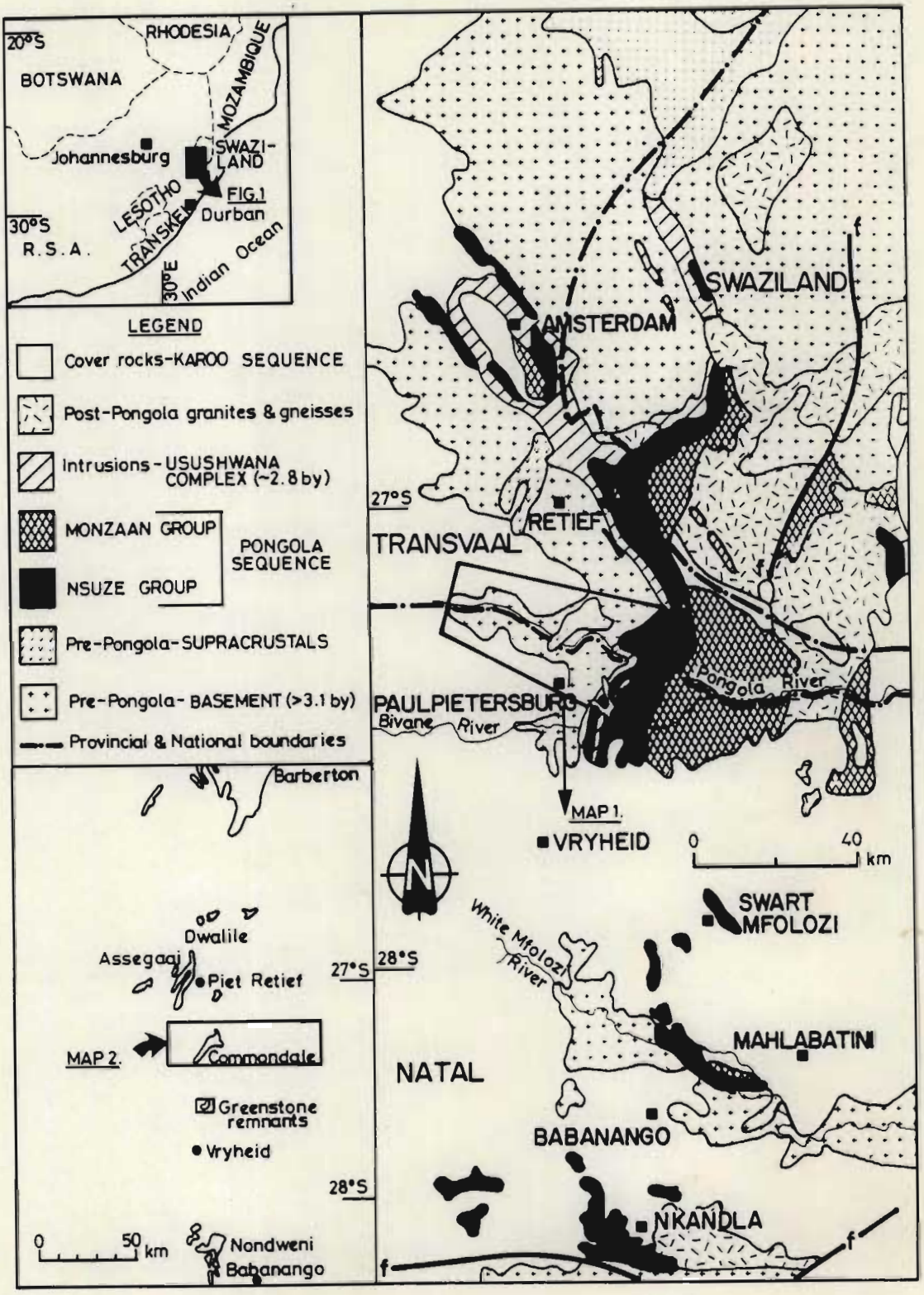

Fig. 1.1. Map showing the location* of the area described and the distribution of the Archaean granitoid basement, Pre-Pongola supracrustals and Post-Pongola granites and gneisses.

*Map 1: - 1:100 000 map of Granite-supracrustal terrane

Map 2: - 1:20 000 map of Commondale supracrustal sequence

alternating cumulate - textured peridotitic komatiites and olivine spinifex rocks at least 640 m thick is preserved (MAP 2). Mapping revealed a strong discordance between the volcano-sedimentary pile and this suite.

The granitoid rocks have been classified into four groups:

1. The Gneiss Complex comprises Layered Gneisses which are lithologically similar to the Bimodal Gneiss Suite of the Ancient Gneiss Complex in Swaziland and the Luneburg Tonalite Gneiss.

2. The Trondhjemite-Tonalite-Granodiorite Suite postdates the Gneiss Complex and supracrustals. Two of the components of this suite, the Bazane Porphyritic Trondhjemite Suite and the Hornblende Granodiorite Suite, clearly intrude the Commondale supracrustals. Neither the Leucotonalite Gneiss nor the Braunschweig Tonalite Gneiss are found in contact with the Commondale supracrustal remnant. These two lithological units are considered to post-date the supracrustal rocks on the basis of their structural styles.

3. The Luneburg Tonalite Gneiss is intruded by a suite of weakly foliated granitoids. Three distinct lithological variants are recognized, namely: sodic granite, medium-grained leucotonalite and biotite granite.

4. The fourth group comprises small intrusions of leucocratic granites and quartz monzonite in the eastern extremity of the map area (MAP 1).

Location and extent of the study area.

The study area covers about 1400 square kilometres (MAP 1). Early Archaean granitoids and supracrustals are unconformably overlain in the north and west by sediments of Karoo age and intrusive dolerite sheets. The Pongola Supergroup into which the Usushwana Complex is intrusive limits the eastern extension of the granitoid-supracrustal terrane.

Access is by way of tar roads from Paulpietersburg, Piet Retief and Pongola. Gravel roads link Paulpietersburg to Luneburg and Hartland. Other minor gravel roads and tracks traverse the area allowing easy access and relatively short walking distances to the remoter parts of the area.

The topography is gently rolling, locally incised by small, steep sided valleys. In the central part of the study area extensive plantations, in which outcrop is extremely poor, hamper mapping. In the western, eastern and northern extremities of the field area the topography is somewhat more rugged. In the western area steep valleys are incised between large granitoid domes and along contacts with Karoo sills. Fresh outcrop is commonly found along streams in this area. In the remainder of the area outcrop quality ranges from poor to excellent, especially along most of the Pongola River. Despite the extensive outcrops exposed in rapids along this river, contacts between the various granitoids and the supracrustal rocks are not common.

Previous work, Aims and Approach.

The study area is of particular interest in that it was last investigated over fifty years ago in a reconnaissance survey by Humphrey and Krige (1931). These authors did not differentiate the granitoid terrane but they did delimit part of the Commondale Supracrustal Suite, although these peridotitic komatiites northwest of Commondale were mapped as 'Karoo dolerites and allied rocks'. No attempt was made by Humphrey and Krige (1931) to investigate the structural complexities of the granitoids and supracrustals.
The object of this study is to establish the structural and stratigraphic relationships between the different granitoids and between the granitoids and suprcrustal sequences. The geochemical nature of both the granitoids and supracrustals is investigated.
The approach of this research is summarized below:

1. Mapping of the 1400 km^2 study area was done directly onto 1:30 000 aerial photographs and the data transcribed onto 1:50 000 topographical sheets, and presented on a scale of 1:100 000 (MAP 1). This scale of mapping was considered adequate

for the granitoids. Where the geology was complex larger scale sketch maps were drawn.

2. The Commondale Supracrustal Suite underlies an area of 100 km^2 and was mapped using aerial photographs of a scale of 1:10 000. The map is presented at a scale of 1:20 000 (MAP 2).

3. Within the core of the southernmost synform of the Commondale Supracrustal Suite, a suite of spinifex and cumulate – textured peridotitic komatiites at least 640 m thick is exposed. A detailed stratigraphic section through the suite was measured. This suite is referred to as the Matshempondo Peridotite Suite.

4. The deformational history of the granitoids was elucidated using numerous S surface measurements, fold axes and axial planes. Detailed structural analysis was undertaken in selected areas particularly in the Layered Gneisses and in some supracrustal remnants. In the Layered Gneisses the minimum strain ellipsoid has been calculated using deformed quartzofeldspathic veins and amphibolite dykes.

5. The petrography of the various granitoids and supracrustals was studied.

6. One hundred and fifty-six samples were analysed by X-ray flourescence spectroscopy for major and trace elements. Granitoids were analysed for eleven major elements and the trace elements La, Sr, Rb, Zr, Nb, Y, Sc, and Ba. Amphibolites and granodiorites were also analysed for Cu, Ni, Zn, Cr and V.

   The Matshempondo peridotites and the supracrustal rocks were analysed for eleven major and eleven trace elements (Cu, Ni, Zn, Nb, Y, Rb, Zr, Sr, V, Cr and Sc).

   These data provide the basis for discussion of magma type, tectonic setting and petrogenesis. The analytical methodology is described in Appendix 2.

7. The effects of metamorphism on these rocks were investigated using thin sections.

Age and chronostratigraphic relationship of the study area to the early Archaean terrane in eastern Transvaal and Swaziland.

The Archaean terrane investigated during this study has a similar geological and tectonic evolution to the granitoid terranes centred about the Barberton, Dwalile, Assegaai and Nondweni supracrustal sequences. The distribution of these 'greenstone' remnants is shown in Fig. 1.1. A chronological summary of the different areas is presented in Table 1.1, with the more pertinent points briefly discussed below.

Layered Gneisses crop out both west and east of the Commondale and Assegaai supracrustal remnants (MAP 3). These Layered Gneisses are lithologically similar to the Bimodal Gneiss Suite in Swaziland (Hunter, pers. comm.). These gneisses are screened from the Commondale Sequence by the clearly intrusive Bazane Porphyritic Trondhjemite Suite.

Four samples collected from the Bazane Porphyritic Trondhjemite Suite yield a (Rb-Sr) whole rock age of 3230 $\pm$ 80 Ma (Alsopp, unpublished data).

Similarly the Anhalt Leucotonalite intrudes at the interface between the Assegaai supracrustals and the Layered Gneisses (Hunter et. al., 1983; Sleigh, 1987). This leucotonalite yields a (Rb-Sr) whole rock age of 3170 Ma (Allsopp, unpublished data). Granitoid suites (Table 1.1) intrusive into the Barberton Sequence in Swaziland are geochronologically younger than the Bimodal Gneiss Suite (Hunter, 1973, 1979; Barton, 1983). Along the southern margin of the Barberton greenstone belt, De Wit et. al. (1983) conclude that the leucotonalite plutons were intruded prior to D_2. Intrusion of several discrete tonalitic and trondhjemitic magmas into or along the orthogneiss-supracrustal contact marked a period of widespread plutonism prior to D_2 in each of these areas. (De Wit et. al., 1983; Jackson, 1984; Hunter et. al., 1986).

TABLE 1.1 CHRONOLOGICAL SUMMARY OF THE ARCHAEAN IN SWAZILAND, EASTERN AND SOUTHEASTERN TRANSVAAL AND NORTHERN NATAL

EASTERN TRANSVAAL[1]	SWAZILAND[1]	SOUTHEASTERN TRANSVAAL - NORTHERN NATAL[2] (PAULPIETERSBURG - COMMONDALE AREA).	SOUTHEASTERN TRANSVAAL[3] (PIET RETIEF AREA).
	Hlatikulu Granite		
	Mhlosheni and Sicunusa Plutons		
	~ 2.6 Ga Kwerta type granite plutons		
	Nhlangono Gneiss		
~ 2.9 Ga Usushwana Complex	USUSHWANA COMPLEX	USUSHWANA COMPLEX	Usushwana Complex
Pongola Mozaan Group	Pongola Mozaan Group	Pongola Mozaan Group	Pongola Mozaan Group
Supergroup Nsuze Group	Supergroup Nsuze Group	Supergroup Nsuze Group	Supergroup Nsuze Group
Dalmein type granodioritic plutons		Quartz monzonite (minor intrusion)	Leucocratic and pegmatitic
Hebron Granodiorite	Mkondo Valley Metamorphic Suite (2)	Leucocratic granite (minor intrusions)	granites
	(Stratigraphic position uncertain:		
	age > 2.6 Ga)		
~ 3.0 Ga Lochiel Granite			~ 3.0 Ga Lochiel granite
~ 3.1 Ga Bosmanskop syenite	~ 3.15 Ga Quartz Monzonite	Granites and leucotonalites (intrusive	
~ 3.2 Ga Leucontonalite plutons	(minor intrusions)	into Luneburg Tonalite Gneiss)	~ 3.2 Intrusion of Anhalt sodic
		Hornblende Granodiorite Suite	granite sheet
	3.3 Ga Granodiorite Suite	Leucotonalite Gneiss	
	Mponono intrusive suite	~ 3.2 Ga Bazane Porphyritic Trondhjemite	
~ 3.2 Ga Kaap Valley tonalite	Tsawela Gneiss pre 3.3 Ga	Suite	
		Braunschweig Tonalite Gneiss	
	Dwalile Metamorhic suite	3.34 Ga Matshempondo Peridotite Suite	
		Commondal Supracrustal Suite	? Assegaai Supracrustal Sequence
	Migmatitic Gneiss (stratigraphic		
	position uncertain)		
3.5 Swaziland Supergroup: Moodies Group, Figtree Group, Onverwacht Group	~ 3.5 Bimodal Gneiss Suite	? 3.5 Ga Lüneburg Tonalite Gneiss	
		Layered Gneisses (bimodal)	? Layered Gneisses (bimodal)

1 Data for Kaap Valley tonalite from Tegtmeyer and Kröner (1987)

1 Data from Tankard et. al. (1982). No relative age sequence is implied with respect to granitoid intrusions aged 3.2 - 3.3 Ga and 2.6 Ga.

2 Data from this study and Hunter et. al. (1986).

3 Data from Hunter et. al. (1986); Sleigh (in prep.)

The Braunschweig Tonalite Gneiss, Kaap Valley tonalite and the Tsawela gneiss in Swaziland are lithologically similar (Hunter. pers. comm.). The Braunschweig Gneiss has a similar structural history to that ascribed to the Tsawela gneiss by Jackson (1984). The remaining components of the gneiss terrane do not apparently have equivalents with the gneiss terrane in Swaziland.

Samples from the Matshempondo Peridotite Suite yields a (Nd-Sm) age of 3337 $\pm$ 13 Ma (Wilson and Smith, in prep). This provides a minimum age for the Commondale Supracrustal Suite. The clearly intrusive 3230 $\pm$ 80 Ma Bazane Porphyritic Trondhjemnite Suite coupled with structural data indicate the Layered Gneisses to predate the Commondale Supracrustal Suite.

CHAPTER 2

GENERAL GEOLOGY.

Various massive and gneissic granitoids within which occur metamorphosed supracrustal remnants constitute the Early Archaean basement to the Late Archaean Pongola Sequence and the Late Palaeozoic - Early Mesozoic Karoo Sequence, Table 2.1. A brief description of the regional geology is essential to a discussion of the geological evolution of the area.

PONGOLA SEQUENCE

The Pongola Sequence comprises a lower, dominantly volcanic Nsuze Group that is overlain by the sedimentary Mozaan Group. This subdivision was first proposed by Humphrey and Krige (1931a). A basalt-rhyolite suite from the Nsuze Group has yielded a Sm-Nd whole rock age of 2934 ± 114 Ma. (Hegner et al., 1984). This date is consistent with the U-Pb age of 2940 ± 22 Ma on zircons from felsic volcanic rocks in the Nsuze Group (Hegner et al., 1984).

Nsuze Group.

The Nsuze Group in the vicinity of the Bivane and White Rivers was investigated by Armstrong (1980) who recognized three major sub-divisions which were assigned formation status* by Armstrong et al., (1982).

i) a lower sedimentary-volcanic unit comprising the Mantonga Formation (± 800 m thick).

* Except for the Bivane Formation these names have not yet been formally recognized. (Hunter, personal communication).

TABLE 2.1 CHRONOLITHOLOGICAL SEQUENCE OF STRATIGRAPHIC UNITS AND THEIR SUBDIVISIONS. AGE RELATIONSHIPS BETWEEN SOME OF THE TRONDHJEMITE - TONALITE - GRANODIORITE SUITE ARE UNCLEAR.

Post Karoo sills and dykes.

KAROO SEQUENCE
- Ecca Group
- Dwyka Formation

~ 2.8Ga USUSHWANA COMPLEX
- Acid Intrusive Suite
- Basic to Intermediate Intrusive suite
- Pyroxenites and dunites

~ 2.9Ga PONGOLA SUPERGROUP
- Mozaan Group
- Nsuze Group
  - Roodewal Fm
  - Bivane Fm
  - Mantonga Fm

~~~~~~~~~~~ unconformity - palaeosaprolite

UNFOLIATED GRANITOIDS
- Quartz Monzonite
- Leucocratic Granite

WEAKLY FOLIATED GRANITOIDS
- Sodic Granite
- Fine grained biotite granite
- Medium grained leucotonalite

TRONDHJEMITE-TONALITE-GRANODIORITE SUITE
- Hornblende Granodiorite Suite
- 3.2 Ga Bazane Porphyritic Trondhjemite Suite
- Braunschweig Tonalite Gneiss
- Leucotonalite Gneiss

~ 3.3Ga MATSHEMPONDO PERIDOTITE SUITE
COMMONDALE SUPRACRUSTAL SEQUENCE

GNEISS COMPLEX
- Luneburg Tonalite Gneiss
- Layered Gneisses.
~~~~~~~~~~~

ii) a middle volcanic unit with minor intercalated volcaniclastic and sedimentary rocks of the Bivane Formation (± 7500 m thick).

iii) an upper volcaniclastic-sedimentary unit of the Roodewal Formation (5 - 600 m thick).

The validity of the Wagendrift Formation proposed by Armstrong (1980) is questioned as a result of the detailed mapping of the granitoid terrane during the present study on the farms Warmbad 18 HU and Wagendrift 12 HU (MAP 1). Quartz wackes cropping out as isolated outliers on Leucotonalite Gneiss, ascribed to the Wagendrift Formation by Armstrong (1980), are considered to be outliers of the Mantonga Formation (MAP 1). It is unknown whether the basaltic lavas previously ascribed to the Wagendrift Formation and cropping out as xenoliths within the quartz diorites and on the southern side of the White River (Armstrong, 1980) are an early volumetrically small volcanic unit predating the Mantonga Formation or whether they are minor basaltic volcanics at the base of the Mantonga Formation.

Along the eastern margin of the study area rocks of the Mantonga Formation unconformably overlie the multiphase Bazane Porphyritic Trondhjemite Suite on the farms Warmbad 18HU, Bendor 211 HT, Zaaiplaats 210 HT and Schaapkraal 20 HU (MAP 1). On these farms a palaeosaprolite is developed at the base of the quartz wackes of the Mantonga Formation (Matthews and Scharrer, 1968; Armstrong, 1980). This is particularly well-developed on the farm Schaapkraal 20 HU where a palaeosaprolite layer 1 - 3 m thick overlies strongly weathered Bazane trondhjemites. The palaeosaprolite layer is in places poorly developed on the farm Bendor 211 HT, where it has been thinned by penecontemporaneous erosion below coarse basal arkosic channel-fill deposits (Matthews and Scharrer, 1968). Matthews and Scharrer (1968) suggest that the palaeosaprolite, a quartz-sericite-vermiculite rock, was derived largely by in situ chemical weathering

of the underlying porphyritic granite. This zone is massive at the base, grading into a crudely bedded zone accompanied by a substantial decrease in the amount of sericitic groundmass. This implies incipient sedimentary sorting of detritus derived from the underlying granite (Matthews and Scharrer, 1968). Palaeosaprolite zones 3 m thick on Zaaiplaats 210 HT and Bendor 211 HT show distinct concentrations of Al_2O_3 and Zr near the unconformity, with an iron maximum at 2 m depth (Moon, 1986). These data are consistent with modern weathering processes, suggesting an origin through in situ weathering rather than hydrothermal activity (Moon, 1986).

The predominant rock types of the Mantonga Formation (±800m thick), are immature, medium- to very coarse-grained quartz wackes with thin (5 - 30 m) intercalated lenses of quartz and arkosic arenites and minor impersistent conglomeratic wackes (50 cm thick). Intercalated lava flows in the Mantonga Formation are prominent south of the White River, ranging in composition from basaltic andesite through andesite and dacite to rhyolite. The flows are laterally impersistent and vary from 2 - 30 m in thickness (Armstrong, 1980). The considerable thickness of immature quartz wackes devoid of feldspars suggests that much of the detritus was derived from weathering of the granitic palaeosaprolite (Armstrong et al., 1982). However, the arkosic arenites and subarkoses indicate that some detritus was derived from weathering of fresh granite (Armstrong et al., 1982), with subsequent in situ alteration of the feldspars.

Lavas of the Bivane Formation comprise basalts, basaltic andesites, andesites, dacites and rhyolites. Individual flows are generally less than 50 m thick. The limited lateral extension of these flows (not more than 10 km) results in a complex interfingering of lavas of similar and different compositions on both regional and local scales (Armstrong et al., 1982). Minor volcaniclastic rocks and subordinate arenaceous sandstones are intercalated with the lavas of the Bivane Formation. These pyroclastic units comprise ash flow tuffs, well-laminated air-fall tuffs, lapilli tuffs, agglomerates and tuffaceous agglomerates which are between 10 and 200 m thick (Armstrong et al., 1982).

The Roodewal Formation is described as a transitional unit between the Nsuze and Mozaan Groups, varying in thickness from 5 - 600 m. It

comprises a number of complexly interfingering facies, representing both pyroclastic and sedimentary deposition (Armstrong et al., 1982). These rock types include fine-grained argillites and air fall tuffs containing arenaceous and volcanic lenses (Armstrong et al., 1982).
North of the White River the strike of the Nsuze Group is northwesterly whereas, south of the White River, the regional strike of the Nsuze Group is approximately northeastwards.

East and southeast of Piet Retief dips of the Nsuze strata steepen to between 55^{o} and 65^{o}. As a result of intense folding and shearing trending northwestwards, the thickness of the Nsuze Group is reduced to between 500 and 2200 m (Smith, 1983). This is substantially less than the 9000 m thick sequence south of the White River reported by Armstrong (1980).

Southeast of Piet Retief rock types ascribed to the Bivane and Roodewal Formations are the dominant rock types (Smith, 1983). In this area the Nsuze Group rocks dip steeply to the northeast. The Bivane Formation comprises basalts, basaltic andesite, andesites, dacites and rhyolites, with intercalations of air fall tuffs and tuffaceous agglomerate lenses. North of the Assegaai River (MAP 3) air fall tuffs, intercalated with agglomerates, pelitic schists, arenaceous sandstones and conglomerates are ascribed to the Roodewal Formation. Tuffaceous agglomerate units up to 1500 m along strike and between 1 and 3 m thick consist of flattened ellipsoidal volcanic fragments within a bedded tuffaceous matrix. Clast supported conglomerate lenses up to 1250 m long and between 1 and 3 m thick are intercalated with finely laminated grey-brown tuffaceous rocks. Pelitic schists composed of pyrophyllite-andalusite-diaspore, together with quartz and aluminous muscovite crop out along strike for 3500 m, varying in thickness between 1 and 5 m. This unit is underlain by rhyolites and dacites and overlain by quartz wackes.

Intrusion of the Usushwana Complex at the interface between the Nsuze Group and the granitoid basement appears to have assimilated the Mantonga Formation which is preserved as large xenoliths in the Usushwana Complex, southeast of Piet Retief.

Mozaan Group.

The Mozaan Group east of the study area is exposed in a series of open structural basins. Between the Bivane and Assegaai Rivers the Roodewal Formation is transitional between the Nsuze and Mozaan Groups (Armstrong, et al.,1982). The Mozaan Group comprises an alternation of arenites and argillites, which reflect three interacting depositional environments, namely offshore shelf, tidal and braided alluvial fan (Watchorn, 1980).

Planar cross-bedded sandstones and subordinate longitudinal gravel bars indicate that sedimentation was dominated by southerly accreting transverse bars in a distal braided river system (Watchorn, 1980). The proximal shelf deposits, which are gradationally overlain by medium- to coarse-grained quartz arenites characterize the base of the tidal sequence. The overlying intertidal zone comprises plane beds, flat topped megaripples and interference ripples interbedded with mud-drapes (Watchorn, 1980). The upper poorly developed heterolithic facies comprises interlaminated sandstones and shales with the proportion of shale increasing upwards. The shelf deposits comprise, from the base upwards banded iron formation, horizontally laminated mudstones, and interlaminated mudstones and rippled siltstones (Watchorn, 1980).

USUSHWANA COMPLEX.

The Usushwana Complex was originally named and defined by Hunter, (1950, quoted in Hunter 1970, p.645) to cover only the ultramafic, mafic and acid rocks exposed between the Usutu and Usushwana Rivers in Swaziland. Hunter (1970) later correlated the gabbroic and granophyric rocks at the base of the Pongola Supergroup in southwestern Swaziland with the Usushwana Complex.

Rock types now ascribed to the Usushwana Complex in the southeastern Transvaal and northern Natal were first mapped by Humphrey and Krige (1931) as a northwesterly and northeasterly trending gabbro-granophyre sheet. These rocks south of the White River were mapped by Armstrong (1980), the area southeast of Piet Retief by Smith (1983) and that northwest of Piet Retief by Hammerbeck (1977).

The Usushwana Complex comprises two dyke-like bodies, one of which extends southeastwards from Amsterdam to its southern extremity in the White River. The other crops out in a subparallel position about 45 km east of Amsterdam in southwestern Swaziland (Map 3). These two dyke-like bodies are linked by a sheet of gabbro and granophyre which intrudes the Nsuze Group (Hunter, 1970, p.645).

An internal (cpx-opx-plag-whole rock) Sm - Nd isochron for a pyroxenite from the Usushwana Complex in Swaziland yields an age of 2871 $\pm$ 30 Ma (Hegner et al., 1984). However, Sm-Nd whole rock data yield an excessively high age of ~ 3.1 Ga (Hegner et al., 1984) which is incompatible with the age data for the Nsuze Group and well-established geological relationships. The date is interpreted as the result of mixing between the Usushwana magma and older continental crust (Hegner et al., 1984).

The Usushwana Complex northeast of Paulpietersburg and southeast of Piet Retief builds a prominant range of hills with gabbroic rock types typically occupying lower lying areas overlain by more resistant, well-jointed granophyres (MAP 3). The Usushwana Complex is intruded between the granitoid basement and the overlying Nsuze Group in Swaziland and the southeastern Transvaal.

In the study area gabbros and granophyres are well exposed on the farms Wagendrift 12HU, Warmbad 18HU and Bendor 211HT, especially along the White and Pongola Rivers and their tributaries. Two main components of the Usushwana Complex are recognizable:

i) Basic to intermediate intrusive suite, in which gabbros, quartz gabbros and granophyric gabbros are the main rock types. Crude layering, defined by changes in mineral proportions and grain size, is developed at some localities. Sporadically developed magnetitite lenses are present, associated with melanocratic gabbros near the top of the gabbroic suite. The outcrop width of the gabbroic rocks varies between 250 m and 2000 m.

ii) Acid intrusive suite, comprising granophyric granites, microgranites and granodiorites. These rock types are gradational into each other and overlie the gabbroic rocks. At the present level of erosion the granophyres are

volumetrically more extensive than the gabbroic rocks.

The abundance of xenoliths, particularly basaltic andesites and quartz wackes, in the granophyric and gabbroic rocks attest to a mechanism of magmatic stoping during emplacement of the Usushwana Complex. The greater volume of granophyre compared to that of gabbro is suggestive of contamination of the magma by assimilation of siliceous roof rocks.

KAROO SEQUENCE.

Dwyka Formation diamictites and fluvioglacial sediments are preserved in pre-Karoo valleys along the northern flank of the Karoo basement. Ecca Group arenites and argillites typically occupy basement highs in and adjacent to the study area.

Dwyka Formation.

Small isolated outcrops of Dwyka Formation diamictite and fluvioglacial sediments are present on the farms Warmbad 18 HU, Talaga 183 HT, Langfontein 182 HT, Schaapkraal 20 HU and Nederland 202 HT (MAP 1). The aerial extent of these outcrops is small, ranging from 20 m^2 to 2 km^2.

On the farm Talaga 183 HT, a massive matrix-supported diamictite contains clasts 1 cm to 1 m in size, varying in shape from angular to well-rounded. The shape of the latter suggests fluvial reworking of some of the material prior to deposition by debris flows. Approximately 1 km south of this outcrop on the farm Nederland 202HT planar crossbedded, arenaceous sandstones are intercalcated with matrix-supported diamictites with a maximum clast size of approximately 10 cm.

Dwyka Formation rocks on Warmbad 18HU build an outlier approximately 2km^2 in extent resting on Layered Gneisses (MAP 1). Matrix-supported cobble to boulder diamictites are interbedded with planar bedded and massive medium-grained sandstones. These are well-exposed in an 8 m vertical section in the valley of the White River. Cobble to boulder size clasts of granitoid and gabbroic rocks can be identified as having been derived from the granitoid basement and Usushwana Complex respectively.

Limited outcrops of Dwyka diamictites and fluvioglacials occupy areas of low relief. Their distribution adjacent to the steep range of hills building the Usushwana Complex suggests their depositon in pre-Dwyka valleys. East of the Usushwana Complex (MAP 3), a large glacial valley extends from north of Mahamba southeastwards along the Swaziland border (Hunter, 1969), where it branches and dissects the Pongola Supergroup parallel to the Klipwal road.

Ecca Group.

Sandstones and argillaceous rocks of the Ecca Group are restricted mainly to the northern and western boundaries of the study area. On the farm Talaga 183HT the contact between the Commondale Supracrustal Suite and Ecca Group siltstones is exposed. At the contact vertically dipping talc and tremolite schists of the Commondale supracrustal remnant are overlain by gently dipping Ecca siltstones. At the base of this unit over a thickness of 1 to 2 m the siltstones are crenulated about the vertically dipping schists as a result of soft sediment deformation The siltstones are overlain by massive, cross-bedded and planar bedded medium-grained sandstones.

POST-KAROO DOLERITE SHEETS.

Along the western, northern and southern margins of the study area abundant dolerite sheets are found varying from tens of metres to hundreds of metres in thickness. These sheets have been intruded at the Archaean granitoid-Karoo Sequence interface as well as at various stratigraphic levels in the Karoo Sequence.

On the farm La Bella Esperance 191 HT (MAP 1) the basal portions of dolerite sheets, that are clearly post-Karoo in age, contain a number of 8 cm thick quartzofeldspathic veins. Xenoliths of Luneburg Tonalite Gneiss and biotite granite are preserved in the dolerite sheets. Also at this locality there is a vertical 'dyke'of dolerite 0.8 - 1.5 m thick that widens towards the top of its present outcrop. It cuts the Luneburg Tonalite Gneiss and is interpreted as a feeder to the overlying sheet. Angular xenoliths of medium-grained leucotonalite are present in thick dolerite sheets on the farm Roodewal 190 HT (MAP 1) west of Luneburg. Occasional thin quartz-

feldspar veins originating from these xenoliths are propagated along joints in the dolerite. These melts of granitic (quartz-feldspar) composition were probably generated by fusion of small amounts of the underlying Luneburg Tonalite Gneiss consequent upon the intrusion of the dolerite. The resultant partial melt migrated along cooling cracks in the dolerite.

Granite-basalt liquid experimental systems described by Watson (1982) indicate that, because of the low diffusivity of SiO_2 and Al_2O_3 into basaltic liquid, xenoliths may be preserved even after extensive exchange of other components. The low diffusivity and buffering of SiO_2, Al_2O_3, K_2O and Na_2O result in quartz and plagioclase being preserved in the xenoliths (Watson, 1982).

MAFIC DYKES.

At least three generations of mafic dykes can be recognized in the study area.

Medium-grained amphibolite dykes up to 1 m wide in the Layered Gneisses cropping out in the Pongola River on the farm Bendor 211 HT (MAP 1) have in some cases been deformed by at least two phases of deformation. Other apparently less deformed amphibolite dykes crop out in the Luneburg and Braunschweig tonalitic gneisses and in the granitic intrusions in the Luneburg Tonalite Gneiss. These amphibolite dykes are the subject of a more detailed discussion in Chapters 3 and 8.

Undeformed dolerite dykes can be traced for distances ranging from several hundred metres to several kilometres. They form swarms aligned either northwest or northeast concordant with the dominant structural trends in the area. These dykes range in width from several metres to several hundred metres in width.

The relative ages of undeformed dykes in the early Archaean are difficult to determine. Dolerite dykes that cut Karoo strata are typically less altered than pre-Karoo dykes, but this is an inadequate basis to classify dykes as pre- or post-Karoo.

CHAPTER 3

GRANITOID LITHOSTRATIGRAPHY.

In this chapter descriptions of the various lithological units and the field relationships on which the stratigraphic sequence (Table 2.1 and Table 3.1) is based will be discussed.

Granitoid Classification.

In this study granitoid classification is based on the parameters indicated in Fig. 3.1 after O'Connor (1965), modified by Barker (1979). This plot based on the normative Ab-An-Or mineralogy allows a geochemically based discrimination of the sodic granitoids, even though this type of classification does not consider the mafic constituents. The limits of the trondhjemite field are also constrained by major element concentrations, which are dependant on the defined petrographic limits and the chemistry of the constituent mineral phases (Barker, 1979) (Fig. 3.1). The ranges for the mafic constituents in the trondhjemite field are; (FeO* + MgO) < 3.4%, and FeO* : MgO commonly 2 - 3. The IUGS classification of igneous rocks (Streckeisen, 1976) describes trondhjemite as a leucotonalite whose plagioclase is oligoclase or andesine. This is consistent with the classification by Barker (1979).

Gneiss Complex.

Two types of quartzofeldspathic gneisses underlie discrete areas of the study area (MAP 1) and are grouped together on structural grounds as the Gneiss Complex (Table 2.1 and Table 3.1). The Luneburg Tonalite Gneiss is restricted to the western part of the study area where it crops out characteristically as domical pavements. Weathered surfaces are friable and generally light brown in colour with darker streaks that result from oxidation of biotite and hornblende. These leucocratic gneisses of tonalitic composition are medium- grained with a crenulate foliation that varies from weak to strong. The foliation is defined by alternating but discontinuous

TABLE 3.1 DETAILED STRATIGRAPHY OF THE GRANITOIDS. LINES WITHIN AND BETWEEN THE FOUR MAIN GROUPS INDICATE INTRUSIVE RELATIONSHIPS (E.G. LEUCOTONALITE GNEISS INTRUDES LAYERED GNEISSES). AGE RELATIONSHIPS WERE DERIVED FROM INTRUSIVE CONTACTS, STRUCTURAL AND SPATIAL RELATIONSHIPS.

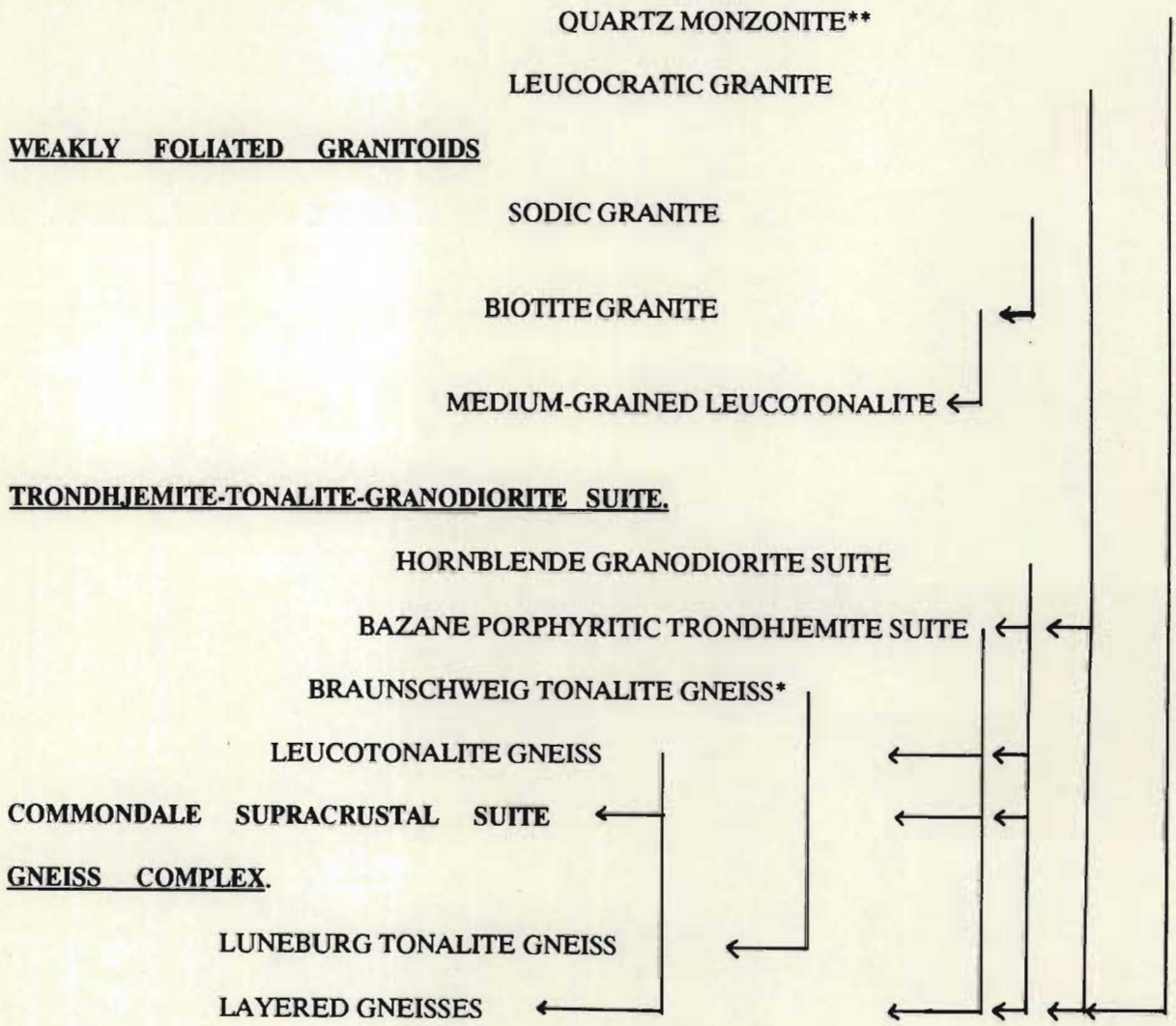

* Age relationship of the Braunschweig Tonalite Gneiss to the rest of the Trondhjemite-Tonalite-Granodiorite Suite. Granitoids unknown.

** Age relationship of quartz monzonite to Leucocratic granite unknown.

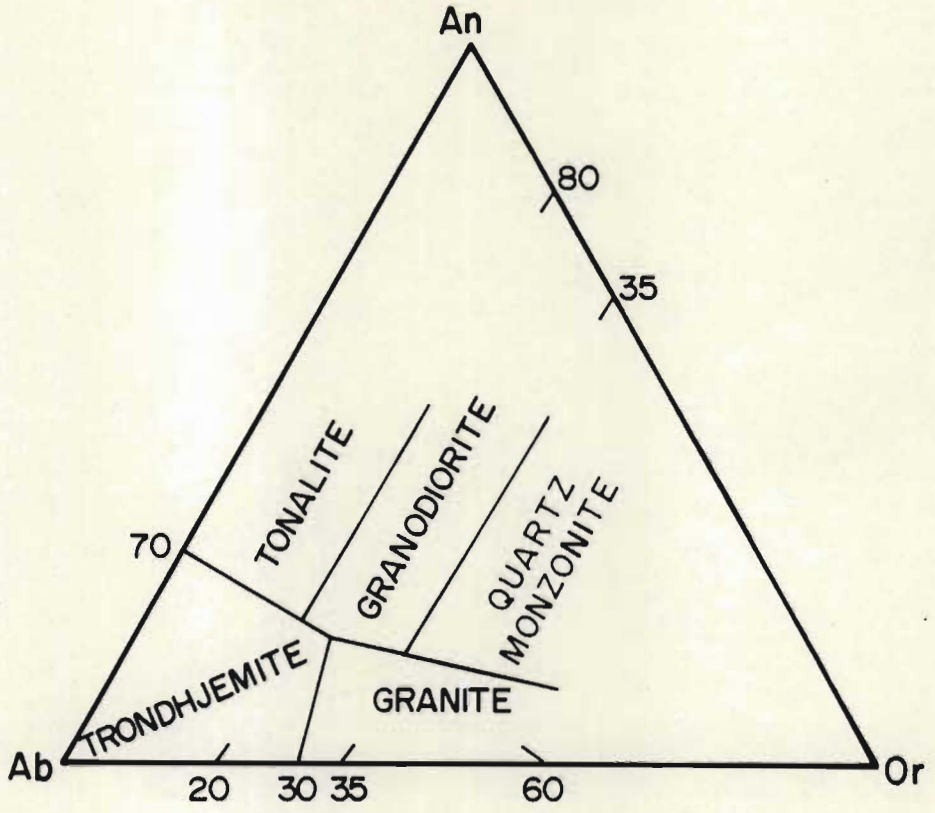

Major element characteristics of trondhjemite.

1. SiO_2 > 68% < 75% SiO_2
2. Al_2O_3 > 15% when SiO_2 ~70% (high Al_2O_3 trondhjemite)

   Al_2O_3 < 14% when SiO_2 ~75% (low Al_2O_3 trondhjemite)
3. (FeO* + MgO) < 3.4%

   FeO* : MgO commonly 2 - 3
4. CaO 4.4 - 4.5 % in calcic trondhjemite. In more sodic varieties CaO 1.5 - 3.0 %.
5. Na_2O 4.0 - 5.5 %.
6. K_2O < 2.5%, and typically < 2%.

Fig. 3.1 Granitoid classification and major element characteristics of trondhjemite (Barker, 1979).

dark, biotite ± hornblende-rich and light quartzofeldspathic layers. The former are 1 - 3 mm thick whereas the light coloured bands are 3 - 7 mm thick. Quartz ribbons are aligned parallel to the foliation defined by the aligned grains of biotite and hornblende. The Luneburg Gneiss encloses small (< 1 km long) remnants of mafic and ultramafic supracrustal rocks, the contacts of which are not exposed but structurally these remnants appear to overlie the Luneburg Gneiss.

Layered Gneisses crop out astride the Pongola River west, east and south of the Commondale Supracrustal Suite and along the White River northeast of Paulpietersburg (MAP 1). These trondhjemitic, tonalitic and granodioritic gneisses are characterized by an alternation of light and dark coloured layers which range in thickness from 2 or 3 mm to 1 - 2 m. Variation in the amount of biotite is responsible for the colour banding in these medium-grained quartzofeldspathic gneisses. The planar foliation is defined by the aligned biotite flakes. Thin highly deformed quartzofeldspathic veins, pegmatites and mafic dykes of a number of different generations are abundant in all components of the Layered Gneiss. The gneisses are concordantly interlayered with amphibolite varying from < 1 cm to several metres in thickness. Amphibolite layers are locally boudinaged but are parallel to the lithological layering with an internal foliation subparallel to that in the gneisses. Hornblende comprises between 60 and 80 vol. % in the amphibolite layers with plagioclase and subordinate quartz constituting the remainder of the rock.The proportion of amphibolite to quartzofeldspathic gneiss is highly variable but amphibolite layers are everywhere subordinate. Whereas many of the amphibolite layers are concordant with the foliation in the tonalite-trondhjemite gneiss, some amphibolites transgress the lithological banding. These discordant amphibolites are interpreted as dykes. The origin of amphibolite units parallel to the lithological layering is enigmatic. However a number of possibilities exist:

i) dykes intruded into the tonalite-trondhjemitic suite and rotated to parallelism due to deformation,

ii) basalts intruded by granitic magmas,

iii) numerous sills intruded into the tonalitic-trondhjemitic suite that remained parallel to the lithological layering during deformation,

iv) intercalated basaltic flows in a felsic volcanic pile.

Astride the Pongola River on the farm Bendor 211 HT individual layers in the layered gneisses are between 1 and 3 metres thick and in places may be up to several tens of metres thick. Three dimensional outcrop and eyed folds indicate the thicknesses of these layers result from structural repetition. Medium-grained, strongly foliated tonalite layers constitute approximately 60% of the rock types along the Pongola River on the farm Bendor 211 HT, with amphibolites and dark, fine- to medium-grained homogeneous tonalites being subordinate. The medium-grained tonalite layers have a strong gneissic foliation defined by biotite and hornblende with sympathetic elongation of quartz grains. These melanocratic tonalites contain patches of melanosome between 5 m x 30 cm and 1 m x 2 cm in size that are elongated in the plane of the foliation. The coarser grained melanosomes are not developed everywhere and consist approximately of 50 vol. % plagioclase, 15 vol. % quartz and 35 vol. % hornblende (Fig. 3.2).

Boudins of pyritic metaquartzite are interlayered with amphibolites, layered amphibolites and calc-silicate gneisses (Fig. 3.3, 3.4, 3.5, 3.6) astride the Pongola River on the farm Tafelberg 186 HT (MAP 1). Leucotonalitic and tonalitic gneisses screen these rock types from apparently more highly deformed tonalitic-leucotonalitic Layered Gneisses. The medium-grained layered amphibolites are composed of alternating plagioclase -amphibole and plagioclase-diopside laminae 0.5 to 5cm thick. The calc-silicates are composed of alternating 0.5 to 1.5cm thick layers of diopside-plagioclase and diopside-microcline. The calc-silicate layers contain abundant zircon and sphene. This sequence crops out over a distance of 250m (Fig. 3.3).

Detailed mapping of this outcrop indicates structural repetition of the units. These aspects and the detailed petrography are discussed in Chapter 4. The quartzites, amphibolites, layered amphibolites and some of the leucotonalitic gneisses may represent the deep root of an older supracrustal sequence, metamorphosed to a higher grade than the

Fig. 3.2. Strongly foliated tonalite gneiss with deformed leucosomes parallel to the foliation. Pen is parallel to the foliation. Layered Gneisses, Pongola River, Bendor 211 HT. Length of pen 15cm.

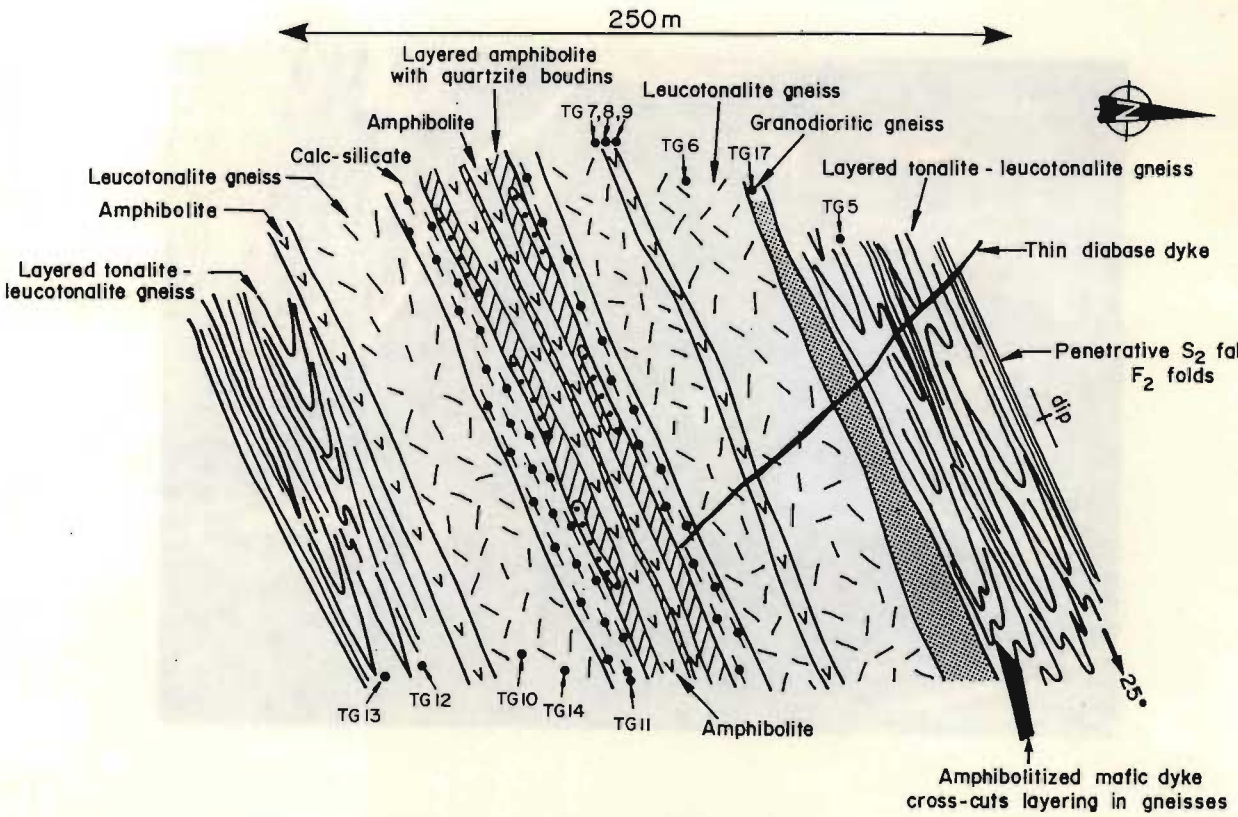

Fig. 3.3. Outcrop map of Layered Gneisses and highly deformed supracrustals. Note the structural repetition in both the supracrustals and Layered Gneisses. Pongola River, Tafelberg 186 HT.

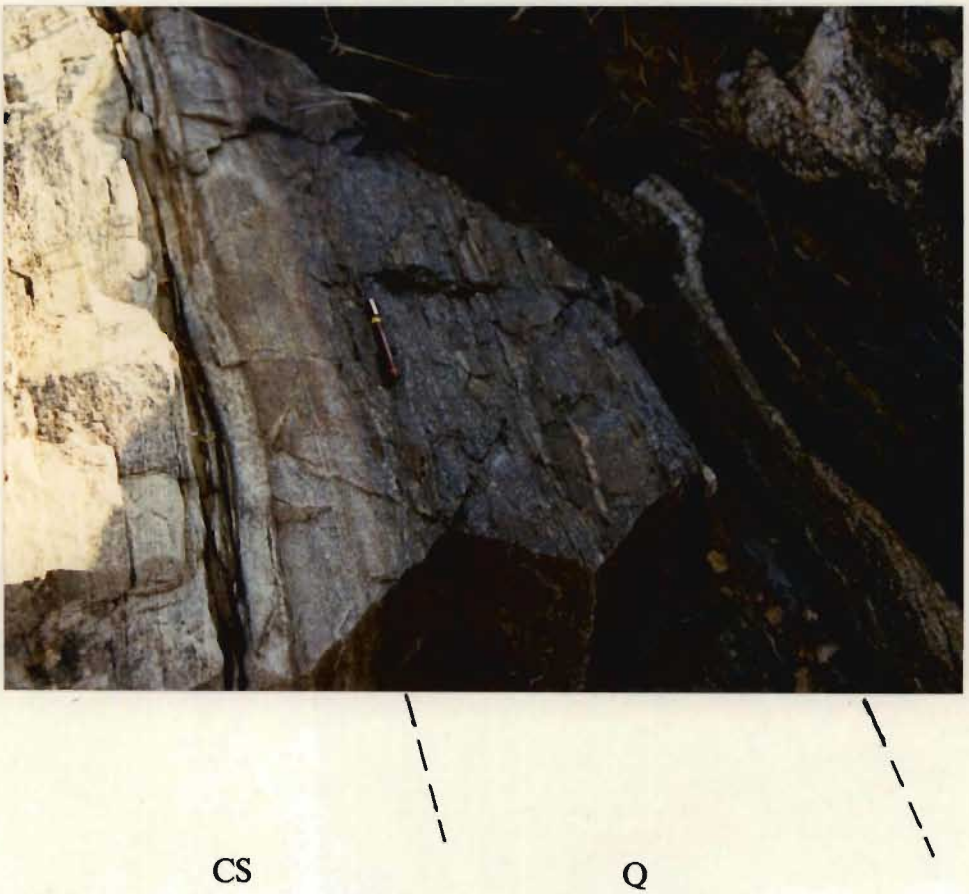

Fig. 3.6. Contact between calc-silicate (CS), pyritic metaquartzite (Q) and layered amphibolite (LA). Pongola River, Tafelberg 186HT. Length of pen 13cm.

stratigraphically and structurally higher Commondale Supracrustal Suite. However, a number of other possibilities fundamental to a better understanding of the layered gneisses exist :

i) The layered amphibolites, calc-silicate gneisses and metaquartzites may be a deep, highly deformed root of the Commondale Supracrustal Suite metamorphosed to a higher grade than the rest of the structurally higher supracrustals.

ii) The Layered Gneisses may represent a felsic volcanic pile intercalated with basaltic flows or sheets, and minor arenaceous sediments. This would imply the existence of a much older siliceous basement than the Layered Gneisses.

iii) Possibility ii) may have been further complicated by the intrusion of granitic and basaltic sheets into the volcanic pile.

Whichever of the four possiblities is correct, the presence of the metaquartzite points to a granitic basement having been in existence prior to the formation of the supracrustal sequences.

Layered Gneisses cropping out along the White River on the farms Wagendrift 12 HU and Warmbad 18 HU are similar to those astride the Pongola River on the farm Tafelberg 186HT (Fig. 3.7 and Fig. 3.8). Outcrops of Layered Gneiss in the White River preserve two small boudins of quartzite (1 x 1,5 m long) enclosed by amphibolite in a fold closure.

The original nature of these layered amphibolites with their associated quartzite boudins is uncertain. Banded amphibolites are reported from the 3.77 Ga Isua supracrustal succession, west Greenland, forming major units in part of the sequence (Gill et al., 1981). The layering is defined by 1 cm thick amphibole-rich lamellae alternating with rocks richer in plagioclase, diopside, epidote, scapolite and quartz. Garnet is preserved locally in pockets and augen that have resisted deformation (Gill et al, 1981). Whether the layering represents primary structures such as stretched pillows or tuffaceous layers, or is due to post-crystallization effects is unknown (Gill et al., 1981).

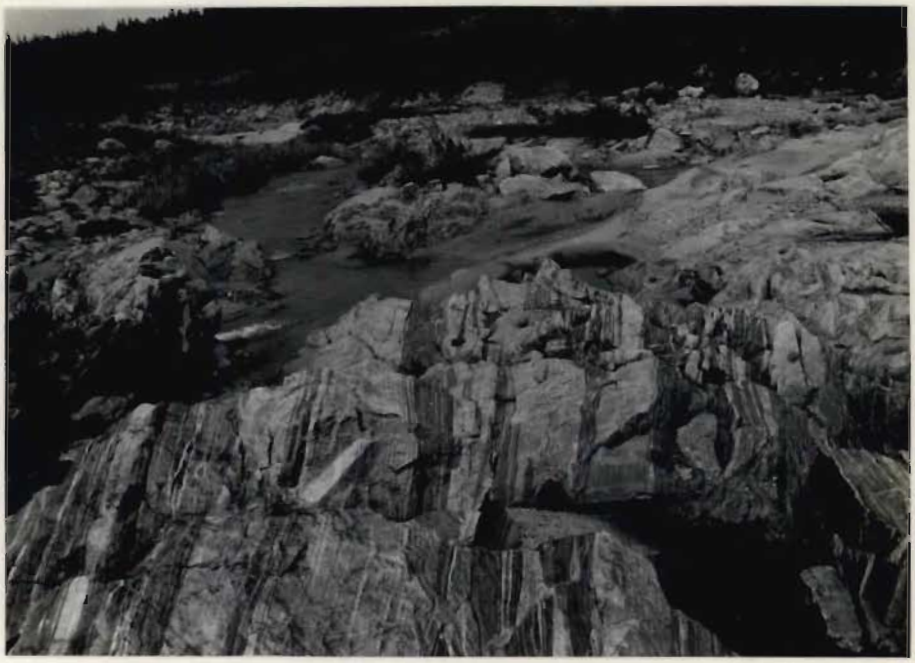

Fig. 3.7. Vertically dipping tonalite-leucotonalite-amphibolite layers in Layered Gneisses in the White River, Witrivier 208 HT.

Fig. 3.8. Meso-scale and centimetre scale layering of fine grained leucotonalites and amphibolite. Highly deformed quartzofeldspathic veins of a number of different generations, especially in the fine grained tonalite. Pongola River, Bendor 211 HT.

Adjacent to the study area on the farms Witrivier 208HT and Wagendrift 12HU layered amphibolites and a poorly exposed quartzite boudin crop out in an arcuate supracrustal remnant preserved within Leucotonalite Gneiss (Sleigh, pers. comm.). These rocks appear to have the same contact relationships to those described on Tafelberg 186HT.

The relationship of the Layered Gneisses to the Commondale Supracrustal Suite is either not exposed or obscured by the intrusion of later granitoids. Contacts between the Luneburg Tonalite Gneiss and Layered Gneisses are nowhere exposed, but due to their apparently similar deformation histories they are interpreted to be of similar age. The greater structural complexity of the Gneiss Complex and discordant boundaries with the intrusive Trondhjemite-Tonalite-Granodiorite Suite indicate that the Gneiss Complex is older than the other granitoids and supracrustals in the study area.

Grouping of the Luneburg Tonalite and Layered Gneiss together as components of the Gneiss Complex does not necessarily imply that they are contemporaneous or cogenetic.

Trondhjemite - Tonalite - Granodiorite Suite.

The Leucotonalite Gneiss, Braunschweig Tonalite Gneiss, Bazane Porphyritic Trondhjemite Suite and Hornblende Granodiorite Suite are grouped together because they all intrude the Gneiss Complex and the supracrustal sequences.
Light coloured Leucotonalite Gneisses underlie the eastern part of the study area and extend north of the White River where they crop out adjacent to the Usushwana Complex (MAP 1). Biotite laths and elongated quartz grains define the foliation of these moderately to strongly foliated, medium-grained gneisses which do not display layering. Outcrop of the gneiss is in many places restricted to occasional boulders, although on the farms Lodewyks Lust 18 HT and Witrivier 208 HT large pavements are exposed south of and in the White River (MAP 1).

The medium- to coarse- grained Bazane Porphyritic Trondhjemite Suite crops out over an area of approximately 250 km^2 on both flanks of the Commondale Supracrustal Suite. Intrusive contacts with the

supracrustal rocks are well-exposed on the farms Talaga 183 HT, Vrye Gunst 199 HT and 201 HT and on Mooiplaats 206 HT (MAP 1). A very strong planar fabric defined by the elongation of quartz ribbons and aligned biotite flakes has destroyed the typical porphyritic character of the Bazane trondhjemites along the western margin of the Commondale Supracrustal Suite. A zone between 10 and 40 m wide adjacent to the supracrustal sequence on the farms Nederland 202HT, Vrye Gunst 201HT and Wachteenbietjies Spruit 44 has an extremely strong mylonitic fabric. Mylonization is in some places so intense that all porphyroclasts are destroyed, but on Nederland 202HT porphyroclasts with long axes in the plane of the mylonitic foliation are preserved. Gradation from the mylonitic granite to the typical porphyritic varieties occurs over a distance of 40 m on the farm Vrye Gunst 201HT.

Away from the contacts with the supracrustals the Bazane trondhjemites displays a moderately strong to strong planar fabric defined by ribbon quartz, aligned biotite plates and parallelism of feldspar porphyroclasts, the latter representing original megacrysts that have been affected by deformation (Fig. 3.9). The size, proportion and type of feldspar phenocrysts are very variable. Megacrysts range in size from 0,3 to 10 cm in length, some are clearly zoned and their abundance varies from 2 to 60 volume %. There is a rapid gradation locally both in size, type and abundance of megacrysts. Trondhjemitic, granodioritic, granitic and quartz monzonitic varieties grade imperceptibly into one another, but lack of outcrop may obscure relationships of lithologies to each other. These varieties are distinguished chemically and mineralogically by varying proportions of K-feldspar, plagioclase, quartz, biotite and hornblende. Biotite is present typically in amounts of 3 vol. % in both the trondhjemitic and more potassic phases. The Bazane Porphyritic Trondhjemite Suite is interpreted as a large texturally and compositionally inhomogeneous sheet-like intrusion emplaced at the interface between the Gneiss Complex and the supracrustal rocks in a similar fashion to that between the Anhalt Leucotonalite and Assegaai Supracrustals (Talbot et al., 1987).

The Hornblende Granodiorite Suite crops out as sporadically distributed pavements and scattered boulders along the northern and eastern margins of the Commondale Supracrustal Suite. On the farm

a

b

Fig. 3.9. Weakly foliated (a) and strongly foliated (b) trondhjemites of the Bazane Porphyritic Trondhjemite Suite. Talaga 183 HT.

Mooiplaats 206 HT west of the main road between Commondale and Moolman where, this suite intrudes supracrustal amphibolites, agmatitic structures are well- developed (Fig. 3.10). Similar but less well-exposed relationships are observed east of the main road between Commondale and Moolman where granodiorites intrude highly deformed metamorphosed pillow lavas.

The hornblende granodiorite is medium-grained, and in places strongly foliated. However, where the hornblende granodiorite intrudes supracrustal amphibolites, hornblende-bearing granodiorites, tonalites and feldspathic amphibolites crop out within several metres of each other. The feldspathic amphibolites are distinguished from the supracrustal amphibolites by their much coarser grain size (3 - 4 mm). Always spatially associated with the granodiorites are muscovite-quartz-plagioclase pegmatites with up to 40% muscovite. A 4 m wide pegmatite on the farm Mooiplaats 206 HT can be traced for 400 - 500 m intruding all rock-types except Karoo dolerites. A similar pegmatite up to 8 m wide crops out in a stream on the farm Jachtdrift 41. Unlike the other granitoids in the area the granodiorites are intruded only by these quartz-muscovite pegmatites.

The complex angular fracturing of the amphibolites clearly indicates brittle disruption during insertion of the granodiorite. This area may represent the roof zone of the granodiorite magma chamber, where the hydrostatic pressure exceeded the lithostatic pressure causing mechanical fracturing of the roof rocks. This suite of rocks may owe its hetrogeneity to assimilation of supracrustal amphibolites during intrusion of the granodiorite.

The Braunschweig Tonalite Gneiss crops out northeast of Luneburg and is best exposed as large pavements on the farm Vaderland 14 (MAP 1). The melanocratic, medium-grained hornblende-bearing gneiss crops out over an area of about 30 km^2. The strong foliation is defined by the alignment of biotite and hornblende which parallels the elongation of the quartz grains. Plagioclase forms porphyroclasts that show crude alignment parallel to the coarse planar fabric. Like the other granitoids in the area, the Braunschweig gneiss is intruded by granitic and pegmatitic veins that range in width from 1 cm to 1 m. Mafic dykes, now amphibilotized, intrude the gneiss (Fig. 3.11).

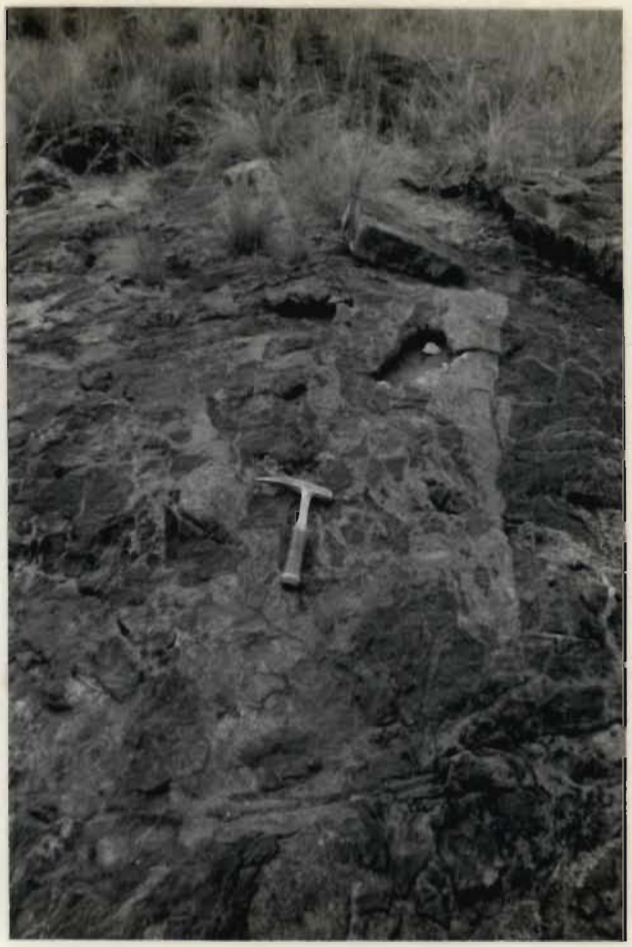

Fig. 3.10. Hornblende Granodiorite Suite (light coloured), intrusive into supracrustal amphibolites. The agmatic structure is well developed in this area. Mooiplaats 206 HT.

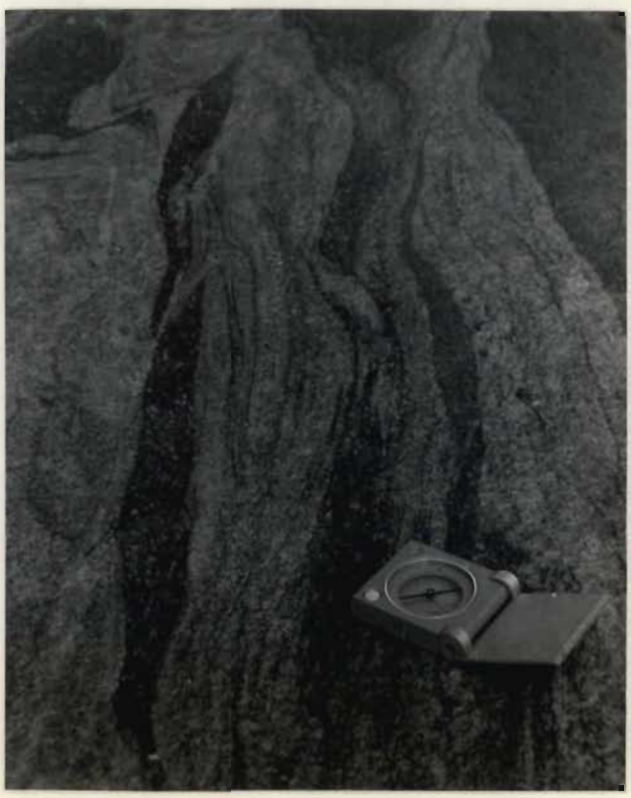

Fig. 3.11. Weakly porphyritic melanochratic Braunschweig Tonalite Gneiss with deformed granitic veins. Vaderland 14.

Although no contacts between the Luneburg and Braunschweig gneisses are exposed, the latter is considered to be intrusive into the Luneburg Gneiss on the basis of structural data (Chapter 8).

Unfoliated and Weakly Foliated Granitoids.

Granitic intrusions in the Luneburg Tonalite Gneiss.

Three distinct granite and leucotonalite bodies, 1 to 10km^2 in extent, intrude the Luneburg gneiss and the metavolcanic remnants.
Medium-grained leucotonalite and biotite granite are typically highly weathered and intrude the Luneburg Tonalite Gneiss in a complex fashion (Fig. 3.12). The medium-grained leucotonalite is distinguished in the field from the biotite granite by its lower proportion of biotite and its typically less weathered appearance. The leucotonalite is seen to intrude the biotite granite on the farm Donkerhoek 172 HT although outcrop is poor. Clear intrusive relationships between the Luneburg Tonalite Gneiss and biotite granite are exposed south of the homestead on La Belle Esperance 191 HT, where anastamosing veins and dykelets originating from more extensive bodies of biotite granite transect the Luneburg Gneiss. Both the biotite granite and the leucotonalite display a weak planar fabric that is defined by subdiomorphic quartz and biotite.

A small (3 km^2) sodic granite intrusion which appears to truncate the biotite granite crops out on the farm Roodewal 190 HT. This fine- to medium-grained granite is devoid of any planar fabric which distinguishes it from the other intrusions into the Luneburg Gneiss. Abundant mafic dykes, now amphibilotized, intrude the granite and Luneburg Tonalite Gneiss.

Leucocratic Granite and Quartz Monzonite.

Leucocratic granites intrude Leucotonalite Gneisses and Layered Gneisses on the farms Witrivier 208 HT and Warmbad 18 HU, respectively. At the former locality sheets and dykes of leucocratic granite up to 15 m thick intrude supracrustal amphibolites and serpentinites (Fig. 3.13). The fine- to medium-grained granite is devoid of fabric, and is intruded by the Usushwana Complex.

Fig. 3.12. Fine-grained biotite granite intrusive into strongly foliated Luneburg Tonalite Gneiss. Roodewal 190 HT.

Fig. 3.13. Supracrustal amphibolites intruded by irregular sheets of Leucocratic Granite. Witrivier 208 HT.

Light pink, medium-grained, unfoliated quartz monzonite intrusive into the Bazane Porphyritic Trondhjemite Suite crops out as a small (1,5 km^2) elliptically shaped body on the farm Schaap Kraal 20 HU. The eastern outcrop of this granite is overlain by Nsuze Group quartzites of the Mantonga Formation. These leucocratic granites and quartz monzonite are both pre-Pongola granitoids.

CHAPTER 4

PETROGRAPHY OF THE GRANITOIDS.

This Chapter describes and discusses the petrography of the granitoids and intimately associated rock-types, particularly those in the Layered Gneisses. The mineralogies of the rock samples are presented in Appendix 1. All sample localities are shown on MAP 1.

GNEISS COMPLEX.

Layered Gneisses.

The Layered Gneisses comprise trondhjemitic-tonalitic and granodioritic rocks that are intimately interlayered with amphibolites, layered amphibolites, calc-silicates gneisses and metaquartzites. The layered amphibolites, calc-silicate gneisses, metaquartzites and some amphibolites may be supracrustals preserved within the Layered Gneisses, as discussed in Chapter 3. Average modal proportions are presented in Table 4.1 and detailed mineralogies are given in Appendix 1 Table 1.

Trondhjemites.

Anhedral to euhedral plagioclase grains (< 4mm) are set in a matrix of finer aggregates of granoblastic plagioclase, quartz, microcline, and biotite, muscovite, apatite, sphene and zircon. Biotite is replaced locally by chlorite and magnetite. The margins of plagioclase grains are saussuritized. Plagioclase is twinned according to the albite twin law.

A mozaic of xenoblastic quartz grains comprises lenticular ribbons that are between 1 and 3mm wide and up to 6mm long. Pleochroic brown-khaki brown biotite (<1mm) laths and hornblende grains (<3mm) parallel the quartz ribbons and wrap around plagioclase porphyroclasts. The subidiomorphic hornblende grains have light brown-green pleochroism. Fractures in plagioclase parallel to the foliation are noted in some samples suggesting brittle deformation possibly postdating the main foliation event. The abundance of curved albite twin lamellae with undulose extinction implies a

TABLE 4.1 AVERAGE MODAL PROPORTIONS OF THE DIFFERENT GRANITOIDS* AND ASSOCIATED ROCKS

GRANITOID TYPE	PLAG	MICRO	QTZ	BIOT	MUSC	HBL	DIOP	ACC
LAYERED GNEISSES								
Tonalites and leucotonalites	31-42	5-10	17-38	12-25	-	9-36	-	Z,A,S
Trondhjemites	41-46	5-10	35-41	5-10	0-3	-	-	Z,A,S
Granodiorite	40	22	26	10	-	-	-	Z
Calc silicate Gneiss								
(diop+plag micro layer)	20	53	-	-	-	-	25	S
(diop+ plag layer)	51	2	2	-	-	-	42	
Layered Amphibolite								
(diop+plag layer)	50	-	-	-	-	-	50	S
(hbl+plag layer)	40	-	-	-	-	60	-	
LUNEBURG TONALITE GNEISS	50-55	4-7	15-20	5-12	-	5-18	-	Z,S,A
LEUCOTONALITE GNEISS	48-60	4-12	21-26	8-16	-	4-7	-	Z,A
BRAUNSCHWEIG TONALITE GNEISS	43-46	5	20-21	8-11	-	20-22	-	Z,A
BAZANE PORPYRITIC TRONDHJEMITE SUITE (See Appendix 1)								
HORNBLENDE GRANODIORITE SUITE								
Granodiorite	40-50	5-15	12-19	9-11	-	7-28	-	Z,A,S
Tonalite	45-50	-	16-20	∿15	-	13-25	-	S
Feldspathic amphibolite	40-50	-	3-8	12-14	-	29-42	-	Z,S
WEAKLY FOLIATED GRANITOIDS								
Medium-grained leucotonalite	∿55	∿ 5	24-27	9-12	-	-	-	A,Z
Biotite Granite	∿20	∿25	∿30	∿25	-	-	-	A,Z
Sodic Granite	35-45	20-25	20-25	∿15	-	-	-	A
UNFOLIATED GRANITOIDS								
Leucocratic Granite	29-32	31-36	∿24	4-8	-	-	-	-
Quartz Monzonite	∿31	∿34	∿18	∿16	-	-	-	Z,S

* Names of granitoids may not be consistent with the modal proportions as they are named by taking into account the geochemical variation within this group of rock-types.

A = apatite; Z = zircon; S = sphene; ACC = accessory minerals
PLAG = plagioclase; MICRO = microcline; QTZ = quartz
BIOT = biotite; MUSC = muscovite; HBL = hornblene; DIOP = diopside

mechanical origin for these twins as a result of shearing (Smith, 1974). Deformation twins or glide twins of albite and pericline form as a result of homogenous shear of lattice points on one side of the twin boundary with respect to the other (Hobbs et al. 1976). In some of the samples chlorite-epidote-quartz symplectites are developed between some hornblende and plagioclase grains. The symplectites are subpoikilitic in the hornblende.

The tonalitic and granodioritic components are texturally similar to the trondhjemites. The tonalites are characterized by a higher proportion of biotite and hornblende than in the trondhjemitic gneisses (Table 4.1). The granodiorites typically have a greater proportion of microcline and mafic minerals than the trondhjemites.

Calc-Silicate Gneisses.

Calc-silicate rocks are a minor component of the Layered Gneisses cropping out in the Pongola River on the farm Tafelberg 186 HT (Fig. 3.3). These banded rocks comprise alternating layers of diopside + plagioclase + microcline and diopside + plagioclase (Table 4.1; Appendix 1 Table 1). Both layers contain < 2% quartz and the diopside + plagioclase layer < 2% microcline. Individual layers are between 3mm and 30mm thick (Fig. 4.1).

The diopside + plagioclase layers comprise subidiomorphic diopside grains (< 3mm) and finer-grained interlocking aggregates of saussuritized plagioclase. The plagioclase is either untwinned or twinned according to the albite twin law and contains abundant inclusions of sphene.

The diopside + plagioclase + microcline layers are characterized by a high proportion (> 50%) of subidiomorphic microcline grains (< 1mm). Diopside and plagioclase grains are elongated and define the foliation which is parallel to the banding. Sphene is a common accessory mineral.

Layered Amphibolites

Enigmatic layering is defined by diopside + plagioclase and hornblende + plagioclase layers between 3mm and 3cm thick. The contact

Fig. 4.1 Photomicrograph of alternating diopside + plagioclase and diopside + microcline layers in calc-silicate gneisses. Microcline + diopside layer is on left, whereas the right hand side of the photograph consists of plagioclase and diopside. Plagioclase is characteristically saussuritized and twin lamellae are obscured. The alteration contrasts with the fresh appearance of microcline. Sample TG11, field of view 10mm, crossed polars.

Fig. 4.2 Photomicrograph of alternating diopside + plagioclase (upper left and lower right hand corners of photograph) hornblende + plagioclase (centre of photograph) layers in layered amphibolites. Sample TG15, field of view 10mm, plane polarized light.

between the layers is sharp. Sphene is an accessory mineral and albite twins in plagioclase are partially saussuritized (Fig. 4.2).

In the amphibolite layers grains (< 3mm) of pleochroic green brownish-green hornblende are surrounded by xenoblastic plagioclase grains (< 1 mm). Hornblende poikilitically encloses small euhedral grains of plagioclase. Plagioclase with broad twin lamellae is twinned according to the albite twin law. These features suggest that the albite twins are the products primary crystallization.

In the diopside-bearing layers subidiomorphic and idiomorphic diopside grains (< 3mm) are surrounded by finer aggregates (< 1mm) of plagioclase. Sphene is a rare accessory mineral. Plagioclase is pervasively saussuritized suggesting a more calcic plagioclase composition than in the amphibolite-bearing layers. Diopside poikilitically encloses small plagioclase euhedra. Chlorite-epidote-quartz symplectites (< 1mm) are developed between some hornblende and plagioclase grains and sporadically between diopside and plagioclase grains. The symplectites may result from differential pressure solution along grain boundaries and migration of components between the hornblende and plagioclase, and diopside and hornblende respectively.

Pyritic metaquartzite.

Ragged xenoblastic grunerite grains (< 4mm), euhedral pyrite grains and magnetite form layers up to 10 mm thick that are separated by quartz-rich layers between 2 and 10 mm thick (Fig. 4.3). The quartz-rich layers comprise polygonal aggregates of quartz, minor pyrite and grunerite. Fibrous and columnar grunerite with fine multiple twinning along the (100) twin plane form aggregates of grains parallel to a poorly developed foliation or elongation of quartz grains. In the quartz-rich layers random aggregates of fibrous grunerite are sporadically developed. The presence of grunerite in the metaquartzites indicates metamorphism at amphibolite facies.

Luneburg Tonalite Gneiss.

Subidiomorphic plagioclase grains (< 8mm) are surrounded by finer aggregates of plagioclase, microcline, quartz, hornblende, biotite,

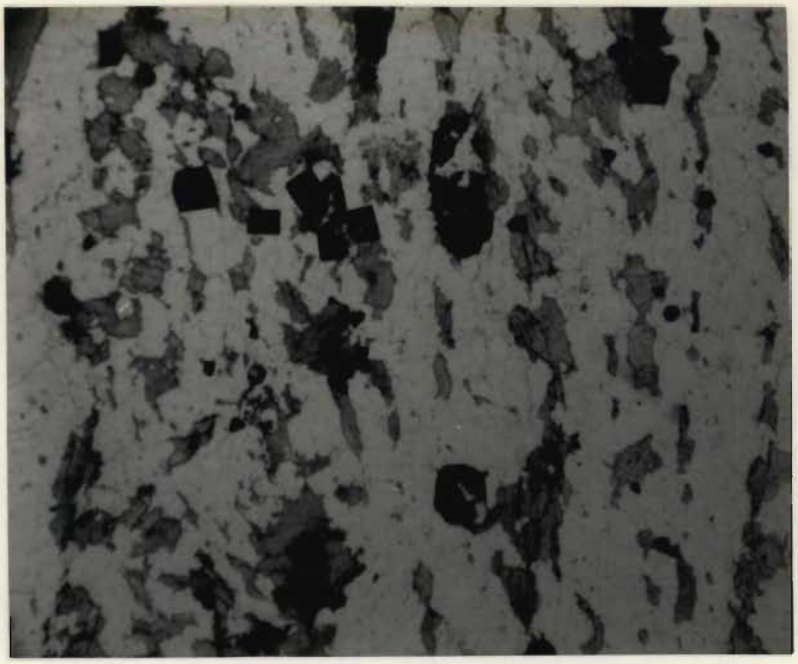

Fig. 4.3 Photomicrograph of xenoblastic grunerite grains (grey) and euhedral pyrite and magnetite (black) separated by quartz rich layers. Pyritic metaquartzite, sample TG16, field of view 10mm, plane polarized light.

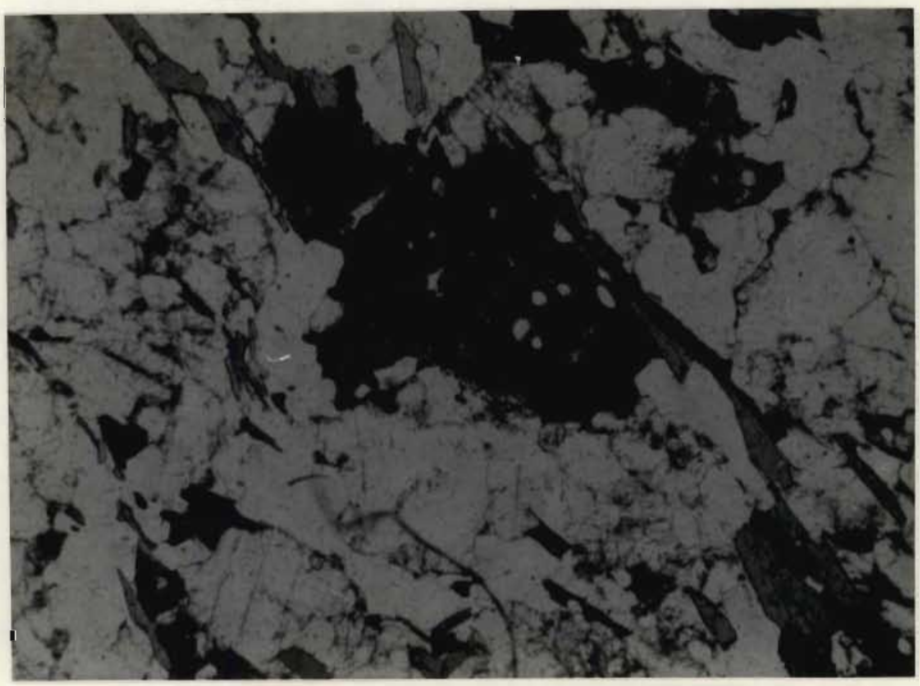

Fig. 4.4 Photomicrograph showing small blebs of quartz in hornblende (centre, black) and biotite laths (grey) wrappping around plagioclase porphyroclasts (upper right). Luneburg Tonalite Gneiss, sample KA2, field of view 4.5mm, plane polarized light.

opaque ore minerals, zircon, sphene and apatite. Hornblende grains (3 mm) poikilitically enclose subhedral plagioclase, sphene, zircon and apatite (Appendix 1 Table 2; Table 4.1). Small blebs of quartz were noted in some of the grains of pleochroic grass green-brownish green subidiomorphic hornblende (Fig. 4.4). Ragged, subidiomorphic biotite grains (< 2mm) locally display broken and kinked plates. The biotite grains have pale brown-brown pleochroism.

Plagioclase is twinned according to the albite-Ala and albite twin laws. Plagioclase grains with a high density of curved twin lamellae are interpreted to be of a mechanical origin. However a large proportion of the plagioclase in these rocks is untwinned. Small bulbous myrmekite heads are sporadically developed where microcline and plagioclase are in mutual contact. The gneissosity is defined by alternating dark biotite $\pm$ hornblende-rich and light quartzofeldspathic layers. The former are 1-3mm thick whereas the lighter coloured bands are 3-7mm thick. Polygonal aggregates of xenoblastic quartz are stretched parallel to the foliation.

Alteration ranges from weak to moderate saussuritization of plagioclase. Biotite is altered to chlorite and magnetite, but is also developed locally at the expense of hornblende.

On the farm Koppie Alleen a coarser grained variety (KA4) is intensely altered. Plagioclase is saussuritized, hornblende is altered to chlorite, magnetite and secondary sphene, and biotite to chlorite.

TRONDHJEMITE-TONALITE-GRANODIORITE SUITE.

Leucotonalite Gneiss.

This Suite comprises several discrete lithologies that are generally less deformed than the Gneiss Complex. In areas of high strain gneissic foliation and a strong mylonitic fabric with pronounced quartz ribbons are well-developed. Texturally the other rock types are generally granoblastic to porphyroclastic. This leucocratic gneiss is broadly similar in appearance to the Luneburg Tonalite Gneiss, but

does not have the same highly folded gneissic layering. It is also distinguished geochemically from the Luneburg Tonalite Gneiss.

Subidiomorphic plagioclase grains (< 6 mm) are set in a groundmass of finer plagioclase, anhedral microcline, quartz, hornblende, biotite, zircon and apatite (Table 4.1; Appendix 1 Table 3). Minor chlorite and epidote replace biotite. Subpoikilitic myrmekite heads are sporadically developed in microperthitic microcline. Myrmekite is developed in some euhedral plagioclase grains in poikilitic microcline. Biotite grains (0.8 mm) and lenticular quartz (6 mm) grains with undulose extinction parallel each other. Locally adjacent to plagioclase porphyroclasts a fine mortar structure is developed. A high density of curved albite twins in plagioclase suggest a mechanical origin for the twins. Samples WTR5, WTR1 and WG1 have a strong foliation characterized by the development of quartz ribbons and a strong mortar structure. Texturally these samples may be referred to as porphyroclastic and in the more extreme cases of cataclasis as protomylonites.

Bazane Porphyritic Trondhjemite Suite.

Petrographically and geochemically the Bazane Porphyritic Trondhjemite Suite may be divided into two facies. The western facies crops out west and east of the Commondale Supracrustal Suite and is separated from the eastern facies, which abuts against the Usushwana Complex and Nsuze Group by a tongue of Leucotonalite Gneiss (MAP 1).

The eastern facies comprises granodiorite, granite, quartz monzonite and trondhjemite. The western facies consists predominantly of trondhjemites with minor granite and granodiorite (see Chapter 5). Compositional variations appear to be gradational into each other but outcrops are commonly inadequate in many areas to confirm the validity of this observation. The rock-types from both the western and eastern facies are typically coarse-grained with porphyroclasts of plagioclase and K-feldspar up to 3 cm and 10 cm respectively. Modal compositions are presented in Appendix 1 Table 5.

Coarse Porphyrtic Trondhjemite.

Coarse (2 - 12 cm) perthitic microcline megacrysts and plagioclase grains (1 - 2 cm) are set in a matrix of finer aggregates of quartz (2-6mm) , plagioclase, microcline, biotite, muscovite, opaque ore minerals, zircon, apatite and sphene. Microcline poikilitically encloses quartz, subhedral biotite and euhedral plagioclase grains (Fig. 4.5). Development of myrmekite heads around the margins of the microcline porphyroclasts and in the plagioclase inclusions is common. Aggregates of xenoblastic quartz grains exhibiting undulatory extinction form ribbons between 4 mm and 5 cm long in the coarser grained varieties. Inclusions of apatite are present in the quartz.

Plagioclase is twinned according to the albite-Ala, albite-pericline, albite and Carlsbad-albite twin laws. Albite twins are the most abundant. Curved albite twins are developed in those rock types with a strongly developed foliation suggesting a mechanical origin for these twins. Large microperthitic microcline crystals are zoned outwards with microcline twinning best developed towards the edges of the crystals. Some of the microcline crystals exhibit both microcline and Carlsbad twins.

Alteration ranges from minor to pervasive, with the latter most common in the deformed varieties that are fractured and display strong mortar textures. In these rocks plagioclase is strongly saussuritized. Biotite is altered to a symplectic intergrowth of chlorite and magnetite. Thin fractures and zones where a strong mortar structure is developed in the interstitial microcline and plagioclase are generally strongly altered to epidote and chlorite with minor calcite. The trondhjemite displays a moderate to strong but variable planar fabric defined by ribbon quartz, aligned biotite flakes and parallelism of feldspar porphyroclasts. The latter represent original inclusion-rich megacrysts affected by deformation. Texturally these rock types are porphyroclastic. Close to the contact with the Commondale Supracrustal Suite protomylonites, mylonites and ultramylonitas are developed.

The rocks classified as granites and granodiorites are distinguished from the trondhjemites by their higher proportion of K-feldspar, biotite and the presence of hornblende in some of the granodiorites.

Fig. 4.5 Photomicrograph of microcline poikilitically enclosing twinned and zoned euhedral crystals of plagioclase. The microcline porphyroclast is in a matrix of xenoblastic quartz (white), saussuritized plagioclase (mottled grey) and mickrocline (faint cross-hatched twins). Bazane Porphyritic Trondhjemite Suite, sample NLD 1, field of view 10mm, crossed polars.

Coarse Porphyritic Quartz Monzonites.

These quartz monzonites are characterized by equal proportions of euhedral plagioclase (1 cm) and microperthitic microcline grains (< 8 cm) . The groundmass comprises finer aggregates of plagioclase, quartz, hornblende, biotite, apatite, sphene, zircon, chlorite, allanite and calcite. Subpoikilitic myrmekite heads are developed in microcline adjacent to plagioclase grains. Myrmekite is also developed in euhedral plagioclase inclusions in microcline megacrysts. Microcline poikilitically encloses plagioclase, hornblende and apatite grains. Biotite plates (4 mm) enclose zircon and apatite.

Quartz ribbons with undulose extinction and feldspar megacrysts are aligned sub-parallel in a matrix of granoblastic plagioclase, hornblende and biotite. Plagioclase is extensively saussuritzed but traces of albite twins can still be recognized. K-feldspar is kaolinized. Biotite is pervasively altered to a symplectic intergrowth of chlorite and magnetite, accompanied by epidote overgrowths. Hornblende is altered to chlorite. Thin fractures are filled by calcite, epidote and quartz.

Braunschweig Tonalite Gneiss.

Subhedral plagioclase porphyroclasts up to 6 mm long are set in a matrix of finer aggregates (3 mm) of quartz, biotite, hornblende, microcline, opaque ore minerals, zircon and apatite. Minor epidote and chlorite replace biotite (Table 4.1; Appendix 1 Table 4).

Quartz with undulatory extinction forms lenticular grains up to 5mm long. A weak mortar texture is developed between the porphyroclasts and finer aggregates. The strong foliation is defined by the alignment of the biotite and hornblende which parallels the elongation of the quartz grains. Long axes of plagioclase porphyroclasts show a crude alignment parallel to the coarse planar fabric.

The plagioclase is twinned according to the albite and pericline twin laws. The albite twins are typically curved and have undulose extinction. The pericline twins are ragged, curved and have a high density of twins in individual phenocrysts. These features suggest

that the albite and pericline twins are of a mechanical origin (Fig. 4.6). However close petrographic observation indicates an older generation of primary albite twins and albite-pericline combination twins. These twins are characterized by broader twin lamellae that are not curved. Plagioclase is reversely zoned, with the rim slightly more calcic than the core. The microcline contains small inclusions (0.1mm) of plagioclase. Sporadically developed myrmekitic heads are embayed into microcline adjacent to plagioclase grains.

Strongly pleochroic tabular green-brown hornblende up to 3 mm in length poikilitically encloses anhedral grains of quartz plagioclase, apatite and zircon euhedra. The presence of quartz inclusions in the hornblende grains is not consistent with a normal mineral paragenesis and probably reflects a two dimensional effect created through thin sectioning. Only a few minute crystals of zircon were identified. Brown-khaki brown biotite sheaves up to 1 mm long are closely associated with and in places partially intergrown with hornblende. In all the samples examined petrographically only minor alteration of biotite to epidote and chlorite, and hornblende to biotite was recognized.

Hornblende Granodiorite Suite.

Rock-types belonging to this suite include granodiorites, tonalites and feldspathic amphibolites. These rock-types are found cropping out where they intrude amphibolites of the Commondale Supracrustal Sequence. The feldspathic amphibolites are distinguished from the supracrustal amphibolites by their coarser grain size, their higher proportion of plagioclase, and their gradational contacts over several metres into tonalites and granodiorites. Modal analyses are presented in Table 4.1 and Appendix 1 Table 6.

Hornblende Granodiorite.

Subhedral to euhedral palgioclase grains (< 5 mm) are set in a matrix of finer aggregates of plagioclase, hornblende, biotite, microcline, quartz, apatite, primary sphene and zircon. Subhedral hornblende grains (< 3 mm) poikilitically enclose apatite, sphene and circular blebs of quartz (Fig. 4.7). Minor epidote, chlorite, magnetite and sphene replace hornblende and biotite.

Fig. 4.6 Photomicrograph of ragged pericline twins in a deformed plagioclase prophyroclast in centre of photograph. Biotite laths (grey) wrap around the plagioclase porphyroclast. Braunschweig Tonalite Gneiss, sample FGT 1, field of view 4.5mm, crossed polars.

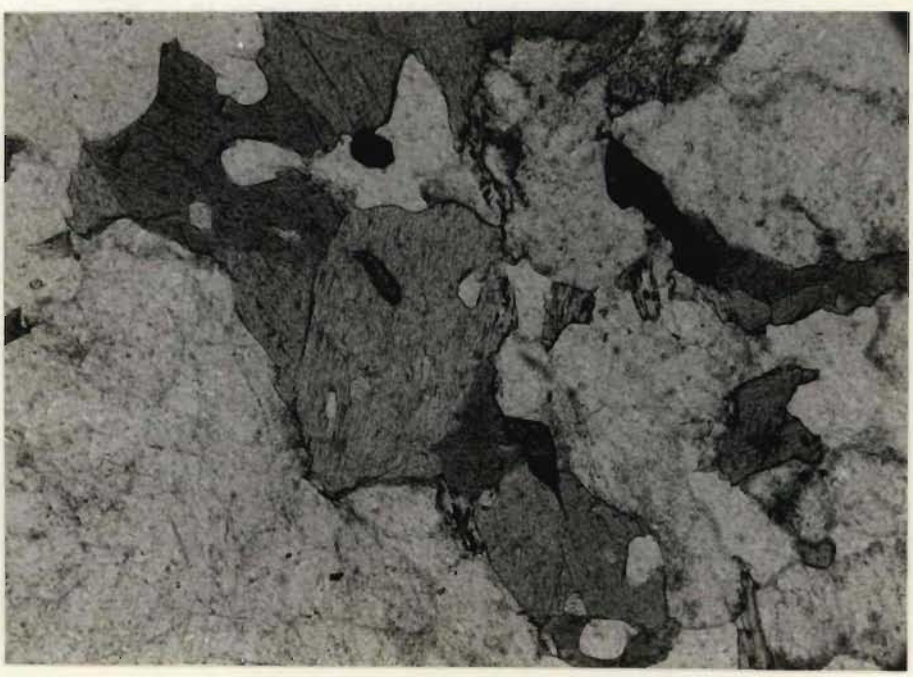

Fig. 4.7 Photomicrograph of subhedral hornblende grains (medium grey with high relief) poikilitically enclosing small grains of sphene (high relief, dark grey to black) and apatite (light grey). Grey background is plagioclase. Hornblende granodiorite, sample LF3, field of view 2mm, plane polarized light.

Plagioclase is twinned according to the albite and Carlsbad twin laws. Quartz with undulose extinction shows a weak preferred orientation that is parallel to laths of pleochroic green hornblende and biotite that defines the weak anastamosing foliation.

Tonalites.

Tonalites are distinguished from granodiorites by the absence of microcline, and their higher proportion of biotite and hornblende.

Subhedral and euhedral plagioclase grains (< 6 mm) and subhedral hornblende grains (< 3 mm) are set in a finer groundmass of biotite, quartz, plagioclase and sphene. Alteration is pervasive locally, with biotite being replaced by chlorite, magnetite and sphene (after ilmenite), and extensive saussuritization of plagioclase.

Euhedral plagioclase crystals (6 mm) are twinned according to the albite law and exhibit oscillatory zoning with an overall normal trend (Fig. 4.8). Many of their Ca-rich cores are saussuritized. Small (< 2 mm) interstitial plagioclase grains are twinned according to the albite-pericline and albite twin laws. Some of these grains are unzoned or only poorly zoned and show no oscillatory zoning. The coarse foliation is defined by the elongation of biotite and hornblende with subparallel alignment of quartz and plagioclase porphyroclasts.

Feldspathic Amphibolites.

Subhedral and euhedral plagioclase (5 mm) and hornblende (4 mm) crystals are present in a groundmass composed of finer aggregates of biotite, plagioclase, magnetite, quartz, zircon and sphene. Plagioclase is strongly altered to saussurite, whereas biotite alters to chlorite and magnetite. Subpoikilitic chlorite-magnetite symplectites are present in some hornblende grains. Plagioclase is twinned according to the albite and albite-pericline twin laws. Hornblende and biotite define a weak fabric wrapping around plagioclase grains.

Fig. 4.8 Photomicrograph of oscillatory zoning in an euhedral plagioclase crystal, bottom right. Note the foliation defined by biotite laths (grey), hornblende (black) and elongated quartz grains (white) wrapping around the plagioclase porphyroclast. Tonalite, sample MP9, field of view 10mm, crossed polars.

WEAKLY FOLIATED GRANITOIDS.

Medium-grained leucotonalite.

Subhedral plagioclase (4 mm) grains are set in a groundmass of plagioclase, quartz, microcline, biotite, apatite and zircon. Locally biotite is entirely replaced by chlorite, magnetite and sphene (after ilmenite), (Table 4.1; Appendix 1 Table 7).

Quartz with undulose extinction, plagioclase and interstitial microcline form polyhedral aggregates. An incipient foliation is defined by a weak parallelism of biotite laths. Plagioclase is twinned according to the albite twin law.

Biotite granite.

Anhedral plagioclase and microcline grains (3 mm) are surrounded by finer aggregates of plagioclase, microcline, quartz, biotite, zircon and apatite. Minor saussurite (epidote, zoizite) replaces plagioclase.

Perthitic microcline poikilitically encloses small euhedral grains of plagioclase, biotite, zircon and apatite, whereas plagioclase contains inclusions of only biotite and apatite. Abundant (5%) myrmekite is developed in microcline adjacent to plagioclase grains, and in plagioclase inclusions. Plagioclase is twinned according to the albite twin law and is commonly anti-perthitic with minor microcline exsolved parallel to the albite twin plane. Quartz with undulose extinction forms lenticular grains (2 mm) that parallel the fine biotite blades (0.5 mm). A weak mortar texture is developed in the zones of foliation (1 mm) immediately adjacent to the biotite.

Sodic granite.

Subhedral plagioclase grains (2 mm) are set in a matrix of finer aggregates of quartz, plagioclase, microcline, biotite and apatite. Minor saussurite replaces plagioclase, and chlorite and epidote replace biotite. Perthitic microcline encloses small euhedral plagioclase grains. Myrmekite heads are developed in microcline adjacent to plagioclase grains. An incipient foliation is defined by

biotite laths (1,5 mm) and polyhedral aggregates of quartz with undulose extinction. Plagioclase is twinned according to the albite, albite-Ala, albite-pericline and Carlsbad twin laws. The former three twin laws are all recognizable in a single crystal.

UNFOLIATED GRANITOIDS

Leucocratic granite.

Euhedral grains (< 2.5 mm) of plagioclase are set in a groundmass of finer aggregates of equigranular quartz, plagioclase, microcline, biotite and minor secondary calcite. Chlorite and magnetite replace biotite and plagioclase is altered to saussurite. Perthitic microcline contains inclusions of strongly altered euhedral plagioclase grains . Plagioclase is twinned according to the albite, albite-pericline, carlsbad-albite twin laws. Fine fractures in biotite laths are filled by epidote. Zircon and apatite are absent.

Equigranular quartz monzonite.

Euhedral plagioclase grains (< 4 mm) are set in a granophyric groundmass of microcline and quartz together with finer aggregates of biotite, hornblende, magnetite, zircon and sphene. Biotite alters partially to chlorite and magnetite. Plagioclase is partially altered to saussurite. The granophyric intergrowths comprise vermicular and cuneiform quartz in the interstitial microcline (Fig. 4.9). Plagioclase is twinned according to the albite and albite-Carlsbad twin laws.

Fig. 4. 9 Photomicrograph of granophyric intergrowths in equigranular quartz monzonite, sample SKL 2, field of view 10mm, crossed polars.

CHAPTER 5

GRANITOID GEOCHEMISTRY AND PETROGENESIS

PART 1 : GRANITOID GEOCHEMISTRY

Ninety samples were analysed for major and trace elements. The analytical methods are described in Appendix 2.

GNEISS COMPLEX

Layered Gneisses

The suite of rocks comprising the Layered Gneisses include tonalite-trondhjemite gneisses, dioritic and granodioritic gneisses, amphibolites and calc-silicate gneisses. The latter two lithologies are intimately associated spatially with, but subordinate to the granitoid gneisses. Their chemistry is therefore considered in this chapter although it is recognized that they may represent supracrustal rocks preserved in deformed keels within the granitoid gneisses.

The analyses of the samples of the Layered Gneisses are presented in Table 5.1 and sample localities are indicated on MAP 1. Detailed sections of sample localities along the Pongola River on the farm Tafelberg 186 HT, and along the White River on the farm Warmbad 18 HU are presented in figures 5.1 and 5.2 respectively. Four samples of quartzofeldspathic gneiss were also collected from outcrops in the Pongola River on the farm Bendor 211 HT. In addition to the suites of samples collected other samples of Layered Gneiss include TG1 (Tafelberg 186 HT), WBS7 (Wachteenbietjies Spuit 44), WTR4 (Wagendrift 12 HU), WB1, WB3 (Warmbad 18 HU).

Quartzofeldspathic Gneisses.

The majority of the quartzofeldspathic gneisses can be classified as tonalitic, based on their normative An-Ab-Or compositions (Fig. 5.3). Twelve of the twenty five samples (Fig. 5.3) plot in the trondhjemite field. However only seven : WR6a, WR6c, WBS7, TG5, TG6, TG10 and TG18 satisfy the major element criteria used to define trondhjemites

TABLE 5.1 MAJOR AND TRACE ELEMENT ANALYSES OF SILICEOUS LAYERED GNEISSES (GROUP A)

	Trondhjemite									Leucotonalite			Tonalite		
	WBS7	TG5	TG6	TG10	TG13	TG18	WR7	WR6a	WR6c	WR2	WR4	WR5	TG1	WR9	WR10
SiO_2	72.73	71.43	73.37	73.39	75.29	73.30	69.19	71.70	70.32	68.34	69.33	68.89	66.74	66.30	65.85
Al_2O_3	13.95	16.50	15.46	15.92	14.93	15.66	17.02	16.07	16.40	16.04	16.27	16.59	16.60	17.59	17.16
Fe_2O_3	0.14	0.24	0.16	0.18	0.13	0.14	0.33	0.24	0.29	0.38	0.33	0.34	0.42	0.41	0.45
FeO	1.14	1.98	1.33	1.47	1.07	1.11	2.65	1.97	2.34	3.06	2.64	2.72	3.38	3.33	3.61
MnO	0.02	0.01	0.01	0.01	0.01	0.01	0.04	0.02	0.03	0.04	0.03	0.03	0.06	0.05	0.04
MgO	0.64	0.63	0.49	0.73	0.51	0.50	1.05	0.67	0.83	1.79	1.14	1.13	1.27	1.40	1.48
CaO	2.53	2.61	2.64	2.62	2.03	2.63	3.04	2.61	2.49	3.85	3.18	3.33	5.16	3.88	3.87
Na_2O	5.40	5.02	5.19	5.13	4.81	5.06	4.92	5.21	5.30	4.44	4.28	4.64	4.84	4.85	4.76
K_2O	1.32	1.61	1.17	1.40	1.86	1.08	1.35	1.28	1.28	1.42	1.61	1.31	1.57	1.19	1.69
TiO_2	0.1759	0.5002	0.2557	0.2817	0.1874	0.2289	0.5488	0.4224	0.5413	0.5004	0.5405	0.5847	0.6474	0.7246	0.7372
P_2O_5	0.08	0.16	0.08	0.08	0.00	0.06	0.13	0.13	0.16	0.22	0.16	0.14	0.26	0.16	0.22
TOTAL	100.13	100.70	100.17	101.21	100.82	99.78	100.25	100.33	99.97	100.08	99.50	100.33	100.93	99.88	99.87
LOI	0.95	0.87	0.73	0.98	0.85	0.79	1.12	0.82	1.07	0.90	0.87	0.88	0.82	1.34	0.92
Nb	1.9	0.3	3.1	3.6	4.0	2.9	9.8	6.8	11.5	10.7	8.0	8.4	2.7	13.2	6.1
Zr	138.6	213.6	160.7	132.4	197.0	149.1	204.4	189.8	200.4	215.7	218.1	166.5	198.2	244.4	189.1
Y	4.9	5.0	5.0	3.4	1.5	1.8	14.1	6.3	16.4	16.6	14.6	14.4	10.3	31.6	14.0
Sr	670.8	942.5	672.8	879.0	529.8	670.1	680.4	598.9	521.1	636.5	762.5	634.1	1046.7	727.0	570.0
Rb	45.9	48.3	47.7	63.6	57.7	38.1	49.7	39.4	46.3	52.6	60.3	39.6	67.0	51.3	56.9
V	6.4	n.d.	n.d.	n.d.	n.d.	n.d.	n.d.	n.d.	n.d.	n.d.	n.d.	n.d.	n.d.	n.d.	n.d.
La	17.6	32.0	44.1	44.0	33.1	19.5	14.8	15.6	14.5	19.8	15.8	14.8	65.1	28.4	26.5
Sc	1.3	2.9	1.4	3.6	1.8	2.2	5.4	3.4	4.5	8.2	4.0	5.5	3.7	5.9	8.1
Ba	413.8	861.4	263.4	390.7	579.1	306.2	283.9	307.3	303.3	382.7	322.8	335.5	560.4	269.9	272.4
Sr/Ba	1.62	1.09	2.55	2.25	0.92	2.19	2.40	1.95	1.72	1.66	2.36	1.89	1.87	2.69	2.09
Rb/Sr	0.07	0.05	0.07	0.07	0.11	0.06	0.07	0.07	0.09	0.08	0.08	0.06	0.06	0.07	0.10
K/Rb	235	277	204	183	268	235	226	270	230	224	222	275	195	193	247
FeO*/MgO	2.00	0.87	0.73	2.26	2.35	2.50	2.84	3.30	3.17	1.92	1.66	2.71	2.99	2.67	2.74

n.d. Not determined; - below detection limit

TABLE 5.1 continued MAJOR AND TRACE ELEMENT ANALYSES OF SILICEOUS LAYERED GNEISSES (GROUP B)

	Leucotonalite			Tonalite				Granodiorite
	WB3	B4	TG14	WB1	B1	B3	TG12	B2
SiO_2	69.47	72.30	68.14	67.78	67.81	66.02	69.94	74.57
Al_2O_3	15.53	15.47	16.00	16.11	16.20	15.55	15.99	14.53
Fe_2O_3	0.42	0.27	0.47	0.45	0.47	0.71	0.37	0.19
FeO	3.42	2.16	3.82	3.61	3.79	5.73	3.00	1.50
MnO	0.05	0.03	0.08	0.06	0.07	0.10	0.04	0.02
MgO	1.67	0.67	1.88	1.72	1.59	1.41	1.36	0.46
CaO	2.48	2.71	4.82	4.24	4.09	4.38	3.31	2.18
Na_2O	4.18	4.43	2.82	4.01	4.32	4.27	4.69	3.77
K_2O	1.87	2.21	1.44	1.57	1.30	1.38	1.51	2.89
TiO_2	0.4857	0.3704	0.5985	0.5326	0.6115	0.8814	0.5341	0.2216
P_2O_5	0.18	0.11	0.17	0.19	0.25	0.31	0.17	0.06
TOTAL	99.77	100.72	100.24	100.27	100.51	100.74	100.92	100.39
LOI	1.34	0.56	1.63	0.79	0.77	0.57	0.66	0.50
Nb	4.2	10.9	14.7	3.9	17.4	8.4	10.5	9.9
Zr	180.8	209.2	185.8	199.9	206.3	160.1	227.1	165.1
Y	7.5	13.8	20.2	10.6	31.8	7.0	19.6	8.8
Sr	261.3	467.9	312.4	404.0	434.2	280.9	548.3	289.2
Rb	60.5	71.2	64.8	69.4	51.8	56.3	79.8	62.9
V	15.4	n.d.	n.d.	14.6	n.d.	n.d.	n.d.	n.d.
La	10.0	46.4	25.5	57.0	45.3	49.5	33.0	49.6
Sc	6.9	5.4	7.1	7.2	9.6	3.5	4.9	4.0
Ba	404.6	638.8	288.6	252.1	147.3	642.0	321.6	669.2
Sr/Ba	0.65	0.73	1.08	1.60	2.95	0.44	1.70	0.43
Rb/Sr	0.23	0.15	0.21	0.17	0.12	0.20	0.15	0.21
K/Rb	257	258	184	188	208	203	157	381
FeO*/MgO	2.30	3.63	2.28	2.36	2.68	4.57	2.48	3.67

n.d. - not determined

TABLE 5.1 continued MAJOR AND TRACE ELEMENT ANALYSES FOR AMPHIBOLITES, CALC-SILICATE GNEISSES AND QUARTZITE

	Amphibolites				Miscellaneous rock-types				
	WTR4	WR1	WR6D	TG8	TG9	TG7	TG11	TG17	TG16
SiO_2	52.70	50.42	51.64	53.31	50.84	62.72	64.40	67.23	89.41
Al_2O_3	15.25	9.50	13.93	7.73	13.82	16.06	15.04	15.26	0.09
Fe_2O_3	1.06	0.94	1.68	1.34	1.53	0.62	0.14	0.35	0.73
FeO	8.56	7.62	13.57	10.87	12.40	5.05	1.13	2.87	5.89
MnO	0.12	0.15	0.20	0.21	0.19	0.09	0.14	0.11	0.32
MgO	8.08	12.80	4.94	13.48	6.57	3.98	3.07	2.29	1.46
CaO	8.80	14.09	7.82	10.71	9.41	5.53	5.28	5.10	1.65
Na_2O	3.14	0.85	2.98	0.91	2.59	4.02	1.90	2.54	-
K_2O	1.44	1.77	1.17	1.11	1.11	0.72	8.61	3.66	-
TiO_2	0.8255	0.9409	1.8673	0.6865	1.2829	0.8476	0.5985	0.6065	0.0089
P_2O_5	0.08	0.94	0.14	0.07	0.14	0.29	0.26	0.27	0.06
TOTAL	100.07	100.03	99.83	100.43	99.82	99.92	100.57	100.30	99.21
LOI	1.52	1.27	0.90	0.88	0.84	1.25	0.47	1.38	0.17
Nb	1.9	15.7	7.1	2.8	5.5	14.9	12.0	18.8	1.0
Zr	45.8	206.1	102.9	54.1	99.2	202.6	228.3	235.7	6.3
Y	11.2	47.9	27.5	17.5	32.8	26.8	23.7	35.0	6.2
Sr	227.7	753.8	265.7	94.7	255.1	520.7	192.6	363.5	7.1
Rb	40.9	79.4	30.1	19.3	41.8	48.8	183.9	133.8	4.4
V	734.0	175.9	337.3	238.8	390.7	91.9	n.d.	n.d.	n.d.
La	8.1	72.6	-	-	-	25.9	33.8	35.7	-
Sc	56.9	42.4	29.0	36.5	43.4	15.1	8.8	10.3	0.9
Ba	90.8	564.2	297.1	123.7	122.7	410.2	2098.4	486.3	20.3
Zn	n.d.	99.0	157.8	108.2	135.9	95.2	55.3	n.d.	n.d.
Cu	n.d.	44.3	230.8	114.4	67.8	3.6	2.2	n.d.	n.d.
Ni	n.d.	211.9	37.5	300.7	125.6	94.7	46.7	n.d.	n.d.
Cr	n.d.	864.9	-	1540.7	165.7	127.1	n.d.	n.d.	n.d.
Sr/Ba	2.51	1.34	0.89	0.37	2.08	1.27	0.09	0.75	-
Rb/Sr	0.18	0.11	0.11	0.20	0.16	0.09	0.96	0.37	

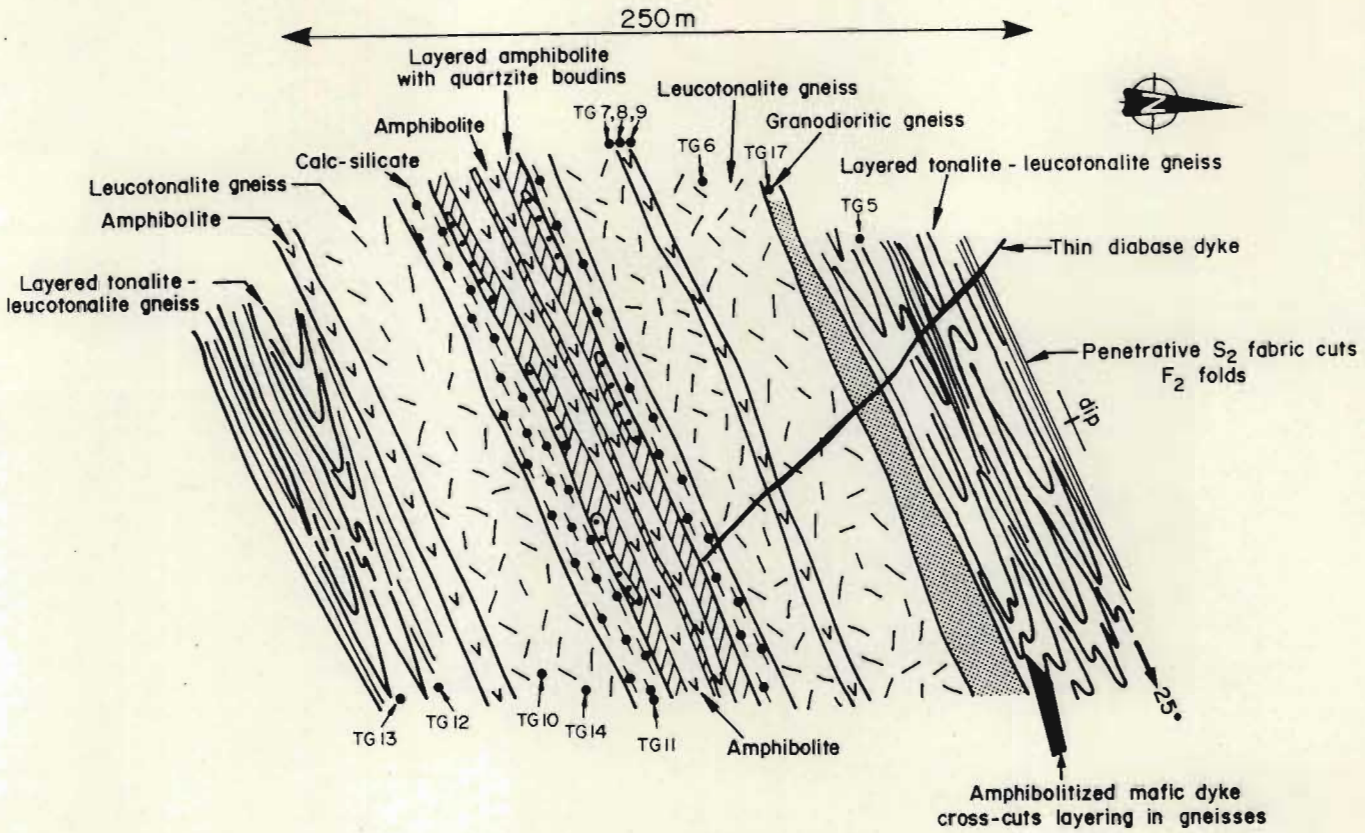

Fig. 5.1 Sample localities of Layered Gneisses cropping out in the Pongola River on the farm Tafelberg 186 HT.

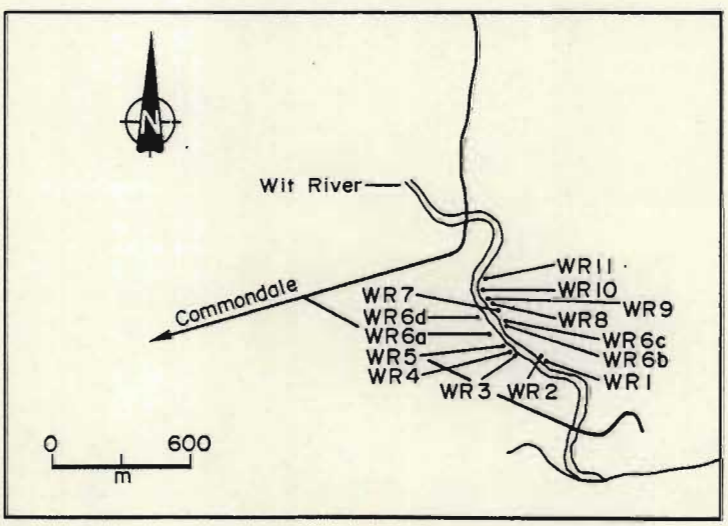

Fig. 5.2 Sample localities of Layered Gneisses cropping out in the White River on the farm Warmbad 18 HU.

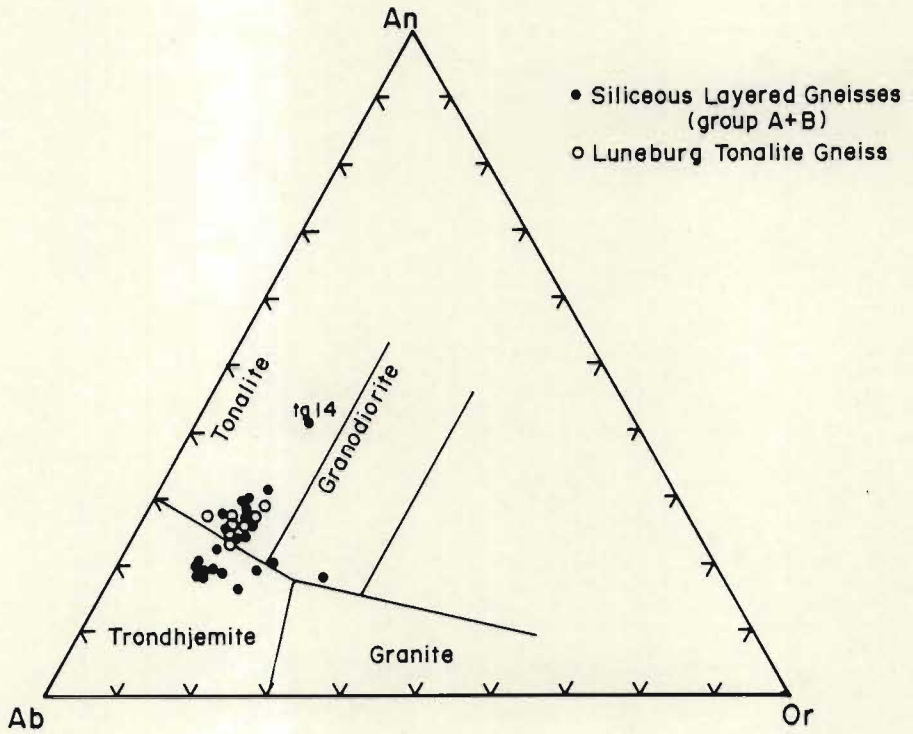

Fig. 5.3 CIPW normative proportions of An-Ab-Or (wt %) in siliceous Layered Gneisses and the Luneburg Tonalite Gneiss. The classification boundaries are after Barker (1979). The calc-silicate gneisses and amphibolites are not included.

(Barker, 1979; Chapter 3, Fig. 3.1).

The granitoid gneisses are characterized by SiO_2 contents between 66 and 75 wt. % with Al_2O_3 varying between 14 and 17 wt. %.
The FeO* / MgO ratio is < 4.6 with 84% of the analyses having FeO* / MgO ratios < 3.0. The content of K_2O is < 2.0 wt. % in all the felsic gneisses. The gneisses are similar to the Type A siliceous gneisses from the Bimodal Gneiss Suite, Swaziland (Hunter et al., 1984). Siliceous gneisses characterized by high SiO_2 (> 75 wt. %) and low (< 12.5 wt. %) Al_2O_3 contents reported from Swaziland have not been identified in the study area. However this does not preclude their existence.

The siliceous Layered Gneisses may be tentatively divided into two groups on the basis of trace element contents. Samples that fall into Group A show the following features:

i) Sr and Zr contents are > 520 ppm and < 244 ppm respectively.

ii) Rb concentrations are > 40 ppm.

iii) The Rb/Sr ratios are < 0.11 with the majority < 0.08.

iv) K/Rb ratios are < 280.

v) Rock/primordial mantle large ion lithophile (LILE) and high field strength (HFSE) element patterns show a greater relative depletion in Nb and Y than in the Group B siliceous gneisses (Fig. 5.32a).

$FeO^* = FeO + 0.8998Fe_2O_3$.

Group B is represented by samples B1, B2, B3, B4, WB1, WB3, TG12 and TG14 (Table 5.1). This group is characterized by :

i) Sr < 470 ppm except sample TG12 (Sr = 548) and Zr within the range of Group A. The depletion in Sr is over the same range of Ca contents as for the Group A gneisses.

ii) Rb concentrations and K/Rb ratios are within the range of Group A siliceous gneisses.

iii) Rb/Sr ratios are > O.12 with 88% greater than 0.15. TG12 has an Rb/Sr ratio of 0.15 and a higher Rb content than the other Group B siliceous gneisses.

The means and standard deviations of Sr contents and Rb/Sr ratios suggest that the separation of the siliceous gneisses into Group A and B is valid:

	Rb/Sr		Sr	
	$\bar{X}$	s.d.	$\bar{X}$	s.d.
Group A	0.074	0.0159	703	150
Group B	0.180	0.0382	375	104

$\bar{X}$ = mean, s.d. = standard deviation

Using the t distribution, confidence levels on the means of the two groups may be tested to establish whether the two groups differ significantly. This is achieved by coding the data for each group, and calculating the standard deviation for both groups collectively. The t value is calculated from this standard deviation and compared to

t table values. The calculated t values for Rb/Sr and Sr are 9.4578 and 5.7940 respectively. The values are higher than the t table values for 20 degrees of freedom at the 95% (t = 2.086), 99% (t = 2.845) and 99.9% (t = 3.850) confidence levels. This indicates that the means are significant and the samples belong to two populations namely Group A and Group B. The method to this approach is from Peters et al. (1974).

The Group A and B siliceous gneisses are in terms of trace element proportions similar to Subgroup A2 and A1 of the Type A siliceous gneisses of the Bimodal Gneiss Suite, Swaziland (Hunter et al., 1984). Subgroup A1 gneisses have steep light REE and flat to gently sloping heavy REE patterns with no major Eu anomaly. Subgroup A2 is characterized by very steep REE patterns with large to small positive Eu anomalies (Hunter et al., 1984). These two groups are clearly distinguished by La/Yb ratios which for Subgroup A1 < 24 and for Subgroup A2 > 100 (Hunter et al., 1984).

Lack of REE data for samples from Groups A and B in this study precludes confirmation that these groups display similar patterns. Whether the classification of the siliceous gneisses into two groups is justified on the basis of subtle differences in trace element chemistry remains equivocal. Additional REE data are required before a firm conclusion can be reached but, nevertheless, differences in Rb/Sr ratios in particular appear to be significant.

The subdivision of the siliceous gneisses into Group A and B gneisses is not reflected on a spatial basis as both types are intimately interlayered in outcrops along the Pongola River on the farm Tafelberg 186 HT, eg. TG10 and TG12 are Group A trondhjemites and TG14 and TG13 are Group B leucotonalite and tonalite respectively. Group B siliceous gneisses from the farm Bendor 211 HT (samples B1 - B4) are apparently not interlayered with Group A gneisses. The sample suite WR1 - WR10 comprise only Group A siliceous gneisses whereas samples WB1 and WB3 to the southeast of this suite have Group B affinities (MAP 1).

The layered siliceous gneisses define a linear trend on the normative Qz-Ab-Or diagram approximately parallel to the QZ-Ab tie line (Fig. 5.4). On the ternary MgO-total Fe-alkalis projection (Fig. 5.5) the

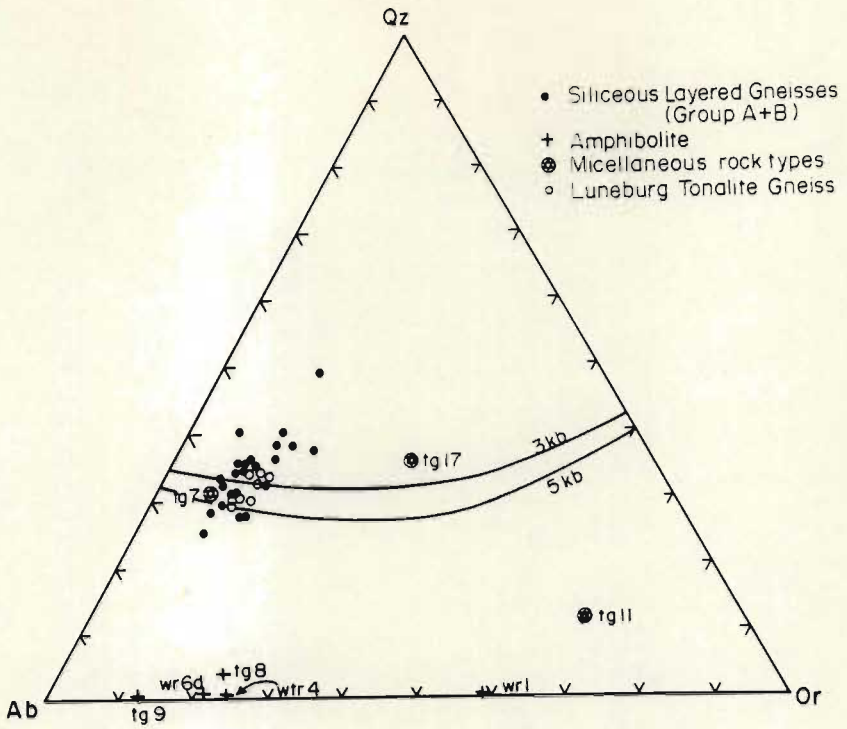

Fig. 5.4 CIPW normative proportions in the siliceous Layered Gneisses, interlayered amphibolites, calc-silicate gneisses and the Luneburg Tonalite Gneiss. Cotectic line for PTOTAL = PH_2O = 3kb from Tuttle and Bowen (1958) and PH_2O = 5kb calculated from Winkler (1979).

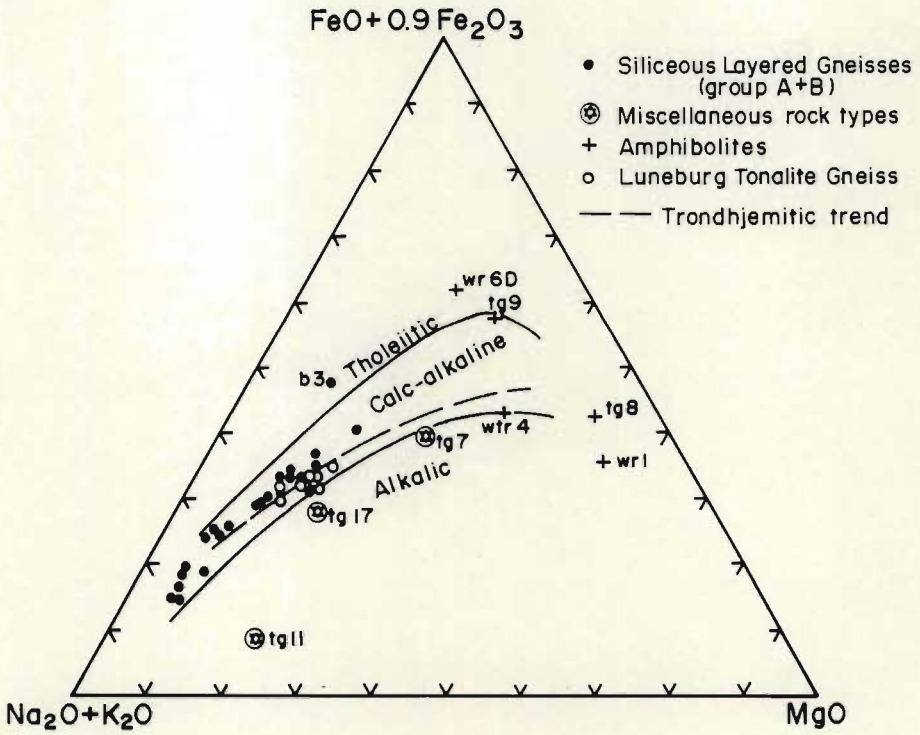

Fig.5.5 Ternary AFM projection showing the siliceous Layered Gneisses, calc-silicate gneisses, amphibolites and the Luneburg Tonalite Gneiss. The tholeiitic and calc-alkaline fields and trondhjemitic trend are from Barker and Arth (1976).

bulk of the siliceous gneisses with the exception of B3 lie within the calc-alkaline field along the trondhjemitic trend of Barker and Arth (1976). On the K-Na-Ca projection (Fig. 5.6) the data points of the layered siliceous gneisses lie towards the Na apex, thus confirming their trondhjemitic affinity.

The mean K/Rb ratio is 230 with a range from 157 to 381. Rubidium contents vary from 38 to 80 ppm (Fig. 5.7). A weak positive correlation between K/Rb and K (plot not shown) in the siliceous gneisses does not suggest extensive redistribution of these elements during deformation and metamorphism. Rather the range in K/Rb ratios appears to reflect varying proportions of biotite, hornblende and microcline and the retrograde reaction of minor hornblende to biotite and of biotite to chlorite. The mean K/Rb ratio of 230 and range of this ratio are similar to those reported from the gneisses in Swaziland (Hunter et al., 1984).

The siliceous Layered Gneisses have Sr/Ba ratios > 0.5 with most > 1.0, but two Group B samples (B2 and B3) have Sr/Ba ratios < 0.5 (Fig. 5.8). The Group A and B siliceous gneisses define two discrete fields on the Rb/Sr plot (Fig. 5.9). Group B gneisses together with the Luneburg Tonalite Gneiss have Rb/Sr ratios > 0.1 whereas the majority of the Group A gneisses have Rb/Sr ratios < 0.1.

Amphibolites.

Amphibolites occupy three discrete fields on the ternary Jensen (1976) diagram (Fig. 5.10). Two samples have compositions appropriate to basaltic komatiites and consequently have low Al_2O_3 (< 9.5 wt. %) and high MgO contents (> 12.5%). Their CaO contents exceed 10.5 wt. % and the Al_2O_3/CaO ratios are about 0.70.

The remaining amphibolites are either Fe or Mg-tholeiites. The former are characterized, in addition to their total Fe (as FeO) contents > 13.5 wt. %, by Al_2O_3 and MgO abundances of 14wt.% and 5 to 6.5 wt.% respectively. The Mg tholeiite has oxide abundances intermediate between the komatiitic basalts and the Fe-rich tholeiites (Table 5.1). All amphibolites have K_2O contents of between 1.1 and 1.8 wt. %. The concentration of Na_2O ranges from 0.85 wt. % in the basaltic komaliites to 3.14 wt. % in the Mg tholeiites.

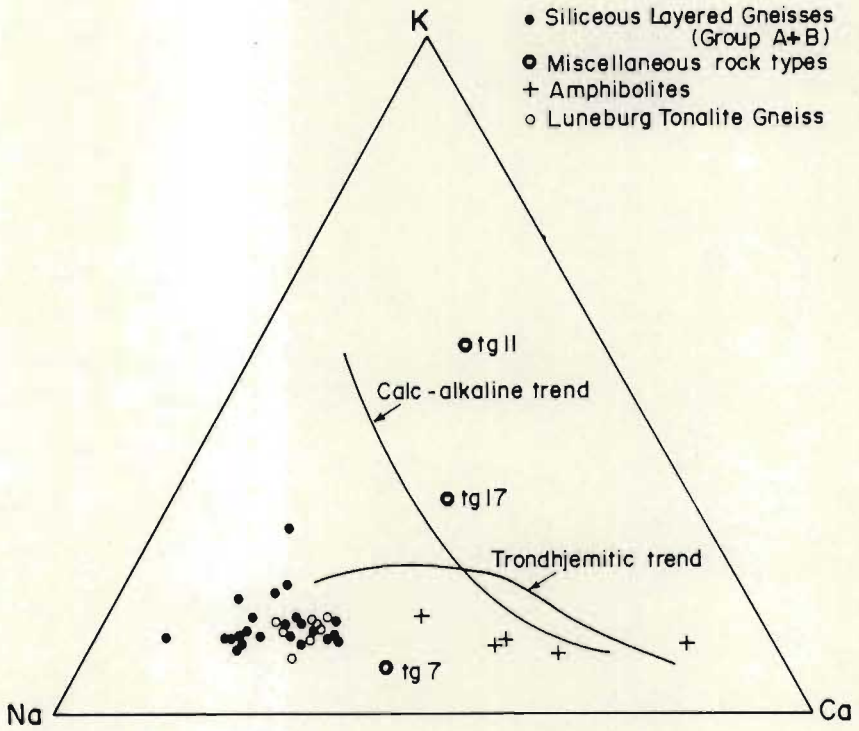

Fig. 5.6 Ternary K-Na-Ca projection showing the trondhjemitic affinity of the siliceous Layered Gneisses, amphibolites and the Luneburg Tonalite Gneiss. The calc-alkaline trend is from Nockolds and Allen (1953) and the trondhjemitic trend from Barker and Arth (1976).

Layered Gneisses
● Group A
✡ Group B
o Luneburg Tonalite Gneiss

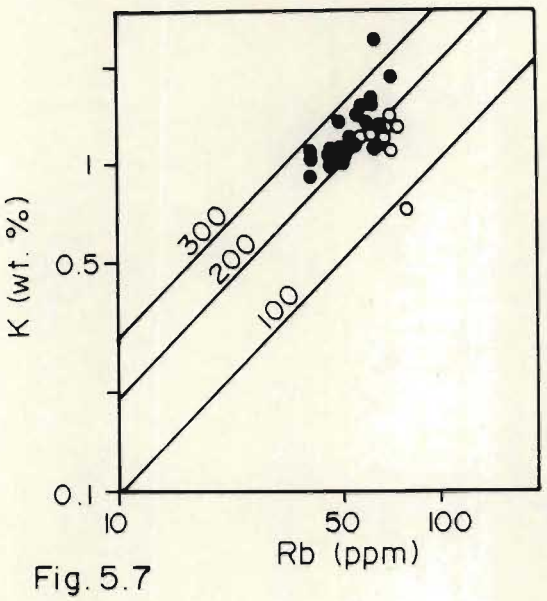

Fig. 5.7

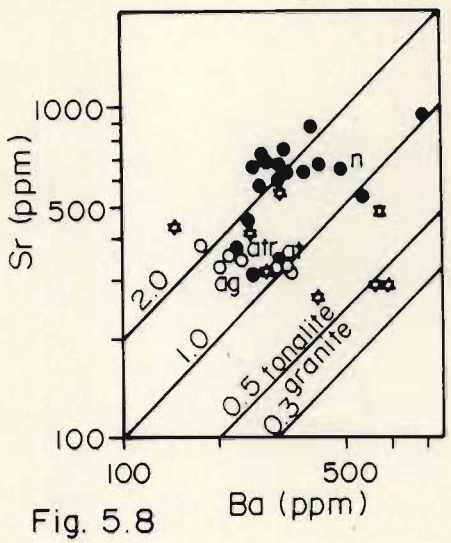

Fig. 5.8

Fig. 5.7 K/Rb plot for Group A and B siliceous Layered Gneisses and the Luneburg Tonalite Gneiss. Symbols as in Fig. 5.6

Fig. 5.8 Sr-Ba plot of Group A and B siliceous Layered Gneisses and the Luneburg Tonalite Gneiss. (AG) average of 3 Type A siliceous gneisses, Bimodal Gneiss Suite, Swaziland (Hunter et al., 1984). (AT) average analysis of Amitsoq Tonalite gneiss (n=25) (McGregor, 1979). (ATR) average analysis of Amitsoq trondhjemite gneiss (n=16) (McGregor, 1979). (N) analysis of trondhemitic Northern Light Gneiss, Thunder Bay Ontario. (Arth and Hanson, 1975 quoted in Collinson and Bridgewater 1979).

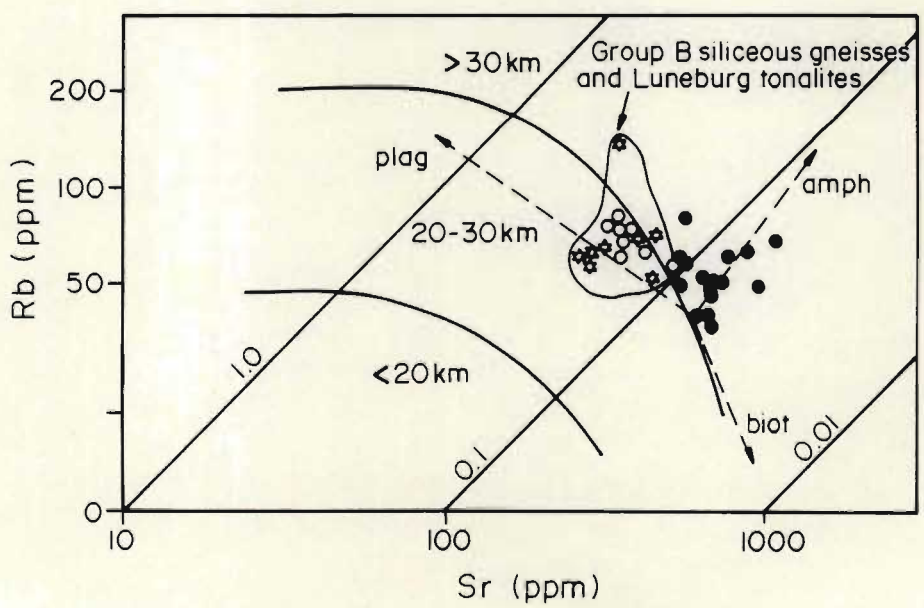

Fig. 5.9 Rb-Sr plot for Group A and B siliceous Layered Gneisses and Luneburg Tonalite Gneiss. Crustal thickness index curves are from Condie (1973). Mineral fractiontion vectors are from Beckinsale (1979). Symbols as in Fig. 5.8.

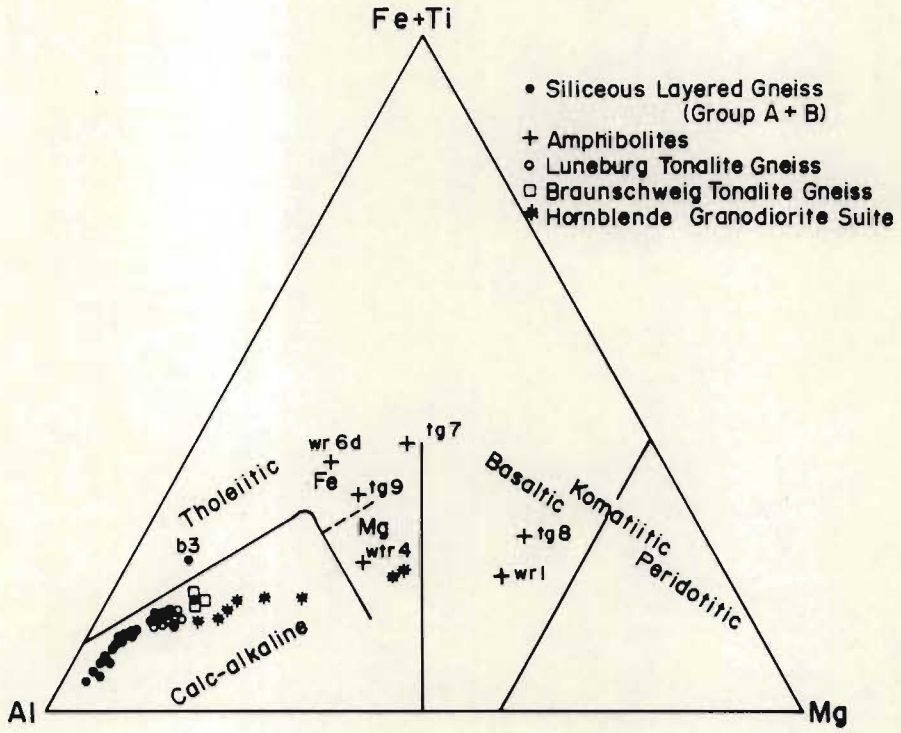

Fig. 5.10 Jensen cation plot of siliceous Layered Gneisses, interlayered amphibolites, Luneburg Tonalite Gneiss, Braunschweig Tonalite Gneiss and Hornblende Granodiorites (after Jensen, 1976). Labelled samples are referred to in the text. The Braunschweig Tonalite Gneiss and Hornblende Granodiorite are discussed under the heading Trondhjemite-Tonalite-Granodiorite Suite.

Samples TG7, 8 and 9 are closely related spatially in outcrops along the Pongola River (Fig. 5.1). TG8 is a coarse grained rock that identified as a basaltic komatiite in Fig. 5.10. This rock type is flanked by a fine-to medium-grained amphibolite (TG9) that lies in the Fe- rich tholeiite field in Fig. 5.10. Sample TG7 is composed of hornblende, plagioclase, quartz and microcline and appears to be interlayered with the amphibolitic rock-types (TG8 and TG9). Table 5.1 list the chemistries of these rock types wherein it can be seen that there is sympathetic decrease in Cr, Ni and MgO contents. Sample TG7 has major element chemistry not dissimilar to that of a quartz diorite but the significant content of microcline negates this classification.

The possibility cannot be excluded that the amphibolite represents either a differentiated intrusion or a sequence of flows of discrete compositions. Sample TG7 may represent a hybrid rock-type resulting from assimilation of siliceous rock types by the intrusion. More detailed sampling is required to resolve this problem.

The amphibolites with the exception of WR1 form a cluster of points on the Qz-Ab-Or diagram along the Ab-Or tie line. There is a marked compositional gap between the fields of the amphibolites and siliceous gneisses (Fig. 5.4). Sample WR1 has a Na content typical of a basaltic komatiite but has a high K_2O content which presumably accounts for its displacement towards the Or apex in Fig. 5.4.

Amphibolite samples TG8 and WR6d suggest that they may define a tholeiitic trend (Fig. 5.5). A tonalite gneiss (B3) also lies in the tholeiitic field in Fig. 5.5 and may constitute a more felsic continuation of the tholeiitic trend. The possibility of rocks of both calc-alkaline and tholeiitic affinities in the layered gneiss sequence in Swaziland has been proposed provisionally by Hunter et al. (1984).

One sample of amphibolite (WTR4) lies close to the boundary of the calc-alkaline and alkaline fields on the MgO-total Fe-alkalis diagram (Fig. 5.5) presumably as a consequence of a sodium content of over 3 wt. % (Table 5.1). On the K-Na-Ca projection the amphibolites parallel the Na-Ca-tie line exhibiting a wide range in Na and Ca contents (Fig. 5.6).

There is no systematic relationship between the spidergram patterns (Fig. 5.11) of the amphibolites and their classification as Mg-tholeiite, Fe-tholeiite or basaltic komatiite. Samples WR1 and WTR4 are enriched in La relative to P, Zr and Ti. In contrast amphibolite samples TG8, TG9 and WR6d are strongly depleted in La relative to Nb and Sr. Lanthanum is present in these amphibolites in abundances that are below detection limit. The very low rock/primordial mantle ratios for La in these samples is indicated schematically in Fig. 5.11.

Examination of the variation diagrams in Fig. 5.12 shows that the elemental ratios of the amphibolites are variable. Samples WTR4, TG8 and TG9 have Nb/Zr and Nb/Y ratios that approach those of primordial mantle, but have Zr/Y ratios greater than primordial mantle (Fig. 5.12). Sample WR6d has Zr/Nb, Zr/Y and Ti/Y ratios that are greater than chondritic but its Ti/Zr ratio is close to chondritic. Plots of elemental ratios for sample WR1 typically show a wide scatter with only the Zr/Nb ratio being close to chondritic.

The wide range in major and trace element chemistry of the interlayered amphibolites suggests different sources and that some of the magmas were possibly contaminated by crustal rocks during emplacement. A more detailed geochemical investigation is required before any significant petrogenetic implications between the geochemically distinct varieties can be made.

Miscellaneous Rock Types.

The rock-types include calc-silicate gneiss (TG11), microcline-rich quartz dioritic gneiss (TG7), granodioritic gneiss (TG17) and pyritic metaquartzite (TG16), (Figs. 5.1). The calc-silicate gneiss and metaquartzite may represent supracrustal rocks preserved in deformed keels in the granitoid gneisses.

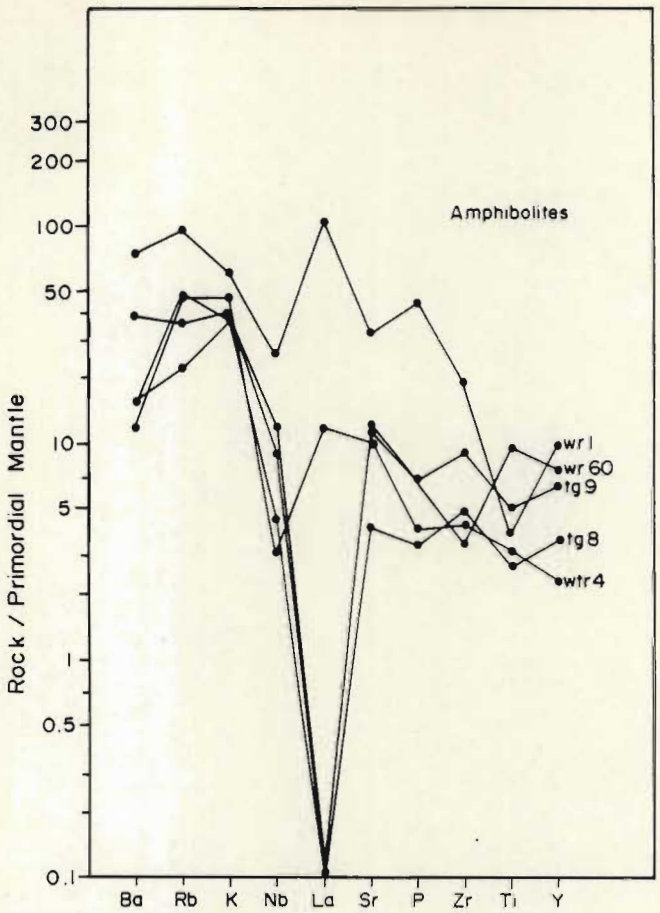

Fig. 5.11 Normalized rock/primordial mantle LILE and HFSE patterns for amphibolites interlayered with siliceous gneisses. Primordial mantle values are from Wood et al. (1979a).

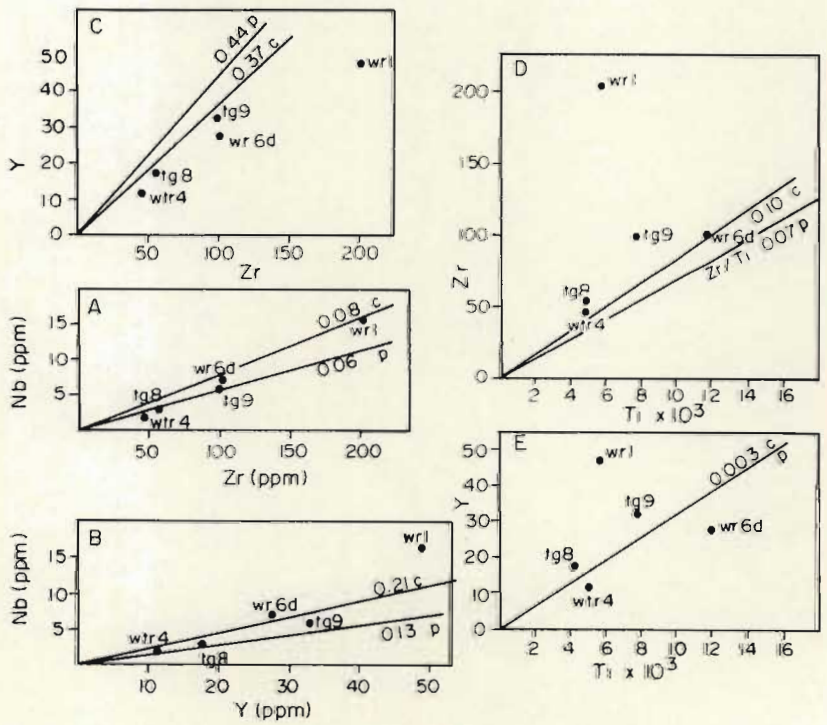

Fig. 5.12 Incompatible element plots for amphibolites interlayered with siliceous Layered Gneisses. Chondritic ratios (c) are from Taylor and McLennan (1981) and primordial mantle ratios (p) from Wood et al., (1979a).

The major and trace element compositions of these gneisses are given in Table 5.1. The three samples TG7, TG11 and TG17 all have similar abundances of Al_2O_3 (15 to 16 %) and CaO (~ 5%) but the contents of the oxides particularly K_2O are very variable. Ba is enriched in TG11 relative to the other samples but Rb is not significantly enriched in the sample (TG 11) that contains over 8% K_2O.

All three samples lie in the alkalic field on the MgO-FeO*-alkalis diagram (Fig. 5.5). TG7 lies in the field of the granitoid gneisses in the Qz-Ab-Or diagram (Fig. 5.6). The remaining samples are widely scattered with TG17 lying close to the cotectic at 3 kb (Tuttle and Bowen, 1958) and TG11 lying towards the Or apex as would be expected from its major element chemistry.

One sample of pyritic metaquartzite was analysed (TG16, Table 5.1). The presence of these quartzite boudins in association with calc-silicate gneiss and amphibolite provides the strongest evidence that these rock types represent a supracrustal sequence.

Luneburg Tonalite Gneiss.

The Luneburg Tonalite Gneisses are interpreted on structural grounds to be part of the Gneiss Complex. The gneisses underlie the western part of the study area. Analyses of the eight Luneburg tonalite samples are presented in Table 5.2 and sample localities are indicated on MAP 1.

All but one of the samples lie in the tonalite field in Fig. 5.3. The sample (ZD1) that lies in the trondhjemite field does satisfy the criteria given by Barker (1979) for inclusion in this rock type. Consequently the Luneburg gneiss is regarded as being tonalitic to leucotonalitic in composition. The Luneburg tonalite has an apparently restricted range in composition with SiO_2 contents between 67 and 70 wt. % and Al_2O_3 from 15 - 16 wt. %. MgO and CaO contents reflect the presence of both hornblende and biotite. Rb, Ba, Nb, Y, Zr and La concentrations are similar to those in the siliceous Layered Gneisses. Sr contents and Rb/Sr ratios are similar to those for Group B siliceous gneisses being < 500 and > 0.11 respectively.

TABLE 5.2 MAJOR AND TRACE ELEMENT ANALYSES FOR LUNEBURG TONALITE GNEISS

	ZD1	KA1	KA2	KA4	LBE1	LBE2	KA6	JT1
SiO_2	70.56	68.13	68.04	66.76	68.72	69.31	66.99	69.18
Al_2O_3	14.95	15.70	15.42	15.81	15.45	15.48	15.92	16.17
Fe_2O_3	0.35	0.42	0.41	0.49	0.40	0.37	0.44	0.37
FeO	2.82	3.36	3.31	4.01	3.23	2.96	3.53	2.97
MnO	0.04	0.06	0.07	0.08	0.07	0.06	0.07	0.05
MgO	1.33	1.88	2.08	2.16	1.66	1.59	1.82	1.31
CaO	3.07	4.00	3.88	3.97	3.78	3.36	4.08	3.38
Na_2O	4.64	4.30	4.48	4.60	4.53	4.30	4.79	4.71
K_2O	1.46	1.69	1.57	1.51	1.54	0.84	1.35	1.44
TiO_2	0.4059	0.4960	0.4661	0.5809	0.4769	0.5977	0.5172	0.5526
P_2O_5	0.14	0.19	0.18	0.22	0.18	0.16	0.20	0.16
TOTAL	99.78	100.23	99.92	100.20	100.03	99.03	99.69	100.28
LOI	0.57	0.69	0.51	1.67	0.56	0.64	0.75	0.56
Nb	3.1	4.6	4.2	4.6	5.0	4.6	4.9	3.7
Zr	143.2	156.6	163.4	200.4	183.6	148.4	183.2	223.9
Y	8.8	11.0	11.1	11.3	11.3	13.5	14.9	11.0
Sr	350.9	346.3	339.3	414.5	324.5	355.7	380.1	507.2
Rb	65.5	70.8	75.8	64.4	60.1	80.2	70.1	56.0
V	2.6	17.0	17.5	12.7	13.1	7.6	8.8	-
La	37.1	33.9	28.3	31.8	27.0	43.5	29.8	42.7
Sc	5.4	7.9	8.2	8.5	7.1	5.8	7.0	5.0
Ba	335.2	308.8	204.4	260.7	346.1	217.2	175.6	324.9
Sr/Ba	1.05	1.12	1.66	1.59	0.94	1.64	2.16	1.56
Rb/Sr	0.19	0.20	0.22	0.16	0.19	0.23	0.18	0.11
K/Rb	185	198	172	195	213	87	160	213

The Luneburg tonalitic gneiss has a mean K/Rb ratio (190) that is slightly lower than that of the layered granitoid gneisses. The mean Rb/Sr (0.19) ratio is close to that of the Group B Layered Gneisses, a feature that is also reflected in the Rb/Sr diagram (Fig. 5.9). Strontium contents in the Luneburg tonalite are typically lower than in the Group A Layered Gneisses which largely accounts for the higher Rb/Sr ratio in the former. As would be expected from their similar chemistry samples of the Luneburg Tonalite Gneiss overlap the field of the layered granitoid gneisses in the Qz-Ab-Or, MgO-FeO*-alkalis and K-Na-Ca diagrams (Figs. 5.4, 5.5, 5.7).

TRONDHJEMITE-TONALITE-GRANODIORITE SUITE.

Leucotonalite Gneiss.

Major and trace element analyses of the six leucotonalitic gneiss samples are presented in Table 5.3 and sample localities are indicated on MAP 1. The analyses lie in the trondhjemite field on the normative An-Ab-Or projection (Fig. 5.13) but are classfied as leucotonalites in terms of their (Feo* + MgO) contents and FeO*/MgO ratios which do not satisfy the criteria for trondhjemite (Chapter 3, Fig. 3.1).

The leucotonalite samples have SiO_2 contents between 70 and 73 wt. % and Al_2O_3 contents between 14.5 and 16 wt. %. The concentration of Na_2O is nearly constant at 5 wt. % and FeO*/MgO ratios are typically close to 3. On the Qz-Ab-Or projection the data points of leucotonalite lie in a compact slightly elongated field parallel to the Qz-Ab tie line (Fig. 5.14). On the MgO-FeO*-alkalis projection the leucotonalites plot towards the alkali enriched apex in the calc-alkaline field along the trondhjemitic trend (Fig. 5.15). Their enrichment in Na and trondhjemitic affinty are further emphasized in the ternary K-Na-Ca plot (Fig. 5.16). Trace elements (with the exception of La) typically show limited variations in abundances (Table 5.3).

Rb/Sr and K/Rb ratios range from 0.10 to 0.16 and 193 to 271 respectively (Figs. 5.17 and 5.18). Sr/Ba ratios are between 1.5 and 2.5 (Fig. 5.19). Abundances of Rb and Sr in the Leucotonalite Gneiss are similar to those in the siliceous Layered Gneisses and Luneburg

TABLE 5.3 MAJOR AND TRACE ELEMENT ANALYSES OF THE LEUCOTONALITE GNEISS

	WG2	LLT1	LLT2	LLT3	WTR1	WTR5
SiO_2	71.30	70.73	72.08	70.38	71.42	70.43
Al_2O_3	15.69	15.84	15.54	15.85	15.71	15.98
Fe_2O_3	0.23	0.28	0.22	0.28	0.25	0.27
FeO	1.90	2.26	1.77	2.31	2.02	2.17
MnO	0.03	0.04	0.03	0.04	0.03	0.04
MgO	0.74	0.93	0.64	0.80	0.85	0.89
CaO	2.99	2.89	2.49	2.85	2.78	2.87
Na_2O	4.99	5.09	4.79	5.02	4.70	4.79
K_2O	1.38	1.69	1.90	1.52	1.81	1.64
TiO_2	0.3689	0.4096	0.3241	0.4477	0.3766	0.4076
P_2O_5	0.12	0.13	0.10	0.15	0.12	0.09
TOTAL	99.75	100.28	99.89	99.63	100.07	99.56
LOI	0.75	0.93	0.96	0.48	1.01	0.91
Nb	2.4	3.2	2.9	2.6	2.5	4.6
Zr	154.8	141.7	136.1	157.1	146.1	146.9
Y	7.5	8.4	9.4	7.4	8.7	8.0
Sr	572.0	426.7	399.5	511.3	412.9	450.3
Rb	55.7	69.1	65.3	65.3	55.4	63.1
La	61.8	11.1	14.4	17.5	22.0	7.1
Sc	2.1	3.6	2.9	2.9	3.7	3.8
Ba	392.8	291.3	292.9	217.2	248.6	285.0
Sr/Ba	1.46	1.46	1.36	2.35	1.66	1.58
Rb/Sr	0.10	0.16	0.16	0.13	0.13	0.14
K/Rb	206	203	242	193	271	216
FeO*/MgO	2.88	2.73	3.11	3.24	2.67	2.74

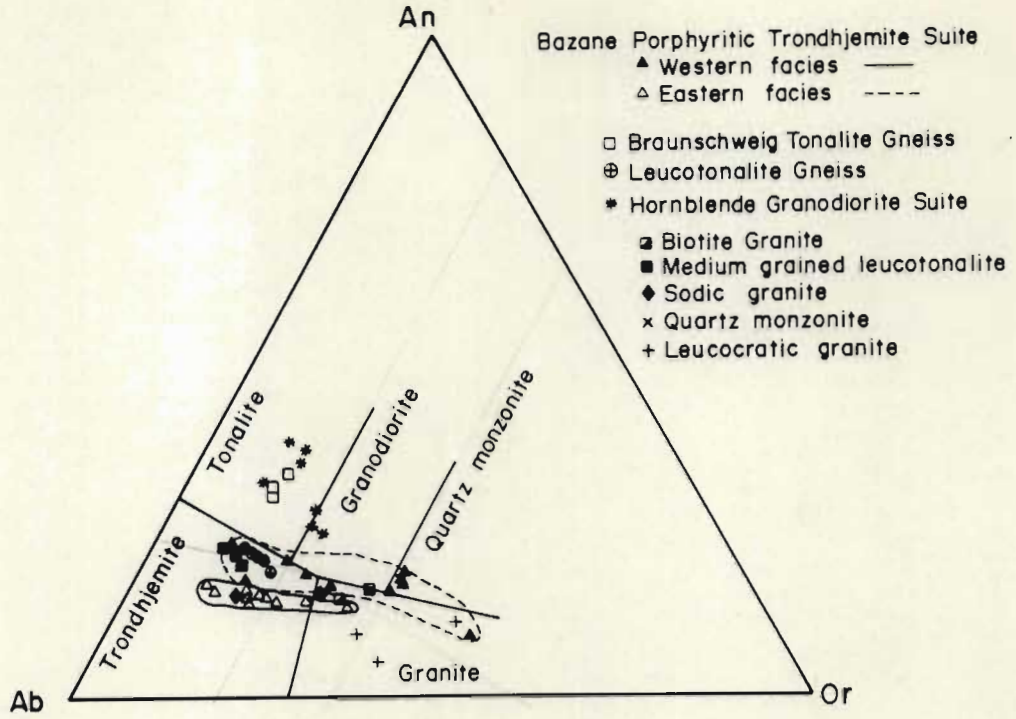

Fig. 5.13 CIPW normative proportions of An-Ab-Or (wt %) in the Trondhjemite-Tonalite-Granodiorite Suite, weakly foliated granitoids and unfoliated granitoids (see Table 3.1). The classification boundaries are after Barker (1979). The plagioclase boundaries at 5kb and 1 kb are after Glikson and Sheraton (1972). Amphibolite components in the Hornblende Granodiorite Suite are not plotted.

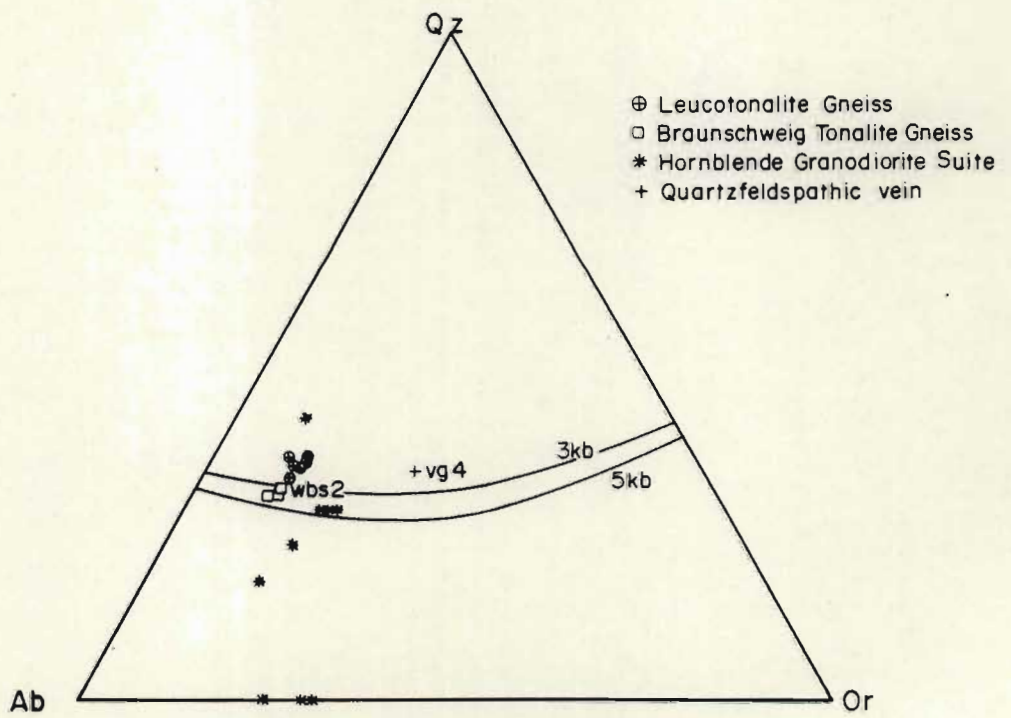

Fig. 5.14 CIPW normative proportions in the Leucotonalite Gneiss, Braunschweig Tonalite Gneiss and Hornblende Granodiorite Suite. Cotectic line PTOTAL = PH_2O = 2kb from Tuttle and Bowen (1958) and for PH_2O = 5kb calculated from Winkler (1979).

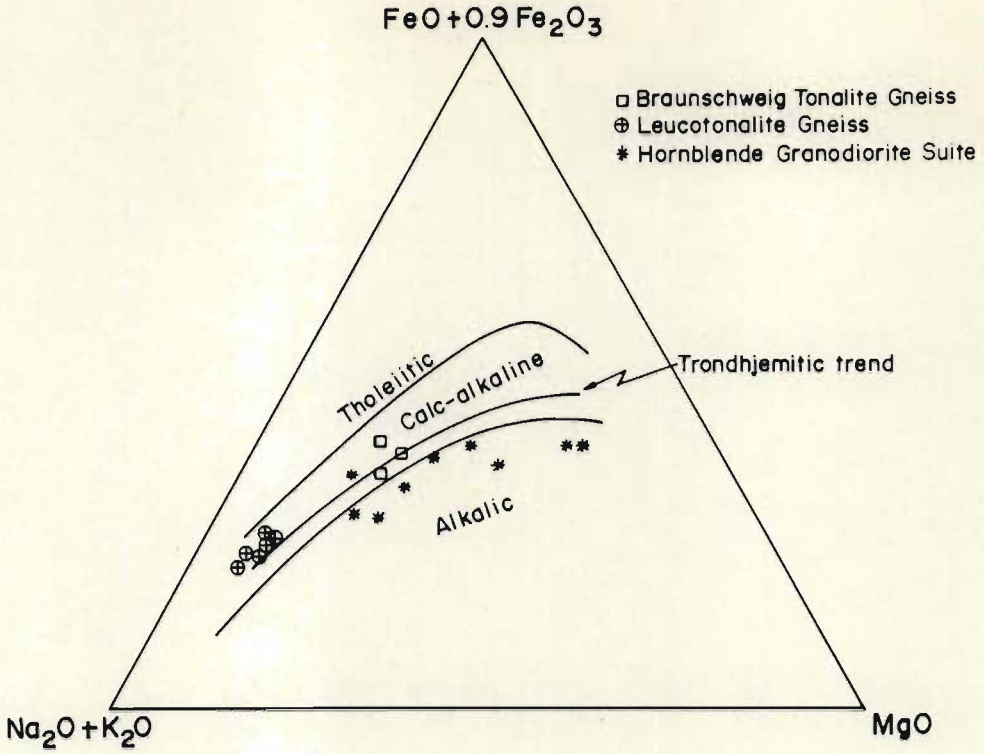

Fig. 5.15 Ternary AFM projection showing the Leucotonalite Gneiss, Braunschweig Tonalite Gneiss and Hornblende Granodiorite Suite. The tholeiitic and calc-alkaline fields and trondhjemitic trend are from Barker and Arth (1976).

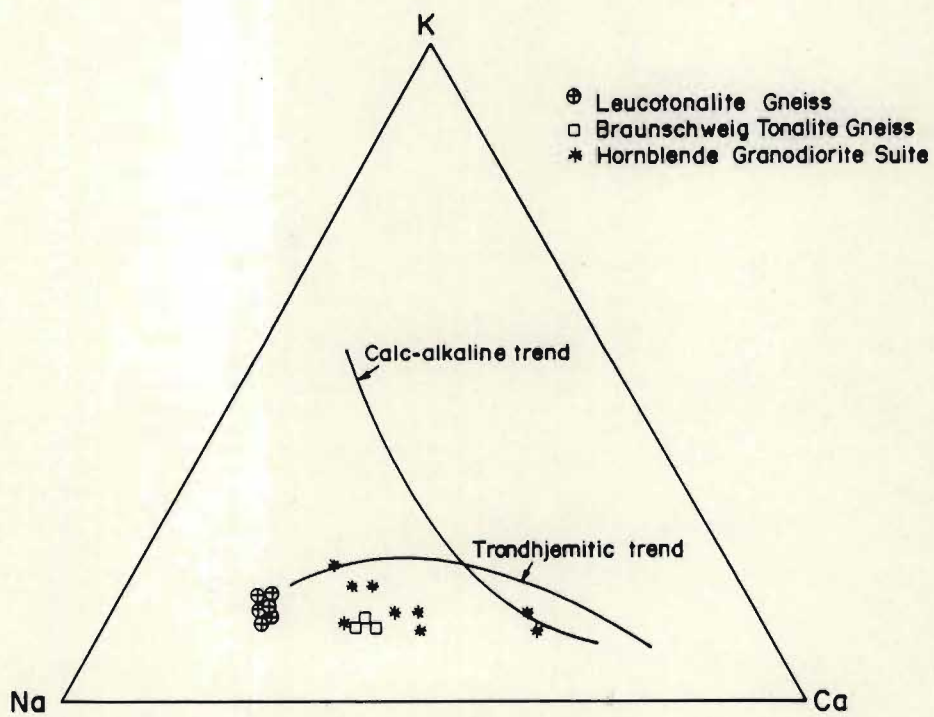

Fig. 5.16 Ternary K-Na-Ca projection showing the trondhjemitic affinity of the Leucotonalite Gneiss, Braunschweig Tonalite Gneiss and Hornblende Granodiorite Suite. The calc-alkaline trend is from Nockolds and Allen (1953) and the trondhjemitic trend from Barker and Arth (1976).

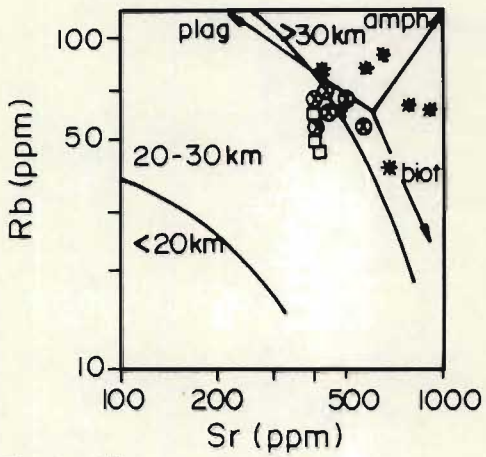

Fig. 5.17

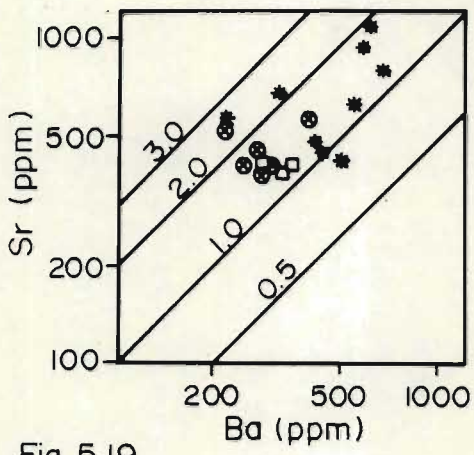

Fig. 5.19

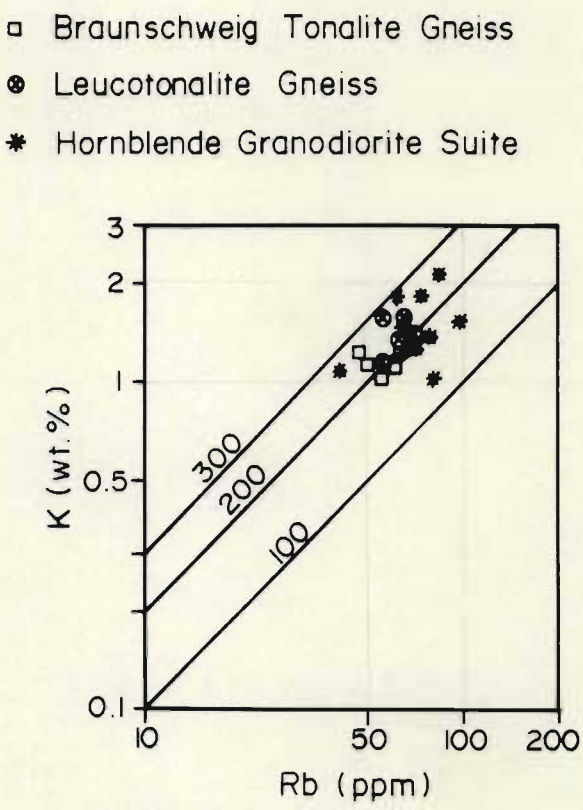

Fig. 5.18

Fig. 5.17 Rb/Sr plot for the Leucotonalite Gneiss, Braunschweig Tonalite Gneiss and Hornblende Granodiorite Suite. Crustal thickness index curves are from Condie (1973). Mineral fractionation vectors are from Beckinsale (1979).

Fig. 5.18 K/Rb plot for the Leucotonalite Gneiss, Braunschweig Tonalite Gneiss and Hornblende Granodiorite Suite.

Fig. 5.19 Sr/Ba plot for the Leucotonalite Gneiss, Braunschweig Tonalite Gneiss and Hornblende Granodiorite Suite.

Tonalite Gneiss. Ba contents are similar to those in the Luneburg gneiss but are typically slightly lower than in the siliceous Layered Gneisses.

Braunschweig Tonalite Gneiss.

Analyses of four melanocratic tonalite samples and one sample of a cross-cutting leucocratic vein are presented in Table 5.4 and sample localities are indicated on MAP 1. SiO_2 and Al_2O_3 contents show no significant variation being 65 wt. % and 16 wt. % respectively. CaO, MgO and FeO contents are also uniform and reflect the higher proportion of hornblende and biotite in this gneiss compared to the leucotonalitic gneisses. FeO*/MgO ratios are < 2.39.

The Braunschweig Tonalite Gneiss is petrographically and geochemically similar to the Tsawela Tonalite Gneiss (Hunter et al., 1984) and the Kaap Valley Pluton (Anhaeusser and Robb, 1983), but has an apparently more restricted range in composition. A greater number of analyses may reveal a wider range in composition.

A sample of one of the leucocratic veins (analysis L15) that cross-cuts the gneiss has 73 wt. % SiO_2, 15.5 wt. % Al_2O_3, 3.6 wt. % CaO, 5.4 wt. % Na_2O and 1 wt. % K_2O. Rb/Sr and K/Rb ratios for the leucocratic vein are 0.05 and 329 respectively.

On the normative An-Ab-Or projection samples lie within the tonalite field (Fig. 5.13). On the Qz-Ab-Or projection the tonalite samples define a restricted field parallel to the Qz-Ab tie line (Fig. 5.14). The Braunschweig tonalites lie along the trondhjemitic trend (Barker and Arth, 1976; Fig. 5.15) in the calc-alkaline field and their Na enrichment relative to K is emphasized in the K-Na-Ca plot (Fig. 5.16). K/Rb and Rb/Sr ratios are < 265 and between 0.11 and 0.16 respectively (Figs. 5.18 and 5.17). The Sr/Ba ratios are between 1 and 2 (Fig. 5.19).

TABLE 5.4 MAJOR AND TRACE ELEMENT ANALYSES OF THE BRAUNSCHWEIG TONALITE GNEISS

	VD1	VD2	FGT1	L14	L15 (leucocratic vein)
SiO_2	64.87	65.44	66.06	64.89	73.42
Al_2O_3	16.29	15.86	16.09	16.12	15.61
Fe_2O_3	0.54	0.55	0.50	0.50	0.13
FeO	4.40	4.46	4.05	4.08	1.02
MnO	0.09	0.08	0.07	0.07	0.02
MgO	2.51	2.10	2.25	1.98	0.42
CaO	4.80	4.79	4.70	5.00	3.02
Na_2O	4.16	4.33	4.46	4.30	5.37
K_2O	1.49	1.39	1.36	1.30	1.03
TiO_2	0.6596	0.6813	0.6168	0.62	0.16
P_2O_5	0.24	0.23	0.22	0.21	0.01
TOTAL	100.06	99.90	100.39	99.07	100.21
LOI	0.54	0.39	0.52	n.d.	n.d.
Nb	4.4	4.6	4.7	13.6	4.4
Zr	195.8	190.4	190.5	203.5	80
Y	11.4	11.4	13.1	20.8	0.8
Sr	415.1	402.9	394.8	416	573
Rb	47.2	50.0	61.1	46	26
V	14.2	8.0	14.1	n.d.	n.d.
La	38.2	26.4	25.0	n.d.	n.d.
Sc	8.3	8.9	9.3	10.5	0.7
Ba	279.6	342.9	341.6	279	271
Sr/Ba	1.48	1.17	1.16	1.49	
Rb/Sr	0.11	0.12	0.16	0.11	0.05
K/Rb	263	231	185	236	329
FeO*/MgO	1.97	2.39	2.02	2.31	

n.d. - not determined

Hornblende Granodiorite Suite.

This suite comprises hornblende-bearing tonalites, granodiorites and feldspathic amphibolites. Major and trace element analyses of nine samples are presented in Table 5.5 and sample localities are indicated on MAP 1.

SiO_2 contents in the hornblende granodiorites and tonalites range between 65 and 68 wt. % and Al_2O_3 between 15.5 and 17 wt. %. CaO abundances are typically between 4 and 6.5 wt. %, whereas Na_2O varies little about a content of 4 wt. %. FeO*/MgO ratios are > 1.32. The feldspathic amphibolites show a wide range of Al_2O_3 contents from 13 to 17.5 wt. % which reflects varying proportions of plagioclase. Both CaO and MgO range from 6 to 9.5 % which in part is a consequence of the variable abundance of hornblende. Trace element contents typically reflect the range from feldspathic amphibolite to granodiorite (Table 5.6). Barium, Sr, V and Cr contents are typically higher in the feldspathic amphibolites than the granodiorites and tonalites.

K/Rb ratios (Fig. 5.18) are > 200 for feldspathic amphibolites and granodiorites, except for MP5 (a low Mg amphibolite) which has a K/Rb ratio of 150. Most tonalites have K/Rb ratios < 200 but one sample, MP 10, has a low Rb content and a K/Rb ratio > 200. The low Rb content may be the result of pervasive saussuritization and retrograde reaction of biotite to chlorite and magnetite. In the other sample alteration is minor. Sr/Ba ratios (Fig. 5.19) are between 1 and 3. Rb/Sr ratios for the feldspathic amphibolites are < 0.09, granodiorites > 0.13 and tonalites generally < 0.14 (Fig. 5.17).

Samples MP9, MP10 and GUT1 lie in the tonalite field whereas samples MP1, LF1, LF3 lie close to the granodiorite-tonalite boundary on the normative An-Ab-Or projection (Fig. 5.13). The latter samples are classified as granodiorite in view of their relatively high K_2O contents (Table 5.6). On the normative Qz-Ab-Or projection (Fig. 5.14) the granodiorites define a compact field whereas the tonalites lie in an elongated field approximately parallel to the Qz-Ab tie line. The feldspathic amphibolites lie along the Ab-Or tie line. A compositional gap between the amphibolites and the least siliceous

TABLE 5.5 MAJOR AND TRACE ELEMENT ANALYSES FOR THE HORNBLENDE GRANODIORITE*

	Granodiorite			Feldspathic Amphibolite			Tonalite		
	LF1	LF3	MP1	MP5	MP7	MP8	MP9	MP10	GUT1
SiO_2	65.34	66.73	67.09	54.67	53.77	52.75	61.32	59.24	68.45
Al_2O_3	15.45	15.47	15.68	17.54	13.60	13.79	16.86	17.18	16.40
Fe_2O_3	0.49	0.41	0.41	0.76	0.94	0.97	0.60	0.69	0.40
FeO	4.00	3.28	3.28	6.14	7.63	7.86	4.82	5.57	3.26
MnO	0.08	0.07	0.07	0.11	0.15	0.16	0.08	0.13	0.08
MgO	3.03	2.79	2.26	6.40	9.23	9.59	3.57	4.61	1.55
CaO	4.74	4.27	3.78	6.58	8.62	9.04	5.54	6.53	4.20
Na_2O	3.99	4.31	4.22	3.87	2.74	2.55	3.95	3.93	3.94
K_2O	2.13	2.13	2.49	1.78	1.76	1.56	1.60	1.31	1.21
TiO_2	0.5440	0.4146	0.4599	0.9904	0.8379	0.8804	0.6831	0.7158	0.5053
P_2O_5	0.19	0.22	0.17	0.38	0.52	0.55	0.26	0.26	0.15
TOTAL	100.00	100.08	99.91	99.22	99.81	99.70	99.28	100.16	100.15
LOI	1.17	0.85	0.91	2.03	1.28	1.41	1.76	1.38	1.51
Nb	3.5	4.5	3.5	9.8	6.5	7.6	6.7	7.5	8.4
Zr	139.4	139.7	140.4	250.9	165.0	129.8	184.2	156.8	189.0
Y	8.7	9.0	10.1	30.5	31.5	34.4	21.1	22.1	23.0
Sr	454.9	484.6	425.9	1082.3	793.5	911.6	629.2	690.2	570.8
Rb	73.5	61.9	84.9	98.8	63.0	61.7	78.3	41.1	81.5
V	63.6	54.4	40.7	162.1	170.9	177.4	98.3	115.7	45.8
La	38.0	31.5	42.2	27.4	33.1	28.8	19.1	28.5	37.9
Sc	12.2	10.0	8.6	23.3	31.5	31.2	16.6	18.3	8.7
Ba	440.3	422.6	499.4	615.4	664.2	570.5	338.6	314.8	221.5
Zn	n.d.	n.d.	n.d.	84.9	114.0	119.7	74.5	94.7	80.2
Cu	n.d.	n.d.	n.d.	31.6	57.7	57.6	20.3	32.8	9.1
Ni	n.d.	n.d.	n.d.	136.7	226.7	225.6	85.1	109.9	45.8
Cr	n.d.	n.d.	n.d.	295.2	545.6	583.5	152.1	214.0	37.0
Sr/Ba	1.03	1.15	0.85	1.76	1.19	1.56	1.86	2.19	2.58
Rb/Sr	0.16	0.13	0.20	0.09	0.08	0.07	0,12	0.06	0.14
K/Rb	241	286	243	150	232	210	170	265	123
FeO*/MgO	1.48	1.32	1.63	1.08	0.93	0.92	1.52	1.36	2.36

n.d. = not determined

* This suite includes granodiorites, tonalites and feldspathic amphibolites.

tonalite is apparent but may reflect incomplete sampling. On the MgO-FeO*-alkalis projection the Hornblende Granodiorite Suite is the only rock-type (excluding Layered Gneiss Samples TG7, TG17 and TG11) in the area that defines an alkalic trend with the exception of one sample (GUT1) that lies in the calc-alkaline field (Fig. 5.15). The alkaline affinity of the Hornblende Granodiorite Suite is confirmed by the binary SiO_2 vs Na_2O + K_2O diagram wherein this suite lies in the sub-alkaline field (Fig. 5.20; Irvine and Baragar, 1971). The ternary K-Na-Ca plot (Fig. 5.16) indicates a trend towards enrichment in sodium.

Alkaline rocks tend to be confined to regions of continental rifting (Sykes, 1978). The Hornblende Granodiorite Suite crops out predominantly along an inferred structural discordance to the west of which the dominant stuctural trend is northeast whereas to the east there is a zone of refoliation aligned northwestwards (MAP 1 and MAP 3). The possiblity of this suite representing an intrusion associated with extensional tectonics is further explored in the final chapter.

Bazane Porphyritic Trondhjemite Suite.

Major and trace element analyses of nineteen samples of the Bazane Porphyritic Trondhjemite Suite are presented in Table 5.6 and sample localities are indicated on MAP 1. On the normative An-Ab-Or projection the western facies of the Bazane trondhjemites adjacent to the Commondale Supracrustal Suite comprises trondhjemites with subordinate granite and granodiorite (Fig. 5.13). The eastern facies adjacent to the Usushwana Complex and Nsuze Group comprises trondhjemites, granites, granodiorites and quartz monzonites (Fig. 5.13).

On the normative Qz-Ab-Or projection (Fig. 5.21) samples of the Bazane trondhjemite lie within a restricted range (35% $\pm$ 5% normative Qz as a proportion of Qz + Ab + Or) parallel to the quartz-alkali feldspar cotectic line for 3 KbPTotal = PH_2O (Tuttle and Bowen, 1958). On the MgO-FeO*-alkalis projection (Fig. 5.22) the samples lie in the calc-alkaline field towards the Na_2O + K_2O apex. One of the disadvantages of the AFM projection in discussing trondhjemitic rock- types is that Na and K represent the one apex thus not allowing one to evaluate the relative proportions of Na_2O + K_2O. Use of the K-Na-Ca ternary diagram (Fig. 5.23) reveals that the Bazane suite occupies a field

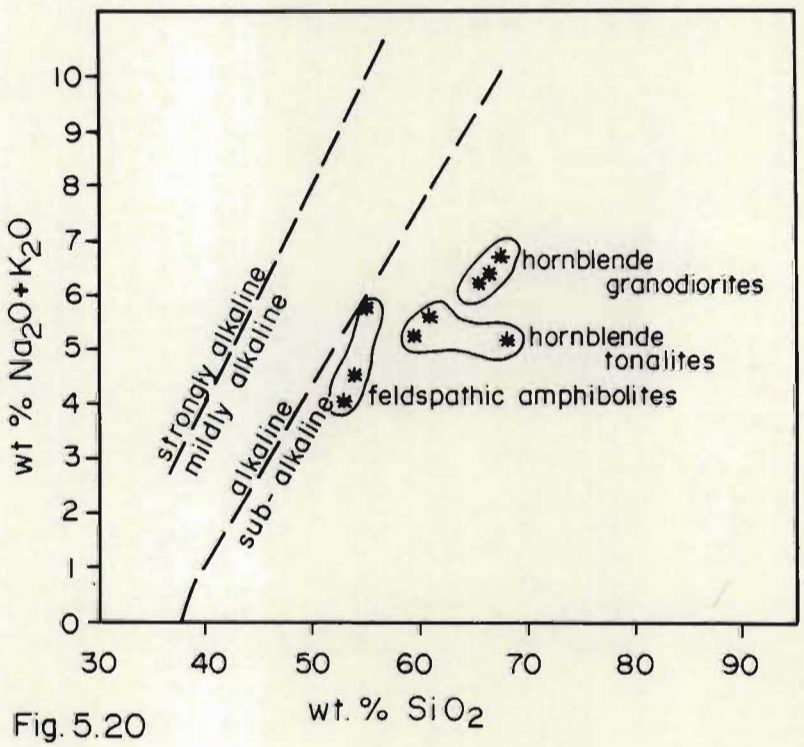

Fig. 5.20

Fig. 5.20 $(Na_2O + K_2O)/SiO_2$ plot for the Hornblende Granodiorite Suite. Alkaline/sub-alkaline boundary is from Irvine and Baragar (1971) and the strongly alkaline/mildly alkaline boundary is from Saggerson and Williams (1964).

TABLE 5.6 MAJOR AND TRACE ELEMENT ANALYSES OF THE BAZANE PORPHYRITIC TRONDHJEMITE*

	Trondhjemite										Granodiorite				Granite		Quartz monzonite		
	WBS1	VG1	VG2	WBS5	WBS6	VG3	TGU1	PK1	RT2	RT3	NLD2	PD1	PD2	ON1	NLD1	RT1	FGT2	FGT3	SKL1
SiO_2	72.15	71.68	72.80	72.54	72.96	72.21	72.54	72.51	72.32	70.02	72.30	72.21	68.32	71.12	72.63	74.16	71.01	68.86	67.23
Al_2O_3	15.81	15.69	15.78	15.99	15.22	15.57	15.65	15.23	15.65	16.09	14.79	15.16	15.96	15.62	14.96	14.31	14.97	15.32	15.78
Fe_2O_3	0.20	0.19	0.18	0.19	0.18	0.21	0.18	0.21	0.22	0.32	0.22	0.20	0.37	0.27	0.23	0.15	0.36	0.28	0.37
FeO	1.63	1.55	1.42	1.51	1.45	1.73	1.50	1.72	1.82	2.55	1.75	1.58	3.03	2.21	1.83	1.21	2.89	3.10	2.99
MnO	0.04	0.05	0.04	0.02	0.03	0.03	0.02	0.02	0.04	0.03	0.04	0.02	0.08	0.03	0.04	0.02	0.04	0.05	0.09
MgO	0.59	0.64	0.54	0.49	0.55	0.62	0.57	0.40	0.71	0.88	0.62	0.56	1.40	0.78	0.49	0.19	0.90	1.15	1.55
CaO	2.42	2.12	2.22	2.10	2.19	2.18	2.09	1.92	1.86	3.11	2.01	2.26	3.02	2.58	1.88	1.02	2.41	2.39	2.79
Na_2O	5.09	5.63	5.20	5.10	5.16	5.18	5.37	4.95	5.16	4.95	4.71	4.23	4.57	4.15	4.22	3.08	3.37	3.98	3.57
K_2O	1.58	1.79	1.61	1.95	0.96	2.02	1.23	2.19	1.82	1.14	2.69	2.79	2.08	2.33	3.17	5.15	3.70	3.98	3.90
TiO_2	0.3004	0.2815	0.2515	0.2574	0.2532	0.3298	0.2801	0.2445	0.3158	0.3719	0.3272	0.2944	0.5035	0.4158	0.3208	0.1931	0.4790	0.5469	0.5660
P_2O_5	0.10	0.09	0.11	0.09	0.09	0.08	0.09	0,07	0,08	0.11	0.11	0.08	0.22	0.15	0.10	0.03	0.21	0.25	0.26
TOTAL	99.91	99.70	100.16	99.84	99.03	100.17	99.52	99.46	99.99	99.56	99.58	99.39	99.58	99.64	99.87	99.52	100.33	100.01	99.08
LOI	1.21	1.37	1.18	0.57	0.79	0.70	0.37	0.54	1.20	0.57	1.05	0.91	1.26	1.07	0.87	0.78	0.92	1.43	1.50
Nb	2.1	1.7	2.0	1.9	1.3	1.8	1.9	2.9	8.3	7.9	3.1	5.2	18.4	7.2	3.5	3.9	7.3	8.8	18.8
Zr	159.4	150.1	145.6	138.9	135.2	149.8	142.3	97.2	216.0	227.8	137.0	114.4	225.0	192.2	180.9	218.3	183.5	256.1	242.4
Y	6.3	5.5	7.2	5.8	7.3	7.1	5.8	7.3	20.2	14.6	8.3	10.4	50.1	10.6	12.1	8.4	17.2	27.7	44.5
Sr	691.9	660.3	614.9	576.5	646.4	613.4	588.5	422.4	619.5	589.6	425.3	560.7	705.4	497.7	345.9	393.3	477.3	433.3	766.9
Rb	57.1	63.6	50.9	53.0	47.1	68.5	51.3	54.8	74.0	69.8	116.3	58.8	79.4	45.2	131.0	122.6	72.6	88.5	89.5
La	18.9	31.0	9.9	13.1	18.8	18.2	35.7	17.7	70.2	32.6	45.7	13.5	64.0	51.6	66.9	83.3	77.1	118.6	79.5
Sc	2.0	1.6	1.6	1.6	1.6	2.2	2.0	1.8	2.5	3.5	3.7	2.3	5.5	6.0	3.4	1.9	6.9	7.9	7.4
Ba	517.7	571.1	396.9	536.5	415.8	474.7	443.1	506.9	452.6	145.6	609.2	634.6	1042.2	764.3	717.6	758.5	913.7	1069.4	1533.6
Sr/Ba	1.34	1.16	1.55	1.07	1.55	1.29	1.33	0.83	1.37	4.05	0.70	0.88	0.68	0.65	0.48	0.52	0.52	0.41	0.50
Rb/Sr	0.08	0.10	0.08	0.09	0.07	0.11	0.09	0.13	0.12	0.12	0.27	0.10	0.11	0.09	0.38	0.31	0.15	0.20	0.12
K/Rb	230	234	263	305	169	245	199	332	204	136	192	394	217	428	201	349	423	373	362

* This suite includes trondhjemite, tonalite, granite, granodiorite and quartz monzonite

n.d. Not determined

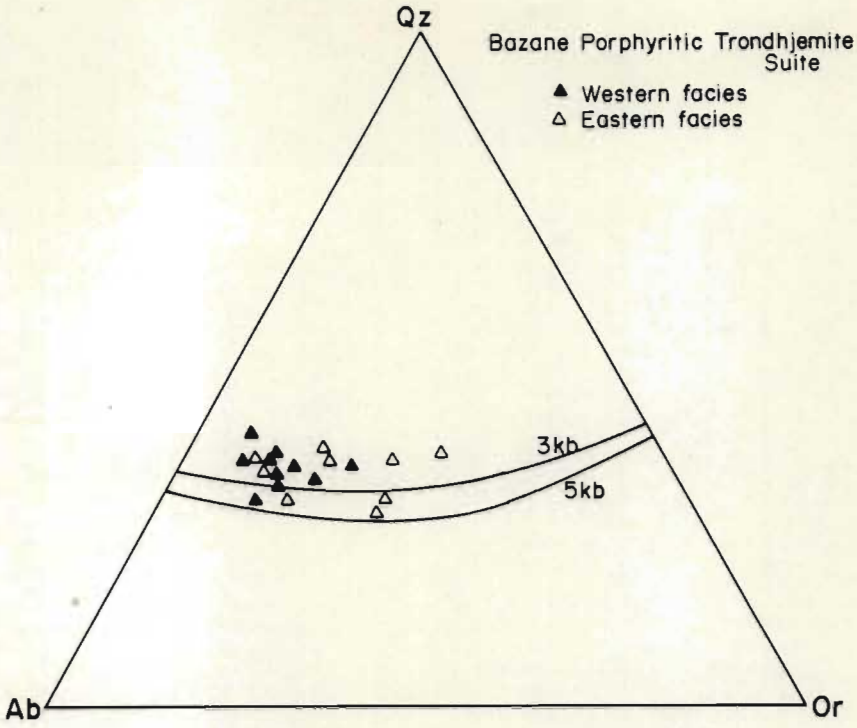

Fig. 5.21 CIPW normative proportions for the Bazane Porphyritic Trondhjemite. Cotectic line for $P_{TOTAL} = PH_2O + 3kb$ is from Tuttle and Bowen (1958), and $PH_2O = 5kb$ calculated from Winkler (1979).

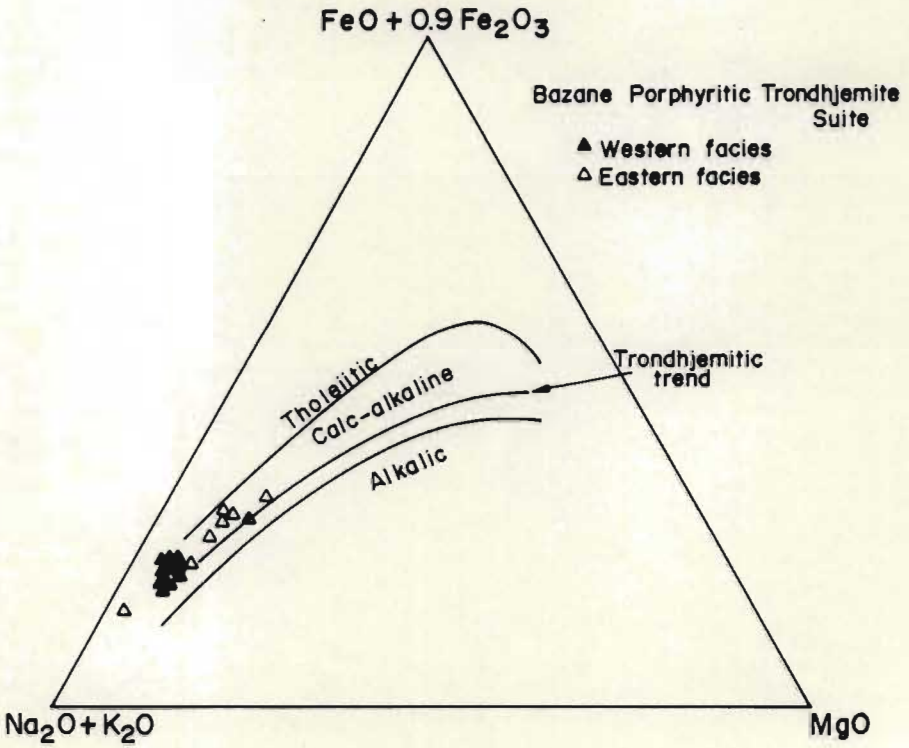

Fig. 5.22 Ternary AFM projection showing the Bazane Porphyritic Trondhjemite. The tholeiitic and calc-alkaline fields and trondhjemitic trend are from Barker and Arth (1976).

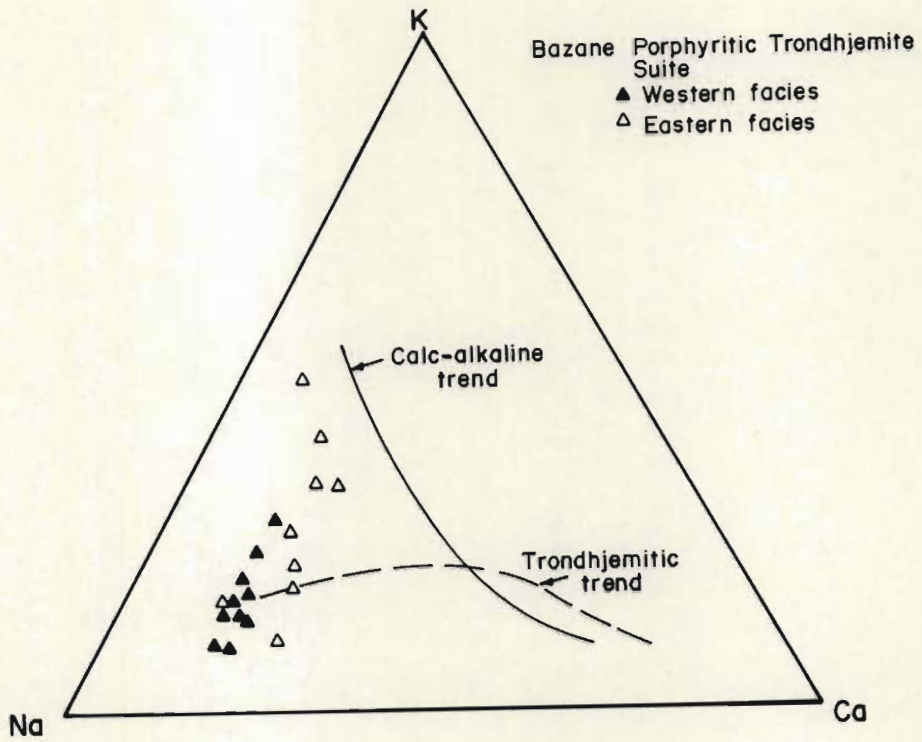

Fig. 5.23 Ternary K-Na-Ca projection showing a differentiated trondhjemite trend for the Bazane Porphyritic Trondhjemite. The calc-alkaline boundary is from Nockolds and Allen (1953) and the trondhjemitic trend from Barker and Arth (1976).

parallel to the K-Na tie line extending from the trondhjemite trend towards the calc-alkaline trend. This is a common feature of the more potassic Archaean granitoids in the eastern Transvaal and Swaziland (D.R. Hunter, pers. comm.). The relationships observed in Figures 5.13; 5.21; 5.22 and 5.23 suggest either :

i) the more evolved potassic rock types may be discrete bodies reflecting multiphase intrusion.

ii) the granites, granodiorites and quartz monzonites may be the products of fractionation of a trondhjemitic magma. Fractionation of plagioclase and quartz from this magma would drive the liquid in terms of the Qz-Ab-Or projection towards the Or apex, involving crystallization along the plagioclase-quartz cotectic surface in the Qz-Ab-Or-An tetrahedron (Carmichael, 1963). The Bazane trondhjemite has been interpreted as a large sheet-like intrusion emplaced at the interface between the Layered Gneisses and the Commondale Supracrustal Suite. The complex geometry of the intrusion along the western margin of the Commondale Supracrustal Suite suggests that the top of the sheet was undulatory, such that the more potassic phases may have accumulated in apical or domical structures. Subsequent deformation and erosion would expose different levels of the Bazane sheet.

Trace element contents typically reflect the range from trondhjemite to granodiorite, quartz monzonite and granite (Table 5.6). Niobium, Zr, Y, La and Ba abundances are greater in the granites, granodiorites and quartz monzonites than in the trondhjemites. In the former three rock types Sr is lower and Rb higher reflecting a higher proportion of microcline than in the trondhjemites. K plotted as a function of Rb (Fig. 5.24) shows that the trondhjemites have K/Rb ratios > ~140. Rock types with K/Rb ratios > 250 - 300 may represent the products of differentiation of these trondhjemitic liquids. Sr/Ba ratios (Fig. 5.25) are between ~0.5 and 5.0. The trondhjemites have Sr/Ba ratios between 1.0 and 5.0 and the more potassic rock types have Sr/Ba ratios < 1.0. The Rb/Sr ratios range between 0.07 for the trondhjemitic rock types and 0.38 for the granitic rock types (Fig. 5.26). The genetic implications of these ratios and the probability that the more potassic members of the suite are the products of fractionation of a

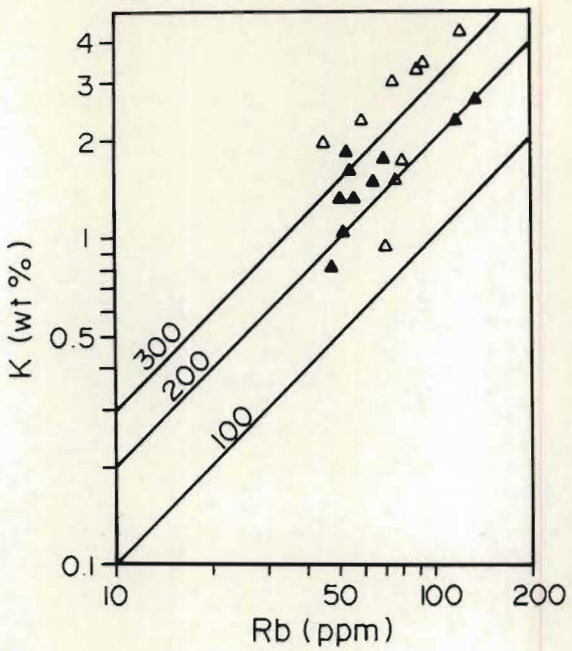

Bazane Porphyritic Trondhjemite Suite
▲ Western facies
△ Eastern facies

Fig. 5.24 K/Rb plot for the Bazane Porphyritic Trondhjemite.

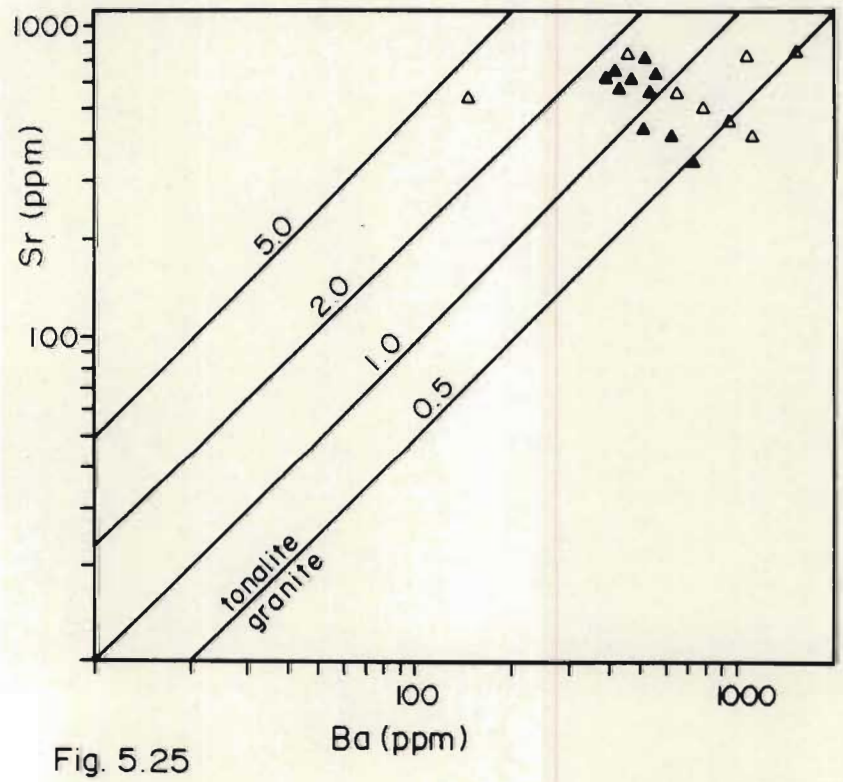

Fig. 5.25

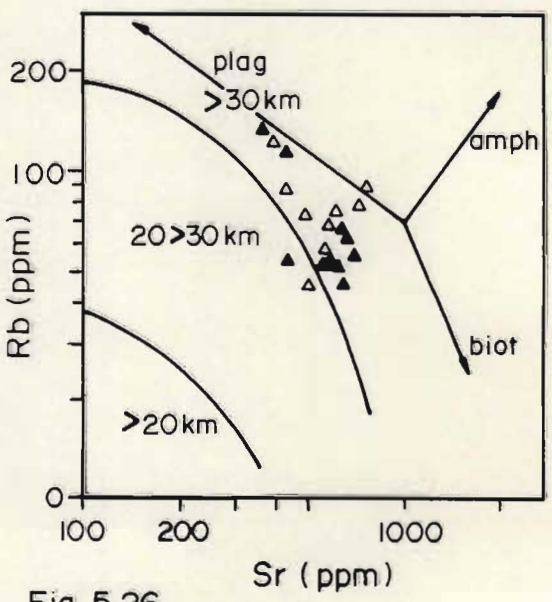

Fig. 5.26

Fig. 5.25 Sr/Ba plot for the Bazane Porphyritic Trondhjemite.

Fig. 5.26 Rb/Sr plot for the Bazane Porphyritic Trondhjemite. Crustal thickness index curves are from Condie (1973). Mineral fractionation vectors are from Beckinsale (1979).

trondhjemitic magma are further explored in a later section.

WEAKLY FOLIATED GRANITOIDS.

The weakly foliated granitoids comprise a suite of medium-grained leucotonalites, biotite granites and sodic granites that intrude the Luneburg Tonalite Gneiss as elliptically shaped bodies. Major and trace element analyses of nine samples are presented in Table 5.7 and sample localities are indicated on MAP 1.

Sodic granites are distinguished from the leucotonalites by somewhat higher contents of SiO_2 and K_2O wheras MgO and CaO are slightly depleted relative to the leucotonalites. Of the trace elements Sr is depleted in the sodic granites relative to the leucotonalites.

Biotite granites have similar SiO_2 contents to the sodic granite but are further enriched in K_2O than the latter. Both Rb and Ba attain their maximum concentrations in the biotite granite (Table 5.7).

The medium-grained leucotonalites plot in the trondhjemite field of the An-Ab-Or projection (Fig. 5.13) but do not satisfy the criteria for classification as trondhjemites (Chapter 3, Fig. 3.1). One of the sodic granite samples plots in the trondhjemite field but also does not satisfy major element criteria for classification as a trondhjemite. The biotite granites plot in the granite field (Fig. 5.13). On the ternary MgO-FeO*-alkalis projection the weakly foliated granitoids occupy the calc-alkaline field (Fig. 5.27). On the Qz-Ab-Or projection the leucotonalites and granites plot in the quartz + plagioclase field towards the cotectic for PH_2O = 5Kb (Fig. 5.28).

Trace element abundances typically reflect the gradation from leucotonalite to granite. Yttrium, Rb and Ba abundance are typically greater in the granites than in the leucotonalites. Strontium and Sc contents are higher in the leucotonalites than granite, with Sr reflecting the higher proportion of plagioclase. K/Rb ratios are < 280 (Fig. 5.29) and Sr/Ba ratios are between 0.5 and 2.0 except for KA 3 which has a Sr/Ba ratio of 0.3 (Fig. 5.30). Rb/Sr ratios are between 0.04 and 0.10 for the leucotonalites and between 0.09 and 0.46 for the granites (Fig. 5.31). The possible genetic relationships between the leucotonalites and granites are discussed in the section

TABLE 5.7 MAJOR AND TRACE ELEMENT ANALYSES FOR MEDIUM-GRAINED LEUCOTONALITE, BIOTITE GRANITE AND SODIC GRANITE

	Medium-grained leucotonalite				Biotite granite		Sodic granite	
	DK3	DK1	DK2	DK4	LBE3	KA3	RD1	RD2
SiO_2	69.21	69.63	70.57	67.94	72.25	72.63	72.85	71.74
Al_2O_3	17.00	16.62	16.04	17.55	15.17	14.71	15.12	16.40
Fe_2O_3	0.26	0.25	0.24	0.29	0.17	0.23	0.20	0.20
FeO	2.10	2.03	1.98	2.33	1.35	1.89	1.64	1.59
MnO	0.03	0.03	0.03	0.03	0.02	0.03	0.03	0.03
MgO	0.97	0.87	0.83	1.12	0.50	0.79	0.65	0.71
CaO	3.01	2.88	2.91	3.44	2.08	2.15	2.05	2.40
Na_2O	5.41	5.16	5.02	5.22	4.58	3.62	4.31	5.65
K_2O	1.53	1.61	1.41	1.20	3.46	3.36	2.77	1.80
TiO_2	0.4021	0.3783	0.3750	0.4542	0.2422	0.3536	0.3109	0.2869
P_2O_5	0.15	0.15	0.13	0.18	0.10	0.12	0.10	0.11
TOTAL	100.08	99.61	99.53	99.76	99.92	99.90	100.05	100.91
LOI	0.78	0.68	1.02	1.49	0.49	0.52	0.63	0.54
Nb	2.4	1.7	2.0	2.0	2.8	3.3	4.2	2.6
Zr	187.5	180.6	175.4	216.9	138.5	215.5	164.0	143.0
Y	7.5	7.6	6.6	5.7	10.0	9.4	10.9	6.3
Sr	817.8	805.0	806.2	952.8	437.9	238.7	319.2	596.7
Rb	62.6	80.4	60.5	35.7	122.6	110.3	103.6	56.0
La	41.6	37.5	47.5	32.4	15.8	75.8	32.1	35.7
Sc	2.6	2.6	2.2	3.2	1.0	1.8	2.7	2.5
Ba	356.6	347.8	325.7	413.8	699.7	972.3	592.3	400.0
Sr/Ba	2.29	2.31	2.48	2.30	0.63	0.25	0.54	1.49
Rb/Sr	0.08	0.10	0.08	0.04	0.28	0.46	0.32	0.09
K/Rb	203	166	193	279	234	253	222	267

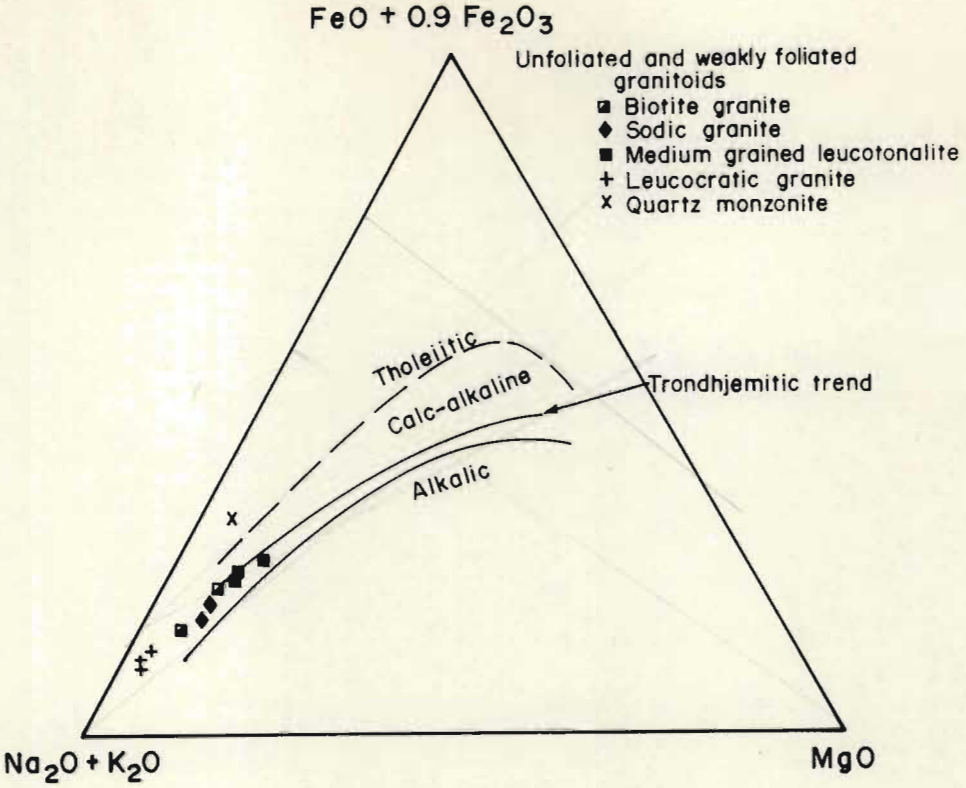

Fig. 5.27 Ternary AFM projection showing the weakly foliated and unfoliated granitoids. The tholeiitic and calc-alkaline fields and the trondhjemitic trend are from Barker and Arth (1976).

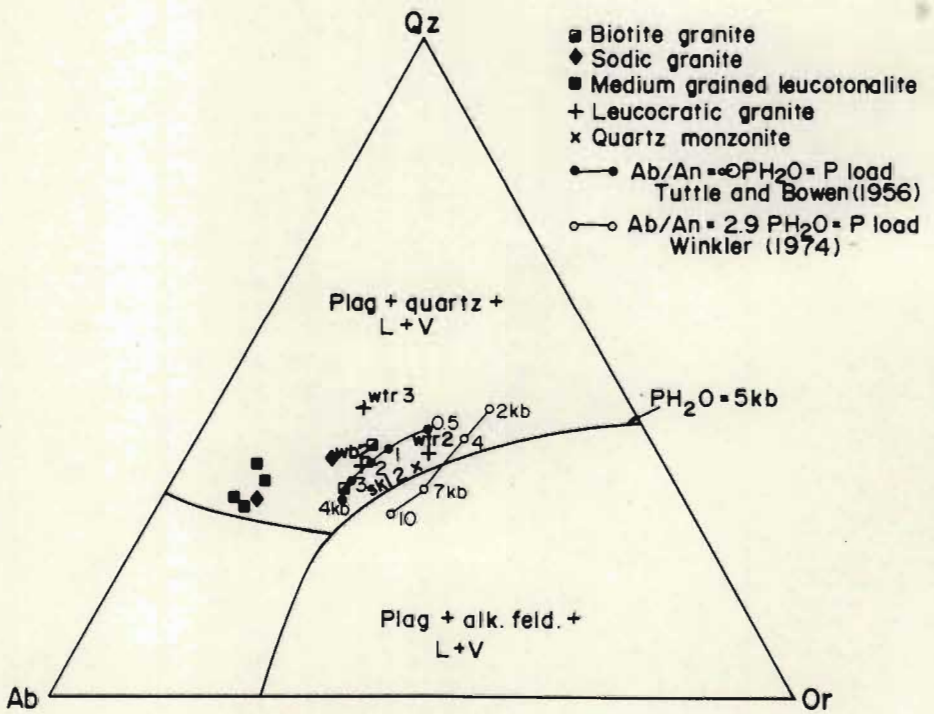

Fig. 5.28 CIPW normative projections in the weakly foliated and unfoliated granitoids in relation to minimum melt compositions derived from experimental studies. Phase boundaries at PH_2O = 5kb from Winkler (1979).

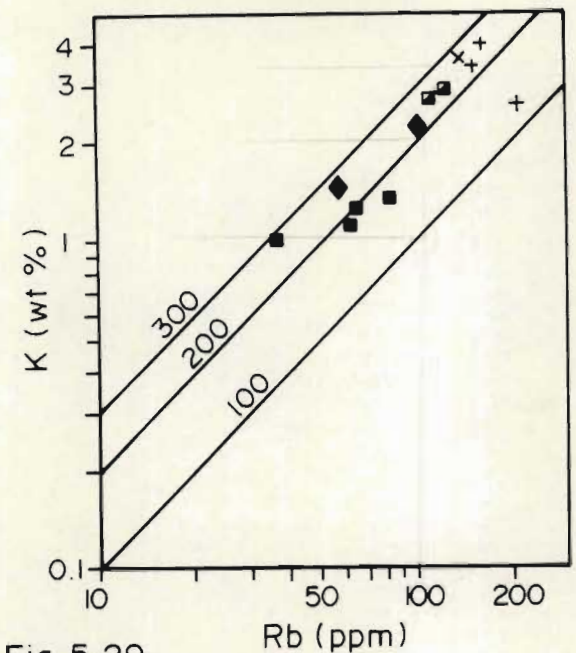

Fig. 5.29

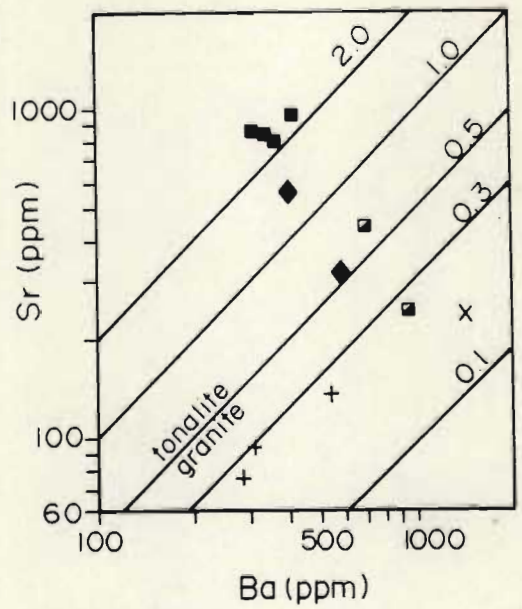

Fig. 5.30

Fig. 5.29 K/Rb plot for weakly foliated and unfoliated granitoids. Ornamentation same as in Fig. 5.28.

Fig. 5.30 Sr/Ba plot for the weakly foliated and unfoliated granitoids. Ornamentation same as in Fig. 5.28.

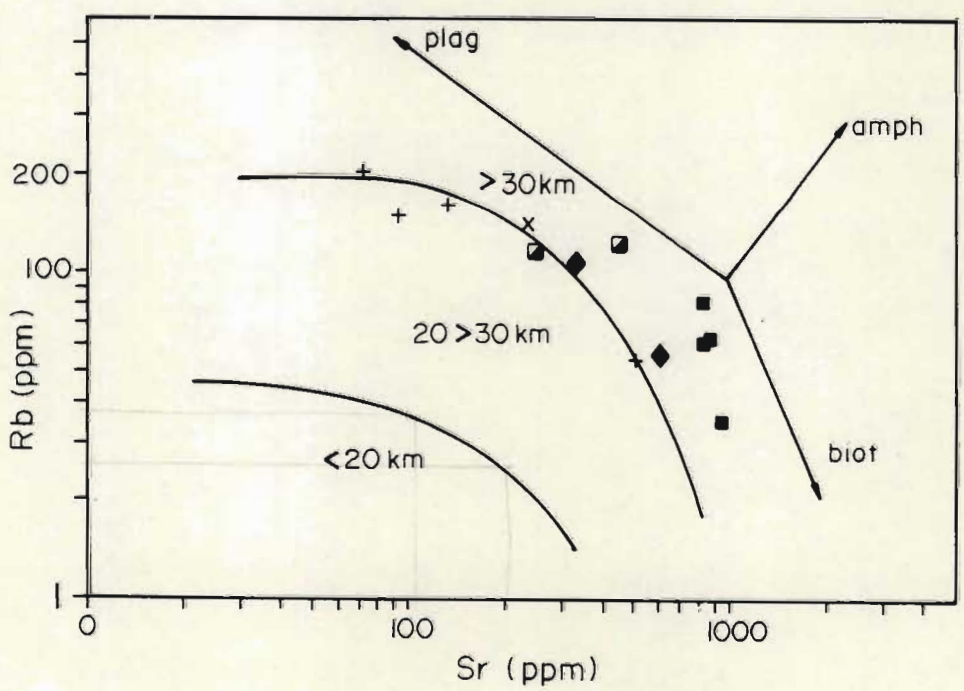

Fig. 5.31 Rb/Sr plot for the weakly foliated and unfoliated granitoids. Ornamentaion same as Fig. 5.28. Crustal thickness index curves are from Condie (1973). Mineral fractionation vectors are from Beckinsale (1979).

on petrogenesis.

UNFOLIATED GRANITOIDS

Major and trace element analyses of three samples of leucocratic granite and one sample of quartz monzonite are presented in Table 5.8. The sample localities are indicated on MAP 1.

The chemical compositions of the leucocratic granites reflect the lack of mafic minerals in these rocks. The oxides SiO_2, Al_2O_3, Na_2O and K_2O constitute 96 wt. % of the rocks. Rubidium exceeds Sr by factors of between 1.2 and 2.8. Zr is present typically in low concentrations whereas Ba contents are variable (Table 5.8). With the exception of one sample (WTR3) the K/Rb ratios are between 225 and 250. Sample WTR3 has a low K/Rb ratio (127) as a consequence of its high Rb concentration.

Only one quartz monzonite sample has been analysed. This differs chemically from the leucocratic granites largely with respect to its lower SiO_2 and high CaO and MgO contents. The trace element chemistry shows more obvious differences with Zr, Sr, Nb, Y and Ba being strongly enriched relative to the leucocratic granites. Rubidium is depleted relative to the leucocratic granites. For the leucocratic granites Sr/Ba and Rb/Sr ratios are < 0.3 and > 1.2 respectively. The quartz monzonite has Sr/Ba and Rb/Sr ratios of 0.16 and 0.60 respectively.

On the normative An-Ab-Or projection (Fig. 5.13) the leucoctratic granites and quartz monzonite plot in their respective fields. The leucocratic granites lie close to the $Na_2O + K_2O$ apex of the ternary alkali-total Fe-MgO diagram and the quartz monzonite sample plots in the tholeiitic field (Fig. 5.27). On the Qz-Ab-Or projection the leucocratic granite and quartz monzonite with the exception of WTR3 plot close to minimum melt compositions or plagioclase-K feldspar-quartz cotectics at PH_2O between 1 and 5 Kb (Fig. 5.28).

TABLE 5.8 MAJOR AND TRACE ELEMENT ANALYSES FOR UNFOLIATED LEUCOCRATIC GRANITE AND QUARTZ MONZONITE*

	WB2	WTR2	WTR3	SKL2
SiO_2	75.54	74.89	75.67	71.42
Al_2O_3	13.57	14.06	14.06	13.33
Fe_2O_3	0.12	0.14	0.14	0.43
FeO	0.95	1.10	1.15	3.49
MnO	0.02	0.02	0.02	0.06
MgO	0.22	0.28	0.22	0.46
CaO	0.69	1.39	1.04	1.88
Na_2O	4.15	3.17	3.68	3.27
K_2O	4.11	4.91	3.14	4.40
TiO_2	0.1165	0.1600	0.0955	0.6002
P_2O_5	0.03	0.04	0.03	0.10
TOTAL	99.51	100.16	99.26	99.44
LOI	0.54	1.54	1.17	1.34
Nb	6.9	3.1	4.5	38.8
Zr	58.0	141.2	89.8	698.6
Y	16.3	12.7	17.4	78.5
Sr	93.1	131.1	74.0	230.8
Rb	149.7	160.3	204.8	138.7
La	41.3	37.8	15.	170.24
Sc	2.1	1.5	1.5	7.6
Ba	312.3	540.3	288.9	1420
Sr/Ba	0.30	0.24	0.26	0.16
Rb/Sr	1.6	1.22	2.77	0.60
K/Rb	228	254	127	263

* quartz monzonite = SKL2

PART 2 : PETROGENESIS.

The Origin of Tonalitic and Trondhjemitic Magmas.

Early Archaean crust comprises in simple terms a complexly interlayered bimodal suite of sodic granitoid gneisses and subordinate amphibolite of basaltic composition within which are preserved remnants of metavolcanic and metasedimentary sequences, the so called greenstone belts. The formation of an early stable continental crust requires the generation of sufficient volumes of granitoid rocks to counter-balance the high density of the basaltic-ultramafic component (Campbell and Jarvis, 1984; Condie, 1986).

The common association of tonalitic and trondhjemitic gneisses with amphibolite has led to the conclusion that these quartzofeldspathic rocks are related to a basaltic source. Geochemical and isotopic evidence in support of this conclusion include :

i) The primitive initial Sr isotopic compositions found in all trondhjemites of all geological eras (Porterman, 1979; Carlson et al., 1983; Arth and Hanson, 1975).

ii) The oxygen isotope ratios of trondhjemites are similar to those of basalts but distinct from those for other granitic rocks (Barker et al., 1976b).

iii) Positive ε_{Nd} values indicate a mantle origin for tonalitic rocks (Carlson et al., 1983).

iv) Experimental melting studies (Green and Ringwood, 1968; Helz, 1973, 1976; Wyllie, 1977), and trace element modelling (for example, Hanson and Goldich, 1972; Condie and Hunter, 1976) suggest a basaltic source for the tonalitic and trondhjemitic magmas.

Many researchers, for example Green and Ringwod (1968); Barker and Arth (1976); Condie and Hunter (1976), envisage the formation of tonalitic magmas as a two-stage process whereby partial melting of the mantle initiated by a mantle plume (Condie and Hunter, 1976; Campbell and Jarvis, 1984) resulted in mafic and ultramafic volcanism. The

second stage involves digestion of the volcanics back into the mantle through mantle sinks (Condie and Hunter, 1976; Condie, 1986) or Archaean style subduction (Campbell and Jarvis, 1984) where partial melting of wet basaltic crust, metamorphosed at amphibolite grade, gives rise to tonalitic and trondhjemitic magmas.

Models for the generation of tonalitic melts involving both fractional crystallization and partial melting have also been proposed. Fractional crystallization models for high Al_2O_3 type trondhjemites were proposed by Goldschmidt (1922), quoted in Arth et al. (1978) and Hietanen (1943) quoted in Arth et al. (1978) for the intrusive suites in the Trondheim area in Norway and the Kalanti area of southwest Finland respectively. Both these areas show a complete range in composition from gabbro through diorite and tonalite to trondhjemite that is consistant with a fractional crystallization model (Arth et al., 1978).

Many of the Archaean terranes however, exhibit a marked bimodality comprising a tonalite-subordinate basalt assemblage in which rocks of intermediate composition such as andesite and diorite are absent (Hunter, 1970b; Hanson and Goldich, 1972; Barker and Arth, 1976). The absence of rocks of intermediate composition suggests that partial melting of wet basaltic magma is a more likely process than fractional crystallization.

Although unanimity exists that trondhjemites and tonalites are formed by partial melting of rocks of basaltic composition the proponents have appealed to both different compositions and modal mineralogies for their starting materials to generate tonalitic liquids and these include:

i) partial melting of amphibolite (Green and Ringwood, 1968; Hanson and Goldich, 1972; Wyllie, 1977; Barker and Arth, 1976 and Tarney et al., 1979)

ii) partial melting of garnet amphibolite (Hunter et al., 1978; O'Nions and Pankhurst, 1978 and Tarney et al., 1979). Partial melting of garnet amphibolites with 30 modal percent plagioclase has also been proposed by Condie, 1986.

iii) partial melting of quartz eclogite (Hanson and Goldich, 1972; Condie and Hunter, 1976; Barker and Arth, 1976 and Arth and Hanson, 1975).

Partial melting of eclogite to produce tonalitic and trondhjemitic melts may not be pertinent for the Archaean as early Archaean terranes at the present levels of exposure contain no eclogite.

Tonalitic and trondhjemitic melts are commonly produced by 15 - 30% partial melting at temperatures (T) between 850 - 1000 degrees C (Helz, 1973, 1976; Wyllie, 1977). The critical factor in applying partial melting models to produce bimodal tonalitic-basalt suites is that the siliceous liquid must be removed from the residue before the fraction of melting exceeds 40% and before the liquid phase becomes andesitic (Barker and Arth, 1976). This is achieved during partial melting where the lower parts of the basaltic pile reach progressively higher pressures and become progressively dehydrated through the upward removal of tonalitic and trondhjemitic liquids such that the deyhdrated residue comprising new hornblende + pyroxene + olivine and other minerals is below the solidus preventing further melting (Barker and Arth, 1976).

The above criteria are consistent with experimental melting relationships for basalts at 5kb PH_2O (Helz 1973, 1976). In the T range 680 - 850 degrees C reaction involves hornblende, plagioclase and melts (Helz, 1973). In the T range 850 - 1000 degrees C hornblende breaks down incongruently changing composition and producing an assemblage of a new hornblende + clinopyroxene + olivine + melt $\pm$ oxides (Helz, 1973). Many Archaean amphibolites such as those of the Ancient Gneiss Complex, Swaziland (Hunter, 1970) and those in the present study area contain a small percentage of quartz. Thus on partial melting of these amphibolites quartz, plagioclase and some hornblende melt first and the excess An component reacts with and becomes incorporated in the residual hornblende (Holloway and Burnham, 1972; Helz, 1973, 1976).

The experimental results of Helz (1973, 1976) reveal that :

i) Melts are extremely quartzofeldspathic within the hornblende stability field. Near and above the hornblende out curve

melt compositions become abruptly richer in FeO and MgO (Holloway and Burnham, 1972; Helz, 1976).

ii) Melt compositions are insensitive to changes in basalt composition within the hornblende stability field except for the Na/Ca ratio which varies directly with that ratio in the source basalt.

iii) Melt composition is insensitive to fO_2 within the hornblende stability field but at higher temperatures MgO, FeO and TiO_2 contents of the melt depend strongly on fO_2.

PETROGENETIC IMPLICATIONS FOR THE ARCHAEAN GRANITOIDS.

General.

The preceding section serves as an introduction to a consideration of the petrogenesis and evolution of early Archaean continental crust. The petrogenesis of the tonalitic and trondhjmeitic gneisses of the study area is modelled using a number of different approaches, that include primordial mantle normalized HFSE and LILE spidergrams that provide a means of comparison of trace abundances in the different gneisses. The possible origins of the various granitoids are tested but the available geochemical data constrain the conclusions. For the Bazane Porphyritic Trondhjemite Suite and the weakly foliated granitoids the possibility that the more potassic components represent the products of fractionation of trondhjemitic and leucotonalitic melts, respectively, is investigated. The significance of Rb/Sr and Sr/Ba ratios is also discussed.

Rock/Primordial mantle LILE and HFSE patterns.

Rock/primordial mantle LILE and HFSE patterns for the various granitoids are presented in Fig. 5.32. The patterns for the tonalitic and trondhjemite gneisses as well as the volumetrically much smaller granitic components are all similar. The patterns show a typical increase relative to primordial mantle from Y to Ba with pronounced troughs at Nb and P and a weak trough at Ti.

Typical spidergram patterns for the Group A and Group B layered

gneisses differ with respect to the relatively greater degree of depletion of Nb, and enrichment of Sr in the Group A gneisses as compared to the Group B gneisses. Some depletion in Y relative to Ti is apparent in the Group A gneisses (Fig. 5.32a). The patterns for the Luneburg Tonalite Gneiss (Fig. 5.32b) are identical to those for the Group B siliceous gneisses and similar to the patterns of the Braunschweigh Tonalite and Leucotonalite Gneiss (Fig. 5.32c). The patterns for the Hornblende Granodiorite Suite (Fig. 5.32d), the Bazane Porphyritic Trondhjemite Suite (Fig. 5.32e) and the weakly foliated granitoids (Fig. 5.32f) similarly all show a typical increase relative to primordial mantle from Y to Ba with troughs at Nb and P with a weak to strong trough at Ti. An exception is the feldspathic amphibolite (MP7) that show a continuous increase from Ti to Nb with no trough at P (Fig. 5.32d).

Patterns for the Bazane Porphyritic Trondhjemite Suite (Fig. 5.32e) show that the relative enrichment from Y to Ba with pronounced troughs at Nb, P and Ti is greater than for more tonalitic compositions. Similarly the relative enrichment in the weakly foliated granitoids from Y to Ba with troughs at Nb, P and Ti characteristic of granitoids in the study area is greater than for tonalitic compositions.

The patterns for the Bazane trondhjemite and medium-grained leucotonalite are steeper than those for the tonalites. This suggests either :

a) a lower degree of partial melting of mafic source rocks so that the relative enrichment in Rb, V, Ba, K and Y is greater than for higher degrees of partial melting, or

b) strong fractionation of mafic source rocks prior to separation of the trondhjemitic melt from the residue may account for the much steeper patterns displayed by the trondhjemites and leucotonalites.

Rock/primordial mantle LILE and HFSE patterns for the unfoliated leucocratic granites and quartz monzonite (Fig. 5.32g) from Y to Ba are very steep with pronounced troughs at Nb, P and Ti. Additional data (Nd) may well reveal that a further trough exists at Sr. This may also be true for two of the Bazane Porphyritic Trondhjemite Suite

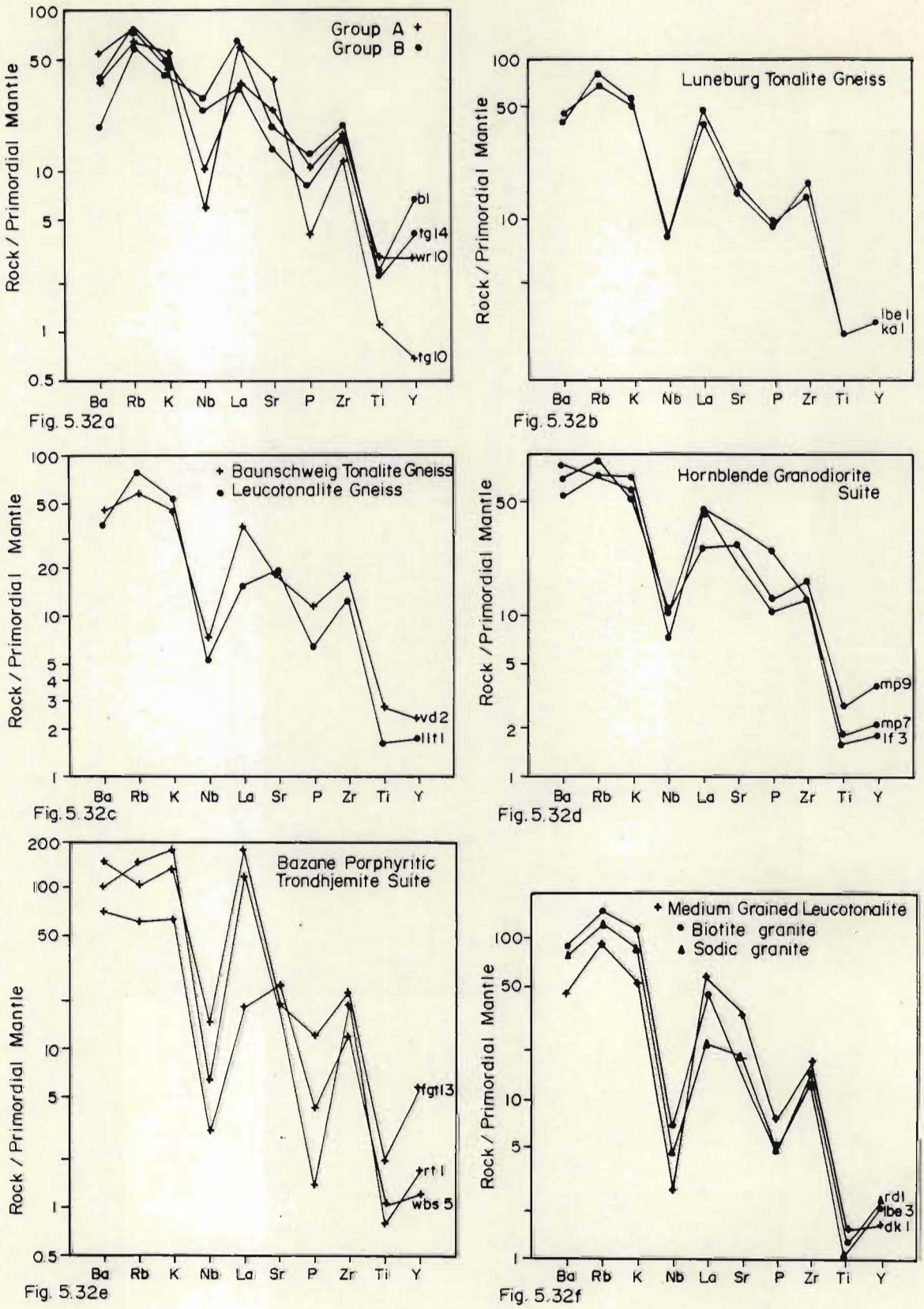

Fig. 5.32 Rock/primordial mantle LILE and HFSE patterns for
a) Layered Gneisses, b) Luneburg Tonalite Gneiss,
c) Braunschweig Tonalite Gneiss and Leucotoanlite Gneiss,
d) Hornblende Granodiorite Suite,
e) Bazane Porphyritic Trondhjemite Suite,
f) weakly foliated granitoids.
Primordial mantle values are from Wood et al. (1979a).

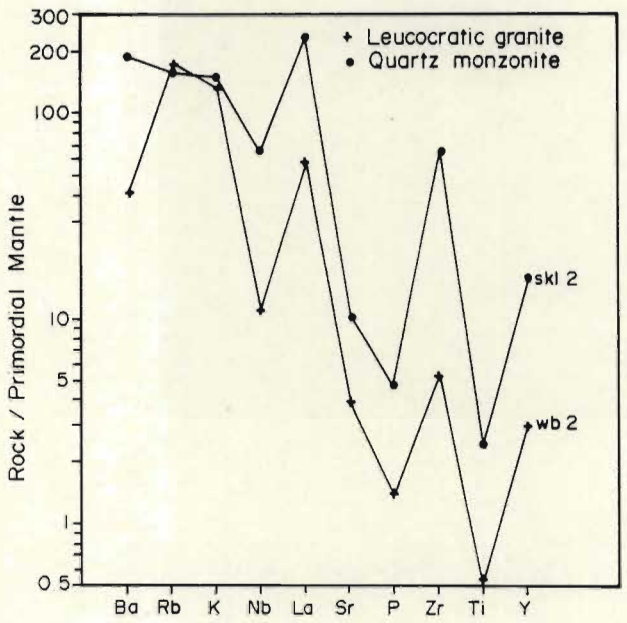

Fig.5.32 continued, Rock/primordial mantle LILE and HFSE patterns for g) unfoliated granitoids. Primordial mantle values from Wood et al. (1979a).

samples (Fig. 5.32e). The patterns are similar to those for samples RT1 and FGT3 of the Bazane Porphyritic Trondhjemite Suite. The unfoliated quartz monzonite (SKL2) shows a relatively strong enrichment in La, Y and Zr compared to compositionally similar rock types in the Bazane Porphyritic Trondhjemite Suite.

The much greater enrichment in LILE (Ba, Rb, K, Nb,La) and depletion in HFSE (P, Zr, Ti) in the unfoliated granitoids compared to the tonalites and trondhjemites suggests an origin through:

i) partial melting of siliceous crustal rocks resulting in a secondary enrichment of LILE and relative depletion of HFSE in the granitic melt.

ii) a very small proportion of partial melting of a mafic source, which is probably unlikely considering that the melt may be unable to separate from the residue and that the Sr/Ba ratios are < 0.5 (O'Nions and Pankhurst, 1978).

A Model for the Tonalitic and Trondhjemitic Gneisses.

The primordial mantle normalized LILE and HFSE trends in Fig. 5.32 suggest similar origins or sources for rocks of tonalitic and trondhjemitic composition. The genesis of these rock types is discussed within the constraints of the available data, as no unequivocal origin or source can be determined without additional data (REE's, Rb-Sr and O isotopes).

Arth (1979) indicates that for a trace element to be reliable as a genetic and tectonic indicator the measured abundances must reflect those of unaltered magma. He suggests that REE may be valid indicators but that Rb is not and the status of Ba and Sr is possibly unreliable. Condie and Hunter (1976) however have shown that where there is a strong coherance in the abundances of Rb, Sr and Ba, it suggests that use of these elements alone may not result in spurious conclusions.

Average K/Rb Rb/Sr and Sr/Ba ratios and their standard deviations for the different granitoids are presented in Table 5.9 which reveals that in some tonalites the standard deviations are relatively small. In

TABLE 5.9: TABULATED AVERAGE DATE FOR THE DIFFERENT GRANITOIDS

Rock-types	n	K/Rb $\bar{x}$	K/Rb s.d.	Rb/Sr $\bar{x}$	Rb/Sr s.d.	Sr/Ba $\bar{x}$	Sr/Ba s.d.
Layered Gneisses Group A	15	232	31	0.07	0.02	1.95	0.50
Group B	8	230	70	0.18	0.04	1.20	0.86
Luneburg Tonalite Gneiss	8	190	20	0.19	0.04	1.47	0.40
Leucotonalite Gneiss	6	222	30	0.14	0.02	1.65	0.36
Braunschweig Tonalite Gneiss	4	229	33	0.13	0.02	.133	0.18
Hornblende Granodiorte Suite							
granodiorite	3	257	25	0.16	0.04	1.01	0.15
tonalite	3	186	72	0.11	0.04	2.21	0.36
feldspathic amphibolite	3	197	42	0.08	0.01	1.50	0.29
Bazane Porphyritie Trondhjemite Suite							
trondhjemite	10	232	60	0.10	0.02	1.28	0.23
granodiorite	4	308	120	0.14	0.09	0.73	0.10
granite	2	275	105	0.35	0.05	0.50	0.03
quartz monzonite	3	386	33	0.16	0.04	0.48	0.06
Medium-grained Leucotonalite	4	210	48	0.08	0.03	2.35	0.09
Biotite Granite	2	244	10	0.37	0.13	0.44	0.27
Sodic Granite	2	245	32	0.21	0.16	1.02	0.67
Leucocratic Granite	3	203	67	1.86	0.81	0.27	0.03
Quartz Monzonite	1	263	-	0.60	-	0.16	-
Veins L15	1	329	-	0.05	-	2.11	-

the petrogenetic models discussed here average trace element abundances have been used for each of the granitoids. Partial melting models are constructed using the batch melting equation,

$Cl/Co = 1/(F + D(1 - F))$ from Hanson and Langmuir (1978) where

Cl is the concentration of a given element in the melt

Co is the concentration of a given element in the total system at the time a given process begins

F is the fraction of melt relative to the original system

D bulk solid/melt distribution coefficient for a given element or oxide at the time of removal of the melt from the solid phases and is given by :

$$Di = \sum_i XiKDi$$

where Xi is the modal proportion of the mineral and KDi is the partition coefficient for a particular element in that mineral.

In the partial melting models the source rocks are considered to have the composition of an enriched Archaean tholeiite (Sample TH2 from Condie, 1981) or an average Archaean low-alkali tholeiite (Condie and Hunter, 1976). Of the models tested for the Group B siliceous Layered Gneisses, Luneburg Tonalite Gneiss, Leucotonalite Gneiss and Braunschweig Tonalite Gneiss the best match exists for Rb, Sr, Ba, Rb/Sr and Ba/Sr in a model involving between 10 and 25 percent partial melting of an enriched Archaean tholeiite (EAT) with modal melting in the proportions hornblende = 78, plagioclase = 20, quartz = 2. The plagioclase amphibolite normalized trends (Fig. 5.33a) suggest that about 20% partial melting of a plagioclase amphibolite of EAT composition, would produce a liquid appropriate to the Luneburg Tonalite Gneiss, whereas lower degrees of partial melting (10 - 20%) of the same source could generate liquids of the composition of Group B trondhjemitic and leucotonalitic gneisses (Fig. 5.33a). The trace element distributions for the Leucotonalite Gneiss and Braunschweig Tonalite Gneiss suggest a model involving partial melting of between 10 and 20% and 20 and 30% respectively of plagioclase amphibolite of EAT composition (Fig. 5.33b). The Ba and Ba/Sr normalized values for some of the granitoids (Fig. 5.34) are greater than those of the model

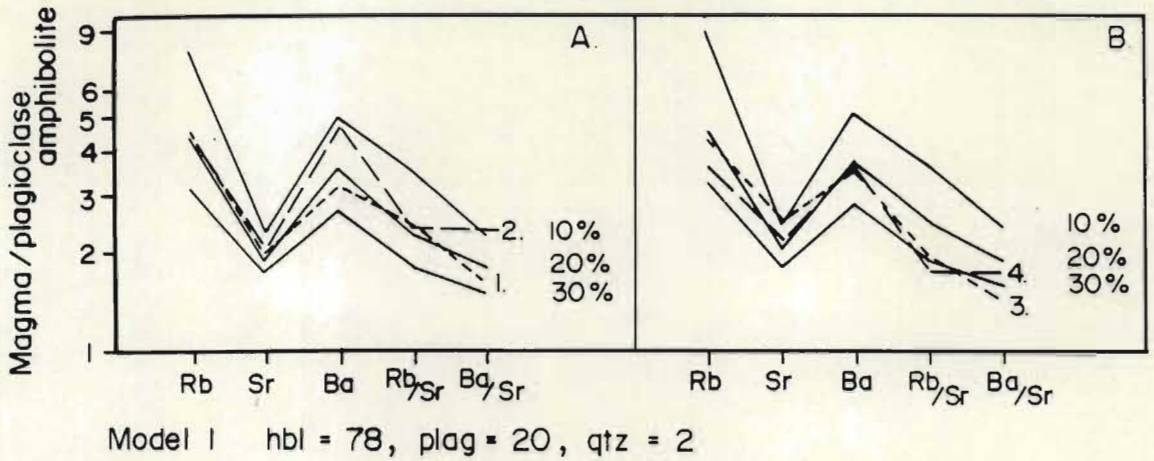

Fig. 5.33A MODEL 1: Plagioclase amphibolite normalized trace element distributions for the average Luneburg Tonalite Gneiss (1), and Group B Layered Gneiss (2); B) the Leucotonalite Gneiss (3), and Braunschweig Tonalite Gneiss (4), compared to those for a model tonalite produced by 10, 20 and 30% batch melting of plagioclase amphibolite. Plagioclase amphibolite composition assumed to be that for enriched Archaean tholeiite (Condie, 1981).

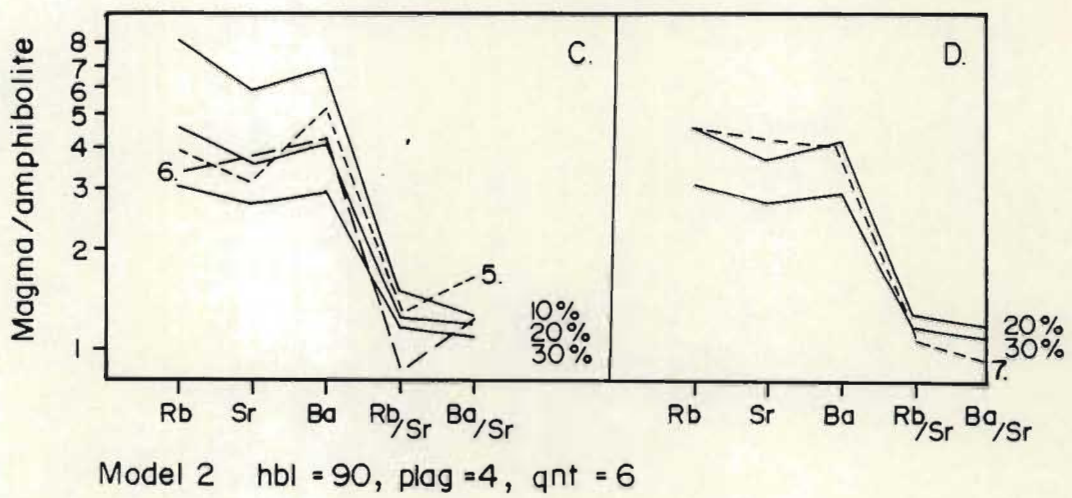

Fig. 5.33C MODEL 2: Amphibolite normalized trace element distributions for the average Bazane Porphyritic Trondhjemite (average of 9 trondhjemite samples), (5); average Group A Layered Gneiss (6); D) the average medium grained Leucotonalite (7) compared to those for 10, 20 and 30% batch melting of amphibolite. Amphibolite composition assumed to be that for enriched Archaean tholeiite (Condie, 1981).

partial melts which may be the result of a small proportion (1 - 2 modal %) of biotite not taken into account during the early stages of partial melting of the plagioclase amphibolite.

Of the models tested for the Group A Layered Gneiss none are adequate and the closest match is achieved in MODEL 2 involving partial melting of enriched Archaean tholeiite with modal melting in the proportions garnet = 6, hornblende = 90 and plagioclase = 4, (Fig. 5.33c). Similar trends are exhibited for trondhjemites of the Bazane Porphyritic Trondhjemite Suite (Fig. 5.33c) and for the medium-grained leucotonalite that intrudes the Luneburg Tonalite Gneiss for which melting between 10 and 20 % is envisaged.

An important difference between those gneisses having patterns broadly similar to MODEL 2 and those having patterns similar to MODEL 1 is that the former have much higher Sr contents for similar CaO abundances but have broadly similar Rb contents. These differences are reflected in the average Rb/Sr ratios (Table 5.9). Although no unequivocal answer is possible with the limited data available it is suggested that fundamental differences may exist between the source rocks for those gneisses with low and high Sr contents and that the proportion of plagioclase is lower in the parent rock that produces the tonalitic and trondhjemitic magmas with high Sr contents.

Field evidence suggests that the Hornblende Granodiorite Suite has assimilated amphibolites of the Commondale Supracrustal Sequence and that their relatively high Rb and Ba contents reflect incorporation of biotite and hornblende from the amphibolites, but it is not improbable that the uncontaminated magmas also owes its origin to partial melting of a plagioclase amphibolite source.

All the tonalitic and trondhjemitic gneisses have Sr/Ba ratios > 0.5 (Table 5.1 - 5.8) and the average Sr/Ba ratios for each rock type are presented in Table 5.10. Sr/Ba ratios > 0.5 are characteristic of those rock types derived from a mafic source whereas rocks with Sr/Ba ratios < 0/.5 are typically derived through partial melting of siliceous crustal rocks (O'Nions and Pankhurst, 1978).

Bazane Porphyritic Trondhjemite Suite:- The product of fractionating trondhjemitic magma.

In the previous section on the Bazane Porphyritic Trondhjemite Suite the suggestion that the granodioritic, granitic and quartz monzonitic components represent the products of fractionation of a trondhjemite magma was advanced. It should be noted that in the An-Ab-Or projection (Fig. 5.13) samples plot in an elongated field, roughly parallel to the Ab-Or tie line and that those samples of granodioritic and quartz monzonitic affinity plot close to the trondhjemite-granodiorite and granite-quartz monzonite joins, respectively.

The following arguments support an origin by fractionation of a trondhjemitic magma for at least some of the more evolved rock types. Samples from the western and eastern facies plotting from left to right on the Qz-Ab-Or projection (Fig. 5.21) show a reasonably consistent decrease in the An/Or ratio (Fig. 5.34) with the An content decreasing from 13.5 to 5% with increasing Or content that is suggestive of a fractional crystallization process. Samples from the western facies of the Bazane trondhjemite display a sympathetic and regular decrease in An with increasing Or (Fig. 5.34) but the samples from the eastern facies show a greater scatter. Samples RT2 and RT3 (both trondhjemites) in particular are displaced from the other eastern facies samples that have characteristically higher normative An contents at equivalent normative Or proportions.

Plots of Rb and Sr versus the Or/Ab ratio show coherent trends with respect to the western facies samples (Fig. 5.35). The eastern facies samples show a greater scatter particularly with respect to Sr (e.g. samples SKL1 and PD2) but nevertheless Rb increases and Sr decreases with increasing Or/Ab ratios. Strontium abundances plotted as a function of normative Or/Ab ratios are considered to be a measure of cotectic differentiation (Barker et al., 1976a). Barker et al. (1976a) have shown that, provided there is a consistent decrease in the An content towards the Or apex of the Qz-Ab-Or projection, the Sr versus normative Or/Ab curves reflect a process of differentiation, for example the Rio Brazos trondhjemite. The Twilight Gneiss, Colorado although displaying a decrease in Sr when plotted as a function of normative Or/Ab does not show a consistent decrease in normative An towards the Or apex of the Qz-Ab-Or projection as would

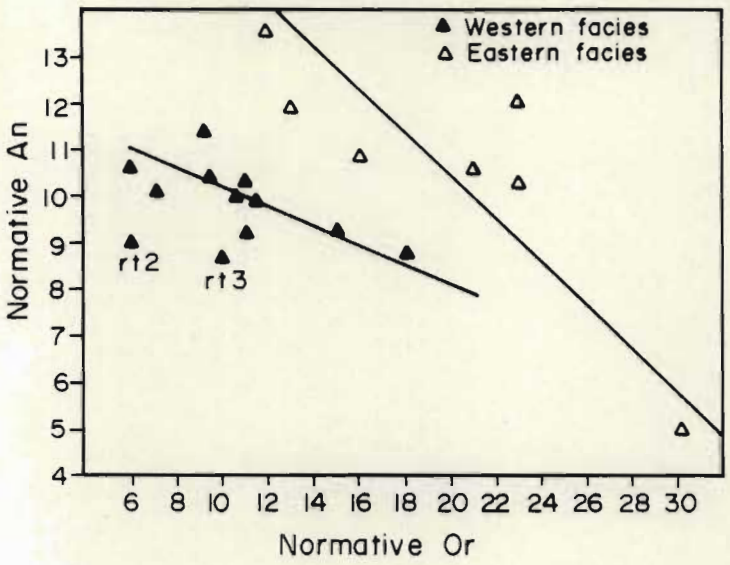

Fig. 5.34 Normative An as a function of normative Or showing a trend consistant with fractiontion for most of the samples from both the western and eastern facies of the Bazane Porphyritic Trondhjemite Suite.

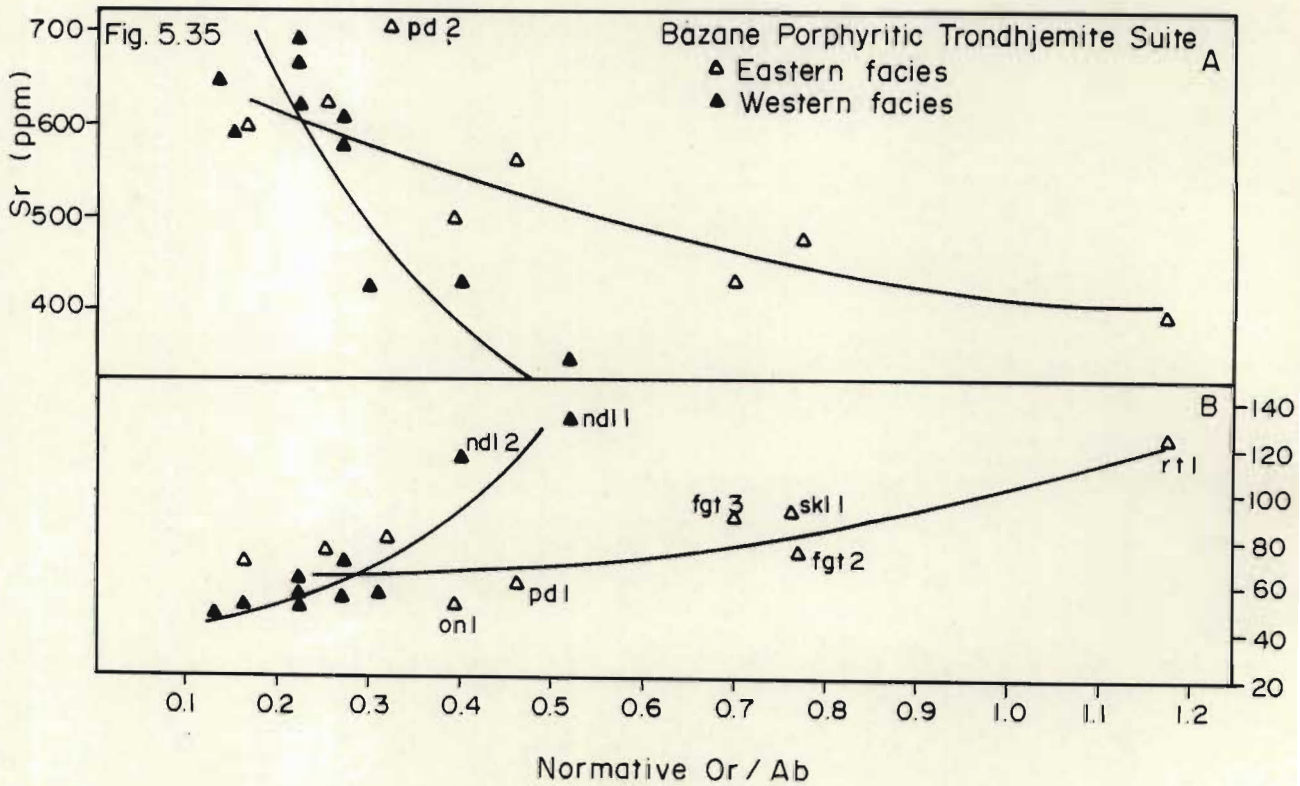

Fig. 5.35 Rb and Sr versus normative Or/Ab for the western and eastern facies of the Bazane Porphyritic Trondhjemite Suite.

be anticipated from fractional crystallization. The relationship between Sr and Or/Ab described here is similar to that for the Rio Brazos trondhjemite (Barker et al., 1976a). Differentiation is inferred only if there is a consistent decrease in normative An towards the Or apex in the Qz-Ab-Or projection. The coherance of Rb with Or/Ab ratios may be the result of differentiation and/or alkali exchange in which Rb follows K (Barker et al., 1976a).

A fundamental difference between the western and eastern facies Bazane trondhjemite suite is reflected in the higher normative An content of the eastern facies at similar normative Or contents. In Fig. 5.36 the compositions of different components are plotted in the An-Ab-Or-Qz-H_2O system at PH_2O = 5kb (Winkler, 1979). The probable crystallization curves have been drawn through the plot and for the western facies (Fig. 5.36a) the crystallization sequence is consistent with the petrography. In the eastern facies (Fig. 5.36b) the higher An content compared to the eastern facies is clearly indicated and except for the 2% hornblende in one of the quartz monzonites, SKL1, the crystallization sequence is consistent with petrography. One of the quartz monzonite samples, FGT2 lies along the crystallization path and the other two samples (FGT3 and SKL1) lie along the ternary cotectic, which is consistent with the petrography.

Modelling the path of a fractionating trondhjemitic liquid was also tested using the Rayleigh fractionation equation $Cl/Co = F^{(D-1)}$. The modelled path starting from a trondhjemite with a low Rb/Sr ratio shows reasonable coherance and consistency with the phase diagram constraints (Figures 5.21 and 5.36). The K/Rb, Sr/Ba and Rb/Sr ratios (Fig. 5.24, 5.25 and 5.26) all define reasonably well-constrained regression curves that are consistent with fractionation. The elongation of the field of the Bazane trondhjemite approximately parallel to the plagioclase vector (Beckinsale, 1979) on the Rb/Sr diagram suggests plagioclase control of fractionation. This is consistent with the phase diagram (Fig. 5.36).

As discussed in the previous section the Bazane trondhjemite is considered to have originated through partial melting of a basaltic source (MODEL 2; amphibolite of enriched Archaean tholeiite composition). The Sr/Ba ratios are consistent with this interpretation. The range in Sr/Ba ratios between 5.0 and 0.50 (Fig.

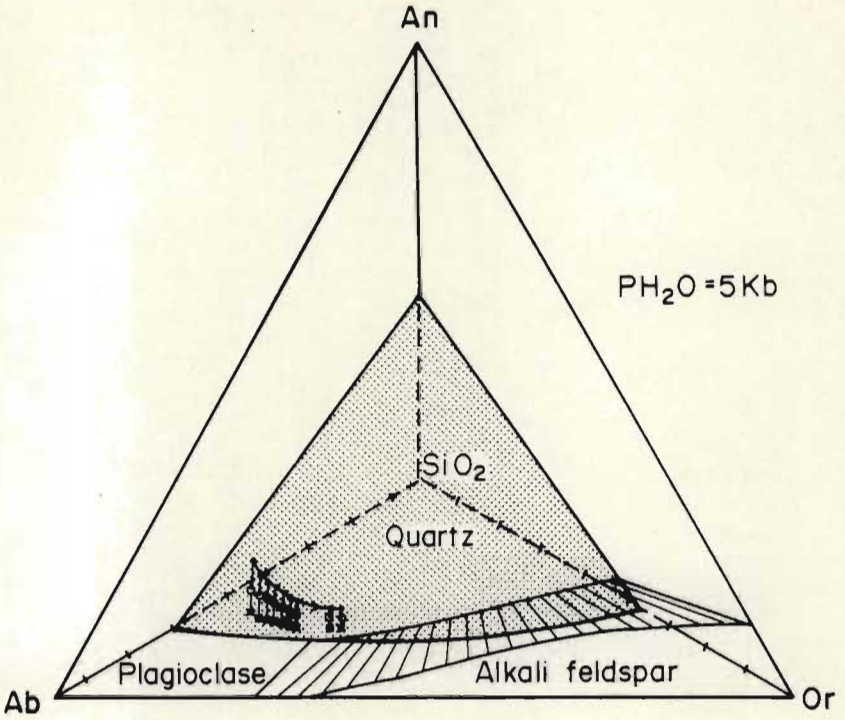

Fig. 5.36a Crystallization path for the western facies of the Bazane Porphyritic Trondhjemite Suite. The predicted phase relationships in the system An-Ab-Or-$Si0_2$-H_20 are those of Winkler (1979).

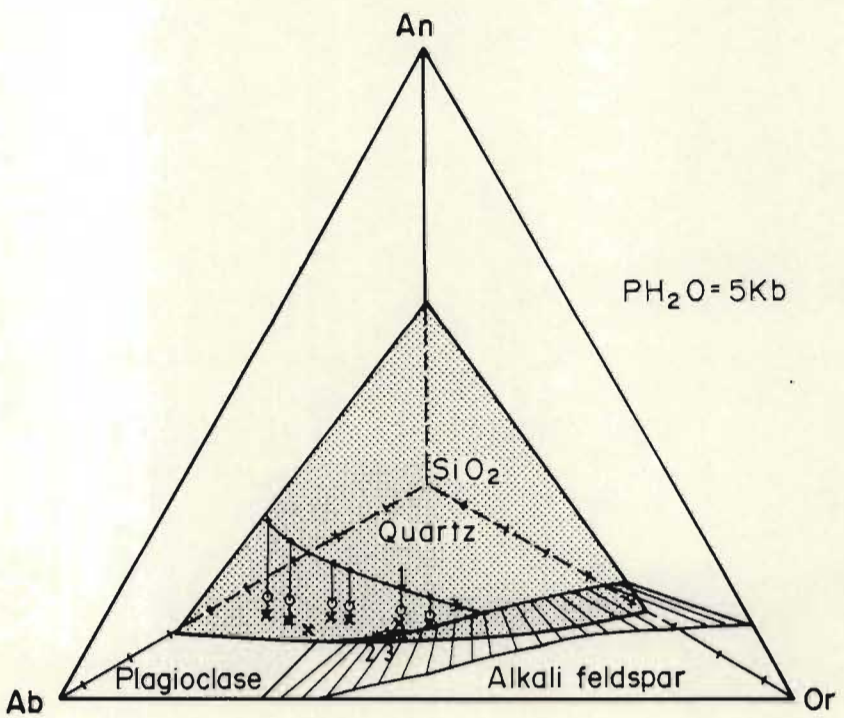

Fig. 5.36b Crystallization path for the eastern facies of the Bazane Porphyritic Trondhjemite Suite. The predicted phase relationships in the system An-Ab-Or-$Si0_2$-H_20 are those of Winkler (1979). 1 = FGT2, 2 = FGT3, 3 = SKLI.

5.25) are consistent with fractionation of a trondhjemitic liquid to produce the more potassic varieties. The Sr/Ba ratios of < 0.50 for two samples, NLD1 and FGT3 may be accounted for through strong fractionation of a trondhjemitic liquid.

Weakly Foliated Granitoids.

This suite comprising leucotonalitic and granitic rock types intrudes the Luneburg Tonalite Gneiss in the complex manner described in Chapter 3. The medium-grained leucotonalite has been interpreted as the product of 10 - 20% partial melting of amphibolite. The granitic varieties may however, be either the product of very small degrees of partial melting of amphibolite or alternatively represent fractionation of a leucotonalitic magma. Direct derivation of granitic rocks from an ultrmafic or low Sr source is unlikely since their Sr contents and Sr/Ba ratios (< 0.5) would require separation of very small degrees of melt (< 0.1%), with a very high proportion of plagioclase in the residue (O'Nions and Pankhurst, 1978).

On the Qz-Ab-Or projection the samples lie in the plagioclase + quartz + liquid + vapour field (Fig. 5.28). A plot of normative An versus Or (Fig. 5.37) suggests that the sodic and biotite granites are the products of a fractionating leucotonalitic magma. The Sr versus normative Or/Ab plot indicates that the leucotonalite and biotite granite lie along a well-constrained regression line whereas that for the leucotonalite and sodic granite is less well-constrained (Fig. 5.38). Plots of the K/Rb, Sr/Ba and Rb/Sr indicate that the samples lie along reasonably well-constrained regression lines (Figures 5.29, 5.30 and 5.31) that are consistent with fractionation. The elongation of the field of these granitoids sub-parallel to the plagioclase vector (Fig. 5.31) suggests that if fractionation occurred, plagioclase was a dominant phase.

At the present level of erosion biotite granites are volumetrically more abundant than the tonalites. This would seemingly preclude fractionation unless the biotite granites represent a hood cover to the tonalitic intrusions that are extensive at depth. More data are required to test the hypothesis that the leucotonalitic rocks were derived through partial melting of amphibolites and that the granitic varieties represent the products of subsequent fractionation.

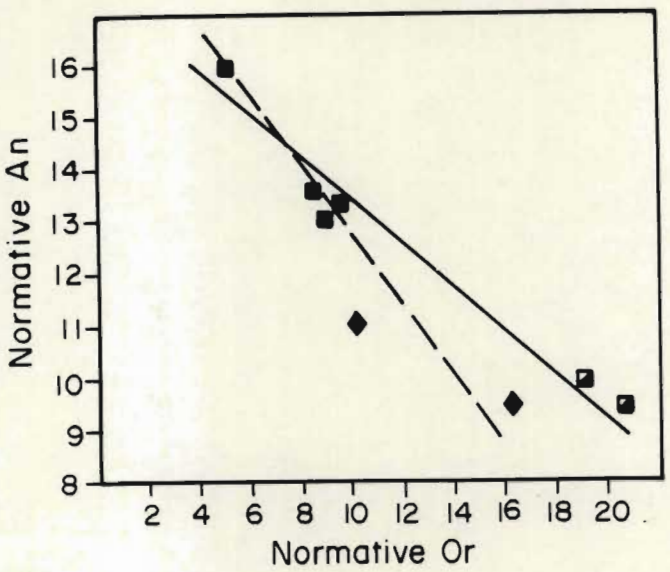

Fig. 5.37 Normative An plotted as a function of normative Or for the weakly foliated granitoids. Symbols same as in Fig. 5.28.

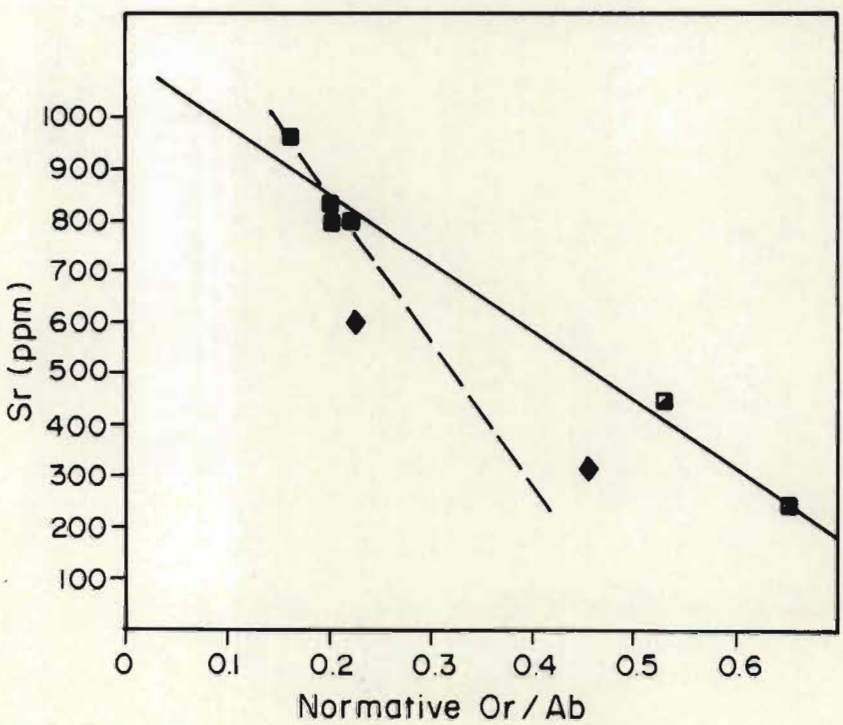

Fig. 5.38 Strontium versus normative Or/Ab for the weakly foliated granitoids. Symbols same as in Fig. 5.28.

Unfoliated Granitoids.

Major element abundances in the leucocratic granites show limited variation but in contrast trace element contents are highly variable. The low Sr/Ba ratios between 0.24 and 0.30 of the leucocratic granites and 0.16 for the quartz monzonite suggest an origin through partial melting of siliceous crustal rocks (O'Nions and Pankhurst, 1978).

Non-modal batch melting models using 10 - 30% melting of tonalitic and trondhjemitic sources were unsuccessful in obtaining trace element proportions similar to those in the leucocratic granites and quartz monzonites. The very low absolute amounts of Sr especially in the leucocratic granites suggests that plagioclase was a residual phase in the source. It should also be recognized that, if these rocks crystallized from liquids formed through partial melting of, for example, Layered Gneisses, various admixtures of tonalite, trondhjemite, granodiorite and amphibolite could produce a range of trace element abundances which would differ from those yielded by the trondhjemite or tonalite used in the model calculations.

If it is assumed that the leucocratic granites solidified from liquids derived by partial melting of siliceous Layered Gneisses in which hornblende is present as a residual phase, the leucocratic granites would have lower K/Rb ratios than those in the source. However small to moderate degrees of partial melting should not significantly alter the K/Rb ratio of the melt (Carmichael et al., 1974). The K/Rb ratios for the leucocratic granites are within the same range as those for the Layered Gneisses but the much higher Rb/Sr ratios in the leucocratic granites reflect the low An component of the plagioclase and the relatively high K_2O content of the leucocratic granites which suggest that small degrees of partial melting of siliceous crust could conceivably produce liquids with K/Rb and Rb/Sr ratios similar to those for the leucocratic granites.

Three samples with variable trace element abundances are however inadequate to speculate unequivocally about the origins of these rocks.

SUMMARY AND CONCLUSIONS

Lack of REE, and Rb and Sr isotopic data militate against identifying unequivocally the origin and petrogenesis of the tonalitic and trondhjemitic gneisses. However available data suggest the following scenario:-

i) The gneiss terrane in the study area is composed almost entirely of leucotonalitic, tonalitic and trondhjemitic gneisses. The Layered Gneisses comprise a bimodal suite of trondhjemitic and tonalitic gneisses interlayered with subordinate, geochemically variable amphibolites.

ii) The Hornblende Granodiorite Suite comprising amphibolites, tonalite and granodiorite of sub-alkaline affinity may reflect a period of extensional tectonics postdating the Gneiss Complex and the intrusion of the Bazane Porphyritic Trondhjemite Suite.

iii) The similarity in the primordial mantle normalized LILE and HFSE patterns for the tonalitic, trondhjemitic and granodioritic gneisses suggest that these are crystallization products of liquids derived from broadly similar sources.

iv) Ten to thirty percent batch melting of plagioclase amphibolite of EAT composition (MODEL 1) could produce liquids similar to those from which the Group B Layered Gneisses, Luneburg Tonalite Gneiss, Leucotonalite Gneiss and Braunschweig Tonalite Gneiss crystallized.

v) Ten to thirty percent batch melting of amphibolite of EAT composition (MODEL 2) could produce liquids from which Group A Layered gneisses, Bazane trondhjemites and the medium-grained leucotonalite crystallized.

vi) The primordial mantle normalized LILE and HFSE patterns of the subordinate unfoliated granitoids (leucocratic granite and quartz monzonite are similar to those of the tonalitic gneisses as a whole and possibly reflects small degrees of partial melting (10 - 20%) of siliceous crustal rocks.

vii) Trace element distributions in the Bazane Porphyritic Trondhjemite Suite and phase diagrams suggest that most of the samples in this suite could represent the products of fractionation of a trondhjemitic liquid.

viii) Phase diagrams and trace element distributions suggest that the biotite and sodic granites may represent crystallization products from a fractionating leucotonalite magma.

ix) Sr/Ba ratios for all the trondhjemitic and tonalitic gneisses are > 0.5 and consistent with the models suggesting an amphibolitic source for these rock types. Sr/Ba ratios of < 0.5 for the leucocratic granite and quartz monzonite (SKL2, unfoliated granitoids) are consistent with an origin involving small degrees of partial melting of siliceous crust.

x) The Rb/Sr crustal thickness index (Condie, 1973) suggests an increase in crustal thickness through the Archaean, especially during the period in which the Bazane Trondhjemite Suite was intruded. These curves also suggest that most of the tonalitic melts were derived at depths between 20 and > 30km. At these depths pressures would be between 5 and 8 Kb and basaltic source rocks would be metamorphosed at amphibolite facies.

CHAPTER 6

COMMONDALE SUPRACRUSTAL SUITE

Introduction

The Commondale Supracrustal Suite underlies an area of approximately 100km^2 and is preserved in two major synformal keels separated by a major shear zone (MAP 2). The Commondale Suite extends southwestwards from east of the Paulpietersburg-Moolman road to south of the Pongola River where it is attenuated to a narrow septa between lobes of the intrusive Bazane Porphyritic Trondhjemite Suite (MAP 2).

The supracrustals are characterized by a predominance of amphibolites, tremolite-actinolite schists, talc-magnesite schists, serpentinites and subordinate banded iron formation (BIF), massive fuchsitic quartzites, argillites, calc-silicates, and mafic and ultramafic intrusive rocks. In the core of the Commondale synform is a 640m thick suite of cumulate and spinifex-textured peridotites that are discordant to the dip of the layering in the volcano-sedimentary pile. These rock-types are now referred to as the Matshempondo Peridotite Suite. The paucity of unequivocal way-up structures and distinct marker units over much of the area underlain by the supracrustal sequence militates against the identification of a stratigraphy.

The objectives of the mapping of the Commondale Supracrustals were to:

i) provide a brief first account of the rock-types that are now ascribed to the Commondale Supracrustal Suite
ii) characterize geochemically the various mafic and ultramafic rock-types
iii) compare structures in the supracrustals to those in the adjacent granitoids
iv) to establish relative ages between the supracrustals and the granitoids.

The main emphasis of this chapter is a description of the mafic and ultramafic volcanics. The field relations and geochemistry of the Matshempondo Peridotite Suite are described in a subsequent chapter (Chapter 7). The structure of the Commondale Supracrustal Suite forms

the subject of a detailed discussion in Chapter 8.

Field Relations

Over much of the area underlain by supracrustal rocks outcrop is extremely poor and in the central portion of the belt is restricted to two major synforms, the Commondale and Nederland synforms (MAP 2). In the Commondale synform units of banded iron formation (BIF) up to 50m thick are interlayered with foliated serpentinites and amphibolites in the fold closure whereas, along the northern limb of the synform, BIF is interlayered with fine-grained grey argillites and massive quartzites (MAP 2). The BIF is characterized by alternating iron-rich (magnetite, haematite) and silica-rich layers (recrystallized quartz) between 1mm and 10cm thick. The core of the Commondale synform comprises the Matshemdpondo Peridotite Suite.

An isolated pavement of highly deformed pillow lavas metamorphosed at amphibolite grade is exposed east of the Commondale-Moolman road (MAP 2). The pillows have light-coloured rims and dark cores. They are now elllipsoid in shape with length to width ratios between 5:1 and 10:1. Cuspate margins recognized at triple junctions between pillows suggests a younging direction to the southwest. This is the only locality where primary textures are preserved in the amphibolites and tremolite-actinolite schists but, on the basis of field relations with other supracrustal rocks, the amphibolites and tremolite actinolite schists are interpreted to be volcanic in origin. Supracrustal rocks along the northeastern margin of the belt are intruded by the Hornblende Granodiorite Suite on Lanfontein 182HT and Mooiplaats 206HT (MAP 2).

The core of the Nederland synform on the farm Mooiplaats 206HT comprises foliated amphibolites interlayered with subordinate BIF and a thin fine-grained grey argillite unit (MAP 2). Further west on Nederland 202HT the same synform is defined by four continuous steeply dipping BIF units interlayered with amphibolites, fuchsitic quartzites, serpentinites, tremolite-actinolite schists and lenses of BIF. A broad zone up to 500m wide comprising talc-magnesite and tremolite-actinolite schists and resistant pods of serpentinite is strongly sheared on the southern limb of the Nederland synform (MAP 2). The western limb of this synform is intruded by the Bazane

Porphyritic Trondhjemite Suite.

Layered sill-like intrusions consisting of dunite, harzburgite, quartz gabbro and quartz diorite crop out in the Nederland synform 300m west of the eastern boundary of the farm Nederland 202HT (MAP 2). The thickness of individual layers range between approximately 12 and 20m. Dunite is commonly strongly foliated. It comprises relict original olivine grains up to 5mm in diameter that are totally altered to serpentine + talc + magnetite. Harzburgites are composed of anhedral rounded and euhedral relict olivine grains up to 20mm in diameter set in a finer-grained groundmass originally consisting of olivine and subhedral pyroxene grains up to 3mm in length. The characteristically fractured olivine grains are totally altered to serpentine + talc + magnetite and the pyroxene to tremolite and chlorite. Quartz gabbro and quartz diorite are medium-grained rocks in which pyroxene and plagioclase are partially altered to tremolite + chlorite and saussurite (chlorite, epidote, zoizite) respectively. The coarse grain size, cumulate textures and mineralogy are consistent with an intrusive origin for these rock-types. The sills were inserted prior to deformation and rotated to their present vertical dips during the deformations that resulted in the development of the Nederland synform.

In the attenuated septa astride the Pongola River the supracrustal rocks are preserved predominantly in synformal and antiformal structures separated by shears (MAP 2). Many of the ultramafic rocks are represented by tremolite-actinolite schists and talc-magnesite-chlorite schists that in some areas enclose more resistant pods of serpentinite. BIF is the only sedimentary rock present in this area. Astride the Pongola River at the western contact with the Bazane Porphyritic Trondhjemite Suite strongly foliated amphibolites up to 2m thick alternate with tremolite-actinolite schists up to 1.5m thick over a distance of approximately 75m.
The supracrustal suite crops out over a width of 240m at its southwestern extremity on the farm Politiek 29HT (MAP 2). Here the suite comprises highly deformed vertically dipping serpentinites, amphibolites, tremolite-actinolite and talc-magnesite-chlorite schists in which isoclinal folds are common.

Intervening between these rock-types is a 10 to 20m thick vertically

dipping ferruginous sediment comprising layers 1 to 6mm thick rich in magnetite and haematite alternating with muscovite + quartz-rich and tremolite-rich layers 1 to 2mm thick. At this locality calc-silicates and amphibolites are characteristic along the western contact with the Bazane Porphyritic Trondhjemite Suite. The calc-silicate rock-types are composed of layers of euhedral grains of diopside up to 10mm long, plagioclase, wollastonite and grossularite alternating with plagioclase-and quartz-rich layers that contain a small proportion of diopside. In thin section the garnet has very high to extreme relief and is light emerald green in colour. Single grains up to 0.2mm in diameter and aggregates of rounded grains are isotropic although the rims of some grains are birefringant in low first order greys. Although garnets are generally isotropic some varieties are not uncommonly birefringant (Heinrich, 1965).

The metavolcanic and calc-silicate rocks adjacent to the intrusive granitoids are metamorphosed typically at amphibolite grade over distances of 100 to 250m from the contacts. Amphibolites are also common in the cores of the Nederland and Commondale synforms. Amphibolite facies assemblages therefore reflect not only the effects of thermal metamorphism adjacent to the intrusive granitoids but also those of regional metamorphism. Later retrograde metamorphism at greenschist grade is also common throughout the supracrustal remnant.

Geochemistry

Sample localities

Three suites comprising a total of twenty samples were collected from different localities. The suite of samples, numbered SP2 to SP12 and comprising amphibolites and tremolite-actinolite schists, was collected from outcrops in the Pongola River on Vrye Gunst 201HT (MAP 1 and Fig. 6.1). Samples C1 and C5 (amphibolite) and C2 and C3 (serpentinite) were collected from between the BIF and Matshempondo Peridotite Suite on Mooiplaats 206HT (MAP 1). Another suite of samples was collected on Politiek 29HT (MAP 1), the locations of the samples being shown in Fig. 6.1. Three of these samples (L1 - L3) are calc-silicate rocks. The other samples (L6 and L7) are tremolite-actinolite schists, L5 is a serpentinite and L4 is an amphibolite. Three of the samples (L5, C2 and C3) albeit pervasively altered to talc + tremolite + magnetite and in the case of C2 and C3 strongly

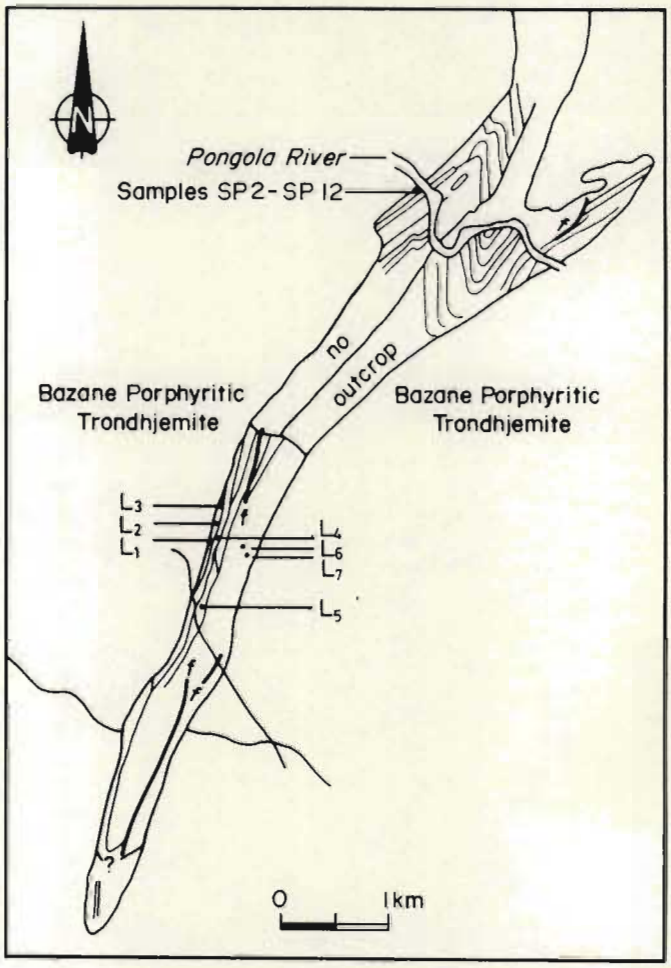

Fig. 6.1 Portion of MAP 1 showing sample localities for the SP and L suites of samples.

foliated are recognizable as original olivine cumulates.

Major and trace elements

The amphibolites are characterized by MgO contents between 8.5 and 13.5 wt. %. SiO_2 varies between 52 and 56 wt. %. CaO and TiO_2 contents vary from ~9 to 12.5 wt. % and ~0.5 to 1.1 wt. % respectively (Table 6.1).

The tremolite-actinolite schists have MgO contents between ~21 and 25 wt. %. SiO_2 contents vary between ~50 and 52 wt. % whereas Al_2O_3 ranges from ~3.5 to 7.4 wt. %. TiO_2 contents are between ~0.3 and 0.4 wt. % and CaO contents between ~7 and 10 wt. % (Table 6.2).

The serpentinites are characterized by high MgO contents between ~38 and 44.5 wt. %. SiO_2 contents are between ~45 and 48.5 wt. % while Al_2O_3 ranges from ~0.5 to 4.6 wt. %. CaO and TiO_2 contents range from ~0.6 to 4.5 wt. % and 0.06 to 0.2 wt. % respectively (Table 6.2).

Calc-silicate rocks from the same unit (Fig. 6.1) have SiO_2 content between ~52 and 55 wt. % while Al_2O_3 varies between ~6 and 11 wt. %. Average CaO and MgO contents are approximately 20 and 9.5 wt. % respectively. The average Cr content is ~0.5 wt. % (Table 6.3).

The amphibolites, tremolite-actinolite schists and serpentinites occupy the fields of basaltic komatiite and peridotitic komatiite respectively on a Jensen (1976) diagram (Fig. 6.2). Because of their relict cumulate textures and high MgO contents the serpentinites (C3, C2 and L5) are referred to as peridotites. The basaltic komatiites, peridotitic komatiites and peridotites (C3 and C2) plot on the same trend as similar rock-types from the Onverwacht Group (Jahn et al., 1982), and above that of Ordivician low Ti komatiitic and boninitic rock-types from Betts Cove (Upadhyay, 1982). Sample L5 plots in the field of the characteristically low Ti, high Al Matshempondo Peridotite Suite (Fig. 6.2). The fields defined on Jensen (1976) plots by the komatiites from the Barberton, Murchison, Pietersburg and Johannesburg greenstone belts in Figures 4.6 and 4.7 in Viljoen et al. (1982) are incorrect as oxide proportions of the components rather than cation proportions were used. These oxide trends plot parallel to but ~5% higher (towards Fe + Ti apex) than that of Jahn et al.

TABLE 6.1 MAJOR AND TRACE ELEMENT ANALYSES OF BASALTIC KOMATIITES FROM THE COMMONDALE SUPRACRUSTAL SUITE

	C1	C5	SP2	SP4	SP6	SP8	SP12	L4
SiO_2	52.79	53.40	54.16	55.62	55.95	55.36	55.31	51.99
Al_2O_3	4.99	7.71	10.80	7.58	7.28	7.55	9.20	9.17
Fe_2O_3	1.79	1.15	1.28	1.31	1.23	1.37	1.47	1.43
FeO	14.53	9.33	10.37	10.58	9.99	11.11	11.91	11.62
MnO	0.33	0.19	0.18	0.19	0.21	0.21	0.22	0.24
MgO	12.38	13.62	10.56	11.75	12.14	10.97	8.57	10.52
CaO	12.12	12.02	9.11	10.30	10.12	10.45	9.06	12.43
Na_2O	0.20	1.27	2.60	1.72	1.54	1.72	2.90	1.22
K_2O	0.32	0.20	-	0.56	0.72	0.54	0.27	0.67
TiO_2	0.5661	0.4681	0.6586	0.5916	0.6296	0.6410	0.7201	1.1062
P_2O_5	0.03	0.03	0.05	0.05	0.04	0.04	0.05	0.14
C_2O_3	0.1700	0.2108	0.0922	0.1668	0.1838	0.1299	0.0504	0.1155
NiO	0.0330	0.0445	0.0222	0.0269	0.0292	0.0253	0.0147	0.0327
TOTAL	100.24	99.64	99.88	100.45	100.05	100.10	99.73	100.69
LOI	0.58	0.59	0.90	0.55	0.60	0.63	0.52	0.40
Nb	1.9	1.2	3.1	2.6	2.0	1.4	3.9	7.3
Zr	37.1	33.7	50.6	55.2	44.8	47.9	49.6	75.4
Y	14.2	12.3	16.9	14.8	14.2	16.7	15.7	20.1
Sr	38.6	80.4	44.4	61.7	123.3	112.0	98.9	126.5
Rb	7.7	11.2	13.4	27.3	37.3	26.5	17.3	15.5
V	170.9	23.3	324.4	217.0	228.6	225.1	255.9	253.7
Ba	63.9	54.8	43.9	54.7	94.1	75.7	72.0	n.d.
Zn	88.5	83.3	112.0	109.9	99.0	111.5	124.0	125.2
Cu	35.3	88.1	108.5	121.9	118.1	137.9	164.8	64.2
Ni	237.5	326.0	173.1	201.0	213.4	194.2	114.5	238.5
Cr	1283	1471	656	1270	1361	959	372	872

- below detection limit

TABLE 6.2 MAJOR AND TRACE ELEMENT ANALYSES FOR PERIDOTITIC KOMATIITES FROM THE COMMONDALE SUPRACRUSTAL SUITE

	SP3	SP5	SP9	SP11	L6	L7	C2	C3	L5
SiO_2	50.34	52.75	52.05	52.42	50.54	51.71	45.25	44.78	48.43
Al_2O_3	7.36	3.26	4.66	3.52	4.30	4.28	0.53	1.93	4.60
Fe_2O_3	1.28	1.26	1.24	1.19	1.31	1.34	1.10	1.11	0.69
FeO	10.39	10.24	10.01	9.62	10.60	10.83	8.90	9.00	5.62
MnO	0.19	0.14	0.25	0.15	0.19	0.20	0.07	0.20	0.11
MgO	21.33	24.91	21.51	24.12	25.04	21.20	44.77	37.95	39.39
CaO	9.25	7.06	10.03	9.30	7.74	10.19	0.68	4.48	2.58
Na_2O	-	-	-	-	-	-	-	-	-
K_2O	0.02	-	0.02	-	-	0.05	-	-	-
TiO_2	0.3952	0.2786	0.3932	0.3247	0.3202	0.4117	0.0789	0.2123	0.0626
P_2O_5	0.03	0.02	0.02	0.01	0.02	0.02	-	0.01	-
Cr_2O_3	0.3543	0.5674	0.4079	0.3161	0.4591	0.3722	0.2362	0.2367	0.4025
NiO	0.1064	0.1611	0.0858	0.1016	0.1424	0.1158	0.3557	0.2946	0.2226
TOTAL	101.04	100.65	100.67	101.08	100.66	100.73	101.96	100.20	102.11
LOI	2.83	3.27	1.89	2.40	3.54	1.82	12.86	10.85	9.99
Nb	2.2	0.2	2.5	1.9	1.5	0.2	0.7	-	1.2
Zr	28.4	25.2	28.6	23.6	26.0	26.5	8.8	17.8	8.4
Y	11.0	7.1	8.1	9.2	11.1	9.8	-	0.3	3.9
Sr	11.6	24.4	20.0	43.7	39.3	46.9	5.9	13.9	9.9
Rb	3.9	5.5	5.2	5.4	11.6	6.0	5.6	0.1	4.9
V	234.8	101.8	139.7	125.3	117.4	143.1	23.3	68.0	81.7
Ba	7.1	19.8	29.4	32.1	10.1	9.9	20.3	9.6	n.d.
Zn	111.0	99.0	131.9	67.7	69.5	74.5	26.9	96.1	37.3
Cu	63.3	118.1	196.5	59.7	7.30	138.6	1.1	21.1	1.6
Ni	768.4	213.4	657.7	802.6	1117.1	874.3	2693.3	1976.1	1640.3
Cr	2998	4156	3099	2467	3256	2798	1471	1830	3247

- below detection limit

TABLE 6.3 MAJOR AND TRACE ELEMENT ANALYSES OF CALC-SILICATES FROM THE COMMONDALE SUPRACRUSTAL SUITE

	L1	L2	L3
SiO_2	55.10	55.20	51.66
Al_2O_3	6.08	11.17	11.17
Fe_2O_3	0.64	0.52	0.76
FeO	5.15	4.22	6.16
MnO	0.76	0.61	0.45
MgO	10.03	8.68	9.69
CaO	21.34	18.37	19.50
Na_2O	0.30	0.96	0.97
K_2O	0.80	0.54	0.40
TiO_2	0.1056	0.1719	0.1687
P_2O_5	0.01	0.01	0.01
Cr_2O_3	0.6176	0.4880	0.4930
NiO	0.0818	0.0753	0.0730
TOTAL	100.90	101.00	101.49
LOI	0.86	1.17	1.21
Nb	0.5	-	-
Zr	11.1	15.8	13.8
Y	8.6	9.7	9.7
Sr	70.7	125.3	207.8
Rb	49.5	37.0	14.1
V	109.4	184.6	186.7
Zn	194.3	96.5	142.8
Cu	4.3	6.4	27.5
Ni	595.3	422.5	540.8
Cr	4488	3526	3804

- below detection limit

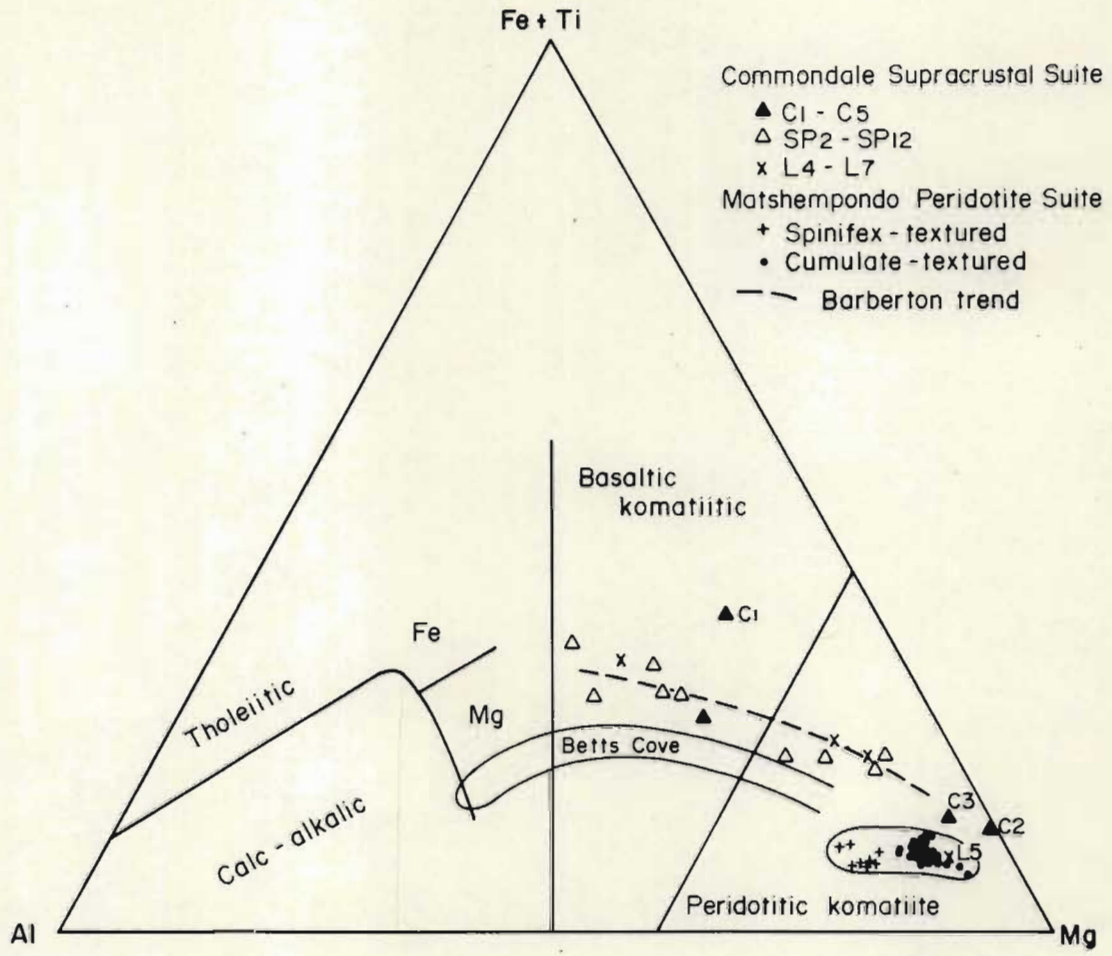

Fig. 6.2 Jensen (1976) cation plot for rock-types from the Commondale Supracrustal Suite and Matshempondo Peridotite Suite. The trend for Barberton is from Jahn et al. (1982) and that for Betts Cove from (Upadhyay, 1982).

(1982) defined by cation proportions.

Major and trace element abundances plotted against MgO for the basaltic and peridotitic komatiites are compared in Fig. 6.3. The most important feature is the compositional gap between ~14 and 20% MgO. Whether this gap reflects a true compositional break between basaltic komatiites and peridotitic komatiites is uncertain with the limited data available. However pronounced compositional gaps have been reported over a similar range of MgO contents from other greenstone belts where a far greater number of samples have been analysed e.g. Nisbet et al. (1977), Binns et al. (1982), Viljoen et al. (1982).

Plots of SiO_2, CaO and Rb versus MgO are scattered for both the basaltic komatiites and peridotitic komatiites. TiO_2, Al_2O_3, FeO, P_2O_5, Zr, Ni, Cr, V, Y and to a lesser extent Nb and Zn plotted against MgO display separate trends for the basaltic komatiites and peridotitic komatiites that appear consistent with fractionation (Fig. 6.3). The higher MgO contents and Mg : Fe ratios (~2) and lower incompatible element contents of the peridotitic komatiites, compared to the basaltic komatiites (Mg : Fe ~ 1), suggests that, if they were derived from a common source, the degree of partial melting required would be significantly different to produce the respective rock-types (Beswick, 1982).

Incompatible element ratios may be used to evaluate whether the Commondale komatiitic rocks were derived from a common source. Incompatible elements plotted against Ti and Zr in Fig. 6.4 define linear trends parallel to, but less than chondritic ratios. In figures 6.4a, b, c and d, Al_2O_3, Ti, V and Y are depleted with respect to Zr or Zr is enriched relative to these elements and oxides. In Figures 6.4e and f, V and Al_2O_3 are depleted with respect to Ti or Ti is enriched relative to these elements and oxides. Except for the Ti/Zr plot (Fig. 6.4b) where samples (C6 - C15) from the Matshempondo Peridotite Suite fall on the same trend as that of the Commondale Suite, interelement ratios in the latter are typically greater than the chondrite ratios. In contrast interelement ratios in the Matshempondo Peridotite Suite are typically less than chondrite. Sample L5 has major and trace element chemistry and incompatible element ratios similar to that for the Matshempondo Peridotite Suite

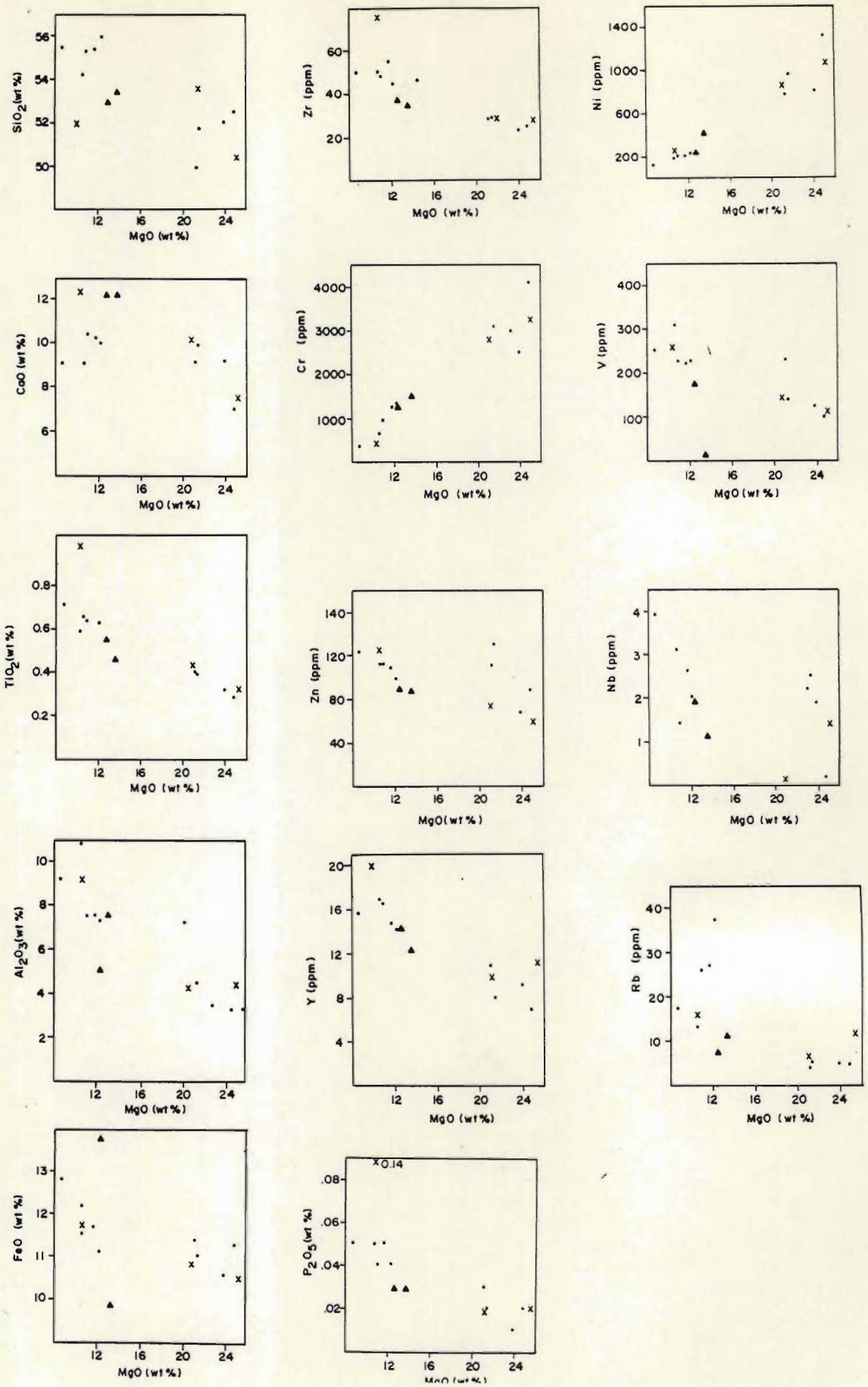

Fig. 6.3 Major and trace element abundances plotted against MgO for basaltic komatiites and peridotitic komatiites from the Commondale Supracrustal Suite. X = L4, L6 and L7, = C1 and C5, = SP2 - SP12.

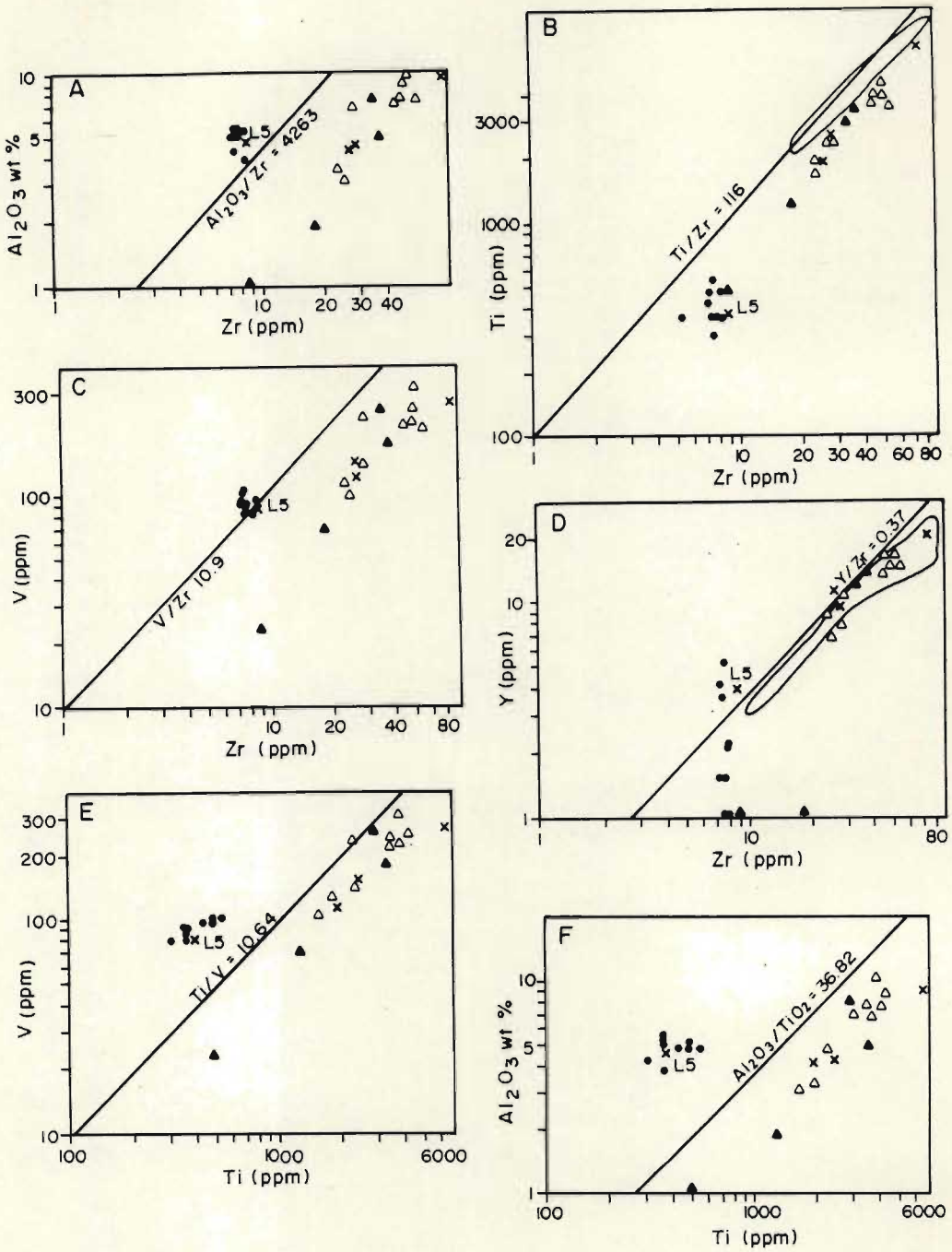

Fig. 6.4 Incompatible major and trace elements plotted against Zr and Ti for basaltic komatiites, peridotitic komatiites and peridotites from the Commondale Supracrustal Suite and compared to cumulate-textured peridotites (C6 - C15) from the Matshempondo Peridotite Suite. Ornamentation as in Fig. 6.2. The fields shown in B and D are for Barberton komatiites and are from Jahn, et al. (1982).

(Figures 6.2 and 6.4). The interelement ratios Ti/Zr, Y/Zr (Fig. 6.4) and Ti/Y ratios for the Commondale Supracrustal Suite are similar to those reported from the Barberton Greenstone Belt (Jahn et al., 1982; Smith and Erlank, 1982).

Despite these differences CaO/Al_2O_3 and Al_2O_3/TiO_2 ratios (Table 6.4 and Fig. 6.5) for the Commondale komatiites and peridotites (C2 and C3) are similar to those for Barberton komatiites, and on the basis of these ratios may be classified as aluminum depleted peridotitic komatiites (ADPK), (Nesbitt et al., 1979). Three Barberton samples (Fig. 6.5), two basaltic komatiites (Komati and Theespruit Formation) and one tholeiite have low CaO/Al_2O_3 and high Al_2O_3/TiO_2 ratios (Jahn et al., 1982) and may be classified as aluminum undepleted peridotitic komatiites (AUPK), (Nesbitt, et al., 1979). These three samples occupy an intermediate position in Fig. 6.5 between the Commondale Supracrustal Suite and the Matshempondo Peridotite Suite.

Summary

i) The Commondale Supracrustal Suite is composed predominantly of mafic and ultramafic volcanic and intrusive rock-types and subordinate BIF. Felsic volcanic rock-types are not recognized in this suite.

ii) Mineral assemblages reflect metamorphism at amphibolite grade with subsequent retrograde metamorphism to greenschist facies.

iii) On the Jensen (1976) cation plot amphibolites, tremolite-actinolite schists and serpentinites range from basaltic komatiites and peridotitic komatiites.

iv) There is a distinct compositional gap between ~14 and 20% MgO which needs to be confirmed by more detailed sampling. The well-defined linear trends on incompatible element variation diagrams (Fig. 6.4) suggest that the komatiites, and peridotitic komatiites could have been derived by partial melting of the same non-chondritic mantle source.

v) The CaO/Al_2O_3 and Al_2O_3/TiO_2 ratios are similar to those for

TABLE 6.4 INCOMPATIBLE ELEMENT RATIOS FOR BASALTIC KOMATIITES AND PERIDOTITIC KOMATIITES FROM THE COMMONDALE SUPRACRUSTAL SUITE

Basaltic komatiites

	MgO	CaO/Al_2O_3	Al_2O_3/TiO_2	Ti/Zr	Ti/Y
C1	12.38	2.43	8.91	91	329
C5	13.62	1.56	16.40	83	228
SP2	10.56	0.84	16.36	78	234
SP4	11.75	1.36	12.85	64	240
SP6	12.14	1.39	11.56	84	266
SP8	10.97	1.38	11.80	80	230
SP12	8.57	0.98	12.78	87	275
L4	10.52	1.36	8.26	88	330
Peridotitic komatiites					
SP3	21.33	1.26	18.40	83	215
SP5	24.91	2.17	11.64	66	235
SP9	21.51	2.15	11.95	82	291
SP11	24.12	2.64	11.00	82	212
L6	25.04	1.80	13.44	74	172
L7	21.20	2.38	10.44	93	252
C2	44.77	1.28	6.63	54	-
C3	37.95	2.32	9.19	71	-
L5	39.39	0.56	76.67	45	96

- Y below detection limit

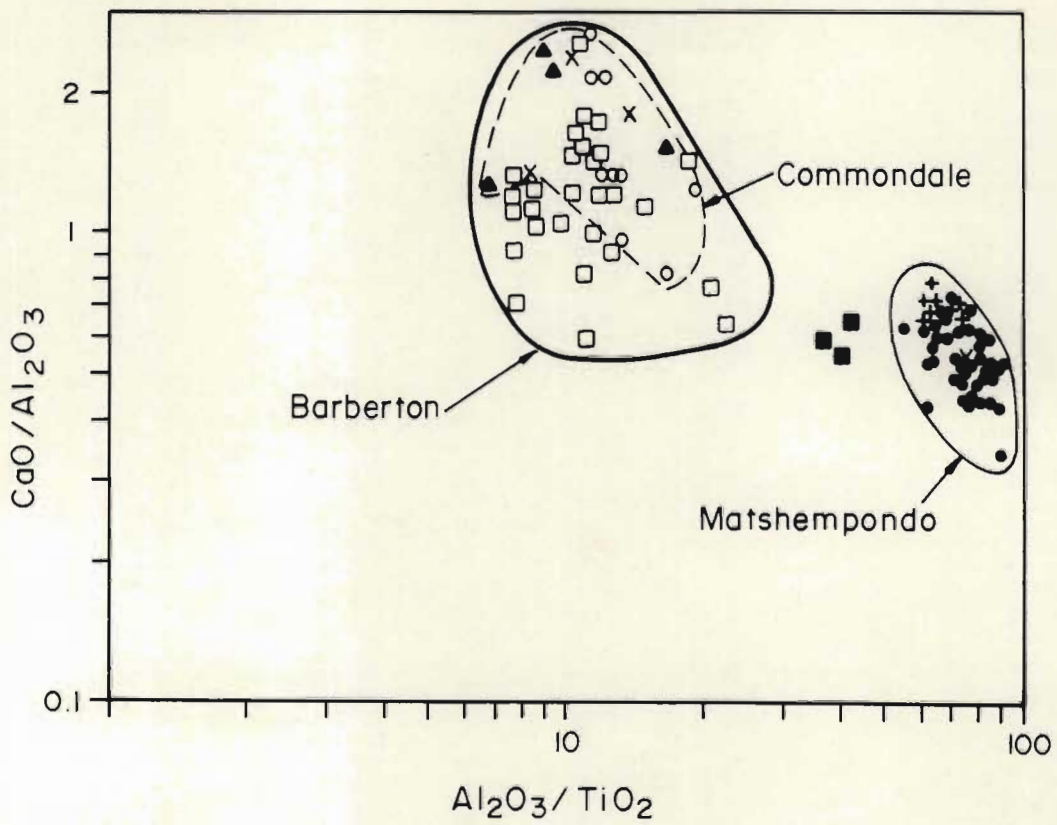

Commondale Supracrustal Suite

▲ C1 - C5

× L4 - L7

○ SP2 - SP12

Matshempondo Peridotite Suite

+ spinifex - textured

● cumulates

Barberton

□ komatiites (Jahn et al., 1982; Viljoen et al., 1983; Smith and Erlank, 1982)

■ basaltic komatiite and tholeiite (Jahn et al., 1982)

Fig. 6.5 Plot of CaO/Al_2O_3 versus Al_2O_3/TiO_2 for Commondale komatiitic rock-types compared to those from Barberton (Jahn et al., 1982; Viljoen et al., 1983; Smith and Erlank, 1982) and the Matshempondo Peridotite Suite.

aluminum depleted peridotitic komatiites (Nesbitt, et al., 1982). The high Ti/Y ratios of the komatiites suggest that during partial melting of the source Y was depleted in the melt by garnet fractionation. These ratios are consistent with generation of the komatiitic liquids at pressures between 70 and 140kb and depths between 200 and 400km (Ohtani, 1984). Over this pressure interval garnet and a small proportion of picritic liquid separate from the ascending diapir resulting in the characteristic ratios Al_2O_3/TiO_2 and CaO/Al_2O_3 ratios in aluminum depleted peridotitic komatiites.

vi) As a general rule analyses of the Commondale Supracrustal Suite can be distinguished from those of the Matshempondo Peridotite Suite on interelement and element ratio diagrams. Sample L5 (serpentinite) however has similar chemical characteristics and incompatible element ratios to peridotites in the Matshempondo Peridotite Suite. Detailed sampling of serpentinite units in other parts of the Commondale Supracrustal Suite may reveal that these chemically distinctive rock-types are not restricted only to the Matshempondo Peridotite Suite and southwestern extension of the supracrustal suite.

vii) The chemical differences between the Matshempondo and Commondale units suggest that the two suites are not co-genetic.

CHAPTER 7

MATSHEMPONDO PERIDOTITE SUITE

Peridotites and peridotitic komatiites preserved in the core of the Commondale synform are part of a sequence of partially serpentininized olivine cumulates and olivine spinifex-textured rocks at least 640 m thick. This suite of rocks first recognized by the author in 1985, has been named the Matshempondo Peridotite Suite. A brief discussion of Archaean komatiites and spinifex-textured rocks in other greenstone terranes provides an introduction to the field relationships, petrological characteristics and geochemistry of the Matshempondo Peridotite Suite.

INTRODUCTION

Archaean komatiites and spinifex-textured rocks.

The term komatiite was introduced by Viljoen and Viljoen (1969c) to describe high magnesium lavas from the Barberton Mountain Land, South Africa. These lavas are characterized by spinifex textures, pillow-like structures and chilled flow tops. Since the recognition of these ultramafic lavas (up to 32 wt. % MgO), with high CaO : Al_2O_3 ratios, similar rock types have been recognized in many greenstone terranes in India, Canada, United States of America, Australia, South America, Zimbabwe and in other greenstone belts in South Africa. With few exceptions these rock-types are restricted to Archaean terranes.

Brooks and Hart (1974) proposed a more rigid definition for komatiite based on the occurrence of spinifex textures and on certain geochemical criteria. The important chemical characteristics are SiO_2 < 53 wt.%, MgO > 9 wt.%, K_2O and TiO_2 < 0.9 wt.% and CaO : Al_2O_3 > 1. Textural characteristics are included to distinguish them from cumulate rocks of diverse origins that have komatiitic compositions. At the Penrose Conference on komatiites (Arndt and Brooks, 1980), 'komatiite' was redefined as an ultramafic volcanic rock which shows the following characteristics (Arndt and Nisbet, 1982) :

i) Volcanic origin of the rock suite indicated by typical and characteristic textures such as chilled flow tops, polyhedral jointing, well developed spinifex textures (tuffs and breccias), quench textures and abundant glass.

ii) An ultramafic composition is indicated by a predominance of olivine and pyroxene in an altered glassy matrix. At ~18 Wt.% MgO, modal and normative olivine proportions are 20-35% and 15-30% respectively, and the total proportion of normative mafic minerals is between 65 and 70%.

These criteria are applied in this study.

Komatiites are more commonly located in the basal stratigraphic levels of broad volcano-sedimentary cycles where they are often associated with ultramafic layered sills that are texturally indistinguishable from the cumulate portions of the lava flows (Naldrett and Mason, 1968; Williams and Hallberg, 1973; Arndt et al., 1979). Komatiites normally occur as lava flows, tens to hundreds of metres thick and are commonly associated with or alternate with sequences of tholeiites of similar or greater thicknesses. Cycles are generally initiated with relatively thin, ultramafic komatiitic flows and are succeeded upwards by thicker, less magnesian mafic komatiites (Arndt et al., 1979).

Archaean ultramafic rocks containing bands of olivine and pyroxene spinifex separated by cumulate layers, interpreted to be discordant peridotite lenses, have been reported from Dundonald and Clerque Townships, Ontario (Naldrett and Mason, 1968). Pyke et al. (1973) describes ultramafic komatiite flows in Munro Township, Ontario, with spinifex-textured upper portions and massive lower sections comprising cumulus olivines. These authors, for the purpose of description, divided the flows into an upper A unit and a lower B unit comprising olivine spinifex and olivine cumulates respectively. This nomenclature has now become widely accepted in the literature, however their divisions of the units into subunits, defined as A1 and A2 and B1 - 4 is not applicable to all komatiitic flows, and is not adhered to in this study. Since the description of Pyke et al. (1973) similar flows have been described by Lajoie and Gelinas (1978), Barnes et al. (1983), Barnes (1985), Arndt (1986a), Auvray et al. (1982), Barley and Bickle (1982) and many others.

Individual flows range in thickness from < 1m (Keays, 1982; Viljoen et al., 1983) to several tens of metres (Arndt, 1977; Barnes, 1985) and to greater than 100m (Arndt, 1977). In some of the thicker flows pyroxene cumulates are developed in addition to the olivine cumulate and olivine spinifex layer (Arndt, 1977).

Part of the komatiite sequence at Pyke Hill, Munro Township, Ontario has been interpreted as having formed as a lava lake (Arndt, 1986b). In this 120m thick sequence comprising olivine cumulates, spinifex veins (5cm - 2m thick with irregular margins) comprising random olivine spinifex and patches of pyroxene spinifex are roughly parallel to the upper contact of the sequence. These veins are interpreted to have formed through intrusion of komatiitic magma along fractures.

Various mechanisms have been proposed for the crystallization of komatiitic flows (summarized by Donaldson, 1982) and recently by Turner et al. (1986) and Arndt (1986a). These recent concepts for the crystallization mechanisms involve growth of the olivine spinifex downwards from the roof into the undepleted lower part of the flow, and as growth continues the olivine-depleted residual liquid is rehomogenized by convection. Continued spinifex growth would decrease the proportion of liquid and slow convection in the phenocryst-free part of the flow permitting granular olivine grains to become concentrated in the lower part of the flow. The cumulate zone would subsequently form.

This general overview provides a basis for an understanding of the significance of spinifex-textured komatiites, and the development of spinifex and cumulate layers within individual cooling units.*

*Cooling unit (after Donaldson, 1982) refers to both the spinifex and cumulate portions of a komatiitic flow or sill, and may be used where uncertainty exists as to the intrusive or extrusive nature of the unit.

Textural Terminology

The term 'spinifex' is correctly used as an adjective to qualify a texture characterized by large randomly oriented or subparallel skeletal, plate or lattice olivine grains, or acicular pyroxene grains set in a finer grained matrix of skeletal or dendritic pyroxene crystals and devitrified glass (Donaldson, 1982). The term spinifex used as a noun, e.g. 'olivine plate spinifex' has become common practice but is not strictly correct (Donaldson, 1982). However it does allow ready identification of the textural type and those minerals that are skeletal. In the following discussion 'spinifex' is used as both an adjective and more loosely as a noun.

Description of spinifex textures requires a morphological classification of the crystals and their relationships to each other : The dominant spinifex textures are summarized below.

1. Olivine Spinifex

a) Hopper olivine : equant to elongate crystals with hollow or embayed cores and euhedral to subhedral outlines (Fig. 7.1a) (Donaldson, 1976, 1982). Randomly oriented equant varieties and elongate varieties are equivalent to the porphyritic spinifex and radiating spinifex respectively of Nesbitt (1971).

b) Olivine plate spinifex : comprises two or more thinly tabular plates (c> a>> b) that are parallel or nearly parallel (Fig. 7.1b) (Donaldson, 1982). Groups of plates that radiate from a common nucleation point to form a fan may be referred to as radiating olivine plate spinifex (Fig. 7.1b).

c) Random olivine plate spinifex : comprises small plates (< 2cm) that show no preferred orientation (Donaldson, 1982).

d) Branching olivine : the linked parallel growth variety comprises roughly parallel dendritic plates or rods (Fig. 7.1c) elongate parallel to a or c crystallographic axes (Donaldson, 1974, 1976 and 1982). The linked parallel growth and olivine plate spinifex variety merge into one another depending on the extent of flattening of the parallel growth units and the internal

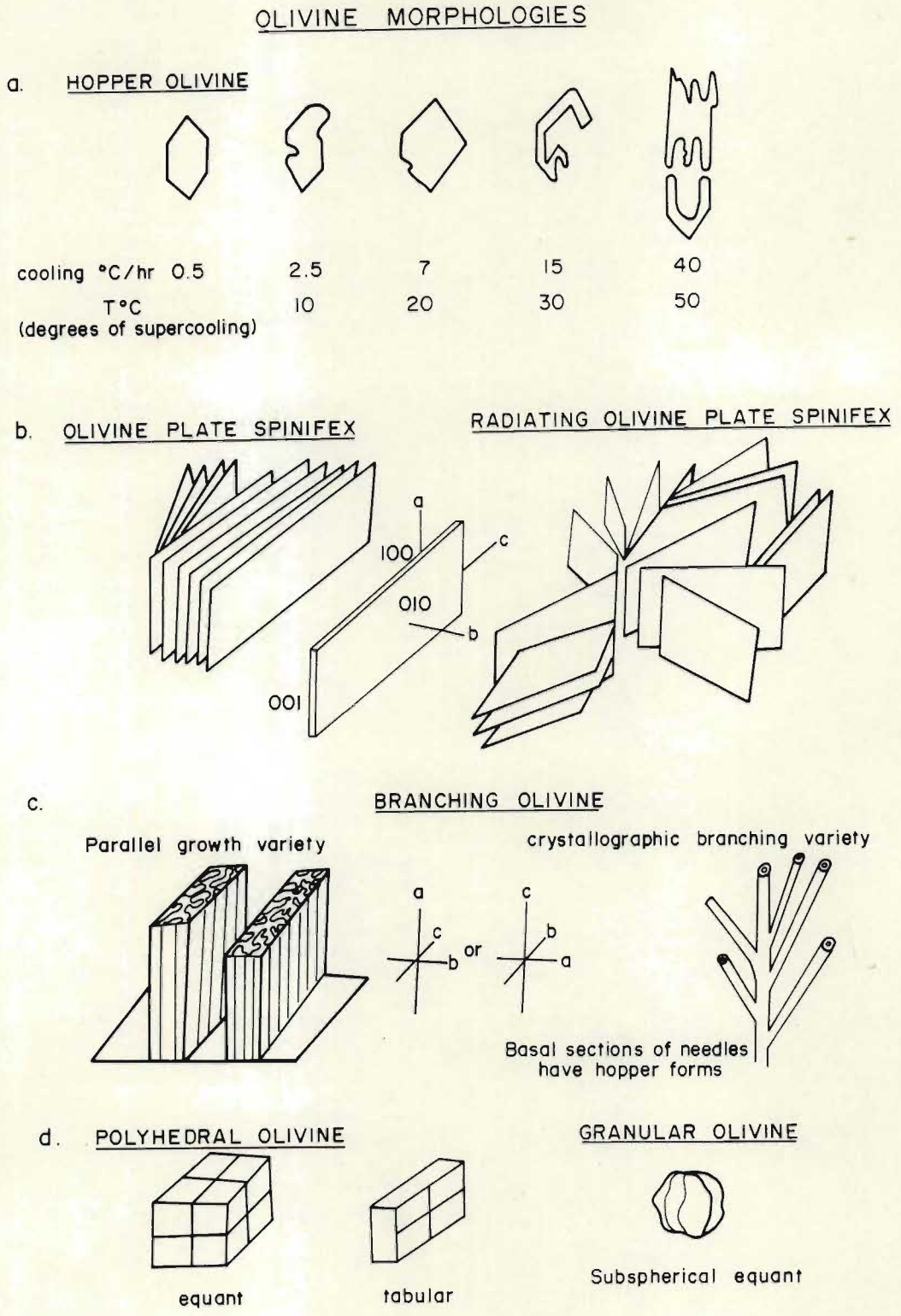

Fig. 7.1 Two and three dimensional sketches of olivine morphologies in spinifex and cumulate units. Hopper olivine, spinifex olivine plate and branching olivine are typical of spinifex textured units. Polyhedral and granular olivine are typical of cumulate units. Sketches of hopper olivine and cooling data are from Donaldson (1976), and that of the parallel growth variety from Donaldson (1982).

dendritic nature of the plates (Donaldson, 1974, 1982). The crystallographic branching variety comprises rods connected by buds or branches parallel to one of the crystallographic axes (Fig. 7.1c) (Donaldson, 1974, 1976).

2. Pyroxene Spinifex

In this textural type skeletal clinopyroxene and orthopyroxene crystals are blade or needle-like in shape. The commonly hollow or tubular needles are distinguished from the relatively tabular blades by longer a or c crystallographic axes. Needles may form parallel growth varieties linked in the (001) plane. Crystallographic branching varieties similar to those for branching olivine are also recognized.

3. Cumulus Olivine

Units with a predominance of discrete granular olivine crystals that are not embayed or hollow represent the cumulate varieties. In these units two types of olivine crystals are found :

a) polyhedral grains with equant to tabular euhedral crystals (Fig. 7.1d).

b) subspherical crytals (Fig. 7.1d).

Orthocumulates are defined as cumulates in which the mesostasis constitutes minerals that account for between 25 and 45% by volume of the rock. The cumulus minerals should reflect closely their original crystallization morphologies (Irvine, 1982). Mesocumulates which are mineralogically similar but distinct from the othocumulates are characterized by a higher proportion of cumulus olivine, and mesostasis that accounts for < 25% by volume of the rock.

PART 1 FIELD RELATIONS AND PETROGRAPHY

FIELD RELATIONS

Geological and structural setting.

The Matshempondo peridotites and peridotitic komatiites constitute a suite of cumulate and spinifex-textured rocks at least 640m thick that crop out over an area of approximately $10km^2$ in the core of the Commondale synform (MAP 2). The suite is bounded by amphibolites, serpentinites and ferruginous sediments in the fold closure (MAP 2) and by ultramafic schists and ferruginous sediments along the northern limb of the Commondale synform. The northern and western boundaries of the peridotite suite are sheared, poorly exposed and characterized by strong serpentinization and talcification often precluding the recognition of primary textures. There is a progressive intensification of the foliation and shearing in the upper 180m of the peridotites on Nederland 202HT.

This suite is preserved predominantly on the northern limb of the Commondale synform. The igneous layering dips at 65 degrees to the north and contrasts to that of the BIF which dips at between 70 and 90 degrees south-southwest (MAP 2) indicating a clear discordance between the peridotites and the volcano-sedimentary pile. The Matshempondo peridotites together with the other Commondale supracrustals were deformed during four major deformation events involving folding, thrusting and shearing resulting in the observed complex geometry of the peridotite suite especially in the closure of the Commondale synform (MAP 2). The D_2 deformation has resulted in the peridotite suite being preserved as a complex hook-shaped fold in the core of the F_2 closure. The structural complexities are discussed in detail in Chapter 8.

The remarkable preservation of primary textures is due largely to the relatively competent behaviour of these rocks and the supracrustal suite during deformation under a relatively low strain regime in the hinge zone of a major synform (see Chapter 8). In the fold closure a strong but widely spaced S_2 axial planar cleavage cross-cuts layering and primary textures.

The Layered Suite

Outcrops of the peridotite suite are confined to the farms Nederland 202HT and Mooiplaats 206HT. The suite is best exposed along section A-B (MAP 2) on the farm Nederland 202HT in the form of low angular outcrops.

In the field, layering is evident as a consequence of the preferential weathering and outcrop patterns of the alternating cumulate and spinifex-textured units. The highly magnesian cumulate layers crop out as ridges between 1 and 3 metres high with the spinifex layers forming depressions between the ridges. Some individual cumulate and spinifex layers are continuous on strike for several hundred metres, but others are discontinuous.

Eighteen cooling units (Fig. 7.2) between 9 and 63 metres thick, each comprising an upper zone of olivine plate spinifex and a lower zone of one or more cumulate layers have been identified. The upper portion of seven of these cooling units are characterized by a microcyclic spinifex-cumulate unit. The cumulate rocks predominate over the spinifex-textured varieties in the succession as a whole as they have a total combined thickness of 572 metres, compared to 68 metres for the olivine spinifex and microcyclic units.

The thickness of individual cumulate layers ranges from 1.6 to 60 metres, the thickest layers being found in the upper 180m of the succession. Here a strong penetrative fabric and pervasive alteration to talc, chlorite, tremolite and serpentine make the cumulate and spinifex layers difficult to distinguish in the field. Individual cumulate layers up to a maximum of 33m thick are recorded in the stratigraphically lower and better preserved portions of the suite where only a weak penetrative fabric is developed.

The seventeen olivine plate spinifex units are between 0.9 and 10.2 metres thick (Fig. 7.2). The lowermost and thickest olivine plate spinifex unit (ML2, 10.2m thick), differs from the other units by development of a lens of orthopyroxene and clinopyroxene spinifex at the top of the unit.
Seven of the cooling units show the development of microcyclic spinifex-cumulate units between 1.6 and 5.6m thick in the upper parts.

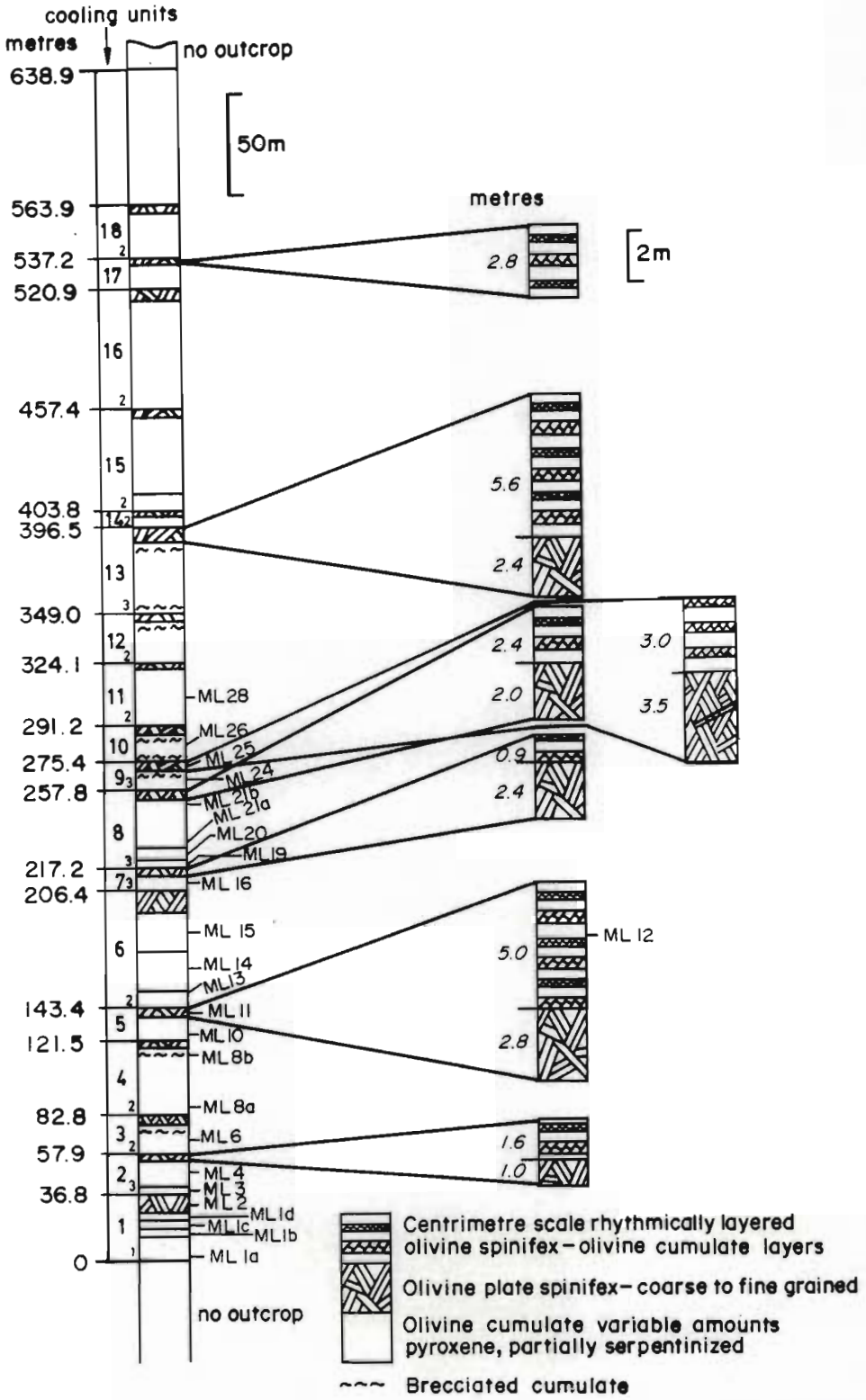

Fig. 7.2 Section through the Matshempondo Peridotite Suite. Numbers ML IA - ML 28 represent samples collected for geochemistry. The left hand column shows the different cooling units comprising cumulate, spinifex and microcyclic units, and the type of cooling unit (1, 2 or 3, see later section). Where microcyclic units overly spinifex units they are represented in the right hand column. The true thickness in metres in the left hand column represents the thickness between successive cooling units, numbered 1 - 18. The section is along line A - B on MAP 2 on the farm Nederland 202HT. The section B-C on line A-B (see Fig. 8.9) represents a 300m thickness over which samples were collected for geochemistry on the southern limb of the F_1 synform (MAP 2 and Fig. 8.9). No samples were collected for geochemistry on the northern limb as alteration and a penetrative foliation are pronounced.

Individual spinifex and cumulate layers or laminae are between 1 and 15cm thick (Fig. 7.3). As many as 41 microcyclic spinifex-cumulate pairs have been recorded in a single unit, but more commonly this ranges from 8 to 25 spinifex-cumulate pairs. To the knowledge of the author these microcyclic units have not previously been reported in Archaean komatiite sequences. Towards the top of the sequence (534.4m from base) a 2.8m thick microcyclic unit overlies serpentinitic rocks in which spinifex textures were not unequivocally recognized due to the strong foliation in the upper part of the suite.

Three distinct types of cooling units or flows are recognized in the Matshempondo Peridotite Suite. Detailed descriptions of the units are hampered by inadequate outcrop in critical areas. The different types have been distinguished on the basis of modal mineralogy, and the presence or absence of microcyclic units and mixed spinifex-cumulate rock-types. The three types are described in the following sections using the best exposed cooling units as examples of each type.

1. TYPE 1 COOLING UNIT

This type of cooling unit (Fig. 7.4), comprises one or more olivine cumulate layers between 3 and 14m thick that collectively represent the B unit. The 10m thick A unit comprises olivine plate spinifex, random olivine plate spinifex and a lens of pyroxene spinifex. Broad subdivision into the A and B units is after Pyke et al., 1973. These units may be further subdivided and the individual subunits from the base upwards are described.

a) B Unit.

The B unit is characterized by cumulate-textured rock-types that are divided into the different subunits on the basis of different modal proportions of cumulus olivine and mesostasis. The mesostasis comprises needle orthopyroxene and skeletal chromite set in a dark coloured matrix interpreted as devitrified mafic glass.

i) B1 subunit.

Modal proportions of cumulus olivine grains up to 3mm in diameter range from ~80 percent by volume at the base to ~75% at the top

Fig. 7.3 Centimetre scale spinifex-cumulate layers in the cooling units. Layers with positive relief are spinifex bearing and those with negative relief are cumulates. The layering dips at 65 degrees towards north.

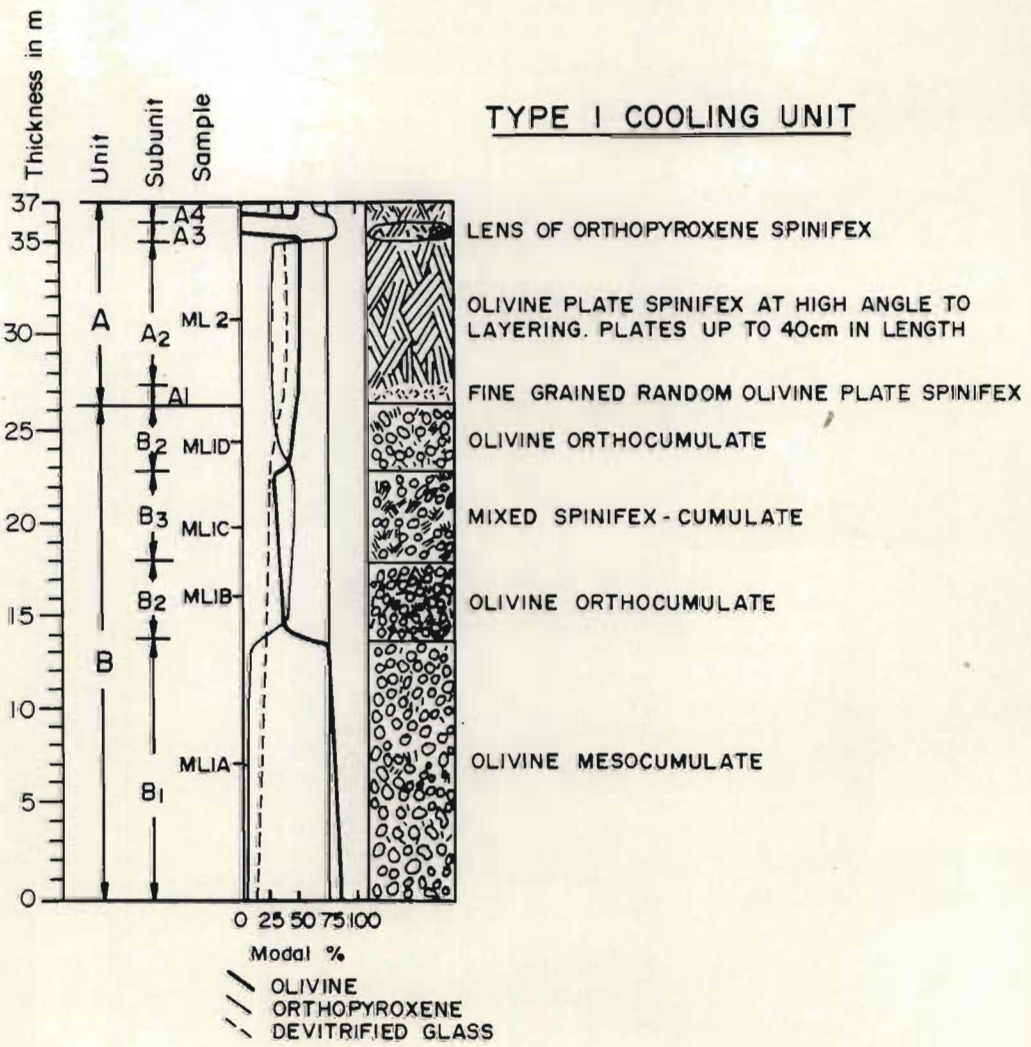

Fig. 7.4 Type 1 cooling unit showing the variations in modal proportions of olivine, orthopyroxene and devitrified glass in the lowest exposed cooling unit (Fig. 7.2, cooling unit 1). In the cumulate zone (ML1A - ML1D) fine strokes between

of the B1 unit (Fig. 7.4). This decrease is accompanied by an increase in the proportion of blade and needle orthopyroxene (needles up to 8mm in length) and devitrified glass. A marked change in the mineral modal proportions distinguishes the B1 and B2 subunits as does the variation in major and trace element contents (see later section).

ii) B2 subunit.

The orthocumulates are characterized by significantly lower modal proportions of cumulus olivine and a higher proportion of mesostasis. At 14m above the base of the cooling unit a significant decrease from 75 to ~50 modal % olivine marks the rapid transition from mesocumulates to orthocumulates (Fig. 7.4). The proportion of modal olivine decreases upwards to 18m where the petrographically distinct B3 subunit is recognized (Fig. 7.4). At 23m (Fig. 7.4) orthocumulates (B2 subunit) form a layer 3m thick beneath the A unit. In this layer there is an upward increase in the proportion of modal olivine from ~35 to 50%.

iii) B3 subunit.

This subunit is a transitional rock-type comprising a mixed zone of spinifex and cumulate textures in an intimate mixture. Granular olivine crystals 1-2mm in diameter and localized zones of up to $2cm^2$ of orthopyroxene needles with individual crystals up to 4mm long occur in a matrix of devitrified glass. In this subunit the proportion of olivine appears to decrease upwards.

As a whole, the B unit shows an upward decrease in the proportion of cumulus olivine to the top of the B3 subunit at 23m after which there is an increase in the proportion of cumulus olivine to the top of the B unit at ~26m. The different B subunits are distinguished in the field by subtle variations in grainsize, colour and texture of the weathered surface. The resistance to weathering and the characteristic appearance of the cumulate layers is dependent on the olivine content. Layers with a high proportion of olivine are preferentially weathered to a characteristic knobbly surface (Fig. 7.5).

Fig. 7.5 Knobbly and rippled surface characteristic of high magnesium cumulate layers, ML3.

b) A Unit

The A unit comprises spinifex-textured olivine, orthopyroxene and clinopryoxene and is divided into the four subunits on the basis of mineralogy, morphology and grainsize.

i) A1 subunit.

The A1 subunit is approximately 70cm in thickness and comprises random and radiating olivine plate spinifex (Fig. 7.4). The fine-grained (< 1cm) random olivine plate spinifex grades upwards into coarser grained (< 3cm) radiating olivine plate spinifex in a matrix of devtrified glass. The proportion of devitrified glass decreases slightly in the coarser grained upper portion of this subunit.

ii) A2 subunit.

Olivine plate spinifex with plates 1-2mm in thickness and varying between 5 and 40cm in length are typically mutually parallel to each other forming books 1 to 15cm thick (Fig. 7.6). The number of olivine plates making up a single book varies for 6 to ~75. Books are inclined to each other, are mutually truncating (Fig. 7.7) and are set at high angles to the layering plane (Fig. 7.4). This coarse-grained subunit is approximately 8m thick where the A3 subunit is not developed.

iii) A3 subunit.

This lenticular subunit occurs immediately below the topmost, A4 layer in the cooling unit (Fig. 7.4) and comprises a lens of pyroxene spinifex 30m in length and 1-2m thick. The habit and grainsize of the orthopyroxene phenocrysts is highly variable. Textures range from parallel sheaves (Fig. 7.8) and fans of hopper orthopyroxene needles up to 3mm in diameter and 15cm in length to short stubby bladed crystals in a groundmass of skeletal clinopyroxene, plagioclase and devitrified glass (Fig. 7.9 and Fig. 7.10). The rubbly nature of the outcrop does not allow the textural relations between the pyroxene spinifex lens and the olivine spinifex to be established.

Fig. 7.6 Olivine plate spinifex in ML2 unit. Random olivine plate spinifex (near pen) grades rapidly upwards into coarse grained (40cm long) olivine plate spinifex. Plates are at a high angle to the random spinifex and the underlying cumulates (not shown).

Fig. 7.7 Olivine plates form books inclined towards each other and appear mutually truncating. ML25 unit.

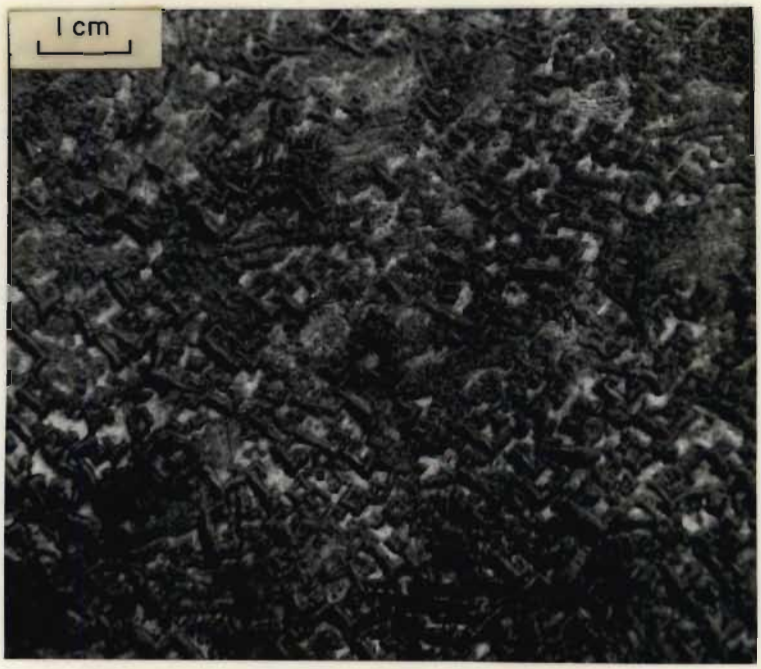

Fig. 7.8 Basal section of a sheaf of parallel tubular orthopyroxene needles. The complex dendritic intergrowth of linked angular basal sections of needles represent a parallel growth structure. Lens of pyroxene spinifex in ML2 unit.

Fig. 7.9 Fans of plumose aggregates of hollow orthopyroxene needles. Lens of pyroxene spinifex in ML2 unit.

Fig. 7.10 Curved and straight stubby blades of orthopyroxene spinifex. Pyroxene spinifex lens in ML2 unit.

iv) A4 subunit.

This subunit comprises the uppermost zone (36-37m in Fig. 7.4) of the A unit and is a medium-grained (~5cm) olivine plate spinifex. Fine-grained chill zones or flow top breccias have not been recognized at the top of the A unit and this apparent deviation from many of the spinifex-textured flow units described in the literature may have an important bearing on the petrogenesis of this succession.

2. TYPE 2 COOLING UNIT.

This cooling unit is similar in mineralogy and textural types to the Type 1 cooling unit but it does not contain the mixed spinifex-cumulate subunit (B3 in Fig. 7.4) or the pryoxene spinifex lens (A3 in Fig. 7.4). In this type the number of cumulate layer varies between 1 and 3. Mesocumulates characteristically at the base of each B unit are succeeded by orthocumulates as in the Type 1 cooling unit. Type 2 cooling units identified in this succession are cooling units 3, 4, 6, 10, 11, 12, 14, 15, 15 and 18 in Fig. 7.4.

3. TYPE 3 COOLING UNIT.

This cooling unit comprises similar layer types to the Type 2 cooling unit but is distinguished by the presence of centimetre-scale microcyclic spinifex-cumulate layers (Fig. 7.11) above the olivine spinifex unit (A unit). As these components of spinifex-bearing flows have not been described in other occurrences it is here identified as the C unit and deviates from the simple classification in Pyke et al. (1973).

Type 3 cooling units identified in the succession are cooling units 2, 5, 7, 8, 9 and 13 (Fig. 7.2). In cooling unit 17 (Fig. 7.2) no A unit is unequivocally recognized due to the strong penetrative foliation in this portion of the sequence. In the different cooling units the C unit ranges in thickness from 1.6 to 5.6m in which between 5 and 41 spinifex-cumulate pairs are recognized. The B unit is characterized by a single B2 subunit or by between 1 and 3 B2 subunits, e.g. cooling unit 8 has three B2 subunits. These different subunits are

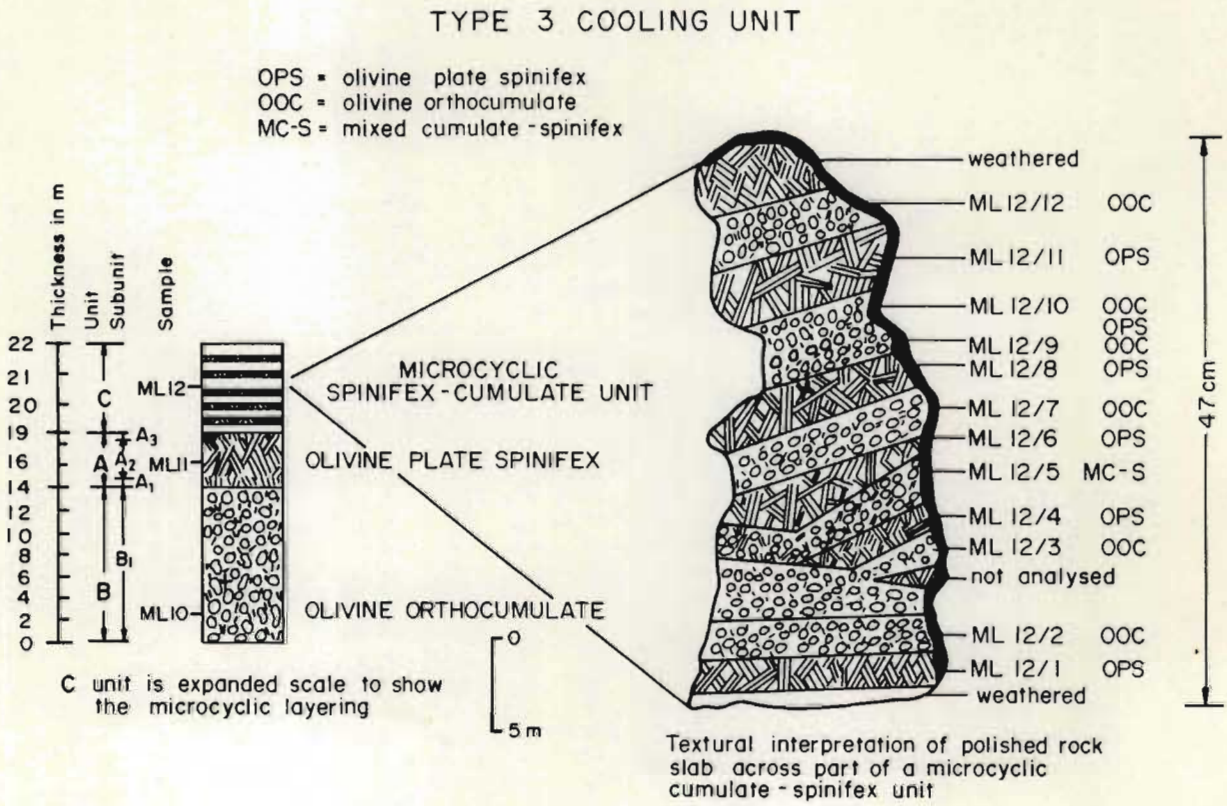

Fig. 7.11 Type 3 cooling unit comprises olivine orthocumulates, olivine plate spinifex and microcyclic spinifex-cumulate units. Textural relationships and sample numbers for each layer in part of the microcyclic unit (ML12) are shown in a sketch of the polished rock slab.

distinguished by different relative proportions of cumulus olivine and mesostasis. The B2 and A1, A2 and A4 subunits of this cooling unit are similar in texture and mineralogy to those described for the Type 1 cooling unit.

The Type 3 cooling unit is described in Fig. 7.11 using cooling unit 5 (Fig. 7.2) as an example. The relations between the relevant A and B subunits are similar to those described for TYPE 1 cooling units. Within the microcyclic spinifex-cumulate unit (C unit) a further fine structure may be observed as shown in a slab 47cm long (Fig. 7.11) comprising five spinifex layers, six orthocumulate layers and one mixed spinifex-cumulate layer. The continuous detail observed in the slab provides an insight into the relations between orthocumulate and spinifex-textured layers. The centimetre-scale spinifex layers comprise fine books of olivine plate spinifex 5 - 40mm long. The mutually truncating plates are perpendicular to or at a high angle to the plane of the layering (Fig. 7.12). The contact between the orthocumulate and spinifex layers is well defined and is recognized as a zone 1 - 3mm thick comprising abundant devitrified glass, random olivine plate spinifex (1 - 2mm in length) and granular olivine.

In any one C unit the frequency of cumulate and spinifex layers is remarkably constant i.e. 10 cumulate layers each 8cm in thickness are separated by spinifex layers 2cm thick (Fig. 7.13a). In another example (Fig. 7.13b) 24 cumulate layers each 6cm thick are separated by spinifex layers 3cm thick. Other examples are shown in Figures 7.13c and 7.13d. Within a single unit there may also be a change in the relative thickness with at least two spinifex-cumulate pairs showing a constant thickness ratio (Fig. 7.14).
Microcyclic units are recognized in all segments of the Matshempondo Peridotite Suite (MAP 2) and can be traced for between 20 and 200m along strike until poor outcrop or zones of ferricrete accumulation between the various segments of the suite militate against positive identification of the same unit in the adjacent block. Individual spinifex layers in the C units can be followed along strike for tens of metres.

Fig. 7.12 Close up of part of the slab in Fig. 7.11 showing the relationship between cumulate and spinifex layers in microcyclic units.

Fig. 7.13 Microcyclic spinifex-cumulate units showing the volumetrically different proportions of spinifex and cumulate layers and the constant thickness ratio of the two textural types in the different cooling units.

a) Part of the microcyclic unit in cooling unit 5 (Fig. 7.2). The spinifex layers (positive relief) are 2cm thick and the intervening cumulate layers 10cm thick.

b) Microcyclic unit in cooling unit 13 (Fig. 7.2). At the base (not shown) of the microcyclic unit spinifex and cumulate layers are 2 and 15cm thick respectively. The ratio decreases towards the top where spinifex and cumulate layers are 3 and 6cm thick respectively (near hammer).

c) Part of the microcyclic unit in cooling unit 2 (Fig. 7.2). The base of the sample shows a thick spinifex layer overlain by spinifex (positive relief) and cumulate layers approximately 2 and 4cm thick respectively. Below the 10cm scale the spinifex layers are trough bedded. These trough-like depressions are also recognized in other microcyclic units.

d) Spinifex (positive relief) and cumulate layers in the microcyclic unit in cooling unit 9 (Fig. 7.2) are approximately 2 and 6cm thick respectively. Trough like structure are recognized in the layering with microlayers pinching out on either side of the trough.

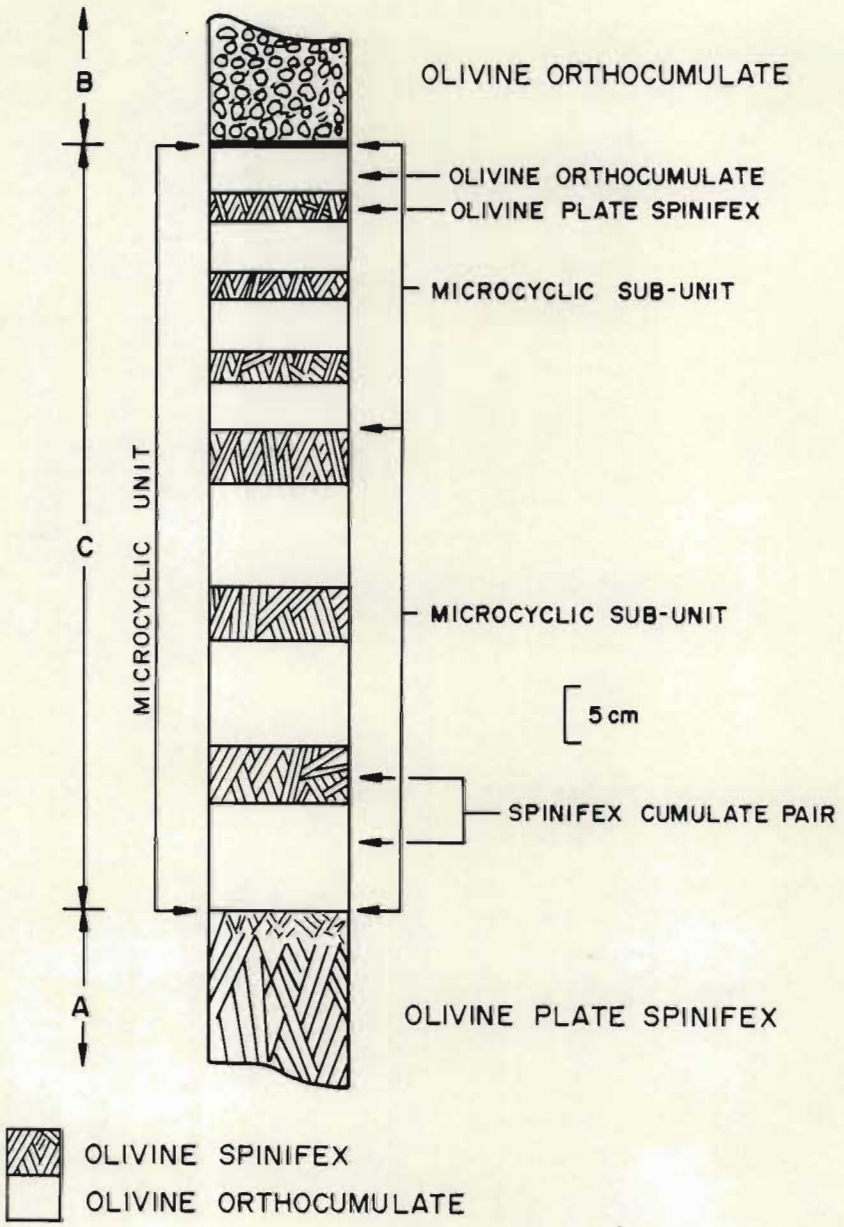

Fig. 7.14 Idealized section of part of a centrimetre scale microcyclic unit through which the thickness of individual layers and the spinifex-cumulate ratio remain relatively constant within each sub-unit. Note the high angle of the olivine plates to the enveloping surface.

Breccia zones and evidence for current action.

Located within a number of the major units in the succession (Fig. 7.2) are zones containing angular fragments 1 - 3cm in diameter (Fig. 7.15). These commonly occur at the tops of some of the cumulate layers and in cooling unit 13 (Fig. 7.2) also occurs at the base of the cumulate unit. These zones essentially represent contrasting olivine cumulates. The fragments of olivine mesocumulate with little mesostasis are enclosed in an olivine orthocumulate. The fine breccia clearly represents disruption of a pre-existing rock type but in relation to the cooling unit as a whole is enigmatic as it does not resemble a flow top texture. Disrupted layering in layered intrusions produces similar microbreccia textures and may be related to strong convection currents within the body of magma.

Strong igneous lamination (Fig. 7.16) is observed in the lowest cumulate layer in cooling unit 8 (Fig. 7.2). The long axes of the olivine are aligned in the layering plane together with subtle changes in modal variation. This lamination is also attributed to the movement of magma during crystallization and deposition of the cumulus olivine.

In the microcyclic units the truncated spinifex layering and trough structures in Fig. 7.13c and Fig. 7.13d may be related to current action as a possible explanation. The truncated spinifex layers are best illustrated in Fig. 7.11.

Polyhedral joints are characteristic throughout the sequence with fractures up to 5mm wide filled by serpentine and magnetite. At the top of spinifex units these joints clearly do not represent flow top breccias.

PETROGRAPHY

Many of the cumulate and spinifex units contain only partially altered mineral assemblages. The partial alteration is olivine to serpentine + magnetite + talc $\pm$ chlorite and orthopyroxene to tremolite + chlorite. Where a foliation is strongly developed, alteration is pervasive. Texturally and mineralogically many of the same rock-types are similar and are discussed collectively in the following sections

Fig. 7.15 Angular fragments of olivine mesocumulate in olivine orthocumulates, in the ML26 unit.

Fig. 7.16 Igneous lamination is well developed in the lower part of the ML13 cumulate unit and parallels the dip of the layering in the microcyclic units. The orientation of the lamination is shown in the figure (----- L). Other fabrics recognized are intersecting joints.

unless referred to specifically. Thin section descriptions are given in Appendix 1.

Olivine plate spinifex.

Many of the textures observed in hand specimen are clearly identified petrographically. Olivine plate spinifex units are medium to coarse-grained with olivine plates between 2mm and 40cm in length.

Olivine forms books of subparallel olivine plates (2 - 30mm long) that are inclined towards each other and are commonly mutually truncating (Fig. 7.17). Many of the olivine plates (0.2 - 2mm thick) are partially altered to serpentine and magnetite, however the hollow and dendritic morphologies of some of the plates are still recognizable. The hollow spaces, 0.005 - 0.01mm wide are altered to chlorite. In the angular polyhedral voids and interplanar spaces controlled by the geometry of the olivine plates hopper and needle orthopyroxene (0.3mm - 1.5cm long) and skeletal chromite crystals are set in a matrix of chloritized devitrified glass.

Sections cut parallel to the C-axis of the orthopyroxene needles reveal that they grew at a high angle to one of the enveloping surfaces (olivine plates) (Fig. 7.17). Sections normal to the C-axis of orthopyroxene needles reveal curvilinear arrays of hopper orthopyroxene (partially altered to chlorite) in optical continuity (Fig. 7.18) suggesting linked parallel growth in the 001 plane (orthopyroxene) with nucleation close to one of the enveloping surfaces (olivine plates). Orthopyroxene crystals between parallel olivine plates are typically mutually parallel or form fans of hollow orthopyroxene needles that radiate from a common apex (Fig. 7.19) or fans of branching needles.

Microprobe analyses of olivine plates and blades in the coarse grained plate spinifex unit (ML25 in Fig. 7.2) suggest a weak zonation across the crystals from Fo_{84} at the centre to Fo_{83} at the edge. Skeletal orthopyroxene crystals between books of olivine plates have compositions between En_{70} and En_{73}. Petrographically the orthopyroxene is identified by low first order grey birefringance, parallel extinction on longitudinal sections and moderate relief.

Fig. 7.17 Photomicrograph of mutually truncating olivine plates partially altered to serpentine and magnetite with tremolite overgrowths. One of the subvertical olivine plates is hollow in some parts. In the triangular space defined by olivine plates curvilinear orthopyroxene crystals grow at high angles to one of the olivine plate. ML25 unit. Crossed-polars, width of view 10mm.

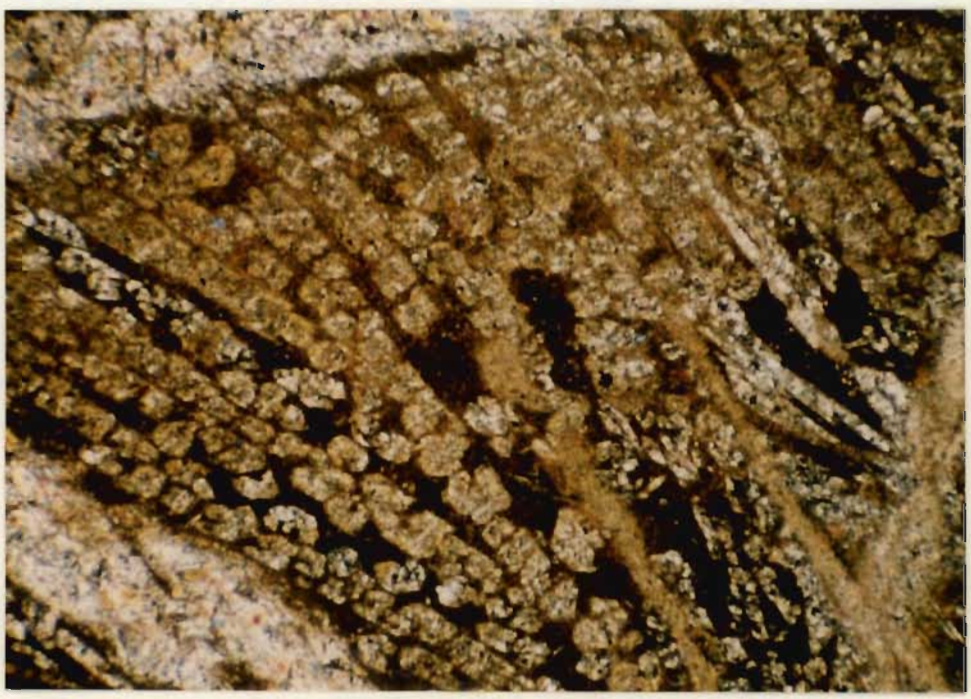

Fig. 7.18 Photomicrograph of an array of hopper orthopyroxene crystals in optical continuity. The crystals are elongated parallel to the C-axes and linked in the 001 plane where crystals nucleate normal to one of the olivine plates, i.e. this photomicrograph is a section cut normal to that in Fig.7.17. Width of view 2.5mm, crossed-polars.

Fig. 7.19 Photomicrograph of branching needles and subparallel orthopyroxene needles between parallel olivine plates that are pervasively altered to serpentine + talc + magnetite with tremolite overgrowths. Skeletal crystals are set in a groundmass of chloritized devitrified glass. Crossed polars, ML2 unit, width of view 10mm.

Textural relations and mineral compositions suggest that within the lattice work produced by the growth and development of the mutually truncating olivine plates small volumes of olivine depleted liquid crystallized orthopyroxene, which grew with a preferred crystallographic orientation, and skeletal chromite. The abundance of skeletal chromite associated with orthopyroxene in a groundmass of devitrified glass suggests that the chromite was not a liquidus phase until orthopyroxene started crystallizing.

Pyroxene spinifex

The lens of pyroxene spinifex at the top of the ML2 unit comprises an apparently random distribution of different pyroxene morphologies. Orthopyroxene crystals show a range in morphologies from stubby (< 2cm in length) blades to blades and tubular needles up to 15cm long. The different pyroxene morphologies are described below.

Orthopyroxene blade spinifex. This texture is characterized by blades between 5mm and 15cm long and up to 1.5cm wide that radiate from a common apex with a tendency to form fans. Basal sections of the orthopyroxene blades are skeletal, with the hollow cores comprising chloritized devitrified glass. Between the orthopyroxene blades are fine cones and plumose radiating clinopryoxene needles up to 3mm long in a groundmass of devitrified glass (Fig 7.20). Clinopyroxene needles are partially or completely altered to tremolite and chlorite. There is no preferred orientation of orthopyroxene fans and cones in thin section or outcrop.

Needle or tubular orthopyroxene spinifex. This texture is characterized by parallel sheaves and fans of hollow orthopyroxene needles between 3mm and 15cm long and up to 3mm in diameter. Orthopyroxene needles are set in a matrix of clinopyroxene needles, altered to tremolite and chlorite and chloritized devitrified glass.

Dendritic orthopyroxene growths show variable forms from bundles of parallel orthopyroxene needles with an internal hopper morphology to complex dendritic intergrowths of essentially angular tubes or needles (Fig. 7.21). The crystals linked in the

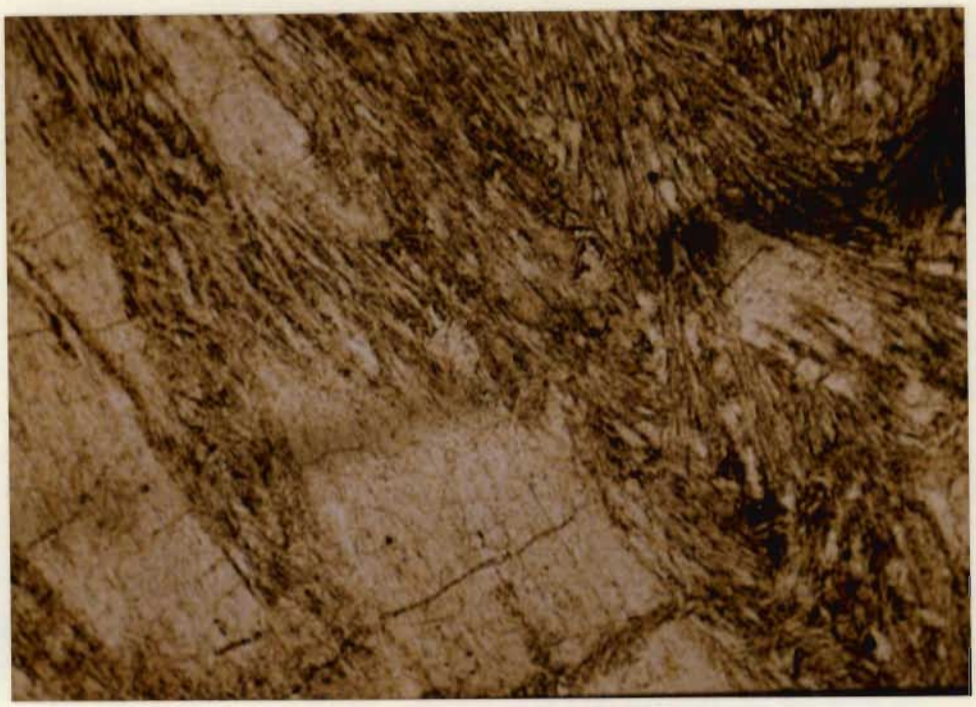

Fig. 7.20 Photomicrograph of fans of needle clinopyroxene and parallel clinopyroxene needles between orthopyroxene blades in a groundmass of devitrified glass. Plane polarized light. Width of view 10mm.

Fig. 7.21 Photomicrograph of complex angular dendritic orthopyroxene in optical continuity in a groundmass of clinopyroxene and tremolite. Crossed polars, width of view 10mm.

001 plane and elongated parallel to the C-axis are in optical continuity. In these dendritic intergrowths orthopyroxene is partially altered to chlorite and skeletal clinopyroxene needles that subpoikilitically enclose parts of the orthopyroxene dendrite are partially to pervasively altered to chlorite and tremolite. The fine-grained matrix of devitrified glass is altered to chlorite but is microcrystalline in plane polarized light.

Olivine mesocumulates

Olivine mesocumulate units comprise 70 - 85% olivine by volume, ~10% orthopyroxene, and tremolite and accessory skeletal chromite in a matrix of devitrified glass (10 - 15%). Subhedral to anhedral olivine grains (granular olivine) < 3mm in diameter are interpreted as the primary cumulus phase. Bladed and tabular hopper orthopyroxene crystals (< 3mm) partially enclose some of the olivine grains and together with fine skeletal chromite (< 0.075mm) and devitrified mafic glass constitute the mesostasis (Fig. 7.22).

In most examples of this rock type primary mineralogies and textures are retained. However partial alteration of olivine to serpentine + talc + magnetite along fractures and of orthopyroxene to chlorite ± tremolite is common. The mafic devitrified glass is in places completely altered to isotropic chlorite.

Olivine orthocumulates

Olivine orthocumulates typically have a higher proportion of mesostasis interstitial to the cumulus olivine compared to the mesocumulates. Components of the mesostasis include hopper needle orthopyroxene crystals, skeletal chromite and devitrified mafic glass. Typical mineral proportions in the rock-type are 45 - 70% olivine, 10 - 35% orthopyroxene, 15 - 30% devitrified glass and accessory skeletal chromite.

The granular cumulus olivine grains are 1 - 3mm in diameter. The orthopyroxene crystals in the matrix occur as blades and needles up to 3.5mm long and the skeletal chromite grains are < 0.1mm in diameter. Straight or curved orthopyroxene needles occur as isolated crystals

Fig. 7.22 Photomicrograph of olivine mesocumulate showing fractured olivine grains in a mesostasis comprising fine needle orthopyroxene and devitrified glass. Width of view 10mm, plane polarized light.

between olivine grains or as small clusters that radiate from a common point (Fig. 7.23). Where orthopyroxene is more abundant there is a significantly larger volume of associated devitrified glass than between cumulus olivine grains. Blade and needle orthopyroxene crystals appear to partially enclose some olivine grains.

Microprobe analyses reveal that the granular olivine grains in one sample (ML24 in Fig. 7.2) are normally zoned, with the centre of the grains having a composition ranging from Fo_{94} - Fo_{95} to Fo_{89} - Fo_{91} at the edge of the grains. Hopper and needle orthopyroxene grains are normally zoned ranging from En_{88} at the centre to En_{84} on the edge.

Textural relations and mineral compositions suggest that olivine crystallized from a liquid that was progressively depleted in magnesium. Orthopyroxene, skeletal chromite and devitrified glass represent the crystallization sequence after olivine.

Mixed spinifex-cumulate rocks.

Only two samples (ML IC and ML 12/5) characteristic of this rock-type were identified, and are from the Type 1 (Fig. 7.4) and Type 3 (Fig. 7.11) cooling unit respectively. They are characterised by a mixture of cumulus olivine with large patches of pyroxene spinifex, and are also geochemically distinctive (see later section). These rocks cannot be regarded as an extreme variant of the olivine orthocumulate as the pyroxene spinifex occurs as a major component. Petrographically they comprise granular olivine crystals 1 - 2mm in diameter, some elongate hopper olivine crystals and tabular to bladed orthopyroxene crystals set in a groundmass of microcrystalline devitrified glass containing skeletal chromite (0.1 - 0.2mm in diameter) (Fig. 7.24).

Between the cumulus olivine patches of devitrified glass up to 8mm in diameter contain subparallel hollow orthopyroxene needles 0.05 - 1mm wide and up to 8mm in length. Needles are also randomly oriented and some clusters of hollow needles exhibit crystallographic branching with budding taking place near the base of the radiate cluster. Skeletal chromite is abundant adjacent to hollow orthopyroxene needles in the large patches of devitrified glass. This suggests that chromite was not a liquidus phase until orthopyroxene started

Fig. 7.23 Photomicrograph of olivine orthocumulate showing fractured olivine grains in a mesostasis comprising a greater proportion of needle orthopyroxene and devitrified glass than that of the mesoscumulates. Width of view 10mm, plane polarized light.

Fig. 7.24 Photomicrograph of mixed spinifex-cumulate rock comprising cumulate olivine in a groundmass of branching and radiating orthopyroxene needles, fine skeletal chromite and devtrified glass. Plane polarized light, width of view 10mm.

crystallizing.

Microcyclic spinifex-cumulate units.

Petrographically the centimetre scale spinifex units comprise mutually truncating books of olivine plates 5 to 40mm long oriented at a high angle to the layering plane. Texturally and mineralogically the spinifex layers are similar to the metre scale spinifex units. The centimetre scale olivine orthocumulate layers comprise between 68 and 85 vol. % granular olivine (1 - 2mm in diameter) and 10 - 15% needle and hopper orthopyroxene in a groundmass of skeletal chromite grains (< 0.1mm) and devitrified glass.

The contact between the centimetre scale spinifex and cumulate layers is well-defined, occurring over a transitional zone of less than 1 to 3mm wide. This zone is characterized by abundant devitrified glass, 1 - 2mm long olivine plates and approximately 5 - 10% granular olivine between 0.5 and 1mm in diameter (Fig. 7.25).

Fig. 7.25 Photomicrograph of contact between centimetre scale olivine spinifex-olivine cumulate layers in the ML12 microcylcic unit. Plane polarized light, width of view 10mm.

PART 2 : GEOCHEMISTRY

Sample Localities

A total of 45 samples collected from two localities in the Matshempondo Peridotite Suite were analysed for both major and trace elements. The samples of spinifex and cumulate-textured peridotites were collected from outcrops on :

i) Nederland 202HT (MAP 2, Section A-B). The 36 samples (ML1 - ML28) were collected from cooling units 1 to 11 (Fig. 7.2), which represent a vertical thickness of 323m above which the peridotites are strongly foliated and have suffered more pervasive alteration to talc + serpentine + chlorite + magnetite. Twelve of the samples were cut from a slab of rock 42cm in length that forms part of the microcyclic unit in cooling unit 5.

ii) Mooiplaats 206HT (MAP 1), in the core of the Commondale synform approximately 1km north of the Commondale Trading Store. Nine cumulate samples (C6 - C15) were collected from this locality.

The nature of the outcrop prevents the collection of a complete suite of samples in most of the cooling units. In the samples collected for analysis alteration is minimal and is interpreted as essentially isochemical except near polyhedral joints.

MAJOR ELEMENTS

Cooling Units

Major element analyses of 33 samples from thick spinifex and cumulate-textured layers (A and B units respectively) from the Matshempondo Peridotite Suite are shown in Table 7.1. The olivine cumulates are characterized by MgO contents ranging from 36.07 to 43.89 wt. %, FeO ranges from 5.50 - 6.85 wt. % and SiO_2 from 45.96 to 48.75 wt. %. The abundance of Al_2O_3 is between 3.52 and 5.35 wt. % and CaO between 1.65 and 3.46 wt. %. Manganese as MnO is between 0.07 and 0.12 wt. % and TiO_2 ranges from 291 to 478 ppm. The average major element proportions are shown in Table 7.2.

Major element abundances in the spinifex (Table 7.1) contrast with those of the cumulates with MgO ranging from 27.89 to 30.87 wt. % and FeO roughly constant at 5.5 wt. %. Silica and CaO contents show

TABLE 7.1 MAJOR AND TRACE ELEMENT ANALYSES OF CUMULATE AND SPINIFEX-TEXTURED MATSHEMPONDO PERIDOTITES

	ML1A	ML1B	ML1C	ML1D	ML2+	ML3	ML4	ML6	ML8A	ML8B	ML10	ML11+	ML13	ML14	ML15	ML16	ML19
SiO_2	47.37	47.52	49.25	47.59	51.15	46.34	45.96	47.66	47.36	46.92	46.76	51.30	47.22	47.10	47.82	47.98	48.24
Al_2O_3	4.59	4.88	6.08	5.00	8.02	3.52	3.66	4.97	4.69	4.41	4.46	7.84	4.56	4.39	4.98	4.83	5.16
Fe_2O_3	0.81	0.77	0.76	0.84	0.69	0.68	0.76	0.77	0.75	0.79	0.77	0.71	0.75	0.73	0.77	0.78	0.73
FeO	6.53	6.21	6.18	6.83	5.56	5.50	6.12	6.20	6.07	6.36	6.23	5.77	6.10	5.93	6.22	6.34	5.94
MnO	0.10	0.12	0.12	0.11	0.11	0.09	0.07	0.12	0.11	0.11	0.12	0.12	0.11	0.11	0.12	0.11	0.11
MgO	38.79	37.61	34.60	37.19	27.89	43.89	42.05	37.67	38.83	39.40	40.01	29.00	38.71	39.95	38.15	38.07	38.27
Cao	2.18	3.55	3.82	2.62	5.88	1.99	1.65	3.13	3.19	2.07	2.46	5.22	2.50	2.53	2.70	2.24	2.56
Na_2O	-	-	-	-	-	-	-	-	-	-	-	0.20	-	-	-	-	-
K_2O	-	-	-	-	0.02	-	-	-	-	-	-	0.02	-	-	-	-	-
TiO_2	0.0597	0.0698	0.0815	0.0658	0.1117	0.0491	0.0486	0.0738	0.0662	0.0605	0.0634	0.1297	0.0631	0.0665	0.0670	0.0619	0.0660
P_2O_5	-	0.01	-	-	-	-	-	-	-	-	-	-	-	-	-	-	-
Cr_2O_3	0.4020	0.4176	0.4581	0.4189	0.5342	0.3559	0.3725	0.4238	0.4121	0.4024	0.4128	0.5459	0.4081	0.4254	0.4132	0.3977	0.4197
NiO	0.2138	0.2287	0.1864	0.2045	0.0909	0.2530	0.2476	0.2074	0.2232	0.2259	0.1905	0.1134	0.2259	0.2223	0.2086	0.2195	0.1964
TOTAL	101.04	101.37	101.52	100.87	100.04	102.68	100.94	101.21	101.70	100.75	101.46	100.96	100.64	101.45	101.45	101.04	101.69
LOI	6.13	5.69	4.63	5.83	4.15	10.41	9.88	6.76	7.49	9.27	8.40	3.47	7.24	7.34	6.89	7.14	6.79
Nb	-	-	-	-	-	-	-	-	-	-	-	-	1.0	0.4	1.4	2.3	2.5
Zr	6.1	7.4	7.8	6.8	9.4	5.8	7.0	7.9	7.4	6.8	6.6	8.3	6.8	7.7	6.9	7.5	7.0
Y	1.2	4.3	4.5	3.8	7.0	7.3	7.7	4.7	2.0	0.2	6.0	6.4	1.0	0.6	2.1	2.3	2.4
Sr	8.7	9.9	4.8	4.2	7.5	-	-	6.5	9.6	1.8	4.5	12.5	7.2	0.1	5.5	4.5	7.9
Rb	-	-	-	-	-	-	-	-	-	1.0	-	0.7	1.8	0.8	2.2	1.5	2.0
V	84.1	86.9	106.9	85.1	138.8	63.4	63.7	87.7	80.9	74.4	78.3	146.0	80.0	81.7	81.8	81.1	78.9
Zn	38.0	39.0	38.9	45.6	29.5	26.5	33.5	42.6	40.1	40.3	43.8	32.5	51.2	40.7	32.4	29.9	60.1
Cu	1.4	1.1	2.2	1.5	4.9	-	1.6	1.2	1.0	1.6	11.8	2.3	2.4	3.8	2.1	2.0	2.0
Ni	1530	1607	1300	1487	685	1767	1745	1492	1585	1598	1300	845	1614	1589	1507	1574	1460
Cr	3390	3225	3698	3325	4263	2697	2635	3193	3178	3157	3178	4041	3156	2953	3218	3121	3153
Ti	358	418	489	394	670	294	291	442	397	364	380	778	378	399	402	371	396

- = below detection limit; + = olivine spinifex-textured peridotites.

TABLE 7.1 MAJOR AND TRACE ELEMENT ANALYSES OF CUMULATE AND SPINIFEX-TEXTURED MATSHEMPONDO PERIDOTITES

	ML20	ML21A	ML21B	ML24	ML25+	ML26	ML28	C6	C7	C8	C9	C10	C12	C13	C14	C15
SiO_2	48.07	47.93	48.75	48.51	50.96	47.18	47.85	47.90	47.89	46.66	47.49	47.83	48.08	47.71	46.96	47.70
Al_2O_3	4.91	5.35	5.49	5.11	6.86	4.24	4.82	4.91	4.94	3.89	5.31	4.98	5.43	5.04	4.27	5.17
Fe_2O_3	0.76	0.79	0.78	0.72	0.64	0.77	0.85	0.74	0.72	0.71	0.83	0.87	0.77	0.80	0.68	0.82
FeO	6.16	6.36	6.28	5.80	5.15	6.20	6.85	5.98	5.87	5.76	6.76	7.09	6.21	6.48	5.54	6.63
MnO	0.11	0.11	0.11	0.11	0.11	0.10	0.12	0.11	0.11	0.09	0.12	0.12	0.11	0.12	0.10	0.12
MgO	38.55	36.66	36.52	37.28	30.87	39.89	38.45	38.43	38.84	40.69	37.36	37.85	36.07	37.64	40.86	36.75
CaO	2.20	2.36	2.61	3.46	5.39	2.23	2.05	2.64	2.52	2.46	3.19	3.17	1.91	3.02	2.40	2.75
Na_2O	-	-	-	-	-	-	-	-	-	-	-	-	-	-	-	-
K_2O	-	-	-	-	-	-	-	-	-	-	-	-	-	-	-	-
TiO_2	0.0569	0.0589	0.0702	0.0759	0.1119	0.0738	0.0795	0.0754	0.0712	0.0614	0.0781	0.0944	0.0648	0.0645	0.0548	0.0633
P_2O_5	-	-	-	-	-	-	-	-	-	-	-	-	-	-	-	-
Cr_2O_3	0.3902	0.4192	0.4310	0.4232	0.5018	0.4096	0.4197	0.4091	0.4120	0.3932	0.4169	0.4237	0.4238	0.4172	0.3898	0.4052
NiO	0.2080	0.2029	0.1752	0.2040	0.1422	0,2340	0.2231	0.2306	0.2274	0.2451	0.2118	0.2012	0.1962	0.2022	0.2389	0.2142
TOTAL	101.41	100.23	101.22	101.69	100.73	101.32	101.70	101.42	101.60	100.95	101.78	102.64	99.26	101.48	101.49	100.61
LOI	6.88	6.40	5.34	6.32	5.77	9.44	10.28	9.38	9.48	9.66	6.73	6.97	7.31	7.62	9.15	6.49
Nb	1.1	3.9	3.4	2.4	2.1	0.9	2.8	1.1	-	-	1.6	7.8	0.4	1.1	0.1	0.6
Zr	6.8	7.5	7.3	7.6	9.3	6.4	8.1	7.4	7.3	8.2	8.3	7.5	7.7	7.4	7.5	7.8
Y	2.8	1.4	-	1.1	2.5	-	0.7	4.2	2.5	-	0.7	5.3	2.1	3.6	1.5	2.1
Sr	8.8	7.6	5.5	5.9	6.6	5.6	5.9	7.9	5.7	1.4	0.9	4.4	7.9	8.9	6.2	4.3
Rb	2.0	1.7	-	0.8	1.4	-	2.8	-	1.3	5.2	2.8	11.7	1.3	1.9	1.6	2.7
V	72.4	82.4	91.7	87.4	126.0	80.9	86.2	99.5	95.7	79.3	94.8	101.6	90.8	91.8	79.7	86.0
Zn	30.5	32.2	53.1	54.3	23.6	39.1	43.7	45.7	44.5	30.4	45.6	42.4	43.5	42.3	38.0	43.1
Cu	4.0	2.6	2.3	3.1	2.5	0.6	1.3	1.6	1.2	2.0	1.4	1.6	2.0	2.8	2.1	1.7
Ni	1463	1466	1277	1474	1051	1683	1578	1718	1630	1797	1534	1500	1363	1444	1599	1495
Cr	2975	3247	3187	3198	4319	3266	3368	3470	3497	3369	3478	3673	3449	3511	3325	3439
Ti	341	359	421	455	671	442	478	452	427	368	468	566	388	387	329	379

TABLE 7.2 AVERAGE MAJOR ELEMENT PROPORTIONS AND STANDARD DEVIATIONS FOR SPINIFEX AND CUMULATE-TEXTURED PERIDOTITIES FROM COOLING UNITS AND MICROCYCLIC UNITS

	Cumulates			
	Cooling units		Microcyclic unit	
	$\bar{x}$	s.d.	$\bar{x}$	s.d.
SiO_2	47.59	0.69	46.78	0.67
Al_2O_3	4.80	0.54	4.45	0.30
Fe_2O_3	0.77	0.05	0.94	0.03
FeO	6.22	0.37	7.60	0.28
MnO	0.11	0.01	0.09	0.05
MgO	38.50	1.84	37.87	0.89
CaO	2.61	0.52	2.33	0.21
TiO_2	0.0669	0.0097	0.0577	0.0045
Cr_2O_3	0.4108	0.0185	0.3895	0.0088
NiO	0.2156	0.0185	0.2249	0.0065
Total	101.28	0.64	100.70	0.61
	Spinifex			
SiO_2	51.14	0.17	50.77	0.30
Al_2O_3	7.57	0.62	7.55	0.19
Fe_2O_3	0.68	0.04	0.55	0.03
FeO	5.49	0.32	4.48	0.21
MnO	0.11	0.01	0.11	0.01
MgO	29.25	1.51	30.31	0.57
CaO	5.50	0.34	5.40	0.30
TiO_2	0.1178	0.0103	0.1159	0.0103
Cr_2O_3	0.5273	0.0228	0.5315	0.0165
NiO	0.1155	0.0257	0.1278	0.0087
Total	100.58	0.48	100.09	0.25

little significant variation at 51 and 5.5 wt. % respectively. Alumina and TiO_2 contents, 6.86 to 8.02 wt. % and 670 to 778 ppm respectively correspond to the higher proportion of SiO_2 in the spinifex-textured rocks compared to the cumulates. Average major element proportions are compared to those for the cumulates in Table 7.2.

The mixed spinifex-cumulate rock-type (Table 7.1, sample ML1C) has major element proportions intermediate between those of the spinifex and cumulate rock-types.

In cooling units 1 to 11 major elements plotted against height for TYPE 1, 2 and 3 cooling units show a systematic variation (Fig. 7.26). The olivine cumulates show a progressive increase in SiO_2 contents upwards in the succession. This tendency is also shown by Al_2O_3, TiO_2 and to a lesser extents by CaO. Magnesia and FeO show similar trends becoming markedly depleted upwards through the sequence (Fig. 7.26). CaO/Al_2O_3 and Al_2O_3/TiO_2 ratios (Fig. 7.26) show an overall upwards decrease through the succession. The plot of $Mg/(Fe^{2+} + Mg)$ against height shows an overall decrease upwards for the cumulate rocks (Fig. 7.26). Within each cooling unit a decrease in $Mg/(Fe^{2+} + Mg)$ upwards reflects a normal fractionation pattern with a small reversal at the base of the cumulate of the next overlying cooling unit.

On the limited data available major element variations can be categorized into three types for cooling units that contain more than one cumulate layer. The fractionation patterns recognized in the different cooling units are :

i) in cooling units 1 and 6 (Fig. 7.2), there is an increase in $Mg/(Fe^{2+} + Mg)$ from the base upwards followed by a decrease in the ratio towards the overlying spinifex unit (Fig. 7.26).

ii) in cooling units 2 and 4 the $Mg/(Fe^{2+} + Mg)$ ratio decreases through the cumulate zone to the overlying spinifex unit.

iii) in cooling unit 8 a decrease in the $Mg/(Fe^{2+} + Mg)$ ratio from the base upwards is followed by an increase towards the overlying spinifex unit (Fig. 7.26).

Other major elements also reflect the variations in the three types. The validity of the three patterns requires more rigorous testing with additional samples.

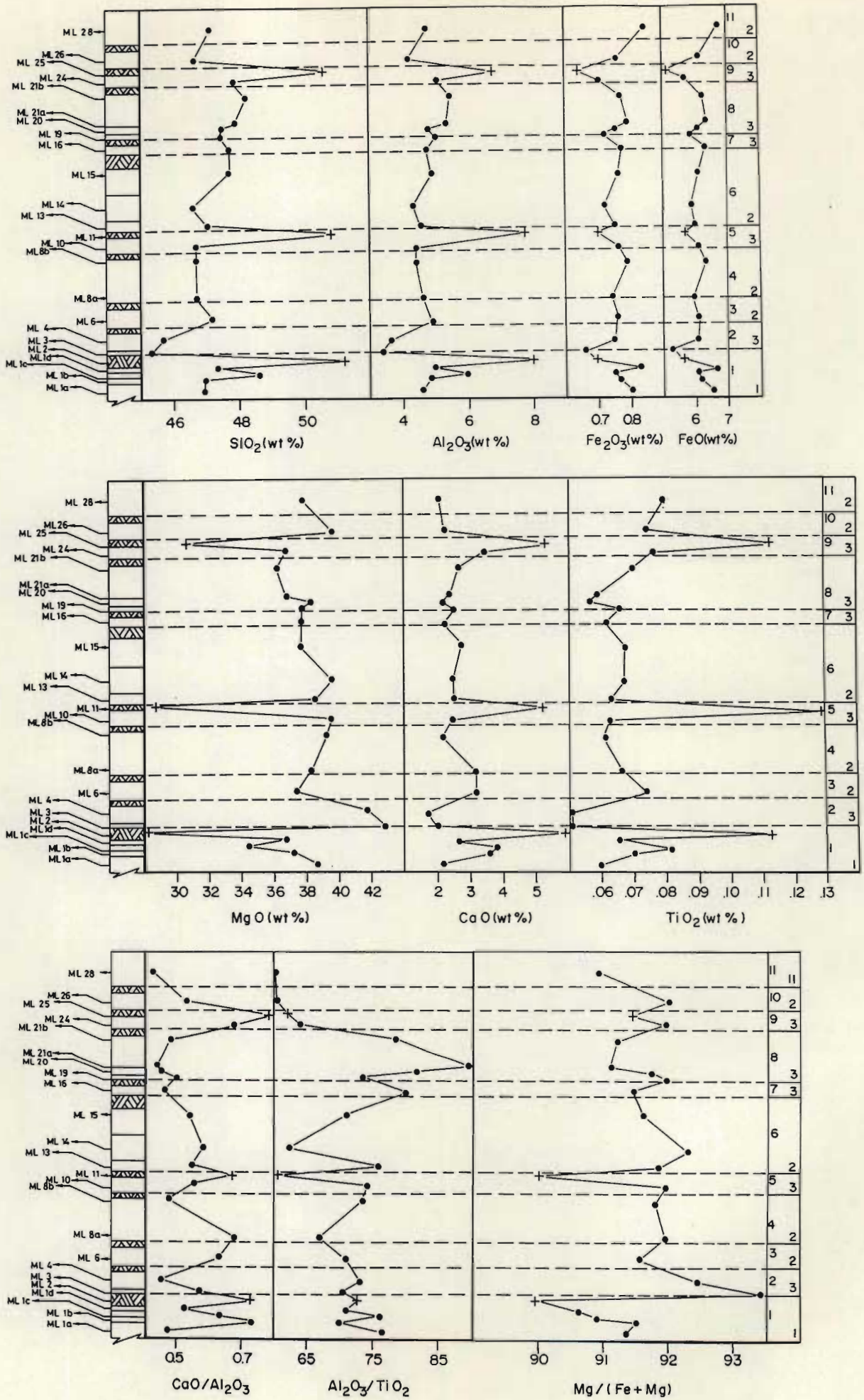

Fig. 7.26 Major element variations through eleven of the cooling units in the Matshempondo Peridotite Suite. The left hand column shows the sample localities (see Fig. 7.2 for thickness of individual cooling units). The right hand column shows the number of the cooling unit and the type of cooling unit (1, 2 or 3). o = olivine cumulate, + = olivine-plate primi-

Microcyclic Units.

Analyses of twelve samples (ML12/1 - ML12/12) from the microcyclic unit shown in Fig. 7.11 are given in Table 7.3, and are plotted against height in Fig. 7.27. Five of these samples are olivine plate spinifex, 7 are olivine orthocumulate and one is a mixed spinifex-cumulate rock. Major element abundances can be correlated to equivalent lithologies in the thick cumulate and spinifex layers through the whole succession. One difference however is the consistently lower (~ 1 wt. %) FeO and higher MgO (~ 0.5 - 2 wt. %) in the centimetre scale spinifex units compared to the metre scale equivalents. The centimetre scale orthocumulate layers however have 1 - 2 wt. % more FeO than large scale equivalents of similar MgO contents. The contrasting compositions for the two lithologies is clearly shown in the plot of FeO versus MgO in Fig. 7.28c. The average compositions of cumulate and spinifex layers are compared to those of the cooling units in Table 7.2.

Major elements plotted against height (Fig. 7.27) show marked variations as related to lithologies with SiO_2, Al_2O_3, TiO_2 and CaO displaying marked enrichment in the spinifex layers compared to the cumulates. Silica, Al_2O_3 and to a lesser extent TiO_2 show a slight increase in abundance with height for all the plate spinifex layers and CaO remains fairly constant. The cumulate layers do not show this systematic compositional variation as a whole, but where more than one sample has been taken from a single layer (ML 12/2 - ML 12/3 and ML 12/9 - ML 12/10 in Fig. 7.27) there appears to be an upward decrease in SiO_2, Al_2O_3 and TiO_2. In these orthocumulate layers MgO and FeO show an upward increase and are inversely correlated to SiO_2. More data are required to confirm these observations.

Interelement variations.

Interelement variations of the major elements of spinifex and cumulate-textured rock-types are shown in Fig. 7.28. The oxides SiO_2, Al_2O_3, CaO and TiO_2 show well constrained inverse correlations against MgO content. In these plots the microcyclic units consistently define a steeper trend than for the large scale cooling units (Fig. 7.28).

TABLE 7.3 MAJOR AND TRACE ELEMENT ANALYSES OF CENTIMETRE SCALE RHYTHMIC CUMULATE AND SPINIFEX-TEXTURED PERIDOTITES

	ML12/1+	ML12/2	ML12/3	ML12/4+	ML12/5+	ML12/6+	ML12/7	ML12/8+	ML12/9	ML12/10	ML12/11+	ML12/12
SiO_2	50.48	46.36	46.04	50.67	48.78	50.74	47.45	51.27	46.88	46.26	50.69	47.67
Al_2O_3	7.73	4.35	4.08	7.32	5.65	7.75	4.93	7.57	4.59	4.22	7.44	4.52
Fe_2O_3	0.57	0.93	0.98	0.59	0.75	0.53	0.89	0.54	0.94	0.97	0.54	0.92
FeO	4.59	7.52	7.93	4.79	6.05	4.26	7.17	4.35	7.64	7.86	4.41	7.46
MnO	0.10	0.12	0.11	0.11	0.11	0.11	-	0.12	0.10	0.11	0.11	0.11
MgO	30.11	38.17	39.01	31.08	34.85	30.70	36.31	29.99	38.17	37.92	29.66	37.61
CaO	5.34	2.42	2.34	4.93	3.52	5.42	2.60	5.55	2.08	2.09	5.74	2.43
Na_2O	-	-	-	-	-	-	-	-	-	-	0.14	-
K_2O	-	-	-	-	-	-	-	0.01	-	-	0.01	-
TiO_2	0.1175	0.0593	0.0567	0.1030	0.0743	0.1078	0.0630	0.1238	0.0613	0.0510	0.1272	0.0546
P_2O_5	-	0.01	-	-	0.01	-	0,01	-	-	-	-	0.01
Cr_2O_3	0.5164	0.3847	0.3815	0.5122	0.4364	0.5498	0.4055	0.5433	0.3854	0.3861	0.5360	0.3935
NiO	0.1333	0.2199	0.2366	0.1377	0.1919	0.1307	0.2191	0.1194	0.2214	0.2260	0.1179	0.2264
TOTAL	99.68	100.53	101.17	100.24	100.42	100.30	100.03	100.18	101.08	100.00	100.04	101.41
LOI	5.31	7.69	8.24	5.32	6.69	5.49	7.89	5.07	9.22	8.76	5.29	8.04
Nb	-	-	-	-	-	-	-	-	-	-	1.2	0.9
Zr	9.0	7.5	6.3	9.4	8.3	8.8	8.0	8.3	7.1	6.2	9.0	6.7
Y	5.2	5.2	5.0	8.1	6.8	7.1	4.1	0.9	4.5	6.0	7.6	8.5
Sr	5.2	6.3	6.8	5.6	6.7	7.2	3.8	6.1	4.1	5.7	6.4	6.7
Rb	-	-	0.2	5.8	1.0	3.8	-	2.4	0.8	0.5	8.0	5.7
V	145.9	78.2	74.0	136.2	103.6	148.5	87.9	147.3	76.1	72.8	151.0	76.7
Zn	28.1	43.6	43.0	30.5	35.7	30.1	39.9	30.4	42.4	44.4	27.9	41.8
Cu	2.8	2.5	2.3	2.7	2.1	3.2	2.4	3.9	2.0	1.8	1.6	4.2
Ni	975	1570	1657	1014	1372	940	1534	892	1578	1606	884	1584
Cr	4447	3218	3230	4378	3589	4637	3418	4528	3152	3236	4559	3332
Ti	704	356	340	617	445	646	378	742	367	306	763	327

- Below detection limit; + = olivine spinifex-textured peridotite

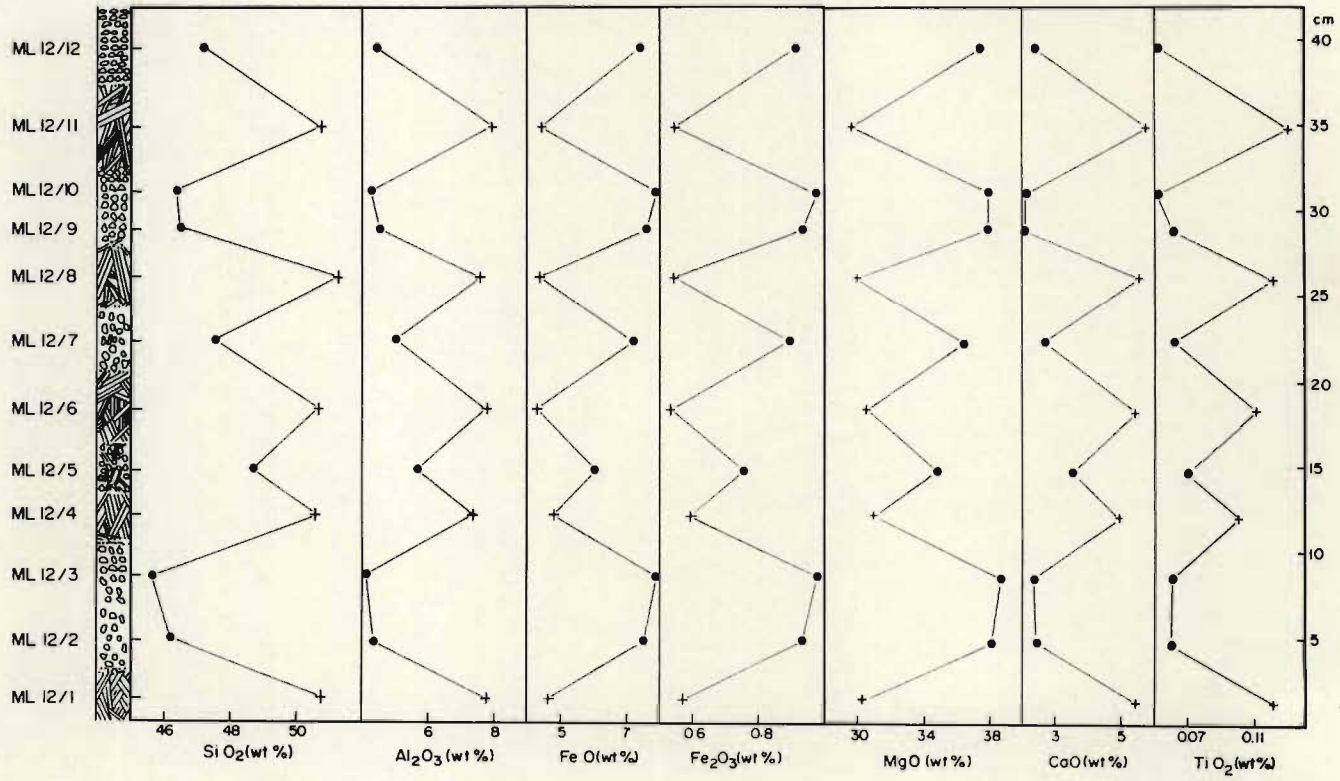

Fig. 7.27 Major element variations through part of the microcylic unit in cooling unit 5. • = olivine cumulate, + = olivine plate spinifex.

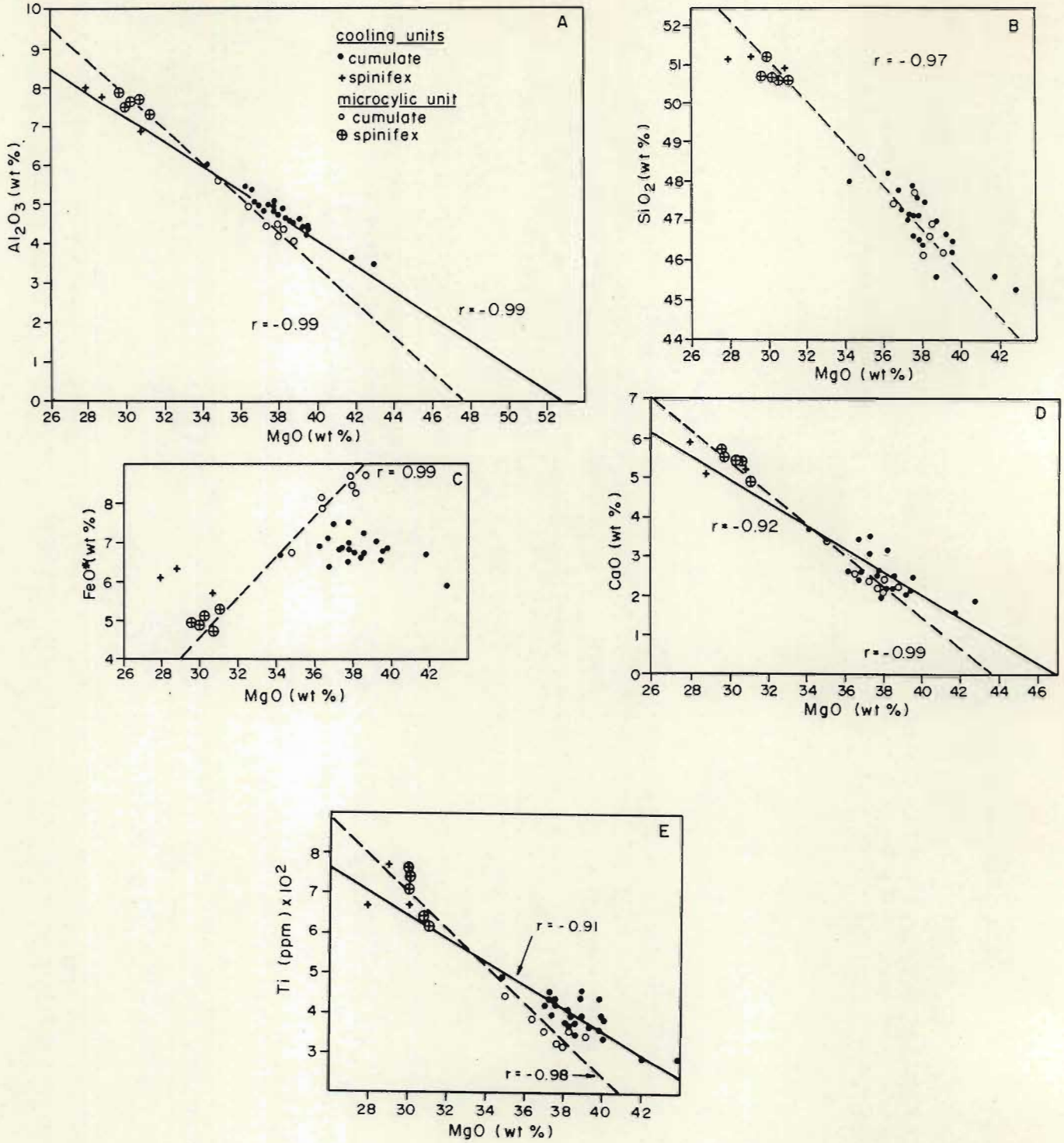

Fig. 7.28 Major element abundances plotted against MgO for spinifex-textured and cumulate rock types from the Matshempondo Peridotite Suite. Dashed regression curves is for sample ML12/1 - ML12/12 (microcyclic unit) and solid regression curve for samples ML1 - ML28 (cooling units).

These trends generally reflect the higher amounts of Al_2O_3, CaO and TiO_2 in the spinifex layers of microcyclic units compared to the metre scale equivalents with similar MgO contents. Similarly the Al_2O_3, CaO and TiO_2 contents in the cumulate layers of microcyclic units are lower than those in metre scale equivalents with similar MgO contents.

TRACE ELEMENTS

Cooling Units.

The trace elements Cr, V, Ni, Zn, Cu, Sr, Y, Zr, Nb and Rb were determined by X-ray fluorescence spectrometry (see Appendix 3 for analytical details). The analyses are presented in Table 7.1. Niobium and Rb were below detection limit for most of the samples analysed.

Variations in trace element content with height for the entire succession are shown in Fig. 7.29. Those trace elements that are incompatible with olivine (Zr, Cr, V and Cu) show a small but discernible overall increase upwards in the succession. In the cumulates Cr increases systematically through the sequence from about 2700 ppm in cooling unit 2 to 3360 in cooling unit 11 (Fig. 7.29). In the lowermost cooling unit (unit 1 in Fig. 7.29) Cr is markedly higher than in the cumulates of the overlying units and varies in proportion to the amount of mesostasis (Fig. 7.4) suggesting an even stronger pyroxene control or possibly the presence of chromium spinel. These data and petrography suggest that pyroxene and chromite crystallized once the liquid had passed out of the olivine stability field, and that the proportion of these components in the mesostasis is inversely correlated to the MgO content of the liquid.

The spinifex units have a much higher Cr content (4041 to 4319 ppm) compared to the cumulate rocks and together with the concomitant lower magnesium values indicates the strong control of pyroxene on the distribution of this element. The non-cumulate control of the Cr is further highlighted by a comparison to the variation of the high field strength incompatible elements Zr, V and Ti. The patterns for these elements are almost identical through the succession.

Nickel, as expected, shows a strong sympathetic behaviour with MgO and

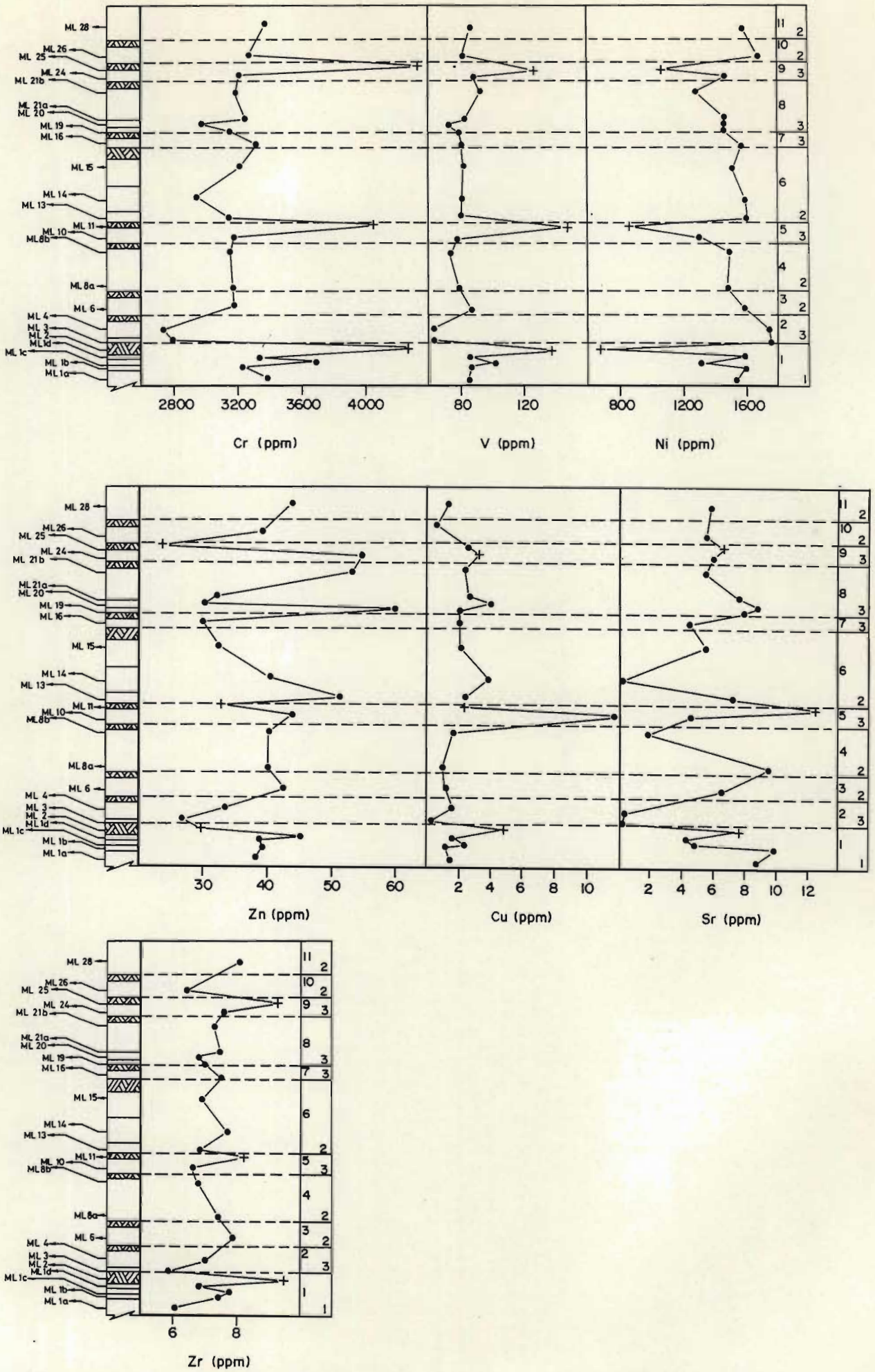

Fig. 7.29 Trace element variations through eleven of the cooling units in the Matshempondo Peridotite Suite. The left hand column shows the sample localities (see Fig. 7.2 for thickness of individual cooling units). The right hand column show the number of the cooling unit and the type of cooling unit (1, 2 or 3). • = olivine cumulate, + = olivine-plate spinif-

is markedly enriched in the olivine cumulates (1300 - 1767 ppm), as compared to olivine spinifex units (685 to 1051 ppm). Two major cycles and parts of two others are defined by the Ni trends through the succession. The Ni trend (Fig. 7.29) show three compositional reversals through the succession, these occurring at the base of cooling units 2, 6 and 10. At the base of each cycle the cumulates have Ni contents between 209 and 314 ppm higher than the top of the underlying cycle. The Ni contents through the two major cycles (cooling units 2 to 5 and 6 to 9) show a consistent upward decrease in the cumulate layers. In the lower cycle (cooling units 2 to 5) (Fig. 7.29) Ni decreases from 1767 ppm at the base of cooling unit 2 to 1300 ppm in the cumulate layer of cooling unit 5. Similarly in the overlying major cycle Ni decreases from 1614 ppm at the base of cooling unit 6 to 1474 ppm in the cumulate layer of cooling unit 9. These apparent cycles may be an artifact of sampling or could be of petrogenetic importance. The variation of MgO through the succession shows similar but less well-defined cycles.

For the alkali and alkali earth elements Rb is below detection limits and Sr is extremely low, varying between 0.2 and 10 ppm in the cumulates. Strontium appears to have remained relatively immobile and not significantly affected by metamorphism and alteration in that this element shows a trend similar to the other incompatible elements, eg Cr and V but is less well constrained (Fig. 7.29).

Microcyclic Unit.

Variations in trace element content with height for the microcyclic unit in Fig. 7.11 are shown in Fig. 7.30. Those trace elements that are incompatible with olivine (Cr, V, Zr and Cu) show a small but discernible overall increase upwards through the microcyclic unit for V, Zr and Cu. The Cr content however increases significantly from 3218 to 3332 ppm and 4447 to 4559 ppm in the cumulate and spinifex layers respectively (Fig. 7.30). This increase reflects the concomitant upward decrease by 0.56 and 0.45 wt. % MgO in the cumulate and spinifex units respectively. Nickel and Zn show a strong sympathetic behaviour with MgO and are strongly enriched in the cumulates as compared to the spinifex-textured layers (Fig. 7.30). The trends for Sr and Y show an overall increase through the microcyclic unit. The variation of these elements through the

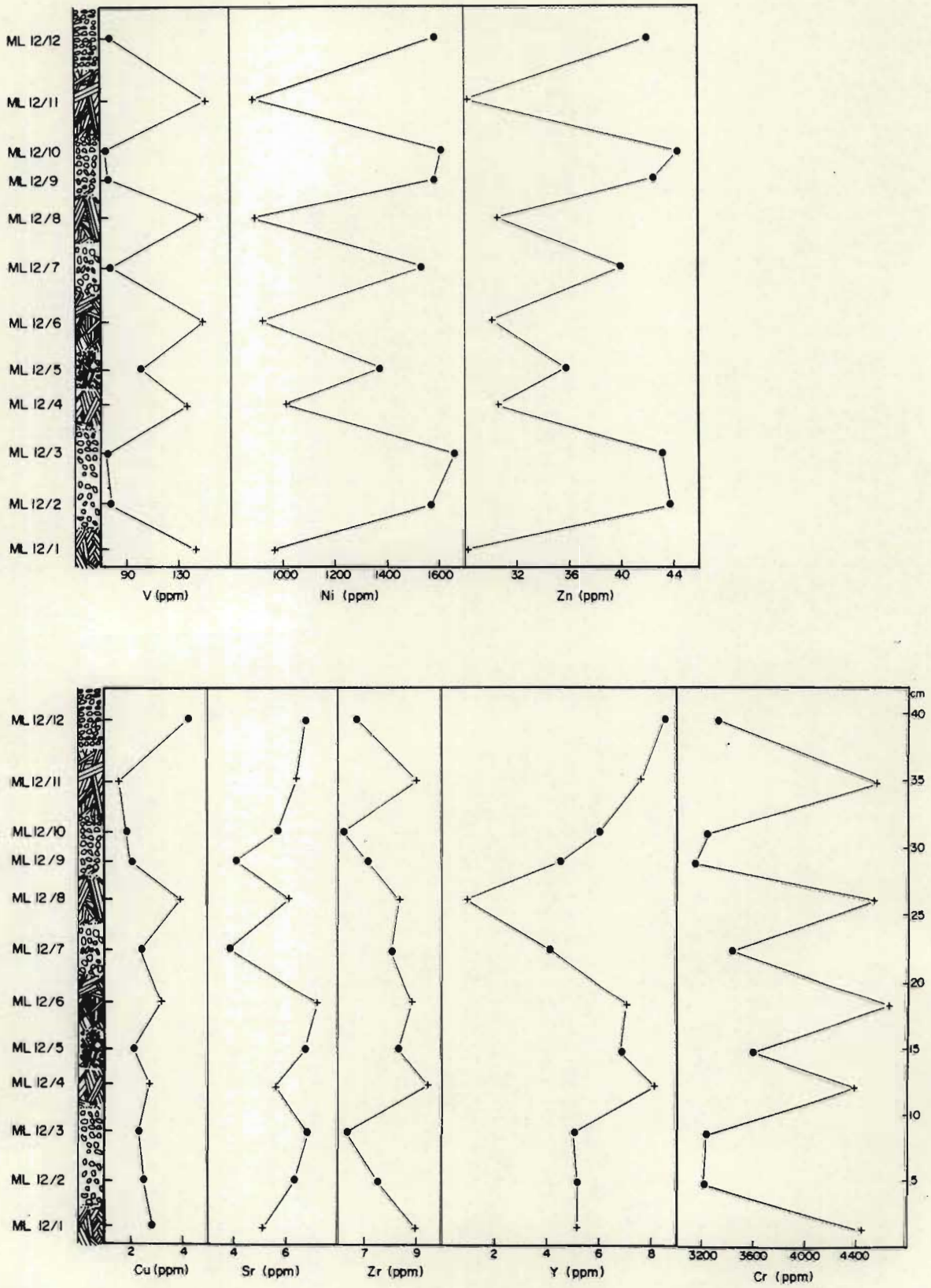

Fig. 7.30 Trace element variations through part of the microcyclic unit in cooling unit 5. • = olivine cumulate, + = olivine plate spinifex.

microcyclic unit suggest three cycles, however the low absolute amounts and small variation in their abundances should not be used as the sole basis for sub-dividing the microcyclic unit. The mixed-spinifex cumulate rock (sample ML 12/5) typically has trace element contents between that of the spinifex and cumulate layers.

Interelement variations

Trace element abundances for the cumulates and spinifex-textured rocks are shown plotted against MgO in Fig. 7.31. Abundances of the trace elements incompatible with olivine, (Cr and V) show well constrained correlations against MgO content (Fig. 7.31 a and b). In these plots the microcyclic units consistently define a steeper trend than for the large scale cooling units (Fig. 7.31). These trends generally reflect the lower and higher abundances of Cr and V in the cumulate and spinifex layers respectively compared to metre scale equivalents with similar MgO contents. In the microcyclic layers Ni is generally depleted in the spinifex layers and enriched in the cumulates compared to similar rocks from the metre scale cooling units (Fig. 7.31c). The plots of Zr and Zn show an overall decrease and increase respectively with increasing MgO contents (Fig. 7.31 d and e).

Effects of alteration on geochemistry

The influence of alteration on the primary compositions of Archaean mafic and ultramafic rocks has received much attention in recent years (Beswick, 1982.)

The well constrained and systematic variation in both major and trace element abundances with height (Figures 7.26, 7.27, 7.29 and 7.30) and the major and trace element variation diagrams (Figures 7.28 and 7.31) suggest that the effects of alteration are not significant for the ML suite of samples. Major and trace element variation diagrams (not shown) for samples C6 - C15 (locality on MAP 1) show well constrained and systematic variations even though significantly more altered than samples from the ML suite. The alteration observed is of greenschist facies involving hydration and alteration of olivine to serpentine and orthopyroxene to chlorite with fine chlorite and tremolite overgrowths in the groundmass of devitrified glass. Petrographic evidence, except

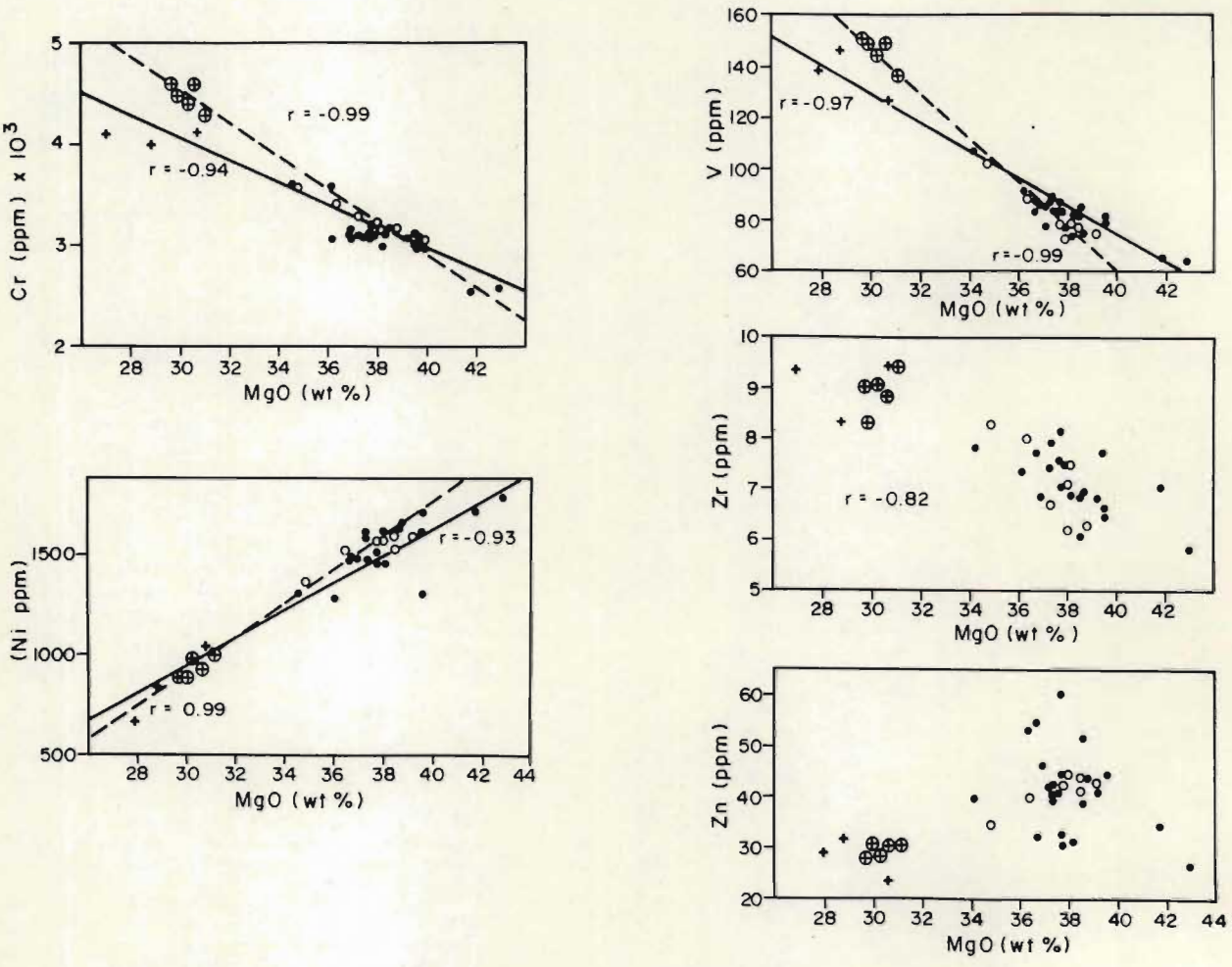

Fig. 7.31 Trace element abundances plotted against MgO for spinifex-textured and cumulate rock-types. Dashed regression curve is for samples ML12/1 - ML12/12 (microcyclic unit) and solid regression curve for samples ML1 - ML28 (cooling units). Ornamentation as in Fig. 7.28.

for samples C6, C7, C8 and ML28, reflects low strains through these portions of the Matshempondo Peridotite Suite, and together with the well constrained compositional variations all alteration effects are regarded as having been isochemical. Loss on ignition values for the cumulates and spinifex-textured rocks range between 4.63 and 10.40 wt. and 3.47 to 6.69 wt. % respectively with an average value of 7.23 wt. %. These observations are confirmed by a plot of loss on ignition versus normative olivine that shows a systematic variation, suggesting the alteration is essentially serpentinization of olivine (Fig. 7.32).

High field strength incompatible elements.

Studies involving the high field strength incompatible elements are important for two aspects :

i) they are not susceptible to changes resulting from low greenshcist facies metamorphism.
ii) as these elements are in many cases incompatible with respect to early formed phases ratios involving these elements have important petrogenetic implications and generally reflect the liquid compositions.

Alteration studies have demonstrated that due to their high field strength (charge/ionic radius) Ti, Zr and Y are relatively immobile during greenschist facies metamorphism (cf. Ludden et al., 1983). The absolute amounts of these elements may change but their ratios are not substantially affected. In ultramafic rocks Ti, Zr and Y are incompatible and their systematic variation reflects increasing concentration in the liquid with fractional crystallization or inversely so with partial melting (Pearce and Cann, 1973; Pearce and Norry, 1979).

In Fig. 7.33 Ti, Zr and Y are plotted against each other and together with ratios involving V, Cr and Al_2O_3 (Table 7.4) are compared to the chondritic ratios. These data indicate the Matshmepondo peridotites to have :

a) Ti/Zr, Y/Zr and Cr/Zr ratios lower than chondritic values
b) V/Zr, Al_2O_3/Zr, Al_2O_3/Ti, V/Ti, Cr/Ti and Y/Ti ratios are greater than chondritic values

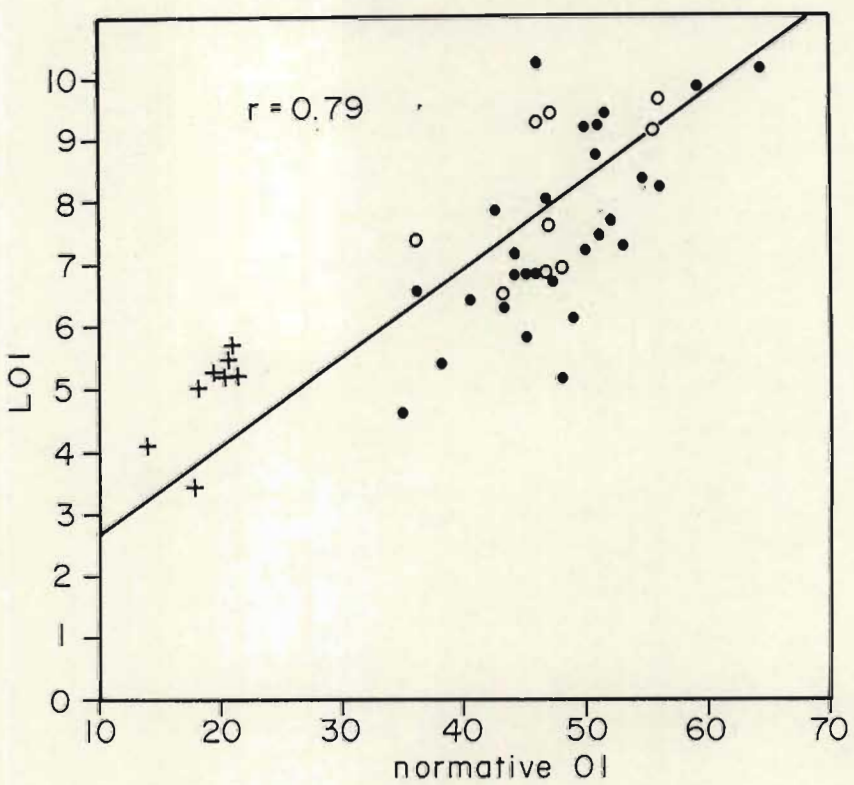

Fig. 7.32 Loss on ignition plotted against normative olivine for samples ML1A to ML28 (• = cumulate, + = spinifex) and C6 - C15 (o = cumulate).

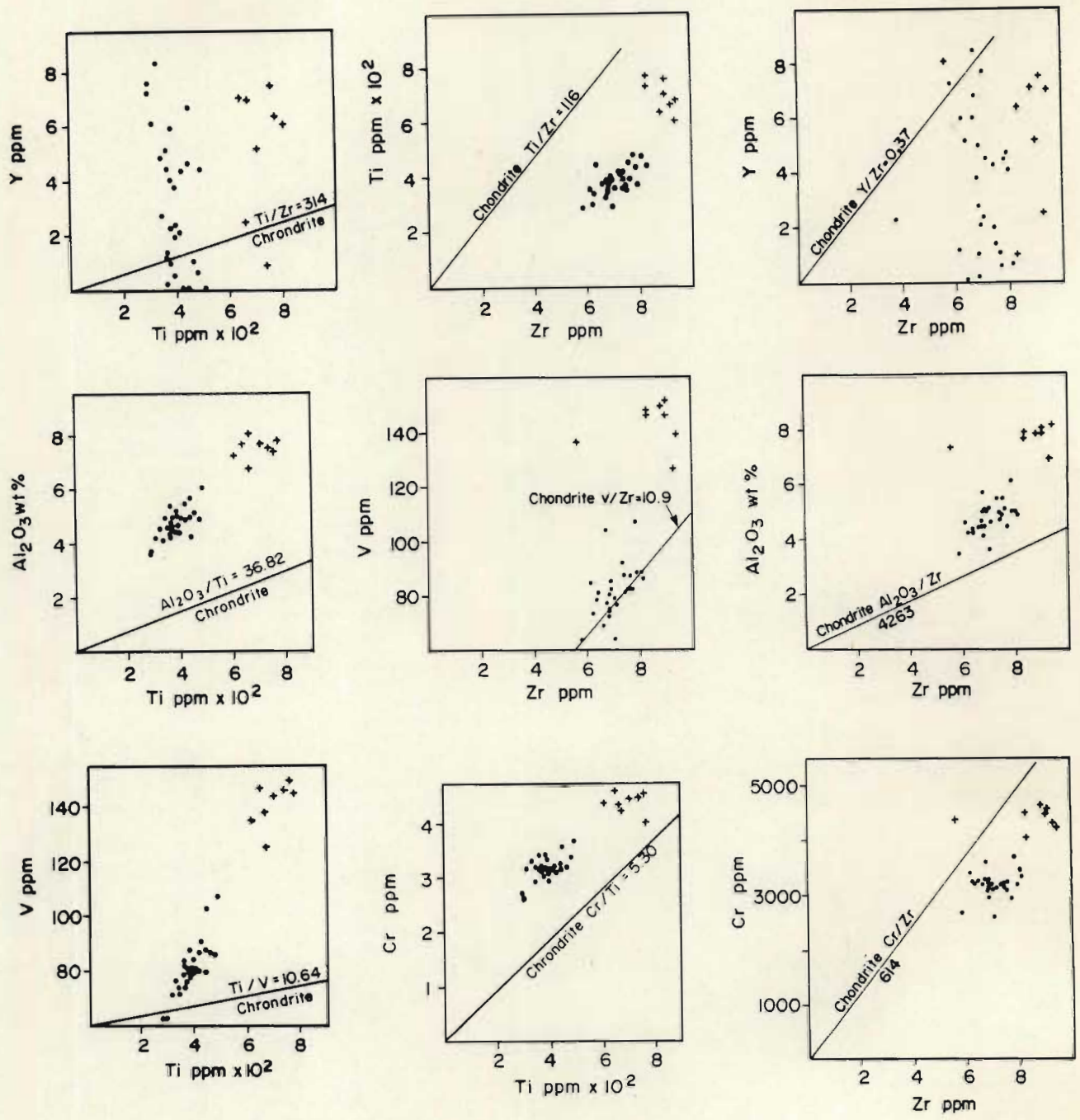

Fig. 7.33 Trace element and incompatible major element variations in spinifex-textured (+) and cumulate (•) rock-types, samples ML1A - ML28. Chondritic ratios are from Taylor and McLennan (1981).

TABLE 7.4 INCOMPATIBLE ELEMENT RATIOS FOR SPINIFEX AND CUMULATES FROM THE MATSHEMPONDO PERIDOTITE SUITE

	Zr/Y	Al_2O_3/Zr	Cr/Zr	V/Zr	Ti/Y	Al_2O_3/Ti	Cr/Ti	Ti/V	Ti/Zr	CaO/Al_2O_3	Al_2O_3/TiO_2
ML1A	5.08	7524	556	13.79	298	128	9.47	4.28	58.69	0.47	76.50
ML1B	1.72	6594	436	11.74	97	116	7.72	4.81	56.49	0.73	69.71
ML1C	1.73	7795	474	13.71	109	124	7.56	4.57	62.69	0.63	76.00
ML1D	1.79	7352	489	12.51	104	127	8.44	4.63	57.94	0.52	71.43
ML2	1.34	8531	453	14.77	96	120	6.36	4.83	71.28	0.73	72.91
ML3	0.79	6069	465	10.93	40	120	9.17	4.64	50.69	0.57	70.40
ML4	0.91	5229	376	9.10	37	125	9.05	4.57	41.57	0.45	73.20
ML6	1.68	6291	404	11.10	94	112	7.22	5.04	55.95	0.63	71.00
ML8A	3.70	6338	429	10.93	198	118	8.01	4.91	53.65	0.68	67.00
ML8B	34.00	6486	464	10.49	1820	121	8.67	4.89	53.53	0.47	73.50
ML10	1.10	6757	481	11.86	63	117	8.36	4.85	57.58	0.55	74.33
ML11	1.30	9446	487	17.59	121	100	5.19	5.33	93.73	0.67	60.31
ML13	6.80	6705	464	11.76	378	120	8.35	4.73	55.59	0.69	64.42
ML14	12.83	5701	383	10.61	665	110	7.40	4.88	51.82	0.58	62.71
ML15	3.29	7217	466	11.86	191	124	8.00	4.91	58.26	0.54	71.14
ML16	3.26	6440	416	10.81	161	130	8.41	4.57	49.47	0.46	80.50
ML19	2.92	7371	450	11.27	165	130	7.96	5.02	56.57	0.50	73.71
ML20	2.43	7220	438	10.65	122	144	8.72	4.71	50.15	0.45	81.83
ML21A	5.36	7133	433	10.99	256	149	9.04	4.36	47.87	0.44	89.17
ML21B	-	7520	436	12.56	-	130	7.57	4.59	57.67	0.48	78.43
ML24	6.91	6724	421	11.50	414	112	7.03	5.21	59.87	0.68	63.88
ML25	3.72	7376	464	13.55	268	102	6.44	5.33	72.15	0.79	62.36
ML26	-	6625	510	12.64	-	96	7.39	5.46	69.06	0.53	60.57
ML28	11.57	5950	416	10.64	683	101	7.05	5.55	59.01	0.43	60.25
C6	1.76	6635	469	13.45	108	108	7.68	4.54	61.08	0.54	61.38
C7	2.92	6767	479	13.11	171	116	8.19	4.46	58.49	0.51	70.57
C8	-	4744	411	9.67	-	106	9.15	4.64	44.88	0.63	64.83
C9	11.86	6398	419	11.42	669	113	7.43	4.94	56.39	0.60	66.37
C10	1.42	6640	490	13.55	107	88	6.49	5.57	75.47	0.64	55.33
C12	3.67	7052	448	11.79	185	140	8.89	4.27	50.39	0.35	90.50
C13	2.06	6810	475	12.41	108	130	9.07	4.22	52.30	0.60	84.00

TABLE 7.4 continued

	Zr/Y	Al_2O_3/Zr	Cr/Zr	V/Zr	Ti/Y	Al_2O_3/Ti	Cr/Ti	Ti/V	Ti/Zr	CaO/Al_2O_3	Al_2O_3/TiO_2
C14	5.0	5693	443	10.63	219	130	10.11	4.13	43.87	0.56	85.40
C15	3.71	6628	441	11.03	180	136	9.07	4.41	48.59	0.53	86.17
ML12/1	1.73	8589	494	16.21	136	110	6.32	4.83	78.22	0.69	69.42
ML12/2	1.44	5800	429	10.43	68	122	9.04	4.55	47.77	0.56	72.50
ML12/3	1.26	6476	513	11.75	68	120	9.50	4.59	53.97	0.57	68.00
ML12/4	1.16	7787	466	14.49	76	119	7.10	4.53	65.64	0.67	73.20
ML12/5	1.22	6807	432	12.48	65	127	8.07	4.30	53.61	0.62	80.71
ML12/6	1.24	8806	527	16.88	91	120	7.18	4.35	73.41	0.70	70.45
ML12/7	1.95	6162	427	10.99	92	130	9.04	4.30	47.25	0.53	82.17
ML12/8	9.22	9120	546	17.75	824	102	6.10	5.04	89.40	0.73	63.08
ML12/9	1.58	6465	444	10.72	82	125	8.59	4.82	51.69	0.45	76.50
ML12/10	1.03	6807	522	11.74	51	138	10.58	4.20	49.35	0.50	84.40
ML12/11	1.18	8267	507	16.78	100	98	5.98	5.05	84.78	0.72	61.08
ML12/12	0.79	6746	497	11.45	38	138	10.22	4.25	48.66	0.54	90.40

- where Y is below detection limit

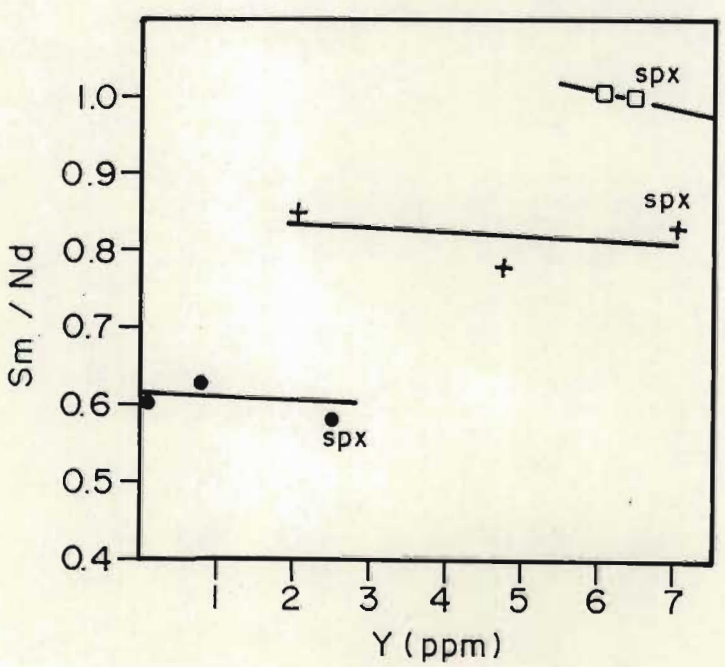

Fig. 7.34 Sm/Nd plotted against Y defines three distinct trends with the spinifex-textured rocks (spx) typically having higher Y contents than the cumulates with similar Sm/Nd ratios. • = ML25, ML26, ML28; ■ = ML10, ML11; + = ML2, ML6, ML8A. Sm and Nd data are given in TABLE 7.5.

c) The variance of Y is significantly greater than Zr or Ti for both the spinifex and cumulates giving rise to an effective constant value and two parallel trends on plots involving Zr and Ti (Fig. 7.33), with the spinifex rocks typically having higher Zr and Ti contents. This behaviour is anomalous and is unlikely to be explained by alteration affects. Alternatively the Y contents may reflect melting of a controlling mineral, such as garnet, that is present in variable amounts in the mantle source. This interpretation is supported by the wide range of Sm/Nd ratios (see later section) indicating quite different rare-earth patterns. The available Sm/Nd data suggest at least three cycles through cooling units 1 to 11 that may be related to the Y abundances and broadly to the cycles defined by reversals in Ni content. In Fig. 7.34 Sm/Nd plotted against Y defines three discrete trends, where the Sm/Nd ratio and Y content are characteristic for the cumulates and spinifex of each group. This pattern (Fig. 7.34) suggests that garnet, controlled the distribution of Y during sequential melting of a mineralogically and isotopically (see later section) inhomogenous source, and would account for the Y/Ti and Y/Zr trends observed in Fig. 7.33.

d) The mantle source for the Matshempondo peridotites is considered to be strongly non-chondritic.

Molecular proportion ratio diagrams.

Molecular proportion ratio diagrams may be used to test the trends of interelement variation to determine whether there is a specific mineral controlling fractionation, and secondly, to observe the possible dispersion due to alteration. Pearce (1968) developed a theoretical basis by which compositional relationships of fractionating species could be examined in terms of the molecular proportions.

Using this approach the molecular proportions of possible fractionating mineral species are normalized to a single incompatible oxide or trace element. The normalizing oxide or trace element must be entirely partitioned into the liquid, so that the absolute amount of the normalizing oxide remains constant. A suite of unaltered samples of variable composition will then reveal the petrogenetic relationships between them in terms of a linear array of points not

passing through the origin (Pearce, 1968). This is achieved provided the parent material is homogeneous and no secondary alteration processes are present. Beswick (1982) shows that molecular proportion ratio diagrams using oxides such as Na_2O and K_2O, which may be mobile during alteration, as the denominator gives rise to a fan shaped scatter of points radiating from the origin. If there has been no alteration selection of appropriate oxides would result in a linear array of points the slope of which would indicate the fractionating mineral.

Chayes (1949) and Rollinson and Roberts (1986) show that ratio correlations using three variables are highly dependent on the coefficient of variation for each of the variables. Strongly enhanced or even spurious correlations can result where the coefficient of variation in the normalizing variable greatly exceeds the coefficients of variation of the numerators.

The validity of any particular application and an assessment of the enhanced correlation may be obtained using random number sets generated within the range of values. For example random number sets for (FeO + MgO), SiO_2 and Al_2O_3 molecular proportions within the range of the Matshempondo peridotites are poorly correlated ($r < 0.45$) in plots between any two of the component oxides. However when Al_2O_3 is used as the normalizing molecular proportion a strong enhanced correlation ($r = 0.839$) results due to the large variance in Al_2O_3. Rollinson and Roberts (1986) conclude that molecular proportion ratio diagrams may not always reflect igneous fractionation in the way suggested by Pearce (1968), Beswick (1982) and Barnes (1985). In some cases the correlations are entirely spurious and critical assessment is required of the coefficients of variation of each of the three variables. The data set is potentially meaningful only where the coefficients of variation of each of the variables are similar, or where a higher degree of correlation is observed between any two of the component oxides (equation 1, Rollinson and Roberts, 1986).

Correlations of oxide proportions in major element analyses arise due to chemical association through petrogenesis, but imposed correlations are also produced due to the closure problem to 100 percent. The applicability of using molecular proportion ratios to test fractionation in rock systems is dependent on the variance of each

component and the correlation coefficient between any two of the component oxides used in molecular proportion ratio plots. Table 7.5 compares the variances and correlation coefficients for interoxide and molecular proportion ratio plots (Fig. 7.35) for the Matshempondo Peridotite Suite. Correlation coefficients in interoxide plots between any two of the three components used in each molecular proportion ratio diagrams (Fig. 7.35) are between 0.930 and 0.992 whereas those in the molecular proportion ratio diagrams range from 0.986 to 0.998 (Table 7.5). Even though the variance in the normalizing oxide is relatively high (Table 7.5) the induced correlation in each of the molecular proportion ratio diagrams is not significant because of the high correlation coefficients between any two oxides used in molecular proportion ratio diagrams.

In this case the data is considered significant and to reflect true correlations between the components arising from petrogenetic processes. In Fig. 7.35 a, b and c, (MgO + FeO*) and SiO_2 molecular proportions (compatible with olivine) are normalized to TiO_2, Al_2O_3 and CaO molecular proportions (incompatible with olivine). In all three plots a linear array of data points (Fig. 7.35) defines a slope of 2:1 which corresponds to olivine control in the fractionation of the peridotites. Cumulates with low incompatible oxide contents plot in the upper right hand portion of the diagrams (Fig. 7.35 a, b and c) and the spinifex-textured rocks with high incompatible element contents representing crystallization from increasingly more fractionated liquids plot towards the lower left hand corner.

Sm-Nd SYSTEMATICS

Five olivine orthocumulate samples and three olivine plate spinifex samples, (ML6, 8A, 10, 26 and 28) and (ML2, 11 and 25) respectively were selected for a Sm-Nd isotopic study. Samples were chosen on the basis of the widest observed range of major and trace element compositions and also to be representative of the entire succession. The analyses were performed by Dr A H Wilson while on sabbatical at the Department of Terrestrial Magnetism of the Carnegie Institution of Washington.

TABLE 7.5 CORRELATION COEFFICIENTS (r) AND VARIANCES FOR DATA FROM THE MATSHEMPONDO PERIDOTITE SUITE

	interoxide variation (r)
$(MgO + FeO^*) - SiO_2$	- 0.984
$(MgO + FeO^*) - Al_2O_3$	- 0.992
$SiO_2 - Al_2O_3$	0.979
$(MgO + FeO^*) - TiO_2$	- 0.946
$SiO_2 - TiO_2$	0.922
$(MgO + FeO^*) - TiO_2$	- 0.966
$SiO_2 - CaO$	0.930
	molecular proportion ratio (r)
$(MgO + FeO^*)/Al_2O_3 - SiO_2/Al_2O_3$	0.998
$(MgO + FeO^*)/TiO_2 - SiO_2/TiO_2$	0.986
$(MgO + FeO^*)/CaO - SiO_2/CaO$	0.993
	variance ($sd/\bar{x}$)
$MgO + FeO^*$	0.103
SiO_2	0.036
Al_2O_3	0.250
TiO_2	0.313
CaO	0.409

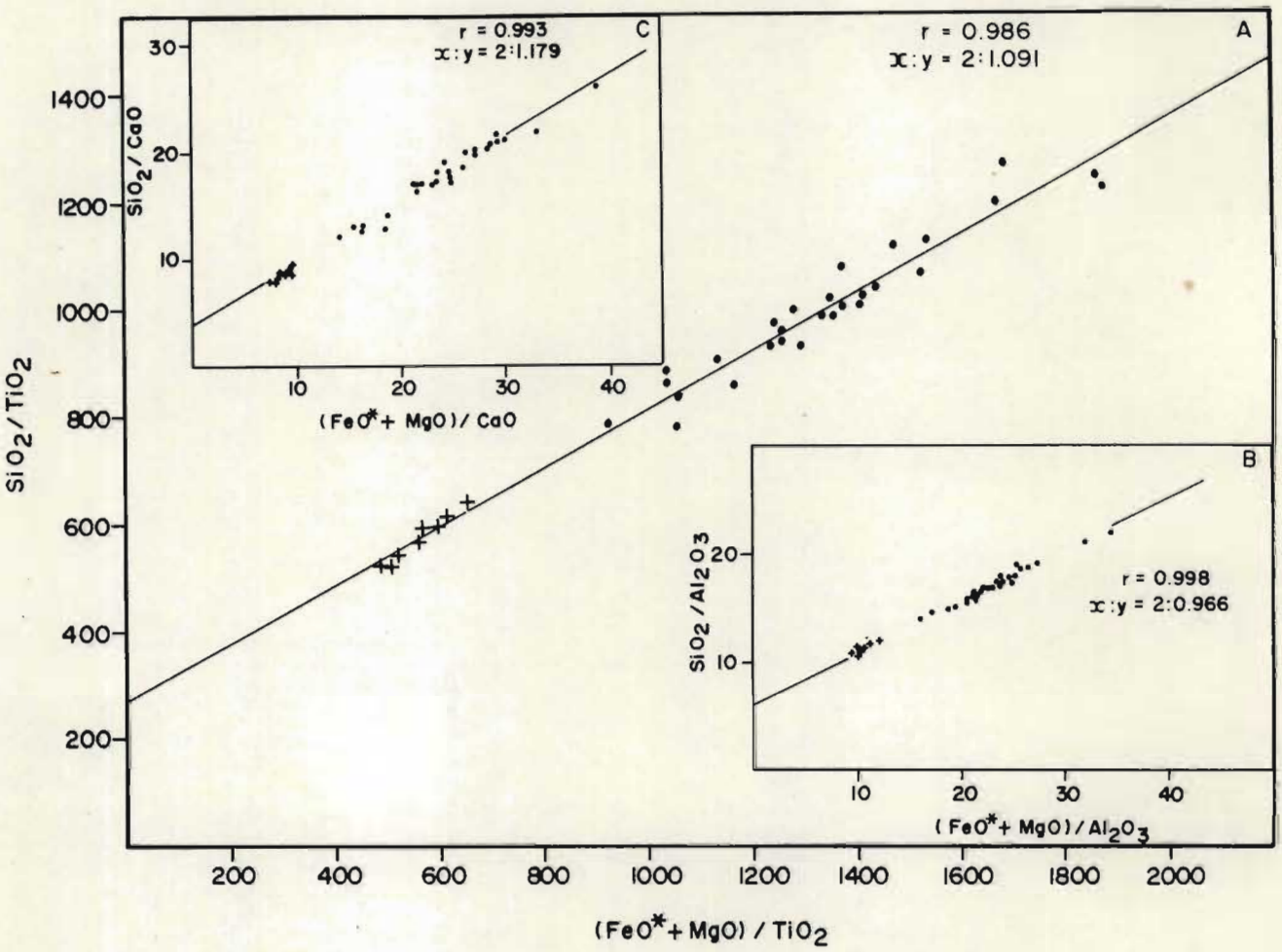

Fig. 7.35 Molecular proportion ratio diagrams in which (MgO + FeO*) and SiO_2 (compatible with olivine) molecular proportions are normalized against an incompatible oxide molecular proportion; TiO_2 in A, Al_2O_3 in B and CaO in C. The 2 : 1 slope indicates olivine control in the fractionation of the spinifex and cumulate-textured rock-types.

Sm-Nd data

Absolute amounts of Sm and Nd are extremely low and vary from 0.0480 to 0.1295 ppm and 0.0362 to 0.2267 ppm respectively (Table 7.6) with abundances of these elements greater in the spinifex than the orthocumulates. In cooling unit 5 (samples ML10 and ML11) the marked difference in the Sm/Nd ratio between the spinifex and cumulate layers is the result of Nd being concentrated in greater amounts than Sm in the more evolved (spinifex) rock-types. The Sm/Nd ratios vary between 0.789 and 0.857 in the lower part of the suite (samples ML2, 6 and 8A in cooling units 1, 3 and 4 in Fig. 7.2). Samples ML10 and ML11 (cooling unit 5) have Sm/Nd ratios of 1.055 and 1.088 whereas samples higher up in the suite (ML25, 26 and 28 from cooling units 9, 10 and 11) have ratios between 0.582 and 0.629 (Table 7.6 column 7). The differences through the suite in Sm/Nd ratios are also reflected by the isotopic ratios $^{147}Sm/^{144}Nd$ and $^{143}Nd/^{144}Nd$ ranging from 0.4762 to 0.6483 and 0.518892 to 0.522702 respectively (Table 7.6).

The $(^{143}Nd/^{144}Nd)$ - $(^{147}Sm/^{144}Nd)$ isochron defines an age of 3337 $\pm$ 13 Ma for the Matshempondo Peridotite Suite (Fig. 7.36). The accuracy of the isochron is attributed to the large range in $(^{147}Sm/^{144}Nd)$ ratios even though the absolute amounts of Sm and Nd are extremely low.

Calculated model dates and epsilon.

ε Nd or ε^{t}_{CHUR} (Faure, 1986) for the Matshempondo Peridotite Suite is 2.03 indicating the suite to be derived from a depleted mantle residue, i.e. CHUR (chondritic universal reservoir) (De Paolo and Warserberg, 1976a quoted in Faure, 1986) is depleted in LILE that are preferentially partitioned into the liquid phase during partial melting. ε^{t}_{CHUR} expresses the difference between the initial ratio of the peridotite suite and the corresponding value (I^{t}_{CHUR}) of this ratio in CHUR at the time of crystallization of the rock whereas I^{0}_{CHUR} makes this comparison at the present time (Faure, 1986).

As the peridotites represent a suite derived from a depleted mantle residue or a non-chondritic mantle one may calculate the date model age (T_{DM}) at which Nd in the peridotites separated from the chondritic reservoir. These ages (T_{DM}) are shown in column 11 of Table 7.6 and the initial $(^{143}Nd/^{144}Nd)$ ratios in CHUR at T_{DM} for the different

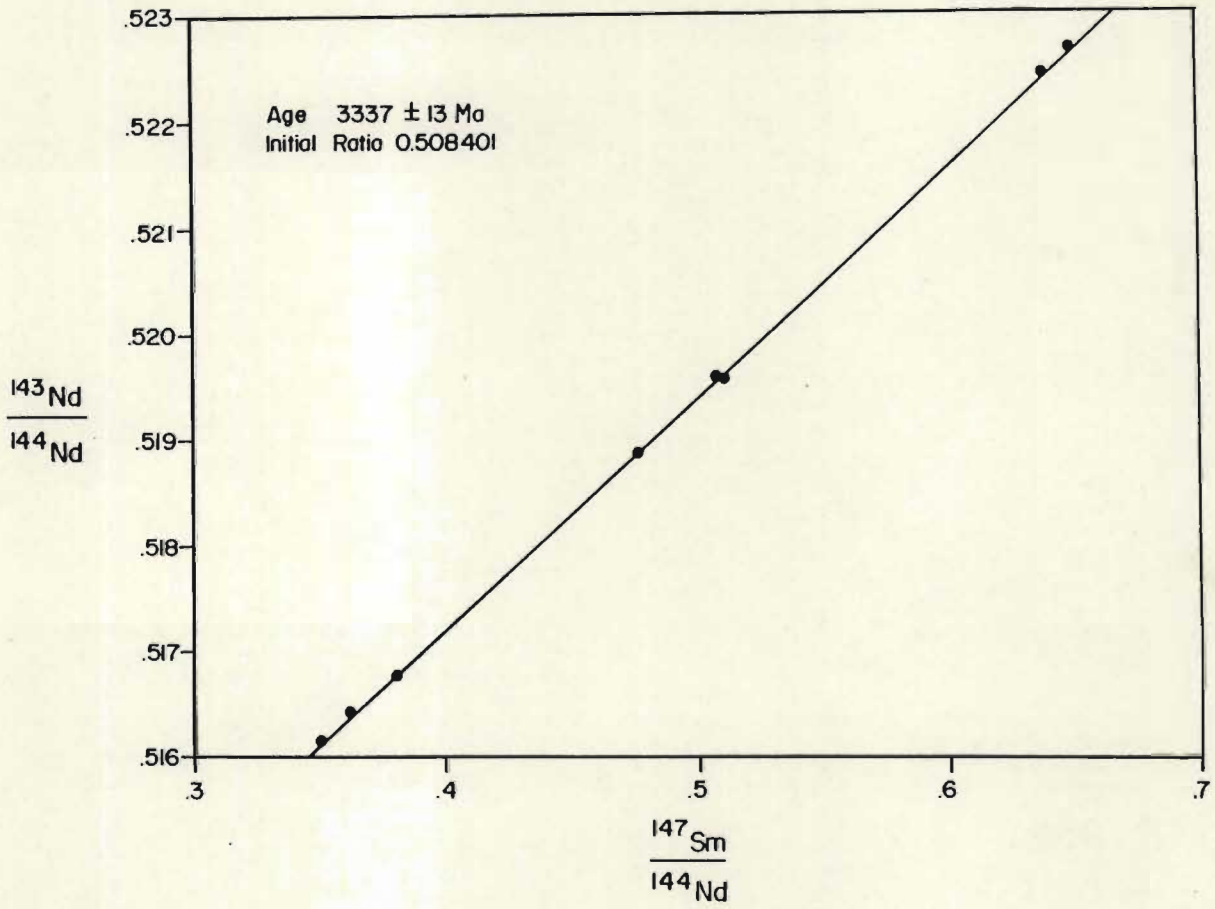

Fig. 7.36 Sm - Nd isochron diagram for the Matshempondo Peridotite Suite. All points have been used in determining the age of t = 3337 ± 13 Ma. The initial ($^{143}Nd/^{144}Nd$) ratio is 0.508401.

TABLE 7.6 Sm-Nd ABUNDANCES, ISOTOPIC RATIOS, EPSILON AND MODEL DATE FOR THE MATSHEMPONDO PERIDOTITE SUITE.
Formulae used to calculate the various parameters are from Faure (1986). Symbols used in columns 12, 13, 14 and 15 are specific to this study, but are calculated using the same basic formulae in Faure (1986).

COLUMN	1	2	3	4	5	6	7	8	9	10	11	12	13	14	15
Sample No.	Rock Type	MgO (wt %)	Sm (ppm)	Nd (ppm)	Sm/Nd	$\frac{^{147}Sm}{^{144}Nd}$	$\frac{^{143}Nd}{^{144}Nd}$	$\bar{x}\ \frac{^{143}Nd}{^{144}Nd}$	±2σ	$\varepsilon^{\circ}_{CHUR}$	T_{DM} (Ma)	$T^{DM}_{CHUR_i}$	T_{DM-IR}	$\left(\frac{^{143}Nd}{^{144}Nd}\right)_{T_{DM-IR}}$	$\left(\frac{^{143}Nd}{^{144}Nd}\right)_{T_{DM-IR}}$ - 0.508401
ML28	orthocumulate	38.45	0.0633	0.1007	0.629	0.3801	0.516776		23	80.7197	3412	0.508213	75	0.508399	- 0.000002
ML26	orthocumulate	39.89	0.0631	0.1050	0.601	0.3632	0.516436	0.5165	26	74.0870	3449	0.508164	112	0.508430	0.000029
ML25	spinifex	30.87	0.1295	0.2267	0.582	0.3510	0.516143		19	68.3718	3434	0.508184	97	0.508407	0.000006
ML11	spinifex	29.00	0.0908	0.0861	1.055	0.6372	0.522474	0.5226	29	191.8703	3377	0.508259	40	0.508426	0.000025
ML10	orthocumulate	40.01	0.0394	0.0362	1.088	0.6483	0.522702		29	196.3179	3370	0.508268	33	0.508408	0.000007
ML8A	orthocumulate	38.83	0.0480	0.0565	0.857	0.5093	0.519638		26	136.5486	3386	0.508247	50	0.508414	0.000013
ML6	orthocumulate	37.67	0.0556	0.0705	0.789	0.4762	0.518892	0.5194	30	121.9964	3384	0.508250	47	0.508396	- 0.000005
ML2	spinifex	27.89	0.0992	0.1179	0.841	0.5082	0.519612		22	136.0414	3386	0.508247	49	0.508410	0.000009

$$\varepsilon^{\circ}_{CHUR} = \left[\frac{(^{143}Nd/^{144}Nd)^{m}}{I^{\circ}_{CHUR}} - 1\right] \times 10^{4} \qquad T_{DM} = \frac{1}{\lambda}\left[\frac{(^{143}Nd/^{144}Nd)^{m} - I^{\circ}_{CHUR}}{(^{147}Sm/^{144}Nd)^{m} - (^{147}Sm/^{144}Nd)^{\circ}_{CHUR}}\right] + 1 \qquad T^{DM}_{CHUR_i} = I^{\circ}_{CHUR} - (^{147}Sm/^{144}Nd)^{\circ}_{CHUR}\,(e^{\lambda T_{DM}} - 1)$$

$$(^{143}Nd/^{144}Nd)_{T_{DM-IR}} = T^{DM}_{CHUR_i} + (^{147}Sm/^{144}Nd)^{m}\,(e^{\lambda(T_{DM-IR})} - 1) \qquad I^{t}_{CHUR} = I^{\circ}_{CHUR} - (^{147}Sm/^{144}Nd)^{\circ}_{CHUR}\,(e^{\lambda t} - 1)$$

where the superscript 'm' on isotopic ratios indicates measured values and '°' isotopic ratios at the present time.

T_{DM} = date modal age for separation from chondritic universal reservoir (CHUR); $T^{DM}_{CHUR_i}$ = initial $(^{143}Nd/^{144}Nd)$ ratio in CHUR at T_{DM}

$(^{143}Nd/^{144}Nd)_{T_{DM-IR}}$ = initial $(^{143}Nd/^{144}Nd)$ ratio after a residence time of T_{DM-IR} where IR = 3337 Ma (age from isochron)

I^{t}_{CHUR} = $(^{143}Nd/^{144}Nd)$ ratio at any time 't' in the past and I°_{CHUR} the ratio at present (0.512638).

$(^{147}Sm/^{144}Nd)^{\circ}_{CHUR}$ = 0.1967

peridotites presented in column 12 of Table 7.6.

The $^{143}Nd/^{144}Nd$ ratios in column 7 of Table 7.6 define three groups, the average ratio for each group shown in column 8 of Table 7.6. Similarly the initial ratios in CHUR at T_{DM} define the same distinct groups (Column 12 of Table 7.6). The average initial $^{143}Nd/^{144}Nd$ ratio of each group is 0.508200, 0.508264 and 0.508248.

In Fig. 7.37 the average initial ratios of the three groups (column 8 of Table 7.6) are plotted through the initial ($^{143}Nd/^{144}Nd$) ratio (from the isochron plot, Fig. 7.36). These lines plotting through the initial ratio diverge and intersect CHUR with an X-axis equivalent to approximately 110Ma (Fig. 7.37). The difference between the model date age (T_{DM}) and the isochron age reflect possible residence periods of depleted mantle residue of between 33 and 112 Ma (column 13 of Table 7.6). These ages as do the ratios in column 7 and 12 of Table 7.6 define three groups. The average residence time indicated for the three groups of data are 95, 37 and 49 Ma.

The Nd isotopic ratios ($^{143}Nd/^{144}Nd)T_{DM-IR}$ (column 14 of Table 7.5) are calculated to test whether the Nd isotopic ratios in CHUR at various ages, T_{DM} evolve after residence periods, T_{DM-IR} of between 33 and 112 Ma to the observed initial ratio (0.508401). Comparison of the data in column 14 of Table 7.6 with the initial ratio of 0.508401 (Fig. 7.36) reveals that the differences (Column 15, Table 7.6) between the calculated and isochron initial ratios are extremely small. These data suggest that :

i) during evolution of the Archaean mantle various components underwent a two stage melting process. The first stage occurred between approximately 3384 and 3449 Ma producing non-chondritic depleted mantle residues. This conclusion is supported by the Nd value of 2.03.

ii) during the periods of the first separation and residence times of between 33 and 112 Ma and the second melting event to produce the observed rocks the depleted mantle sources would have evolved isotopically.

iii) at 3337 Ma these components had approximately similar $^{143}Nd/^{144}Nd$ isotopic ratios. Considering the decay constant of 6.54×10^{-12} y^{-1}, over such short residence times differences in the isotopic ratios of the three groups would be

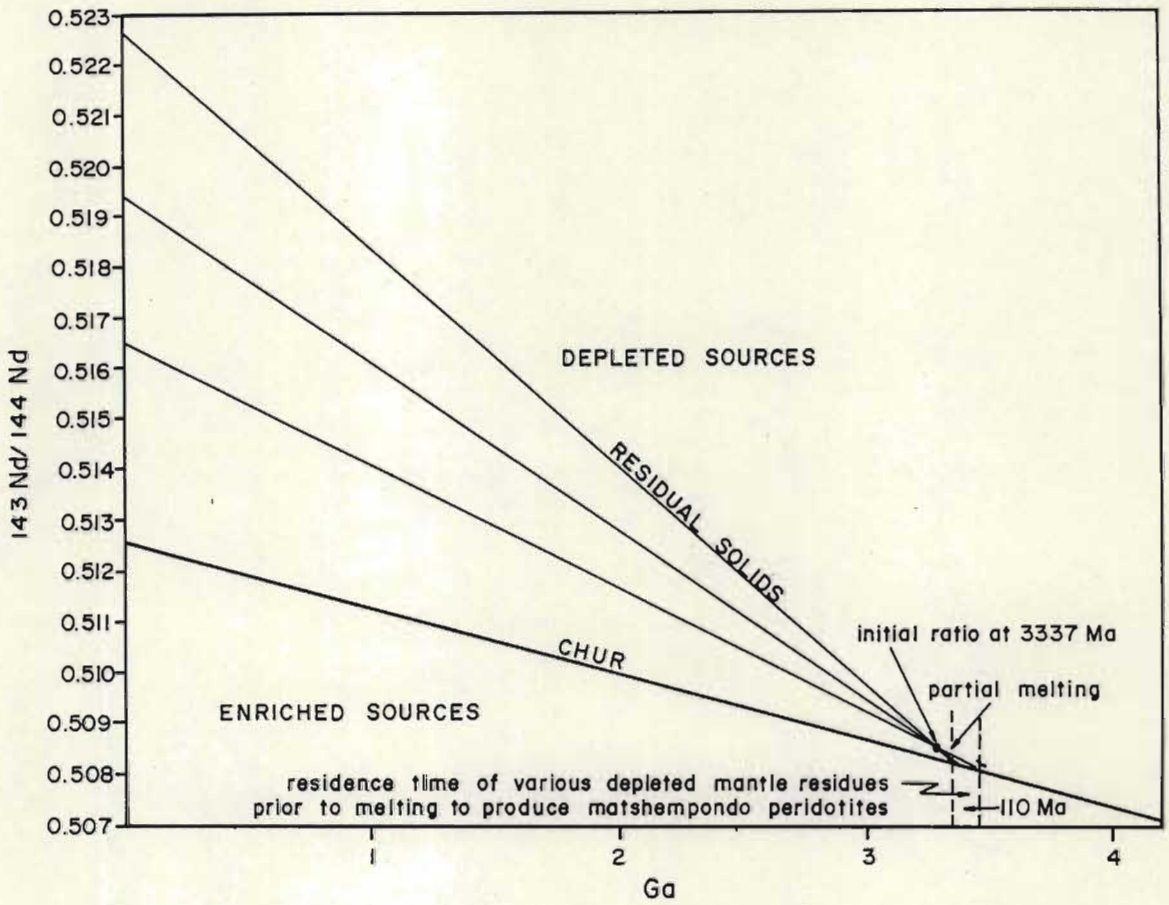

Fig. 3.37 ($^{143}Nd/^{144}Nd$) versus age (Ga) plot showing the residence times of depleted mantle residues of up to ~ 110Ma prior to partial melting. The model date indicates the time at which Nd in the crystal rocks separated from the chondritic reservoir (CHUR). At 3337 Ma isotopic ratios of the possibly different components were similar after crustal residence periods of between 33 and 112 Ma (columns 13 and 14, TABLE 7.4). Evolution of isotopic ratios towards the present time clearly reveal the differences in the depleted mantle sources.

indistinguishable. It can therefore be assumed that the initial ratio from the isochron is the same as that in the three groups at 3337 Ma (see column 14 and 15 of Table 7.6).

iv) depleted and isotopically inhomogeneous mantle components were sequentially melted and extruded forming the observed sequence of cooling units.

v) lines constrained by measured $^{143}Nd/^{144}Nd$ ratios and T^{DM}_{CHURi} and passing through the initial ratio (Fig. 7.37) reflect isotopic inhomogeneities in the depleted mantle source rocks. The isotopic ratios and Sm and Nd abundances would not be consistent with an origin of partial melting of an isotopically homogeneous source and subsequent fractionation.

CRYSTALLIZATION AND DIFFERENTIATION OF THE MATSHEMPONDO PERIDOTITE SUITE

Introduction

The Matshempondo Peridotite Suite is strongly discordant with the adjacent metavolcanic pile and may represent a primary unconformity enhanced by later deformation events. The primary discordance may be the result of topography accentuated by thermal erosion of the meta-volcanic pile by high temperature, turbulent komatiite lava flows. Subsequent increments of lava would become ponded and crystallized in a lava lake environment. Thermal erosion channels are typically several to hundreds of kilometres in length, however their length is limited by the dimensions and topography of the basins into which komatiites erupt (Huppert and Sparks, 1985). An alternate suggestion is that the peridotites may represent a sub-volcanic intrusion. Whichever of these options is correct the internal cooling and differentiation mechanisms would be similar although overall heat losses would be greatest for the lava lake. The constant thickness of the spinifex and cumulate units along strike suggests that these rock types do not represent komatiite flows.

Textures similar to the observed olivine spinifex textures are not restricted to komatiitic flows and have been reported from layered intrusions e.g. Rhum intrusion (Wager and Brown, 1968), Rognsund gabbro, Norway (Robin's 1973), in peridotite lenses in Cleque

Township, Ontario (Naldrett and Mason 1968), and in a sequence of olivine cumulates in Munro Township, Ontario interpreted as a lava lake (Arndt, 1986b). Centimetre-scale rhythmic olivine spinifex-olivine cumulate layering and harrisitic olivine (olivine plate spinifex) have been recorded in the ultramafic Tertiary Rhum Intrusion and their origin attributed to supercooling (Wadsworth, 1961). The rhythmic alternation of olivine cumulates and crescumulates exhibited by certain sections across the Rhum Intrusion is a type of layering not described from other layered intrusions (Robins, 1973). A major textural difference, however, between the Rhum intrusion and the Matshempondo Peridotite Suite is the presence of glass (now devitrified) in the latter. This indicates that, although similar processes may have been operative, the Matshempondo Peridotite Suite represents a situation of much greater heat loss. Microcyclic layering has not previously been documented in komatiitic flows and as such represents an important variant for generally similar occurrences reported in the literature.

Liquid compositions

Spinifex-textured zones in komatiite flows have in the past been interpreted as frozen silicate melts e.g. Donaldson (1976) and Viljoen and Viljoen (1969c). In the case of fine-grained random spinifex they may well represent compositions close to that of the liquid e.g. Lewis and Williams (1973). Recent studies show that many of these spinifex units contain abundant excess modal olivine and do not therefore represent primitive mantle melts, e.g. (Barnes et al., 1983; Campbell and Arndt, 1983; Kinzler and Grove, 1985; Arndt, 1986a, 1986b).

The linear trends in the variation diagrams (Fig. 7.28) of major element abundances plotted against MgO are consistent with fractionation of olivine and further supported from the petrological and mineralogical observations. The compositions of liquidus olivines crystallizing from the initial liquid may be estimated from plots of MgO against an element incompatible with olivine e.g. Al_2O_3 or TiO_2. Using this approach and other criteria, liquid compositions may be calculated for both spinifex and cumulate units (A and B units respectively).

The MgO content of the first formed liquidus olivines, calculated from

the x-intercept in the Al_2O_3 versus MgO plot (Fig. 7.28) is 52.8% which corresponds to an olivine composition of $Fo_{94.5}$ in the metre scale A and B units (Fig. 7.4 and 7.11). The x-intercept using samples ML24* and ML25* from the same cooling unit corresponds to 52.6 wt. % MgO and therefore agrees with the entire data set used in Fig. 7.28. The composition of olivine in equilibrium with ultramafic liquids may be calculated using the relationship from Roeder and Emslie (1970) :

$$0.3 = \frac{X^{ol}_{FeO} \cdot X^{liq}_{MgO}}{X^{liq}_{FeO} \cdot X^{ol}_{MgO}}$$

all components as molecular proportions

All the iron in the liquid is assumed to be Fe^{2+} (Bickle, 1982; Arndt, 1986a). Olivine compositions calculated to be in equilibrium with the bulk compositions of samples ML24 (orthocumulate) and ML25 (olivine plate spinifex) are $Fo_{97.2}$ and $Fo_{96.9}$ respectively. These data are significantly higher than those calculated by the x-intercept method ($Fo_{94.5}$) and as determined by microprobe ($Fo_{94.8}$ for cumulus olivine and $Fo_{83.5}$ for spinifex olivine), (Table 7.7). This is attributed to the fact that the rocks are enriched in olivine and as such do not represent bulk liquid compositions. The amount of excess modal olivine may be calculated using mass balance considerations and taking the composition of olivine ($Fo_{94.5}$ from Al_2O_3 - MgO plot) to be in equilibrium with the liquid. The method involves the removal of a percentage of olivine of composition $Fo_{94.5}$ from the bulk rock composition and recalculation of the bulk rock back to 100 percent. The Roeder and Emslie (1970) equation enables the new Fo content of the olivine in equilibrium with the bulk rock to be determined. When the calculated Fo content is the same as that determined from direct measurement or the Al_2O_3 - MgO plot the excess modal olivine content and liquid composition can be determined.

* Only these samples are used in this discussion as microprobe compositional data is available.

1) orthocumulate unit (ML24).

Microprobe analyses of several granular olivine grains in sample ML24 reveal a maximum Fo content of $Fo_{94.8}$ in the centre of grains with a normal zonation to $Fo_{88.6}$ at the edge of some grains. The maximum Fo content of probed grains ($Fo_{94.8}$) is almost identical to that deduced from the olivine control line ($Fo_{94.5}$) in the Al_2O_3 - MgO plot (Fig. 7.28). The zonation in the cumulus olivine grains reflects the continued growth of crystals in a locally fractionating liquid becoming progressively depleted in MgO. The higher Fo composition calculated using the Mg-Fe distribution coefficient for the bulk rock therefore reflects excess modal olivine in the orthocumulate units.

Using mass balance considerations and an olivine composition of $Fo_{94.5}$ the excess modal olivine in the orthocumulates is calculated to be 50% (Fig. 7.38) and the MgO content of the liquid from which it crystallized 21.66 wt. %. The composition of this liquid is shown in Table 7.7.

Compositions of needle orthopyroxene as determined by microprobe analyses in a matrix of devitrified glass are zoned from the centre En_{89} to edge En_{85} and reflect crystallization and fractionation in a liquid already depleted by extensive crytallization of olivine. This conclusion may be tested by calculating the Mg/Fe ratio of the liquid from which the orthopyroxene crystallized using the relationship from Wilson (1977).

$$0.26 = \frac{X_{FeO}^{opx} \cdot X_{MgO}^{liq}}{X_{FeO}^{liq} \cdot X_{MgO}^{opx}}$$

all components as molecular proportions.

The Mg-Fe ratio for the liquid changed from 2.10 to 1.36 during the crystallization of the orthopyroxene whereas the earlier formed olivine shows the change in this ratio to be 5.46 to 2.32. The order of crystallization for these two minerals is clearly demonstrated by these relationships as well as the progressive change during the crystallization.

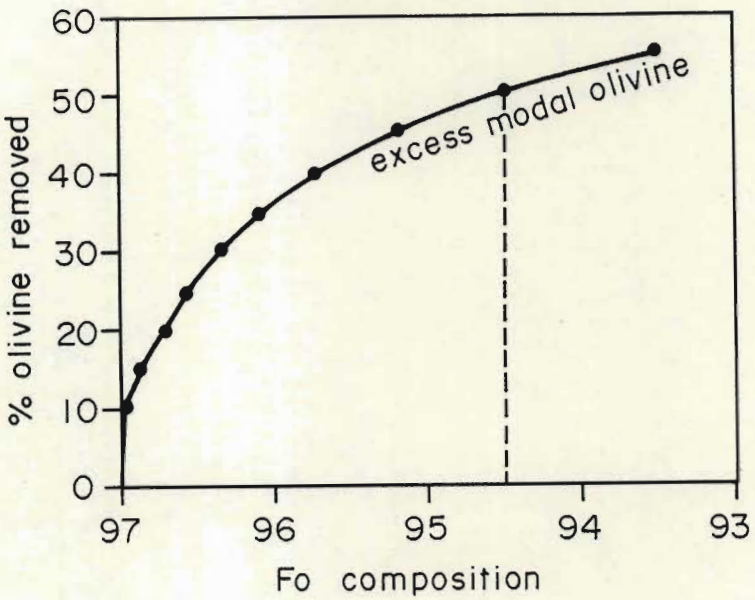

Fig. 7.38 Percentage olivine removed from the orthocumulate (ML24) plotted as a function of Fo content. The excess modal olivine curve shows the change in olivine composition after removal of different percentages of olivine ($Fo_{94.5}$) from the bulk rock composition.

TABLE 7.7 MEASURED AND CALCULATED OLIVINE COMPOSITIONS, LIQUID COMPOSITIONS AND EXCESS MODAL OLIVINE PROPORTIONS

Unit	MgO wt % (rock)	olivine compositions (F_O) measured	calculated	X-intercept Al_2O_3/MgO	excess modal olivine %	calculated MgO in liquid (wt %)	Liquid in equilibrium with F_O 83.5 excess modal olivine %	calculated MgO in liquid wt %
ML24 orthocumulate	37.28	94.8	97.2	94.5	50	21.67	-	-
ML25 plate spinifex	30.69	83.5	96.9	94.5	40	16.04	54	5.00

LIQUID COMPOSITIONS CALCULATED FROM MASS BALANCE.*

	1	2	3
SiO_2	55.22	56.52	60.97
Al_2O_3	9.80	11.31	14.70
FeO*	7.40	5.83	5.94
MnO	0.22	0.18	0.24
MgO	21.67	16.04	5.00
CaO	4.39	8.88	11.55
TiO_2	0.11	0.18	0.24
Cr_2O_3	0.78	0.83	1.08
NiO	0.42	0.23	0.31
TOTAL	100.00	100.00	100.00

* 1. Liquid composition for orthocumulate (ML24)

2. Liquid composition for olivine plate spinifex (ML25)

3. Residual liquid composition, i.e. that in equilibrium with Fo83.5 in spinifex unit (ML25)

2) Olivine plate spinifex unit (ML25).

Microprobe analyses of three olivine spinifex plates reveal that the olivine is weakly zoned with a maximum composition of Fo_{84} in the centre and Fo_{83} at the edge. The compositions are less magnesian than those calculated from the Al_2O_3 - MgO plot ($Fo_{94.5}$) and the Mg-Fe distribution coefficient ($Fo_{96.9}$ (Table 7.7). The sample, ML25, is coarse-grained (> 25 cm) olivine plate spinifex from the middle of the 3.5m thick spinifex unit. The microprobe analyses may not reflect the initial compositions of the olivines as modification by Fe-Mg diffusion can significantly reduce the Fo content of the olivines (Arndt, 1986b). The olivine control line on the Al_2O_3 - MgO diagram (Fig. 7.28) should however reflect the composition of the olivine crystallizing from the initial liquid.

Using mass balance considerations and assuming that $Fo_{94.5}$ represents the olivine liquidus composition of the initial liquid the excess modal olivine reflected by the bulk composition of the rock is calculated to be 40% (Fig. 7.39). The calculated MgO content of the liquid from which the spinifex unit crystallized is 16.04 wt. %. The composition of this liquid is shown in Table 7.7.

Mass balance calculations indicate the MgO content of the liquid in equilibrium with olivine of composition $Fo_{83.5}$ (average of probed data) to be 7.5 wt. % and the excess modal olivine 54%. The composition of this liquid is shown in Table 7.7.

Orthopryoxene spinifex that crystallized between olivine plates ranges in composition from En_{90} to En_{70} (determined by microprobe) and represents a change in Mg/Fe ratio of the liquid from 2.34 to 1.52. This contrasts with an Mg/Fe ratio for the liquid of 5.15 based on the olivine composition of $Fo_{94.5}$ determined by the intercept method. However this determined composition is at variance with the observed range in olivine composition of Fo_{84} to Fo_{83} which would represent a range in liquid compositions for Mg/Fe of 1.57 to 1.46. Textural relations clearly indicate that olivine crystallized before the orthopyroxene. It is therefore concluded that the observed

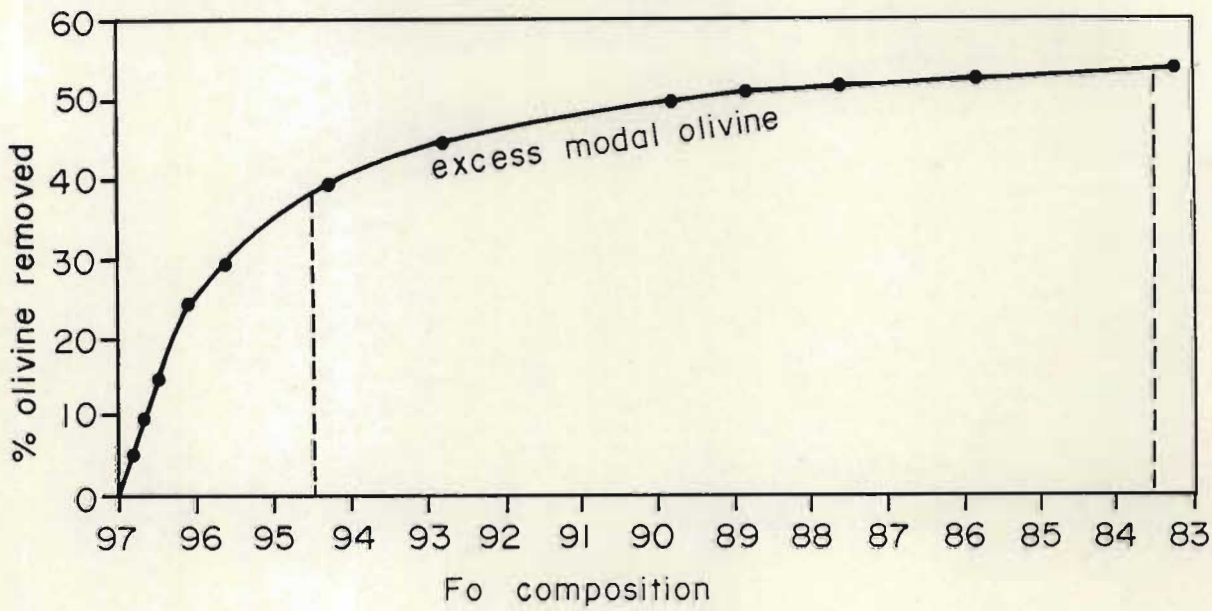

Fig. 7.39 Percentage olivine removed from the olivine plate spinifex (ML25) plotted as a function of Fo content. The excess modal olivine curve shows the change in olivine composition after removal of different percentages of olivine ($Fo_{94.5}$) from the bulk rock composition.

compositions of the olivine (and subsequently calculated values of Mg/Fe for the liquid) reflect post liquidus modification of the original magnesian olivine.

The differences in probed olivine compositions are interpreted to reflect different internal processes in the orthocumulate and spinifex layers during crystallization of the cooling unit. The possible reasons for these differences are discussed in the following sections.

Crystallization and differentiation in the cooling units.

Calculation of liquid and olivine compositions and the proportion of excess modal olivine provides a means of modelling the crystallization history of the spinifex and cumulus layers. This may be achieved utilizing the experimental data and interpretations of Huppert et al. (1984) and Turner et al. (1986) who propose a crystallization and differentiation model for cooling units involving compositional convection. In contrast to the approach of these authors, Arndt (1986a) proposes a model in which the differentiation is achieved solely by redistribution of olivine phenocrysts.

A successful model applied to the Matshempondo Peridotite Suite should answer the following questions :

a) Do the different cooling units in the Matshempondo peridotites each represent successive pulses of magma?
b) Did spinifex layers crystallize from each pulse of magma, or do some of the cumulate units represent individual pulses?
c) Could this peridotite sheet have been a single continuous emplacement of magma in which the cyclicity of layering was produced by double diffusion convection in a gravitational field (McBirnery and Noyes, 1979)?
d) Does this peridotite suite represent a sub-volcanic intrusion, a lava lake or a sequence of laterally extensive komatiite flows?

Internal processes operating would be similar for the subvolcanic intrusion and lava lake with heat flow dominated from the upper surface. Microcyclic layering involving repeated layers of cumulate and skeletal olivine have been reported from layered intrusions such as Rhum (Wager and Brown, 1968) but have not previously been

documented in komatiitic flows. A major textural difference however, is the presence of glass (now devitrified) in the Matshempondo Peridotite Suite. This indicates that, although similar processes may have been operative, the Matshempondo peridotites represent a situation of much greater heat loss.

It is also considered unlikely that the suite crystallized from a single pulse of magma. Sm-Nd isotopic data suggest derivation of the suite from several isotopically distinct mantle sources. This is consistent with field observations of the complex cyclical nature of the layering and suggests that each cooling unit represents a separate emplacement of magma.

Crystallization mechanisms envisaged for the A (spinifex-textured) and B (cumulate) units of TYPE 1, 2 and 3 cooling units are essentially similar and are discussed collectively. The crystallization mechanism to produce the microcyclic layering (C unit) of TYPE 3 cooling units is discussed as a separate problem.

1) Crystallization mechanism for A and B units in TYPE 1, 2 and 3 cooling units.

The A and B units are essential features of spinifex-textured flows and crystallization mechanisms have been described in detail by many workers with refinements being advanced in a few more recent publications (Huppert et al., 1984; Turner et al., 1986; Arndt, 1986b). The mechanism proposed for cooling units in the Matshempondo Peridotite Suite applies these well established principles.

Emplacement of the magma body may have occurred as single or multiple events either as a high level intrusion or as a thick ponded flow. Ponding of highly mobile komatiitic lavas behind a solidified flow front has been suggested by Huppert and Sparks (1985). In both cases heat loss will be dominant from the upper surface with vigorous convection taking place within the body of magma.

Supersaturation and high nucleation rates that favour the formation of olivine spinifex are attained by elevating the liquidus temperature relative to the magma temperature. This may

be achieved by a sudden decrease in the hydrostatic pressure or by changes in PH_2O of the liquid (Donaldson, 1974).

Fine olivine spinifex crystals would have nucleated at the top of the flow where heat loss was greatest and grown downwards into the convecting liquid (Fig. 7.40). The olivine plates would have continued to grow by constitutional supercooling largely controlled by compositional convection of the liquid in the lower part of the flow (Turner et al., 1986). Liquid in the immediate vicinity of the rapidly growing plates would have become depleted in the olivine components promoting propagation of the tips of the crystals beyond this differentiated layer into the convecting and undepleted lower region. This preferential growth would have produced the observed characteristic vertically oriented spinifex texture (Fig. 7.40). Growth of the spinifex zone by compositional convection would have caused the granular olivine crystals to remain suspended within the turbulently convecting lower layer (Turner et al., 1986). This process could have continued until the concentration of the cumulus crystals in the lower convecting part of the flow approached 70%, however it is likely that convective motions would have ceased before such high concentrations were attained (Turner et al., 1986). For example a komatiitic liquid with a 30% MgO content would crystallize 40 - 50% olivine in cooling from 1600 to 1200 degrees C. Only 20 to 30 % of the liquid need be transferred upwards in order to raise the concentration to 70% olivine (Turner et al., 1986). These observations are consistent with the data for the mesocumulates in the Matshempondo Peridotite Suite. The orthocumulates however typically have between 35 and 60% olivine and a high proportion of orthopyroxene needle spinifex and devitrified glass.

This crystallization mechanism may account for the observed differences in the olivine composition in the cumulus and spinifex layers for the following reasons :

a) The normal zonation of Fo contents of cumulus olivine grains reflect continued growth in a fractionating liquid. The fact that olivine compositions do not reflect re-equilibration with the interstitial liquid indicates removal of a substantial amount of the less dense lower magnesian liquid by compositional

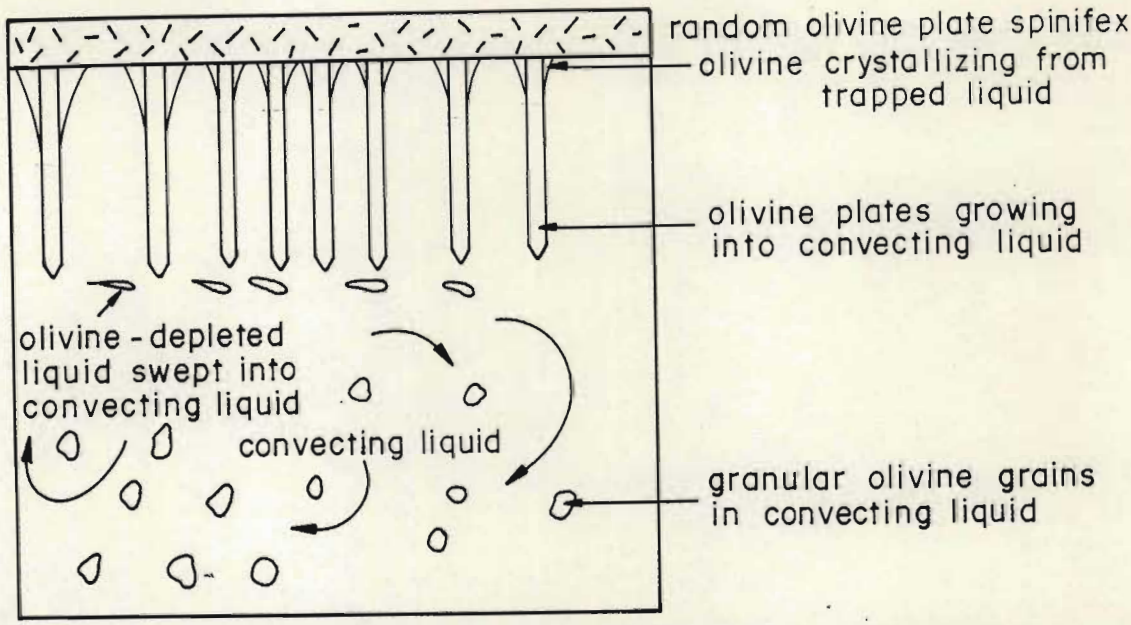

Fig. 7.40 A. Crystallization model showing growth of olivine plates downwards into a compositionally convecting liquid crystallizing granular olivine in the lower part of the cooling unit.

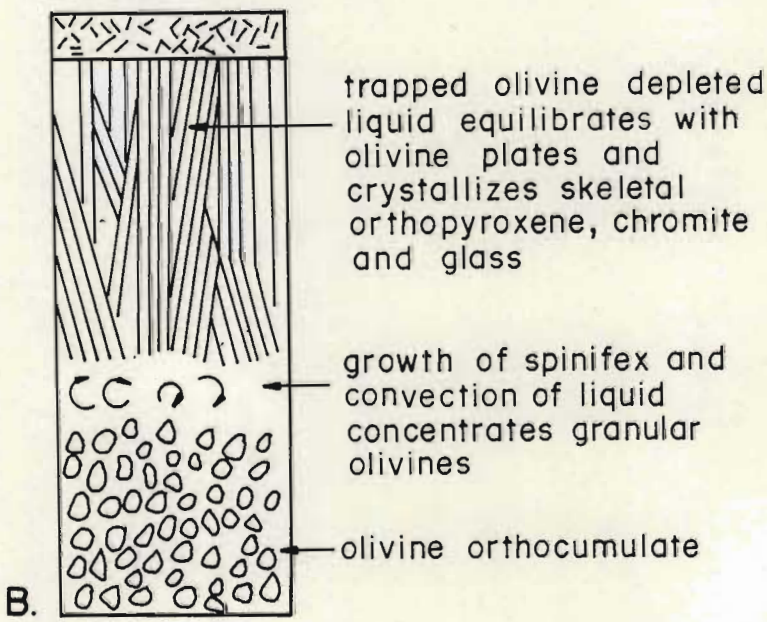

Fig. 7.40 B. Continued crystallization and upward displacement of the convecting liquid increases the proportion of granular olivine in the lower part of the cooling unit.

convection to the upper layer. The Mg-Fe ratio of the interstitial liquid indicated by orthopyroxene compositions suggest that skeletal orthopyroxene crystallized and was subsequently enclosed in a matrix of glass after the olivine had crystallized to $Fo_{88.6}$ on the edges of grains. The skeletal morphologies of orthopyroxene indicate rapid crystallization however the granular olivine morphology is consistent with crystallization at lower rates. A possible explanation is that the residual liquid between cumulus olivine grains was supersaturated with respect to orthopyroxene. This would have resulted from supercooling (by conduction and convective cooling) causing supersaturation that resulted in the crystallization and rapid growth of orthopyroxene in a matrix of mafic glass.

b) The probed compositions of plate olivine suggest substantial Mg-Fe diffusion between the olivine plates and interstitial liquid. The geometric configuration of the olivine plates (Fig. 7.40) would constrain the crystal-liquid relations as a result of the interstitial liquid being trapped in a three dimensional space that is effectively sealed from the convecting liquid below the spinifex layer. This trapped liquid would continue to equilibrate with the bounding olivine plates and also crystallize needle orthopyroxene and skeletal chromite which then became enclosed in mafic glass. This mechanism may account for the low Fo contents of probed olivines.

The excess modal olivine proportions and calculated MgO contents of liquids from which spinifex and orthocumulate rocks in the Matshempondo Peridotite Suite crystallized are comparable to those of similar rock-types with similar MgO contents (Donaldson, 1974; Arndt, 1986a, 1986b).

2) Crystallization mechanism for microcyclic units.

The microcyclic layering of repeated spinifex and cumulus layers in C units at the top of TYPE 3 cooling units (Fig. 7.11) represents a specific condition that existed within the magma body and which contrasts with that giving rise to the major A and B units. Broadly the textures are similar to those observed in the larger scale units but chemical characteristics and limited

modelling suggest that Mg-Fe diffusion between the spinifex and cumulus layers was significant and that subtly different controlling factors were operative. Furthermore, as this type of layering has not been described from other spinifex bearing occurrences any proposed mechanism must deviate from those which explain the larger scale features.

Flow top breccias which characterize most spinifex-bearing komatiite flows are absent in the Matshempondo peridotites indicating repeated influxes of magma into a large reservoir. The absence of flow top breccias suggests that at no stage did solidification of a pre-existing flow take place before the influx of a new batch of magma.

Essentially the evaluation of the small-scale microcyclic layering becomes similar to that for large layered intrusions in which double diffusion convection (McBirney and Noyes, 1979) and constitutional supercooling play important roles. These controls would have been all the more important in the very low viscosity Matshempondo magma (~ 100 poises). The recurrence of microcyclic units at similar stratigraphic positions within the larger scale units (Fig. 7.11) suggests that this results from an internal mechanism as opposed to extrusion of new flows or influxes of new magma.

Any proposed mechanism must account for the periodic supersaturation necessary for high nucleation rates and growth of olivine plate spinifex. Double diffusion convection in a body of magma and diffusion controlled crystallization in the proximity of the cooling surface of a solidifying magma may result in small scale rhythmic layering (McBirney and Noyes, 1979). The low viscosity and high temperature Matshempondo magma would have rapidly broken down into a series of double diffusion layers each undergoing convection, heat transfer and periodic supersaturation.

The scope of the study does not allow a vigorous evaluation of the thermal conditions necessary to produce the observed layering. However it is strongly indicated that varying conditions of supersaturation and equilibrium crystallization occurred.

COMPARISON OF GEOCHEMISTRY AND SOURCE OF THE MATSHEMPONDO PERIDOTITE SUITE TO KOMATIITES FROM OTHER GREENSTONE BELTS.

General aspects of the geochemistry of the Matshempondo Peridotite Suite are compared to peridotitic komatiites with similar MgO contents from other greenstone belts. In particular comparisons are made using trace and major elements incompatible with olivine.

A high degree of partial melting (> 40%) of a mantle source is required to produce peridotitic melts and, if Ti is regarded as completely incompatible at high degrees of partial melting then all the Ti should be partitioned into the melt (Nesbitt et al., 1979). Calcium and Al should behave similarly provided there is no residual phase in the source (garnet or clinopyroxene) that would retain significant amounts of these elements. As a consequence of the above reasoning Nesbitt et al. (1979) divides peridotitic komatiites into two groups on the basis of CaO/Al_2O_3 and Al_2O_3/TiO_2 ratios :

i) aluminum undepleted peridotitic komatiites typically have CaO/Al_2O_3 and Al_2O_3/TiO_2 ratios of ~ 1 and ~ 20 respectively whereas,

ii) aluminum depleted peridotitic komatiites have CaO/Al_2O_3 and Al_2O_3/TiO_2 ratios of ~ 1.5 and ~ 11 respectively.

These peridotitic komatiite types are suggested to have been generated in the mantle at depths < 200km and ~200 to 400km respectively (Ohtani, 1984).

The Matshempondo peridotites on the basis of these ratios are aluminum undepleted peridotitic komatiites. The low CaO/Al_2O_3 ratios and the extremely high Al_2O_3/TiO_2 ratios reflect the characteristic high Al_2O_3 and the low Ti contents of the magmas (Table 7.8) and therefore presumably also the source region. The Ti contents of the spinifex-textured peridotites vary between ~620 and 780 ppm and are approximately a factor of two lower compared to the abundances in peridotitic komatiites from other greenstone occurrences of similar

TABLE 7.8 SELECTED MAJOR AND TRACE ELEMENT DATA OF PERIDOTITIC KOMATIITES FROM THE MATSHEMPONDO PERIDOTITE SUITE, BARBERTON, ALEXO, BELINGWE AND THE YILGARN BLOCK

		Ti ppm	Ti/Zr	Ti/Y	Al_2O_3/ TiO_2	CaO/ Al_2O_3	SiO_2 wt. %	MgO wt. %	Al_2O_3 wt. %
MATSHEMPONDO									
Spx	ML2	670	71	96	72.91	0.73	51.17	27.90	8.02
	ML11	778	94	121	60.31	0.67	50.86	28.75	7.84
	ML25	670	72	268	62.36	0.79	50.66	30.69	6.86
	ML12/1	704	78	129	64.42	0.69	50.70	30.24	7.73
	ML12/4	617	76	110	73.20	0.67	50.62	31.05	7.32
	ML12/6	646	73	91	70.45	0.70	50.65	30.65	7.75
	ML12/11	762	84	100	61.08	0.72	50.74	29.69	7.44
Selected samples from Barberton - Smith and Erlank (1982)									
HSS88C	CM	1679	84	268	10.38	2.47	49.51	24.09	4.05
HSS95	ST	1619	125	289	18.22	1.50	47.34	25.68	4.92
HSS109	ST	1679	83	223	11.11	1.53	46.53	32.91	3.11
HSS523	Pillow	2278	70	295	10.52	1.62	47.38	29.42	4.00
HSS87	Ap. Lava	2098	83	233	10.20	1.55	46.20	30.60	3.57
Selected samples from Richards Flow, Barberton - Viljoen et al. (1983)									
MDF3		2218	84	254	11.14	1.72	47.65	27.86	4.12
MDF4		2278	84	256	11.16	1.72	47.48	27.28	4.24
Selected samples from Belingwe - Nisbet et al. (1982)									
AT8	ST	1559	-	-	21.12	0.96	46.83	31.13	5.49
B4	ST	1858	-	-	20.32	1.00	46.76	27.93	6.30
SF134	ST	1679	-	-	21.75	1.04	47.74	28.66	6.09
Alexo, Ontario - Arndt (1986a)									
M662		1918	141	236	19.68	0.95	45.00	29.60	6.30
Yilgarn Block, Australia - Nesbitt and Sun (1976)									
1	ST	1679	103	283	19.14	0.84	44.43	31.72	5.36
3	ST	1618	119	237	20.85	1.00	45.42	31.46	5.63

MgO contents (Table 7.8). The Matshempondo peridotites are characterized compositionally by silica contents which are up to 3.5% in excess of those from other occurrences (Table 7.8). There is no geochemical nor petrographic evidence to suggest that these rocks have been silicified and therefore the high silica contents are interpreted to be primary and in particular to reflect the high orthopyroxene content observed in both the orthocumulate and spinifex bearing lithologies.

Ti/Y ratios (89 - 129 with value of one 268) (Table 7.8) for the spinifex-textured peridotites are considerably lower than those for peridotitic komatiites from Barberton, Alexo, and the Yilgarn Block (Table 7.8), whereas Ti/Zr ratios are similar (Table 7.8). Absolute amounts of Y in the Matshempondo peridotites are similar to abundances in peridotitic komatiites from Barberton (Smith and Erlank, 1982), Alexo (Arndt, 1986) and La Motte (Ludden and Gelinas, 1982).

Fractionation of clinopyroxene and/or garnet in the mantle would result in an increase in the Ti/Y ratio of the melt as Y cannot be regarded as an incompatible element for these minerals. The consistently high Ti/Y ratios in the Barberton komatiites (Smith and Erlank, 1982) are interpreted to reflect garnet fractionation during generation of the komatiitic liquid (Sun and Nesbitt, 1978) at depths >200km (Ohtani, 1984). The very low Ti/Y ratios in the Matshempondo peridotites is also not inconsistent with garnet or clinopyroxene fractionation in the mantle but indicates a source depleted in Ti. Considering the relative incompatibilities, Zr > Ti > Y (Sun et al., 1979), the depletion of the mantle in these elements should also be reflected in the relative Zr, Ti and Y abundances in the liquid. The abundances of these trace elements suggest that the liquid from which the Matshempondo Peridotite Suite crystallized was strongly depleted in Zr and Ti with respect to Y. The relative proportions of Ti, Zr and Y suggests that the source had previously been depleted in Ti and Zr by an earlier melting event. That the Matshempondo peridotites are derived by partial melting of a depleted mantle residue is supported by Sm-Nd isotopic data (see earlier section). It is envisaged that during the melting event fusion of garnet and/or clinopyroxene introduced Y into the liquid in non-chondritic ratios with respect to Ti and Zr (Fig. 7.33). The trace and major element characteristics may be attributed to very high degrees of partial melting of

isotopically inhomogeneous depleted garnet peridotites.

SUMMARY AND CONCLUSIONS

i. The Matshempondo Peridotite Suite comprises a suite of cumulate and spinifex-textured peridotites and peridotitic komatiites at least 640m thick that crop out over an area of approximately $10km^2$.

ii. Three broad types of cooling units have been identified. TYPE 1 and 2 cooling units are similar in many respects to those described from komatiitic flows in other greenstone belts. The TYPE 3 cooling unit, in addition to the A and B units, contains an upper C unit characterized by microcyclic spinifex-cumulate layering. Microcyclic layering has not previously been documented in Archaean komatiitic flows.

iii. The absence of flow top breccias suggests that at no stage did solidification of a pre-existing influx of magma take place before the influx of a new batch of magma. It is considered that the most likely environment in which the Matshempondo peridotites crystallized was a ponded lava lake.

iv. Elements incompatible with olivine plotted against MgO and molecular proportion ratio diagrams indicate olivine control of the fractionation which is consistent with the observed mineralogy and petrology.

v. Mass balance considerations applied to cooling unit 9 (samples ML24 and ML25) indicate excess modal olivine proportions of 50 and 40% for the orthocumulate and spinifex layers respectively. Calculated liquid compositions suggest that the orthocumulate and spinifex layers crystallized from liquids with MgO contents of 21.67 wt. % and 16.04 wt. % respectively. These MgO contents do not reflect those of the original liquid in the cooling unit prior to crystallization, however the MgO content of the liquid determined from the orthocumulate unit is within the range of that of reported initial liquids that would crystallize these rock-types.

vi. The Matshempondo peridotites are on the basis of CaO/Al_2O_3 and Al_2O_3/TiO_2 ratios classified as aluminum undepleted peridotitic komatiites, whereas the associated basaltic komatiites and peridotitic komatiites in the Commondale Supracrustal Suite are aluminum depleted peridotitic komatiites. On the basis of these ratios the mantle sources of the rock-types are interpeted to be mineralogically different and liquids are suggested to have been derived at depths of < 200km and between 200 and 400km (Nesbitt et al., 1979; Ohtani, 1984) for aluminum undepleted and aluminum depleted peridotitic komatiites respectively. Al_2O_3/TiO_2 ratios in the range between 60 and 90 for the Matshempondo Peridotite Suite have not previously been documented in Archaean peridotitic komatiites which typically have ratios between 10 and 20 (chondritic). Several komatiites from Barberton with Al_2O_3/TiO_2 ratios $\geq$ 40 share geochemical characteristics of modern boninites (Jahn et al., 1982).

vii. Sm-Nd isotopic data indicate partial melting of isotopically inhomogeneous depleted mantle to produce the liquids from which the Matshempondo peridotites crystallized. The depleted mantle residues from which the second stage Matshempondo liquids separated had residence times between 33 and 110 Ma in the mantle after the first melting event.

viii. The absolute abundances and relative proportions of Ti, Zr and Y suggests that the source had been depleted in Ti and Zr by an earlier melting event. During the second stage melting event that produced the Matshempondo liquid Y was introduced, by the fusion of garnet and/or clinopyroxene into the liquid in non-chondritic ratios with respect to Ti and Zr. Melting of the isotopically inhomogeneous mantle that gave rise to the distinctly different Sm/Nd ratios through the sequence is also reflected by Y contents that increase with increasing Sm/Nd ratios. The variable abundances of Y may be attributed to mantle inhomogeneities and the degree of partial melting.

CHAPTER 8

STRUCTURE

INTRODUCTION

At least seven episodes of deformation are recorded in the granitoid-supracrustal terrane (MAP 1 and MAP 3) and these are designated D_1 to D_7 (Table 8.1). Three phases of folding, F_1, F_2 and F_4 are identified and are related to D_1, D_2 and D_4 respectively. The numbering of the deformational events starts with the earliest recorded in the supracrustals and neglects any preceding events in the Gneiss Complex.

F_1 in both the greenstones and granitoids is recognized as original westward verging recumbent nappes separated by late D_1 thrusts. F_2 folds are tight to isoclinal with northeasterly trending steeply inclined to vertical, axial surfaces. Fold axes plunge between 25 and 80 degrees northeast and less commonly southwest. F_1 is recognized in Type 3 interference structures (hook folds; Ramsay, 1967, p. 533-535) with F_2 on all scales. Axial surfaces of open F_4 folds are steeply inclined to vertical, trend northwesterly, and most folds plunge between 30 and 50 degrees towards the northwest. Regional scale Type 1 interference structures (dome and basin; Ramsay, 1967, p. 521-525) between F_2 and F_4 are recognized (MAP 1) in the Luneburg Tonalite Gneisses and in the area centered about the Commondale supracrustals). The other deformational events include northeasterly mylonitization and shearing developed during late D_2 and D_3 respectively, shearing and folding in a northwesterly direction during D_5, and development of pull apart graben and late mylonitic shearing during D_6 and D_7 respectively. D_5 and later events are not discussed in any detail, as they are poorly understood and require a detailed regional structural study of adjacent areas to elucidate their relation to earlier, possibly coaxial deformations.

Rotation through up to ninety degrees of the recumbent D_1 structures during D_2 provides a map scale section of hook folds and possible D_1 thrust geometries (MAP 2 and Fig. 8.9). These folds are best preserved in the lower strain hinge zone of the F_2 Commondale synform and on the western limb of the Nederland synform (MAP 2). The fortuitous preservation of possible late D_1 thrust geometries in the hinge of the

TABLE 8.1 TECTONIC EVOLUTION OF THE GRANITOID-SUPRACRUSTAL TERRANE WEST AND EAST OF COMMONDALE*

GEOLOGICAL EVENTS	STRUCTURAL EVENTS
1. Tonalitic, trondhjemitic and subordinate basaltic liquids intruded or extruded to form the Gneiss Complex (Layered Gneisses, Luneburg Tonalite Gneiss).	
2. Extrusion of mafic and ultramafic volcanics, chemical and clastic sedimentation, sub-volcanic layered intrusions (Commondale Supracrustal Suite and Matshempondo Peridotite Suite). N1 quartzofeldspathic veins in (1).	
	D_1 SL fabric formation (L_1^1 min and axial planar S_1) and recumbent westward-verging N and S-plunging F_1 folding of (1), (2) and (N1) about flat-lying axial surfaces. In (2) L_1^0 min is parallel to F_1 fold axes in thinly bedded metasediments. D_1 westward-thrusting parallel to axial surfaces of F_1 folds.
3. Intrusion of Braunschweig Tonalite Gneiss.	
4. Intrusion of Bazane Porphyritic Trondhjemite Suite.	
5. Intrusion of Leucotonalite Gneiss.	
6. Intrusion of biotite granite, sodic granite and meidum-grained leucotonalite into Luneburg Tonalite Gneiss. N_2 leucocratic granite veins in (3) N_3 mafic dykes (amphibolite) in (1) (3) (4) (6) N_4 thin quartz feldspar veins in (3) (4) (6) (N_3) N_5 sodic pegmatites in (1) (3) (4) (6) N_6 potassic pegmatites in (4)	
7. Intrusion of Hornblende Granodiorite Suite (Sub-alkaline) possibly related to crustal extension. N_7 coarse quartz-mica-feldspar pegmatite in (7) (1) (2).	
	D_2 SL fabric formation (L_2^1 min and axial planar S_2) in (1) (2) (3) (4) (5) (7) and weakly in (6). In (2) L_2^0 min is parallel to F_2 fold axes in thinly bedded metasediments. Intense F_2 folding in (1) (2) (4) and N_1 - N_4 and varying intensitites of S_2 fabric axial planar to NNE to NE trending fold surfaces. As a result of intense F_2 folding and boudinage and penetrative S_2 refoliation S_1 is transposed and hard to recognize except where it is folded. Ductile and brittle ductile shear zones subparallel to F_2 axial surfaces in (1).

TABLE 8.1 continued

GEOLOGICAL EVENTS	STRUCTURAL EVENTS
	Late D_2 Dextral shearing at Bazane Porphyritic Trondhjemite and supracrustal contact, proto-mylonite to ultramylonite development. (S - C mylonites). (Sense of movement NE).
	D_3 NE - SW ductile and brittle sinistral shearing in Commondale Supracrustal Suite (sense of movement SW).
	D_4 Open to tight folding (1) (2) (4) (5) about steeply inclined NW-trending axial surfaces. Post D_4 granitoids (4) (5) have open to tight refolded S_2 fabric defining F_4. Localized shearing about NW axis in (1) recognized by foliation curved into shear plane.
8. Intrusion of leucocratic granites and quartz monzonite. N_8 grey granite veins in (1) (5) N_9 potassic granites and pegmatites in (1) (5) and cutting (N_8) and (N_9).	
9. Deposition and extrusion of Pongola Sequence (indicating stable craton).	
	D_5 Sinistral (left lateral) shearing ($\pm$ 40 km displacement) and folding about steep NW axial surfaces.
	D_6 Development pull-apart graben associated with zone of NW refoliation east of Piet Retief.
10. Intrusion of Usushwana Complex as dyke-like body east of Piet Retief.	
	D_7 WNW mylonitic shearing with lateral displacement of gneissis layering and supracrustal remnants. NW shearing parallel to the Usushwana Complex - granitoid contact and NE faulting across the complex S_7 is a mylonitic foliation in the Usushwana gabbros and adjacent granitoids.
	$D_7 + n$ Various phases of younger deformation, faulting, mylonitization, etc.

* Numbering of deformation events starts with the earliest deformation recognized in the supracrustals and neglects any preceding events in the Gneiss Complex.

Commondale synform allows recognition of structures, the angular relation of which would otherwise be obscured on fold limbs by high flattening and shear strains.

The open refolding during D_4 results in complex interference structures incorporating three fold phases complicated by thrusts and shears, of which map scale examples are easily recognizable (MAP 1 and MAP 2) and clearly show the Commondale synform as the right hand limb of a large open F_4 antiform in the core of which Layered Gneisses and Bazane Porphyritic Trondhjemite Suite are preserved. This limb is a refolded Type 3 interference structure in which the F_1 and F_2 fold axes and axial surfaces were rotated about F_4 axial surfaces.

D_1

D_1 in the Gneiss Complex.

A strong flat-lying S_1 gneissosity in the layered Gneisses and Luneburg Tonalite Gneiss developed during D_1. The S_1 fabric in the Layered Gneisses is parallel to the lithological banding, S_0 and a L_1^1 mineral lineation, defined by plagioclase or quartz, is sporadically developed (Table 8.2).

S_1 foliations in the Luneburg Tonalite Gneiss, west of Luneburg, are relatively flat-lying and define a crude dome and basin structure as a result of refolding about F_2 and F_4 axial surfaces. The remainder of the granitoid terrane is characterized by steeply inclined fabrics and only locally has the F_1 fabric survived subsequent deformation. The originally flat-lying S_1 fabric is unequivocally distinguished from younger foliations where :

a) S_1 is folded about F_2 axial surfaces in areas of lower strain adjacent to zones of strong penetrative S_2 refoliation that obliterates S_1 (Fig. 8.1)

b) In hook folds where S_1 axial planar to F_1 is folded about the F_2 axial surface (Fig. 8.2). In many instances hook folds in quartzofeldspathic veins are extremely flattened in the XY plane of the strain ellipsoid, to the extent where F_1 axial surfaces parallel those of F_2 on the limbs but are normal to them in the hinge.

TABLE 8.2 EXPLANATION OF SOME STRUCTURAL SYMBOLS USED IN THE TEXT AND ON STEREONETS.

S_0	pole to lithological layering
S_1	pole to S_1 foliation
S_2	pole to S_2 foliation
L_1^0	D_1 lineation on S_0 surface
L_1^1	D_1 lineation on S_1 surface
L_2^0	D_2 lineation on S_0 surface
L_2^1	D_2 lineation on S_1 surface
L_2^2	D_2 lineation on S_2 surface
AT	axial trace
AP	axial plane
π	pole to π girdle

Fig. 8.1 Layered Gneisses exposed in a pavement on the north bank of the Pongola River on the farm Tafelberg 186 HT, display similar F_2 folds deforming S_1 and S_O. A 5m wide zone of penetrative S_2 refoliation is preserved to the left of the hammer.

Fig. 8.2 a) Quartzofeldspathic vein defining a hook fold in pre D_1 amphibolite sheet. S_1 is axial planar to F_1 and folded about F_2. Layered Gneisses, Pongola River, Bendor 211 HT.

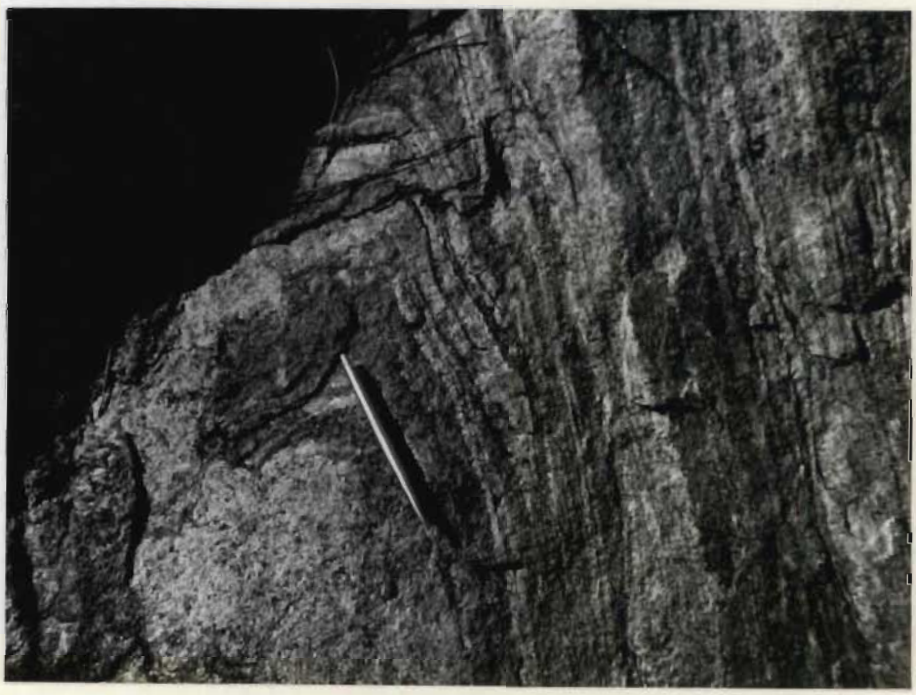

Fig. 8.2 b) Centimetre scale hook fold in Layered Gneisses. Photograph is detail of fold closures in Fig. 8.1.

Layered Gneisses on the farms Bendor 211 HT, Tafelberg 186 HT, Warmbad 18 HU and Wagendrift 12 HU contain a number of generations of quartzofeldspathic veins and amphibolitic sheets, some of which are clearly dykes, (Table 8.1). An early suite of thin omnidirectional quartzofeldspathic veins in homogeneous, dark coloured tonalites and feldspathic amphibolites is interpreted as pre-D_1 on the basis of interference structures (hook folds). Calculation of the bulk minimum strain ellipsoid using these veins and pre-D_2 amphibolite dykes is discussed in a later section. Thrust faults interpreted as late D_1 disrupt S_1 and the lithological layering in the Layered Gneisses on Bendor 211 HT (Fig. 8.3). Within a zone about 10m wide numerous thrusts faults exhibiting ramps, flats and horse structures (Butler, 1982; Boyer and Elliot, 1982) are recognized. Thrust breccia zones up to 4cm thick are common along the thrust surfaces and comprise angular fragments of tonalitic and amphibolitic gneisses in a silicified matrix (Fig. 8.4). Displacements along the thrusts vary between 5 and 10 m. The thrust surfaces were rotated to a vertical orientation during D_2 to provide a section view of the thrust geometries. These thrusts may alternatively be considered late D_2 wrench faults that produced thrust like geometries although it is unlikely that the well-developed flats, ramps and horses could develop during lateral movement along a vertical plane.

D_1 in the Supracrustals.

D_1 in the Commondale Supracrustal Suite and other smaller supracrustal remnants is characterized by :-

1. small to macroscale recumbent folds (F_1) defined by folding of lithological layering (S_0) in BIF and the Matshempondo peridotites

2. penetrative axial planar foliation (S_1) and locally L_1^1 mineral lineations

3. detailed mapping in the hinge of the Commondale synform suggests that thrusting was important during D_1.

Fig. 8.3 D_1 thrust fault in Layered Gneisses displaces lithological layering and S_1. Displacement of thrust, is 5.5m. Pavement, Pongola River on Bendor 211 HT.

Fig. 8.4 Breccias along thrust fault surfaces in Fig. 8.3a comprise angular fragments of tonalitic and amphibolitic gneisses in a silicified matrix.

In the ferruginous quartzites, BIF and Matshempondo peridotites, S_1 is oblique to S_0. In the BIF S_1 is hard to recognize in the field, but in thin section S_0, S_1 and S_2 are clearly displayed. S_1 is defined in the quartz-rich layers by strained and elongated grains in optical continuity but oriented oblique to the magnetite-haematite layers. The S_2 fabric, defined by elongate and recrystallized quartz grains, is penetrative through S_1 and normal to S_0 (Fig. 8.5).

In the Matshempondo periodotite suite the unique centimetre scale cyclic spinifex-cumulate layers (Chapter 7) define S_0 (Fig. 8.6). S_1 is better developed in the cumulate layers than the spinifex layers and manifests itself as thin layers (0.5mm thick) in which the olivine grains are fractured and a higher proportion of serpentine and magnetite are present. The S_0 - S_1 relations are readily observed in most outcrops of the Matshempondo Peridotite Suite.

A strong S_1 fabric is also well-developed in the tremolite-actinolite schists and amphibolites. Locally an L_1^1 mineral lineation is recognized.

Few F_1 folds have resisted subsequent deformational events but on the northern limb of the Commondale synform relatively undeformed F_1 westward verging recumbent mesoscale folds are preserved in ferruginous metaquartzites (Fig. 8.7).

F_1 structures folded by F_2 produce hook folds with amplitudes that range from centimetres to kilometres in the Commondale and Nederland synforms. Small and mesoscale structures are easily recognized (Fig. 8.8) whereas the large scale structures are recognized through cleavage-bedding relations and the symmetries of second order folds. In the Commondale synform the identification of large-scale hook folds is complicated by poor outcrop in critical areas, late D_1 thrusting, and intrusion of the Bazane Porphyritic Trondhjemite Suite prior to D_2. Cleavage-bedding relations (S_1 - S_0) in the Matshempondo peridotites suggest recumbent-folding during D_1 and refolding about vertical F_2 axial surfaces to produce a complex hook fold (Fig. 8.9).

On the western limb of the Nederland synform second order F_2 folds have S symmetry and plunge northeast indicating a synformal closure to the southwest (MAP 2). Second order folds on the same limb

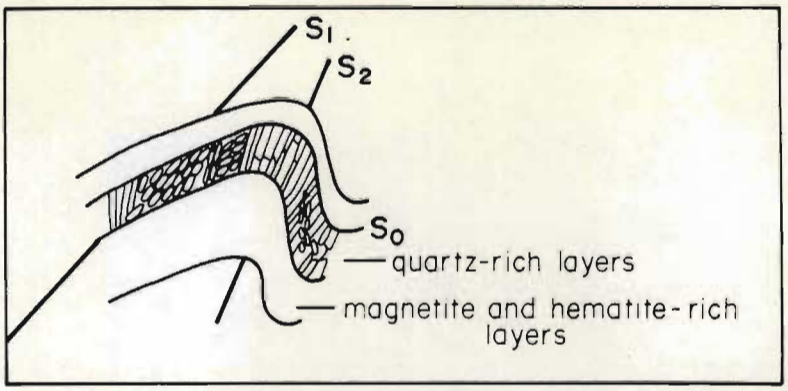

Fig. 8.5 S_O, S_1 and S_2 cleavage-bedding relationships in banded iron formation in the hinge of the Commondale synform. Mooiplaats 206 HT.

Fig. 8.6 Centimetre scale spinifex-cumulate layering (S_O) in the Matshempondo Peridotite Suite. Spinifex textured layers (positive relief) show only weak S_1 development whereas cumulate layers (negative relief) show strong S_1 development that is clearly distinguishable from the igneous lamination. Nederland 202 HT.

Fig. 8.7 Westward verging recumbent F_1 folds in banded iron formation. Northern limb of the Commondale synform, Mooiplaats 206 HT.

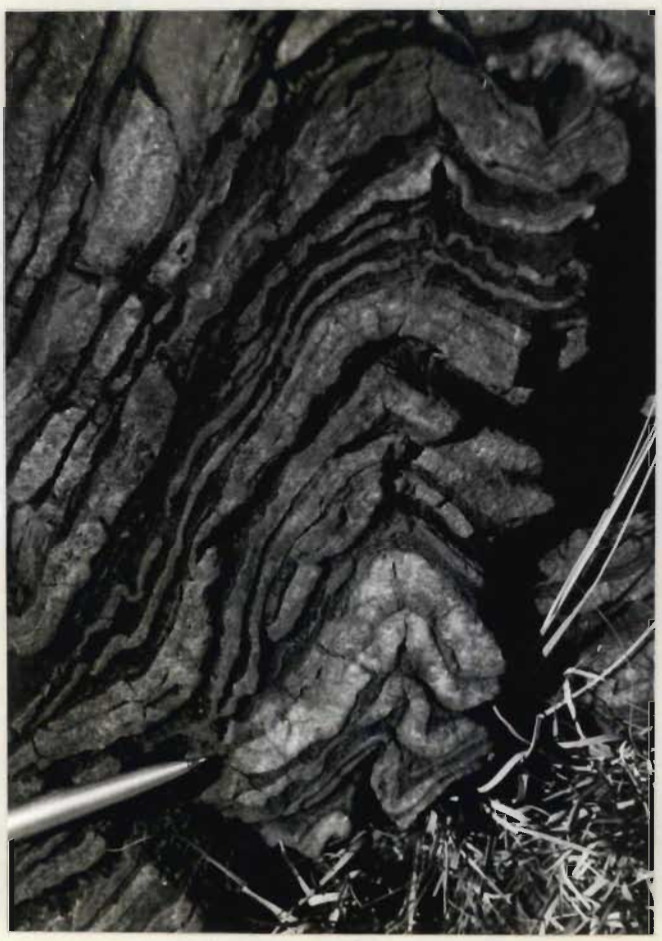

a

b

Fig. 8.8 a) Intrafolial hook fold and b) metre scale hook fold in ferruginous quartzites, Commondale synform. Mooiplaats 206 HT.

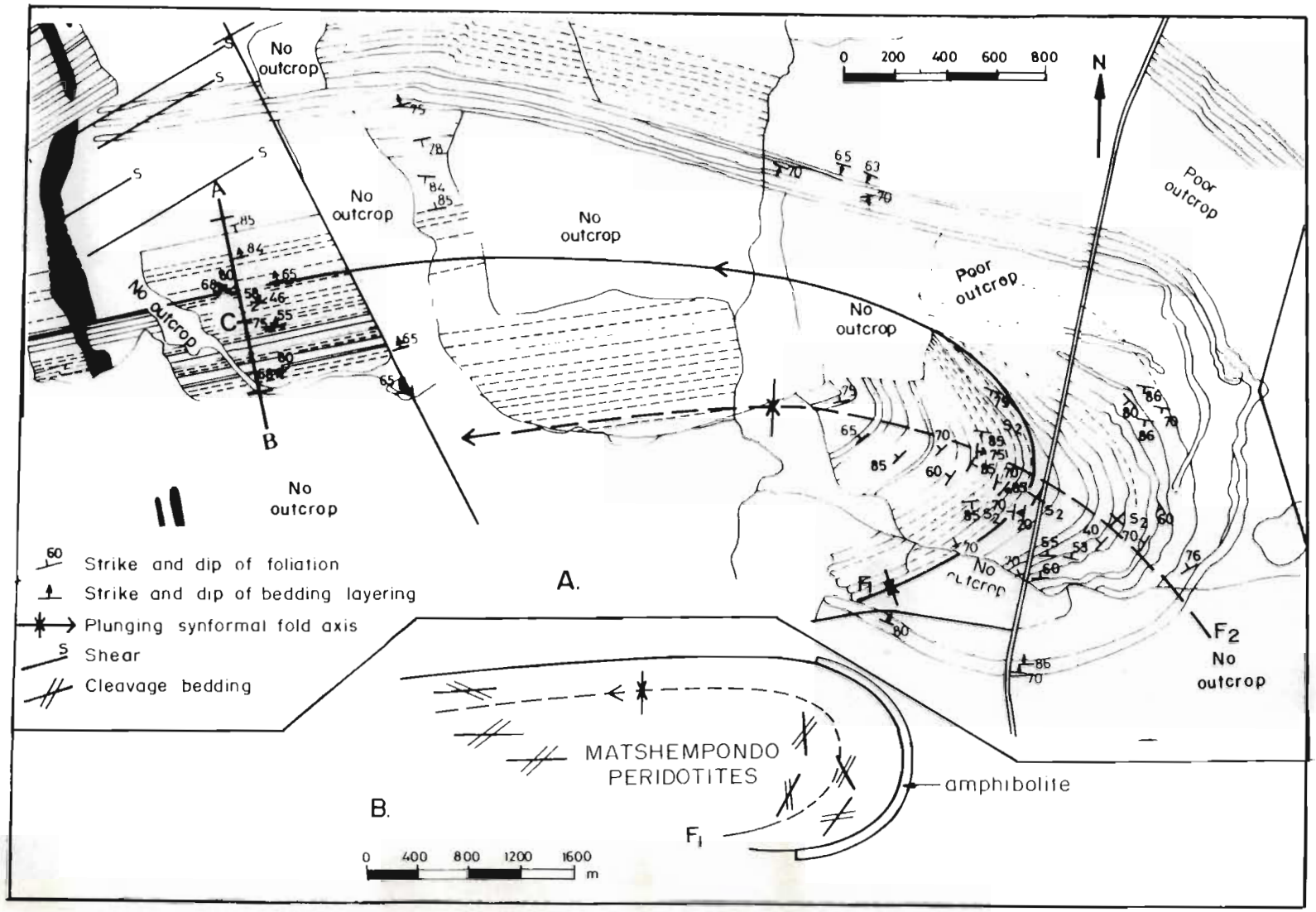

Fig. 8.9 a) Simplified Map of the Commondale synform showing S_O, S_1, S_2 in relation to F_1 and F_2 axial traces. See Fig. 7.2 for explanation of Section A - B.

b) Sketch map of the cleavage bedding relationships in the Matshempondo peridotites that enable recognition of the F_1 fold duplicating part of the peridotite suite. The sketch map is a simplification of (a).

(ferruginous quartzite) in the northern corner of the farm Nederland 202 HT (MAP 2) have Z symmetry and plunge south-southeast indicating a synformal closure to the northeast, that is exposed close to the contact with the Karoo Sequence. The symmetry and F_1 and F_2 axial traces are indicated in a simplified map of the Nederland synform (Fig. 8.10). On the farm Mooiplaats 206 HT (MAP 2 and Fig. 8.10) a hook fold, defined by the banded iron-formation, with a wavelength of approximately 40m is exposed in an area of poor outcrop. The location and sketch of the structure are shown in Fig. 8.10.

Inspection of the hinge zone of the Commondale Synform (MAP 2) reveals a number of interesting features :

1) Serpentinites chemically distinct from the Matshempondo peridotites are up to 200m thick on the northern limb but are only a few tens of metres thick on the southern limb. This suggests that :-

   a) the southern limb was sheared during D_2, or

   b) late D_1 thrusts have eliminated some of the thickness of the serpentinites, or

   c) the thickness was reduced as a consequence of thrusting which was reactivated by weak shearing during D_2.

2) In the hinge six quartzite units define discontinuous outcrops around the fold closure. This may be the result of either :-
   a) boudinaging during D_1, or

   b) thrusting during late D_1.

The interpretation of the structures as thrust-related is preferred for the following reasons. Some of the ferruginous quartzite units appear to truncate metapelitic layers and overide and encapsulate amphibolite layers that were originally more extensive. Small scale recumbent nappes in ferruginous quartzites are separated from unfolded layers by thrusts (Fig. 8.11). The zone of thrusting comprises metapelitic material in which thin quartz-rich layers are disrupted and rotated. The sectional view of D_1 structures in F_2 structures

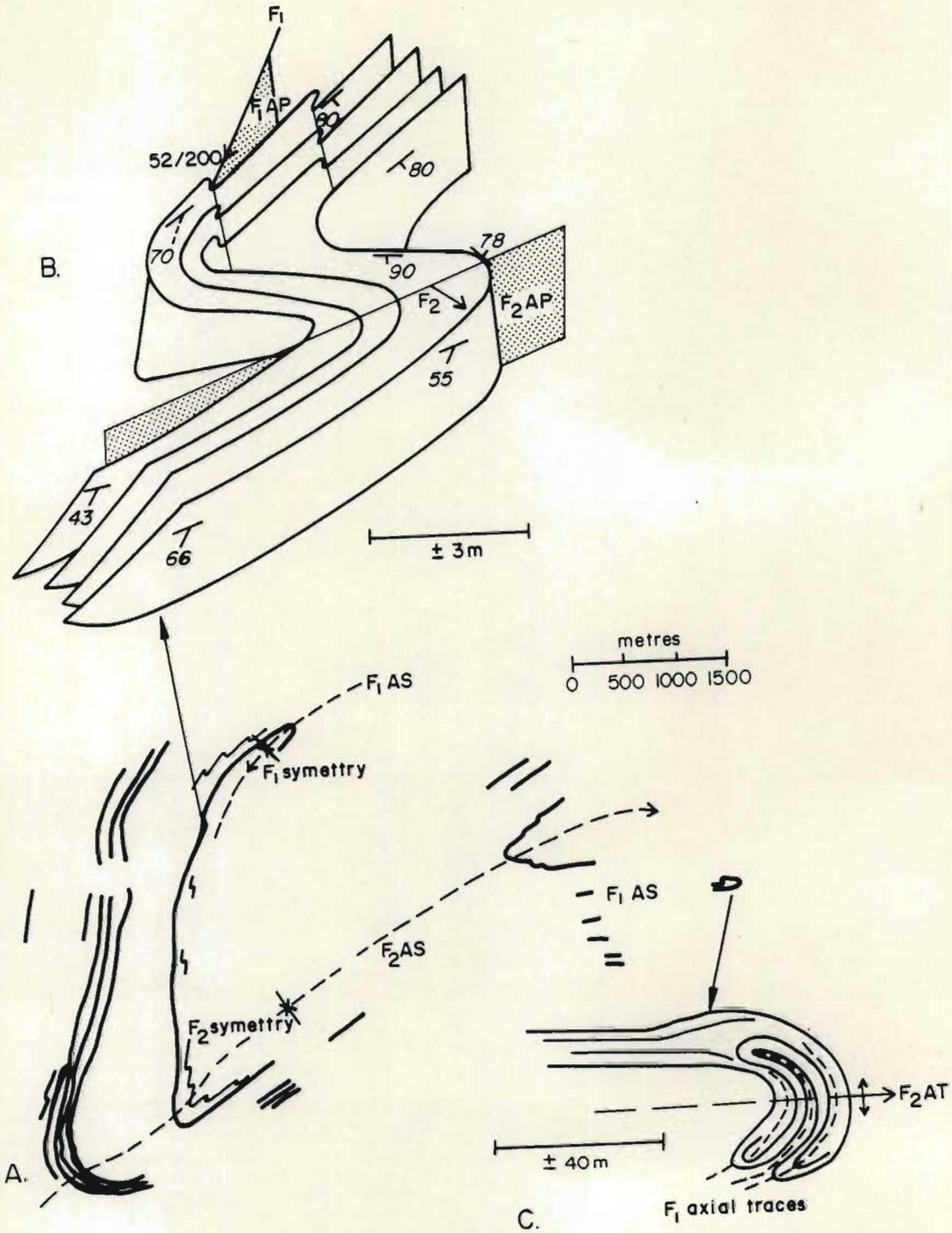

Fig. 8.10 a) Simplified map showing the quartzite and ferruginous quartzite units in the Nederland synform. Note the different sense of symmetry between F_1 and F_2 structures and the F_1 hook on the western limb of the Nederland synform.

b) Mesoscale S on Z interference structure between F_1 and F_2 are affected by later open folding F_4.

c) Type 3 interference structure (hook fold) between F_1 and F_2.

Fig. 8.11 Small scale recumbent nappe separated from straight quartz rich layers by a thrust fault in an argillaceous layer in which the quartz rich layer is imbricated. Commondale synform, Mooiplaats 206 HT.

(MAP 2) and the construction of down plunge profiles, longitudinal and cross-sections through the D_2 structures lend support for the existence of D_1 thrusts (MAP 2, Commondale synform and sections). Strongly foliated amphibolites and altered serpentinites mark the trace of the proposed thrusts in the Commondale synform.

Outcrop is unfortunately inadequate to erect a stratigraphy or employ stratigraphic polarity principles (Strydom and Visser, 1986) as indicators of thrusts.

D_2

D_2 in the Gneiss Complex and Commondale Supracrustal Suite.

The D_2 deformation is characterized by folding about steeply inclined to vertical northeasterly trending axial surfaces. Folds vary from several centimetres to greater than five kilometres in amplitude. Accompanying the formation of the F_2 folds is a strong penetrative S_2 axial planar fabric, L_2^2, L_2^0 and L_2^8 (Table 8.2) stretching mineral lineations. Late D_2 deformation includes dextral shearing and development of mylonite in the contact zone of the Bazane trondhjemite adjacent to the supracrustal suite (MAP 1).

Major F_2 structures in the supracrustals are reclined tight to isoclinal similar folds (MAP 1 and MAP 2) that constitute the Nederland and Commondale synforms. These synforms plunge steeply to the northeast and northwest respectively. Tight steeply plunging normal and reclined (antiformal and synformal respectively) F_2 folds are dominant astride the Pongola River on the farm Vrye Gunst 201 HT and further south along the western margin of the supracrustal suite (MAP 2). A major shear, interpreted on the basis of lineations as D_3, is marked by vein quartz on Vrye Gunst 201 HT and by strongly sheared talc-chlorite-magnesite schists and peridotites on Nederland 202 HT. This shear separates the two major synforms and the smaller folds astride the Pongola River (MAP 2 and, see cross-sections on MAP 1).

F_2 in the Luneburg Tonalite Gneiss is defined by open to tight refolding of S_1 about a northeasterly axial surface. In much of the area west of Luneburg (MAP 1) foliations in the tonalite dip at angles between 16 and 45 degrees to the southeast and northwest (MAP 1). In

contrast the terrane east of Luneburg has a predominantly vertical fabric, much of which is a penetrative S_2 foliation (MAP 1, section A-H).

In the Layered Gneisses mesoscale F_2 similar folds plunge most commonly to the northeast between 10 and 35 degrees (Fig. 8.12). Poor outcrop of the Layered Gneisses in most areas precludes recognition of any large scale structures that may be present. Individual layers in these folds with an average amplitude/wavelength ratio of 1.58 are thickened in the nose and thinned on the limbs. These F_2 folds (defined by folding of S_0 and S_1, Fig. 8.12) are separated by zones of intense axial planar S_2 refoliation which in most areas totally overprints S_1 (Fig. 8.1 and Fig. 8.13). The apparent long axes (Fig. 8.12) and S_1 in the boudins is oblique to the S_2 refoliation (Fig. 8.1 and Fig. 8.13). In the Layered Gneisses on Bendor 211 HT eyed folds in tonalitic gneisses are defined by strongly deformed quartz veins.

Similar type F_2 folds in the Commondale Supracrustal Suite are characterized by thickened hinge zones and thinned limbs, which are particularly apparent in the Commondale and Nederland synforms (MAP 2). S_1 and S_0 are folded about F_2 axial surfaces (Fig. 8.14) and the S_2 axial planar cleavage in the Matshempondo peridotites and BIF is spaced from < 1cm to several metres. S_2 crenulation cleavage is developed in the mafic and ultramafic schists, especially the talc-magnesite-chlorite schists.
F_2 fold axes in the supracrustals also have variable but much steeper plunges than those in the Gneiss Complex due to the variations in the attitudes of the layers being folded that result from the earlier D_1 event and variations in strain across the supracrustal suite.

The F_2 axes plunge between 50 and 90 degrees (Fig. 8.15) to the northeast or southwest and when refolded during D_4 plunge east-northeast and west-northwest in the Nederland and Commondale synforms respectively. Hook folds that are apparently far more abundant in the supracrustals than the Layered Gneisses have resulted in F_1 and F_2 fold axes being co-axial in many instances.

In areas of lower strain where buckled S_1 surfaces in the Layered Gneisses are preserved the L_2 stretching lineation defined by elongated quartz and plagioclase grains is parallel to F_2 fold axes.

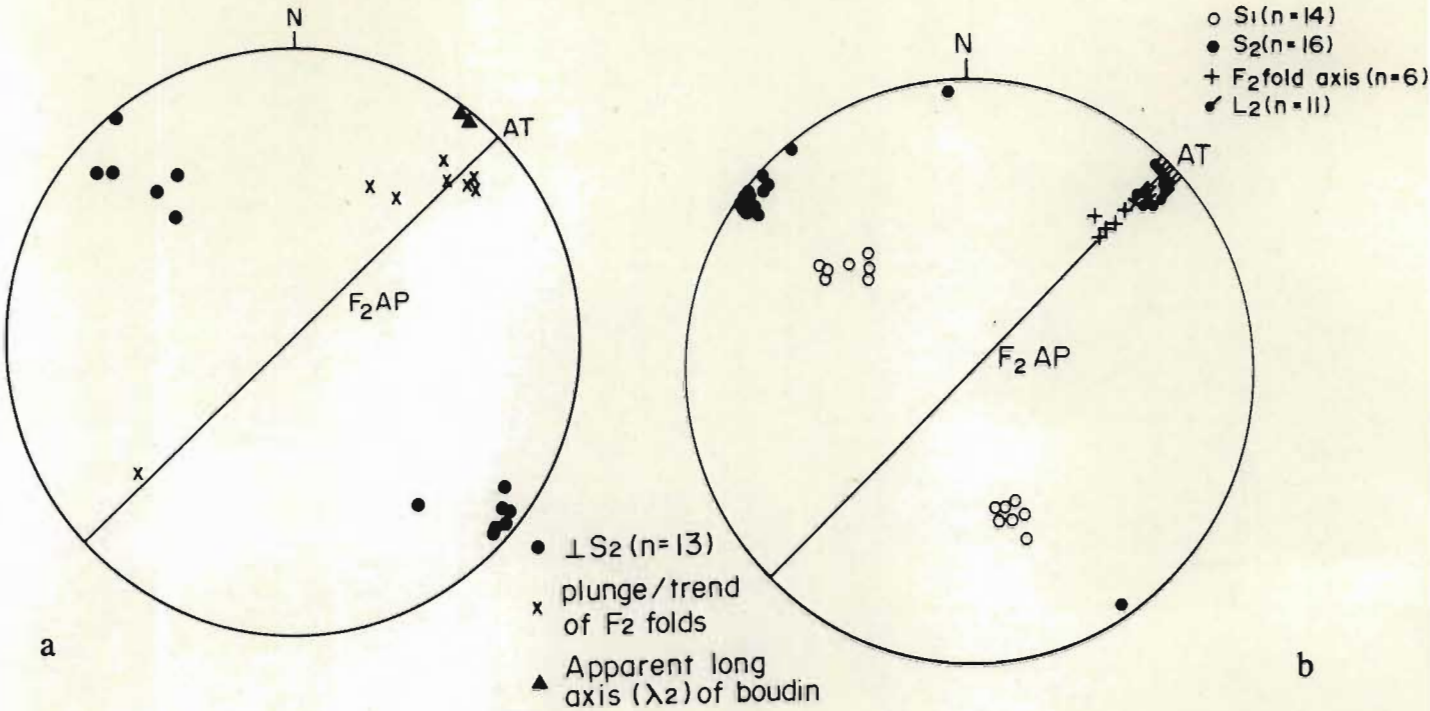

Fig. 8.12 Equal area projections for S_1, S_2, L_2^1 and F_2 components in the Layered Gneisses on a) Wachteenbietjies Spruit 44 and b) Tafelberg 186 HT (See MAP 1). S_2 is axial planar to F_2 and S_1 is folded about F_2 axial surfaces. F_2 fold axes are parallel to the L_2^1 stretching lineation.

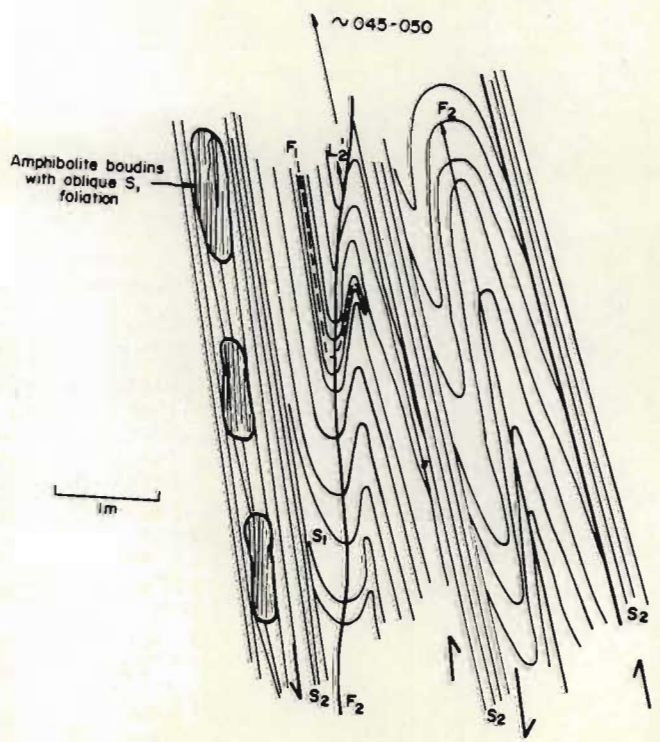

Fig. 8.13 Field sketch showing S_1, S_2, F_1 and F_2 relationships in Layered Gneisses on the farm Tafelberg 186 HT. Note the oblique S_1 foliation in the amphibolite boudins, and the sinstral sense of shear indicated by the F_2 fold symmetry.

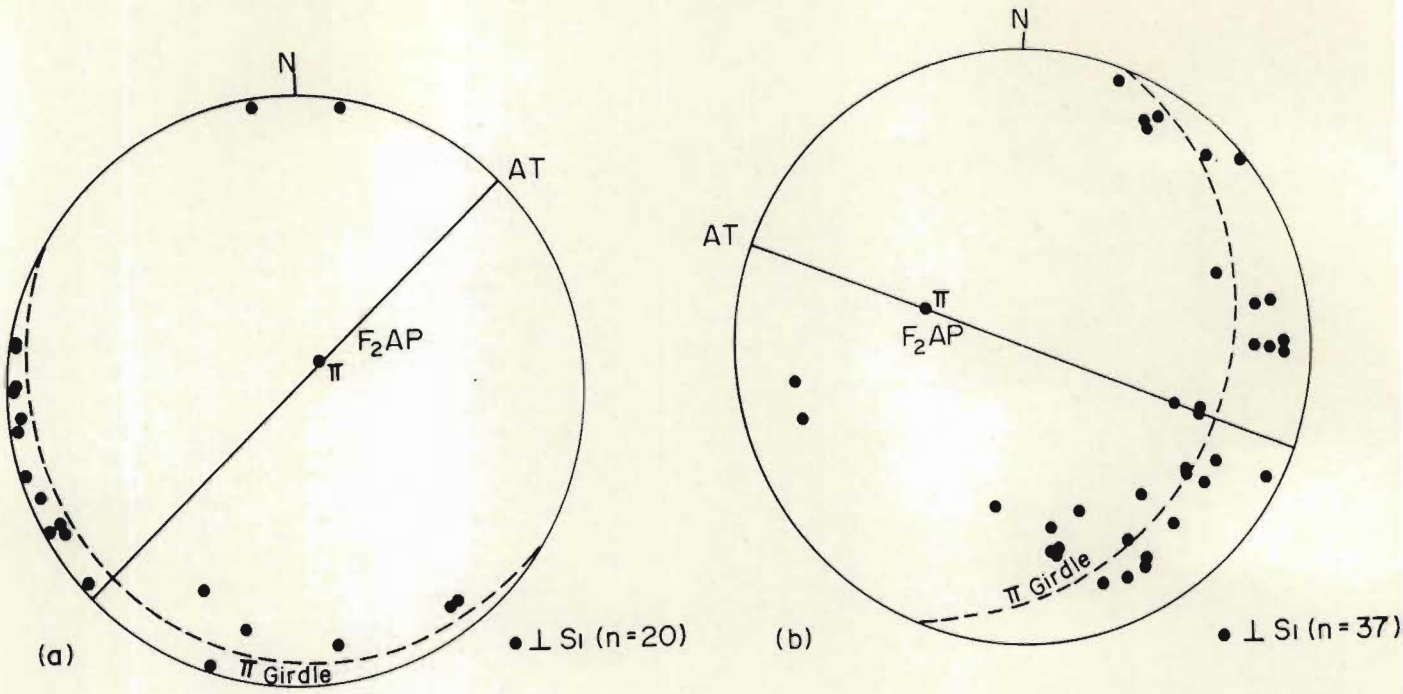

Fig. 8.14 Equal area projection of poles to S_1 in a) Nederland synform and b) Commondale synform. The northwesterly orientation of the F_2 axial plane in Commondale synform reflects folding about F_4 axial surfaces.

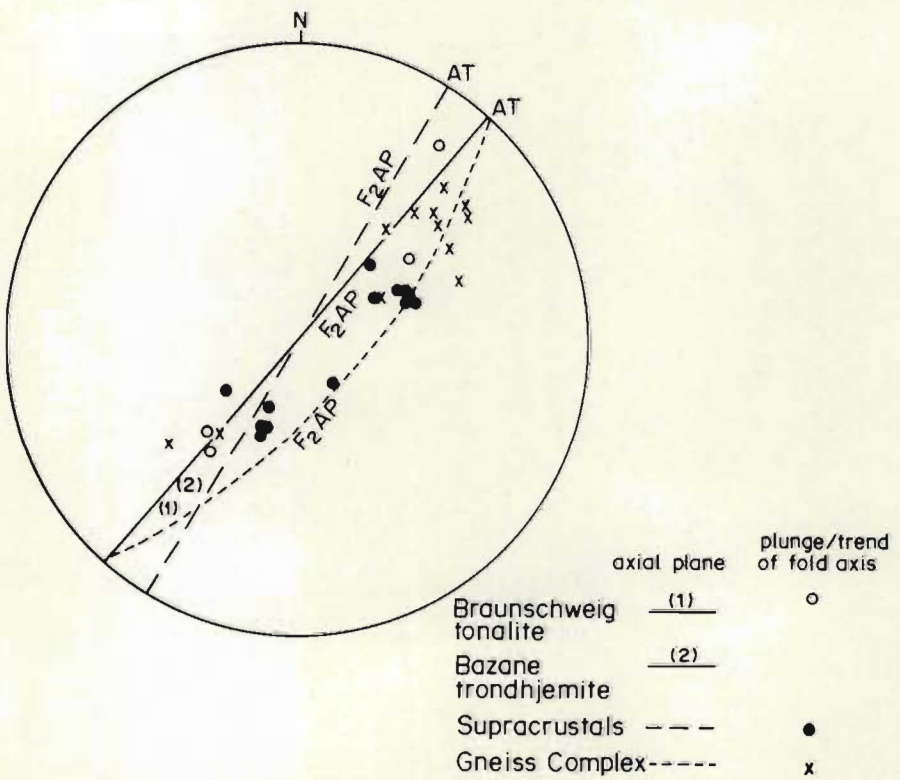

Fig. 8.15 Equal area projection of F_2 axial planes and fold axes in the Gneiss Complex, Braunschweig Tonalite Gneiss, Bazane Porphyritic Trondhjemite Suite and Commondale Supracrustal Suite. F_2 fold axes in the supracrustals are typically steeply plunging while those in the gneisses plunge at shallow to moderate angles.

On an equal area projection L_2^1 lineations plot as a point maxima about the F_2 axial plane (Fig. 8.12b). Similarly in the supracrustals L_2^0, L_2^1 and probably L_1^0 stretching mineral lineations are parallel to the F_2 fold axes. The distribution of lineations suggests that fold axes have rotated towards parallelism with the stretching lineation (Ridley, 1986). The stretching lineation indicates the transport or shear direction and is characteristic of rocks that have been deformed by shearing (Ridley, 1986), where folds form with axial planes parallel to the flattening plane (XY) and perpendicular to the Z axis of the strain ellipsoid. The parallelism of fold axes and lineations is achieved through small irregularities amplified during progressive strain (Cobbold and Quinquis, 1980), or because a wrench shear component is part of the strain history (Coward and Potts, 1983).

Fold shapes, and the initial obliquity of fold axes and parallel lineations to the slip direction suggests that homogeneous simple shear comprising a dominant wrench and minor thrust component (Ridley, 1986) was an important mechanism for the formation of the F_2 folds. The tightness of upright folds in a wrench shear dominated regime depends on the mechanical positioning of strain between homogeneous simple shear and buckling leading to folding (Ridley, 1986). Fold symmetry in the Layered Gneisses on Tafelberg 186 HT indicates sinistral shearing that postdates the buckling of S_1 and S_0 to produce F_2 folds. S_1 approximately parallels S_2 on the limbs and becomes progressively superimposed by S_2 the greater the distance from the fold closure along the limbs (Fig. 8.13).

The Commondale and Nederland synforms in their D_2 orientation plunge southwest and northeast respectively and are separated by a prominent D_3 shear zone (MAP 2). The D_3 shearing may have removed an intervening antiformal structure although no conclusive evidence of this is apparent. Alternatively the Commondale and Nederland synforms may represent a complex sheath-like structure. Poor outcrop in part of the Commondale synform does not provide, by means of cross and longitudinal sections, firm control on the orientation of the fold axis at depth. However, sections through the Nederland synform (not shown) suggest that fold axes plunge less steeply in the core of the F_2 fold indicating the fold axes to be non-cylindrical (Fig. 8.16)

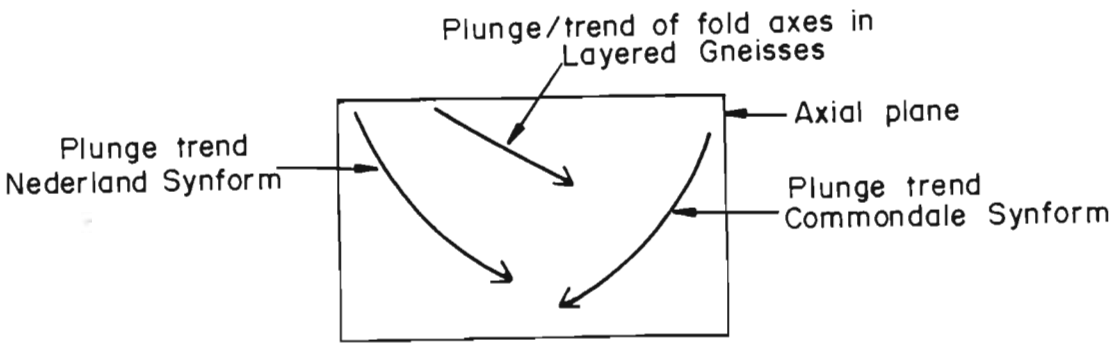

Fig. 8.16 Sketch of the F_2 axial plane comparing the apparent orientation of the axes of non-cylindrical folds in the Commondale Supracrustals, and the shallowly plunging fold axes in the Layered Gneisses, where folds are also non-cylindrical.

Variable orientations of S_0 and D_1 structures may account for the opposing plunges in the Commondale and Nederland synforms, however as discussed above the geometry of the folds may be strongly modified during shear strain where initially slightly curved fold axes are strongly rotated (Ramsay and Huber, 1987). Evidence (see above and section on S-C mylonites) suggests that during late D_2 a simple shear regime prevailed. If this is so it would not be unreasonable to predict the development of sheath-like structures. These structures may, for instance, be produced where variations in the intial dips of layering are developed into fold hinge line variations that become pronounced during flattening strains and produce eyed or sheath folds (Ramsay and Huber, 1987).

Throughout the study area fold axes in the supracrustals plunge more steeply than those in the Gneiss Complex, Braunschweig Tonalite Gneiss and Bazane Porphyritic Trondhjemite Suite (Fig. 8.15). This suggests that the gneisses and supracrustals responded differently to the D_2 deformation. Similar type F_2 folds, intense shearing and high flattening strains (see later section) suggest that the major deformation mechanism during D_2 is progressive simple shear. The orientation of the F_2 fold axis on the axial surface is dependent on the competency and rate of deformation of the deforming layer. Fold axes therefore lie on the intersection between this plane and the plane of the layer (Flinn, 1962). One would therefore anticipate that planar anisotropies and different rates of deformation in relation to the orientation of the strain ellipsoid would account for the varying plunges of F_2 axes within the axial plane (Fig. 8.16).

The supracrustals are preserved as a complex structural enclave separated from the Layered Gneisses by the tabular Bazane Porphyritic Trondhjemite Suite which was emplaced post D_1 - pre D_2. The Layered Gneisses being at a greater depth, would deform incompetently during D_2, i.e. at a higher rate than the supracrustals. This suggestion is supported by the strong S_2 refoliation and ductile shearing of felsic layers in the Layered Gneisses.

D_2 in the Trondhjemite-Tonalite-Granodiorite Suite.

Post-D_1 granitoids intrude the Gneiss Complex and Commondale Supracrustal Suite and are characterized by a strong S_2 foliation. Smaller poorly foliated leucotonalitic and granitic bodies intrude the Luneburg Tonalite Gneiss.

The Braunschweig Tonalite Gneiss, Leucotonalite Gneiss and Bazane Porphyritic Trondhjemite Suite are all host to a number of generations of post-D_1 quartzofeldspathic veins, sodic pegmatites and amphibolitic sheets (Table 8.1). The quartzofeldspathic veins deform competently whereas the amphibolitic sheets deform as incompetent planar elements. (see later discussion of post-D_1 dykes in Layered Gneisses). The planar elements are folded about steeply inclined to vertical northeasterly trending F_2 axial surfaces and fold axes plunge both northeast and southwest (Fig. 8.15).

The axial planar S_2 foliation (Fig. 8.17) is defined by the elongation and flattening of quartz grains, plagioclase porphyroclasts and gneissic layering (see Chapter 4) which for the Bazane Porphyritic Trondhjemite Suite and Hornblende Granodiorite Suite is in places oblique to intrusive contacts with the supracrustals. The lack of fabric reflecting D_1 and the absence of evidence that S_2 is transposed S_1 indicates that these granitoids were intruded post-D_1 acquiring their strong S_2 fabric during D_2.

S - C mylonites and fabric relationships.

Mylonites in a zone up to 50m wide are developed along the contact with the Commondale Supracrustal Suite in the Bazane trondhjemites (MAP 1). Protomylonites and mylonites crop out along the western margin of the supracrustals on Nederland 202 HT (Fig. 8.18). On Vrye Gunst 201 HT, Wachteenbietjies Spruit 44 and Politiek 29 mylonites and ultramylonites are developed in which the porphyroclastic character of the Bazane trondhjemites is totally destroyed. In other less deformed areas porphyroclasts are reduced in size and sigmoidal in shape.

In the mylonite zone both S and C fabrics are developed. S surfaces are related to the accumulation of finite strain and C surfaces to

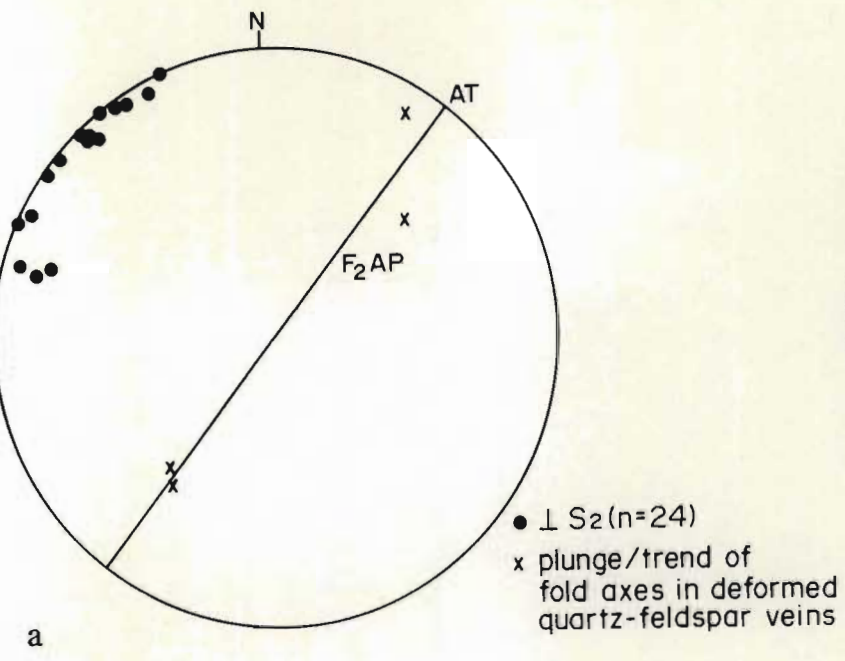

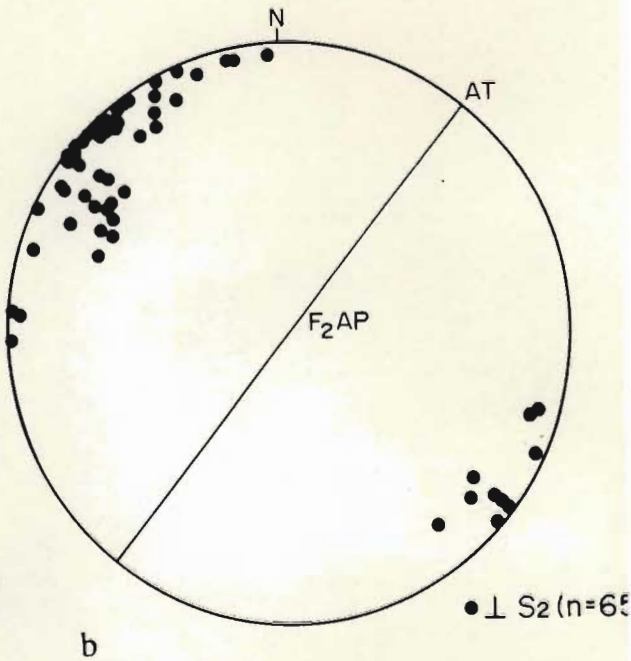

Fig. 8.17 Equal are projection of poles to the S_2 axial planar foliation in the, a) Braunschweig Tonalite Gneiss and, b) Bazane Porphyritic Trondhjemite Suite.

Fig. 8.18 Deformed plagioclase and microcline porphyroclasts in mylonites in the Bazane Porphyritic Trondhjemite Suite at the contact with the Commondale Supracrustal Suite. Nederland 202 HT.

displacement discontinuities or zones of relatively high strain (Berthe et al., 1979). Stretching lineations on the C surfaces (planes of relative movement) indicate an essentially horizontal sense of displacement. The oblique S surfaces define the plane of preferred mineral orientation (Berthe et al., 1979), and lie in the XY plane of the finite strain ellipsoid. During the initial stages of orthogneiss and mylonite development, the angle between the S and C surfaces is 45 degrees. During progressive deformation S surfaces adopt a sigmoidal shape, rotate and at the ultramylonite stage are indistinguishable from C surfaces (Berthe et al., 1979). In mylonite zones an increase in the intensity of non-coaxial deformation (Lister and Snoke, 1984) is expressed by a decrease in grainsize, recrystallization and increase in the density of C surfaces.

The distinction should be made between S - C tectonites and gneisses where an S_1 - S_2 terminology is justified. The S - C terminology is applied when both surfaces form during the same deformational event (Berthe, et al., 1979; Lister and Snoke, 1984). The mylonitic foliation, S, forms early during the deformation and C later in response to the development of anisotropy (Lister and Snoke, 1984). S_1 - S_2 terminology is used where an earlier deformed gneiss is involved in a later shear zone, where older S_1 surfaces are transected by S_2 and C surfaces produced during the younger deformation (Lister and Snoke, 1984). In many S - C tectonites the dominant foliation is an older modified fabric, that can be misleading in terms of the qualitative assessment of strain during mylonitization (Lister and Snoke, 1984).

During S - C fabric development, feldspar porphyroclasts in the S plane develop flattened mantles and sigmoidal tails of dynamically recrystallized feldspar. The tails are derived from an originally large clast by grain size reduction (Passchier and Simpson, 1986) in a more ductile and fine-grained matrix (Simpson and Schmid, 1983). Foliation planes are asymmetrically distributed around the porphyroclasts so that the grains have a retort shape with tails of finer grained recrystallized material of the same composition of the porphyroclasts extending along the foliation plane in the direction of shear (Simpson and Schmid, 1983). The shape of the deformed feldspar porphyroclasts, fold symmetry, tension gashes and marker units may be used as kinematic indicators to reflect the direction and sense of

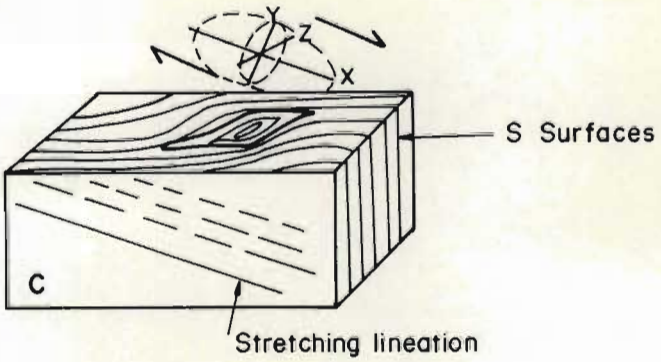

Fig. 8 19 a) Block diagram showing the orientation of the oblate ellipsoid and dextral sense of rotation or shear determined from linear and planar elements illustrated in the block diagram. The shape of the ellipsoid reflects qualitatively the high flattening strains. Drawing is from block cut with surfaces normal to the axes of the strain ellipsoid.

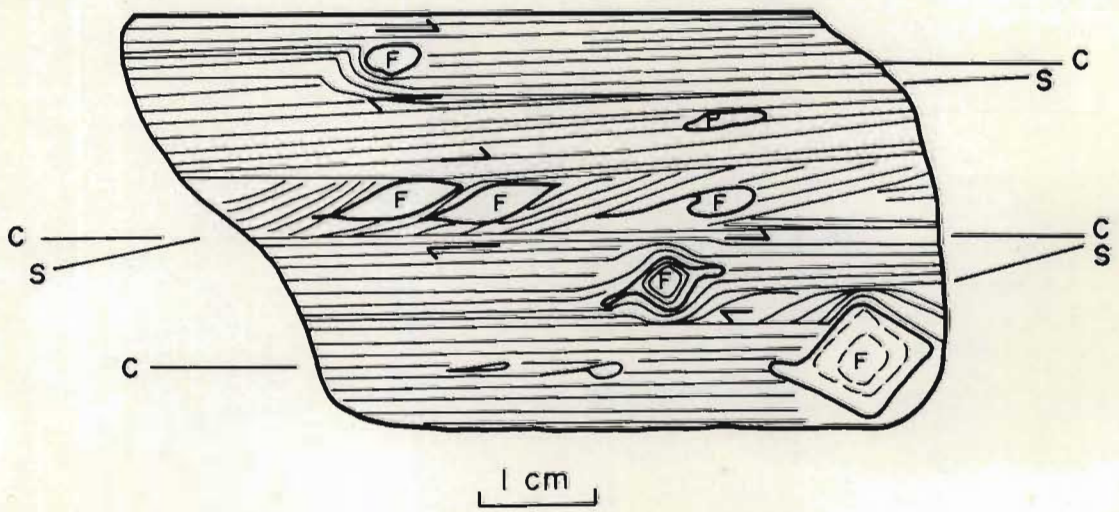

Fig. 8.19 b) S-C relationships and deformed feldspar porphyroclasts reflecting dextral shearing and mylonite formation in the Bazane Porphyritic Trondhjemite Suite along the western margin of the Commondale supracrustals on the farm Nederland 202 HT. Drawing is from slab normal to the Y axis of the strain ellipsoid.

shearing (Simpson and Schmid, 1983; Sugden, 1987 and others).

In the protomylonites and mylonites developed adjacent to the Commondale Supracrustal Suite on Nederland 202 HT S - C relationships and deformed feldspar porphyroclasts (Fig. 8.18) indicate a dextral sense of shearing (Fig. 8.19). Similarly fold symmetries and S_1 - S_2 relationships in the Layered Gneisses on Tafelberg 186 HT reflect a sinistral sense of shearing during D_2 (Fig. 8.13) in which fold axes parallel the shear direction suggesting sheath fold development.

Deformation of competent and incompetent planar elements and determination of the minimum strain ellipsoid.

Quartzofeldspathic veins as strain markers.

A suite of omnidirectional pre-D_1 quartzofeldspathic veins between 5mm and 10cm in thickness are abundant in feldspathic amphibolites and dark, homogeneous tonalite gneisses. These veins were intensely deformed during at least D_1 and D_2 (Fig. 8.20). They are prominent in the gneisses exposed on Tafelberg 186 HT and Bendor 211 HT. Quartzofeldspathic veins and their imposed or inherited planar sub-fabrics may be used as strain markers when they strain at rates different to those of their less competent host (Talbot, 1970; Talbot, 1987; Talbot et al., 1987). This is because they strain as single layers and any inhomogeneities they introduce into the strain of the rock complex of host-plus-veins are localized to within one wavelength of the structures that form in each planar element of the sub-fabric (Talbot, 1987). Deformed veins at these localities provide the only means of estimating the strain in the Layered Gneisses.

If one is to assume homogeneous strain during ductile deformation in a terrane that has been deformed inhomogeneously on a regional scale a small area should be chosen where the overall strain in the host-plus-vein complex may be regarded as homogeneous. Two such areas, 6 x 3 x 1.5m and 20 x 10 x 0.5m were chosen on Tafelberg 186 HT and Bendor 211 HT respectively. At the former locality the veins are hosted in amphibolite and tonalite in which a strong penetrative S_2 fabric is characteristic. At this locality only the veins hosted in tonalite were used in the strain analysis. On Bendor 211 HT the zone of homogeneous tonalites and quartzofeldspathic veins comprises

Fig. 8.20 Suite of thin omnidirectional veins deformed during D_1 and D_2 and exposed in a shallowly plunging S_2 synform. The host rocks are medium grained homogeneous tonalites. Pavement in Pongola River on Bendor 211 HT.

Fig. 8.21 Hook fold in thin quartzofeldspathic vein. Outcrop in Pongola River on Tafelberg 186 HT.

transposed S_1 fabrics in shallowly plunging isoclinal F_2 folds. Locally an S_2 penetrative fabric is developed. At both these localities the presence of hook folds in the quartzofeldspathic veins (Fig. 8.21) indicate this suite of veins as pre D_1.

The basic assumptions of this method, developed by Talbot (1970), to calculate the minimum strain ellipsoid are :

a) quartz veins are approximately parallel sided straight planar sheets before strain,

b) folds in the veins imply shortening, and

c) necking and boudinaging of the veins imply extension. Many of the thin quartzofeldspathic veins in the XY plane appear unstrained, but close observation indicates a strong internal foliation implying that the veins have been thinned uniformally without necking during ductile deformation.

To quantify the shape of the minimum strain ellipsoid, the orientations of veins that are extended, partially folded and folded are plotted on a lower hemisphere equal area projection (Talbot, 1970). The area containing the poles to extended planar units (quartzofeldspathic veins) on the stereonent is the field of overall extension (Talbot, 1970). If the deformation is homogeneous this field is elliptical, centred on Z, elongate in the ZX principal plane (where strain axes, X > Y > Z) and defines the surface of no finite longitudinal strain (snfls). Linear or planar elements parallel to the snfls are assumed to be their original lengths, and do not show any strain structures (Talbot, 1970). Planar elements lying wholly on one side of the cones bounded by the snfls have decreased in length through folding whereas those on the other side have increased in length through necking, boudinage and straight planar elongation (Talbot, 1970; Talbot, 1987). The shape and orientation of an ellipsoid strained by any mechanism can be derived from the shape and orientation of the snfls using formulae derived by Flinn (1962) and shown graphically by Talbot (1970). The angular relationships ψ XZ and ψ YZ (measured from snfls on an equal area projection) allow the derivation of the axial ratios where a = X/Y and b = Y/Z (Talbot, 1970). The axial ratios are calculated using the equations defined by Flinn (1962) and applied in the same manner as Talbot (1970),

where for oblate ellipsoids

$$\cos^2 \psi YZ = \frac{a^{-2/3}b^{2/3} - b^2}{1 - b^2}$$

so that for oblate ellipsoids

$$b^2 = \frac{-A \pm \left(A^2 + 4\left(\frac{n}{1-n}\right)^3\right)^{\frac{1}{2}}}{2}$$

Where

$$A = \frac{(1-n)^2 (1+2n) + \left(\frac{n}{m} - 1\right)}{(1-n)^3}$$

Where $n = \cos^2 \psi YZ$ measured from equal area projection

$m = \cos^2 \psi XZ$

and $$\frac{1}{a} = \frac{\left(b^2 (1-n) + n\right)^{3/2}}{b}$$

Assuming no volume change and the ellipsoid to be derived from a unit sphere (Talbot, 1970) one may define the magnitude of the axes (Flinn, 1962; Flinn, 1978) such that :

$$XYZ = 1$$

therefore $X = a^{2/3}b^{1/3}$, $Y = a^{-1/3}b^{1/3}$, $Z = a^{-1/3}b^{-2/3}$

Further theoretical aspects and methodology are described in Talbot (1970) and in the appendix of Talbot (1987).

Lower hemisphere equal area projections for deformed quartzofeldspathic veins on Tafelberg 186 HT and Bendor 211 HT presented in Fig. 8.22 describe the minimum finite strain ellipsoids that reflect the bulk deformation. No direct information about the deformation path and history are available from these figures. Some important differences between these strain ellipsoids are apparent. The shape and orientation of the extension fields are different resulting in obvious differences in the orientation of the strain axes

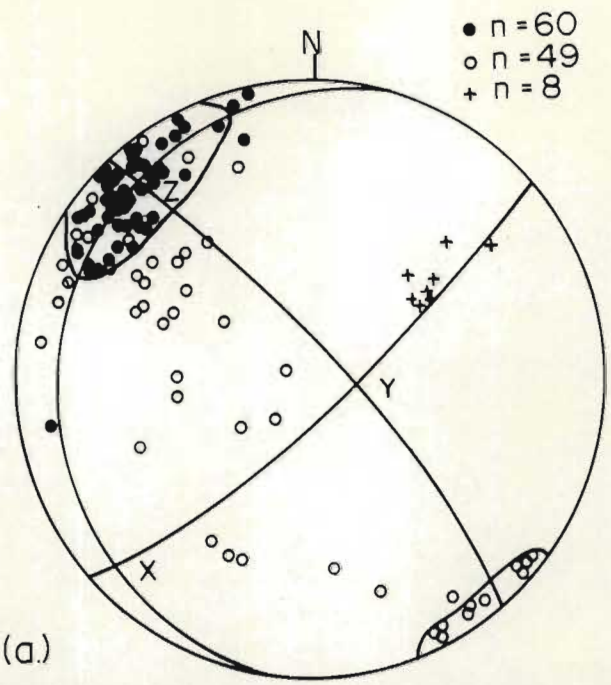

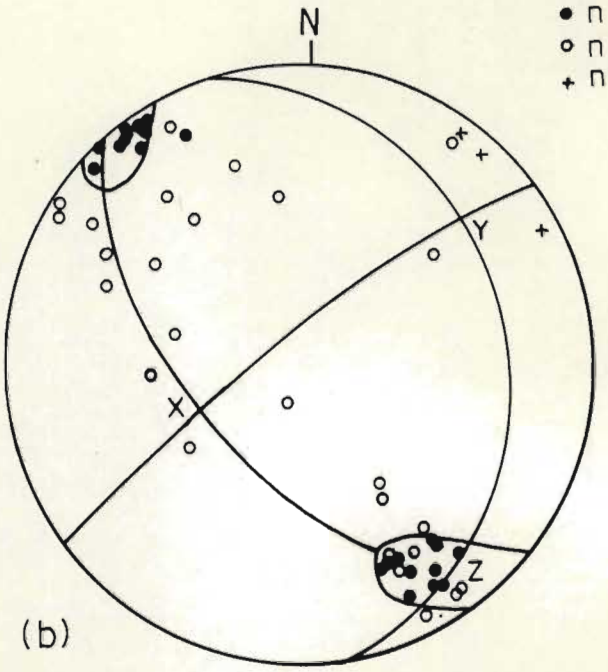

- Poles to extended veins, necked and straight
- o Poles to partially folded veins
- \+ Fold axis

a) Tafelberg 186HT		b) Bendor 211HT
21°	ψXZ	24°
14°	ψYZ	10°
1.69	a=X/Y	1.94
3.01	b=Y/Z	2.35

a) Tafelberg 186HT		b) Bendor 211HT
2.05	X	2.07
1.21	Y	1.07
0.40	Z	0.45
0.48	k	0.78
0.35	ν	0.13
1.24	ε	1.14

a=b X/Y, b=Y/Z and k= (1na)/(1nb), Lode factor $\nu = \left(\frac{1nb-1na}{1nb+1na}\right)$

and natural strain $\varepsilon = (^2/_3)^{\frac{1}{2}} \left((1na)+(1nb)^2 + 1na.1nb \right)^{\frac{1}{2}}$

are tabulated above

Fig. 8.22 Lower hemisphere equal area projections of strain data from a) Layered Gneisses, Tafelberg; b) Layered Gneisses, Bendor. ψZX and ψYZ are the angular dimensions of the extension fields measured from Z in the principal planes.

in three dimensional space. Poles to partially folded veins cluster around the ZX plane in Fig. 8.22b and in Fig. 8.22a tend to plot between the ZX and ZY planes. On Tafelberg 186 HT the X axis of the strain ellipsoid plunges at 10 degrees to the southwest whereas on Bendor 211 HT the Y axis lies in a subhorizontal plane plunging at 30 degrees to the northeast. The major differences in the orientation of the strain ellipsoids are presumably related to different amounts of strain (greater strain in the case of the Layered Gneisses on Tafelberg 186 HT) that may reflect deformation at different crustal levels.

The minimum strain ellipsoids represent the bulk deformation (D_1 + D_2). The orientation of the XY plane of the strain ellipsoid parallels that of F_2 axial surfaces reflecting a major influence by D_2 on the orientation of the bulk finite strain ellipsoid. In both cases K indicates flattening strains that are theoretically associated with the development of a penetrative S fabric (Fig. 8.23). Thus the strain ellipsoid (k = 0.78) for the Layered Gneisses on Bendor indicates moderate flattening strains consistent with field observations. The bulk strain ellipsoid (k = 0.48) for the Layered Gneisses on Tafelberg 186 HT indicates higher flattening strains (Fig. 8.23) which is consistent with tight to isoclinal folds and a penetrative S_2 fabric that in places overprints S_1.

The bulk minimum strain ratios are compared to those determined by similar techniques from the Motjane schist belt, Swaziland (Jackson and Robertson, 1983) and from Layered Gneisses southwest of Piet Retief (Talbot et al., 1987) in Fig. 8.25. Layered Gneisses on Bendor 211HT have been shortened by about 55% whereas those on Tafelberg by 60%, which is similar to that recorded from southwest of Piet Retief. Strains in the Motjane schist belt reflect shortening between ~70% and 80%.

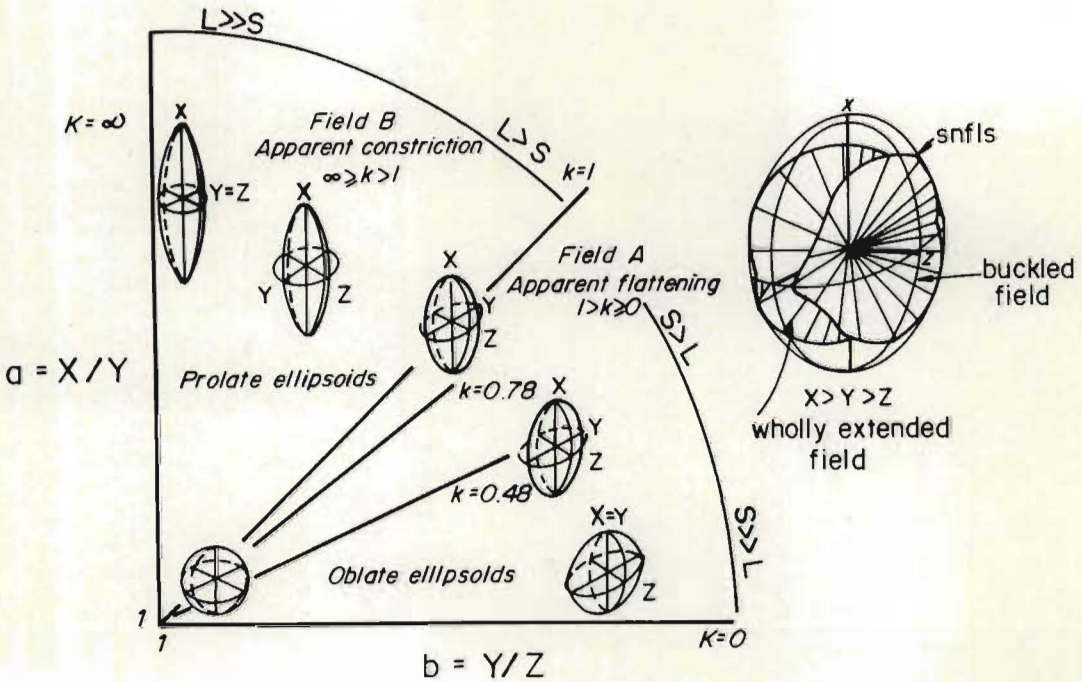

Fig. 8.23 Flinn plot showing the fields of constriction and flattening. K is a parameter expressing the shape of the strain ellipsoid (prolateness or oblateness). The inset is a typical oblate strain ellipsoid where the surfaces of no finite longitudinal strain (snfls) are represented by two cones centred about the Z axis and elongate in the ZX plane. The lines k = 0.48 and k = 0.78 represent the ellispoids from Tafelberg 186 HT and Bendor 211 HT. The former represents a higher flattening strain and greater development of penetrative S fabrics. Flinn plot modified from Ramsay and Huber (1983).

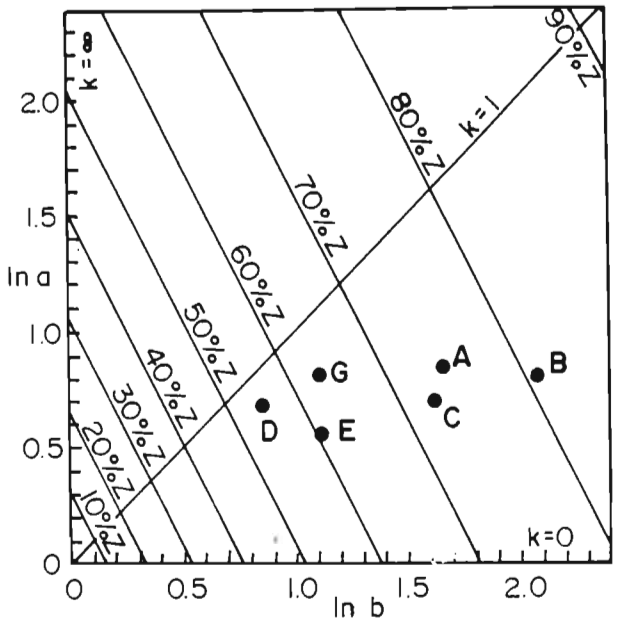

Fig. 8.25 Three dimensional bulk minimum strain ratios measured from deformed quartzofeldspathic veins. A, B and C are localities in the Motjane schist belt, Swaziland (Jackson and Robertson, 1983). D is Layered Gneiss on Bendor 211 HT, E Layered Gneisses on Tafelberg 186 HT, G Layered Gneisses southwest of Piet Retief (Talbot, et al., 1987). Data are plotted on a natural logarithmic Flinn diagram showing contours of percentage shortening parallel to Z.

Amphibolite dykes as strain markers.

The Layered, Braunschweig and Leucotonalite Gneisses and the Bazane Porphyritic Trondhjemite Suite are host to a number of generations of mafic dykes in addition to quartzfeldspathic veins (Table 8.1). These dykes were intruded prior to D_2 and also pre-D_1 in the Layered Gneisses. In the Layered Gneisses on Bendor 211 HT post D_1 - pre D_2 amphibolitic dykes between 0.5 and 1m in thickness were deformed during D_2 and may be followed along strike for up to 80m. S_2 where developed is axial planar to folds in these sheets that cross-cut S_1. In places the S_1 fabric is transposed and parallels localized zones of S_2 refoliation. Depending on the orientation of these amphibolitic sheets with respect to the strain ellipsoid they are necked and boudinaged, undeformed or partly or strongly folded (Fig. 8.26 and Fig. 8.27).

The relative incompetency of the amphibolitic sheets in the tonalitic host produces inverse mullions or cuspate margins (Talbot, 1982) in these sheets where they are folded. The foliation in the mafic sheets is sigmoidal and oblique to the enveloping surfaces. Oblique foliations in mafic sheet intrusions are interpreted to be the result of layer parallel shears along the sheets propagated by the rotation and deformation of the sheet as a single layer due to the bulk strain of the country rock (Talbot, 1982). The oblique foliations provide information about the geometry of strain of the bulk rock mass.

The post D_1 - pre D_2 suite of mafic dykes on Bendor 211 HT are interpreted to have been metamorphosed at amphibolite facies during D_2. During this event an internal sigmoidal S_2 foliation defined by the elongation of plagioclase and hornblende oblique to the dyke margins and locally an S_2 fabric in the tonalitic gneiss developed. Figures 8.26 and 8.27 illustrate some examples on different scales of these deformed dykes in which classical shapes such as inverse mullions, cuspate or lobate margins and an oblique internal foliation are characteristic. In thinner sheets the foliation is planar but in the thicker sheets it is sigmoidal due to the enhanced strain gradient across the sheet (Talbot, 1982).

In Fig. 8.26a the margins of the amphibolitic sheet are cuspate or inverse mullion. The dyke has an internal sigmoidal foliation

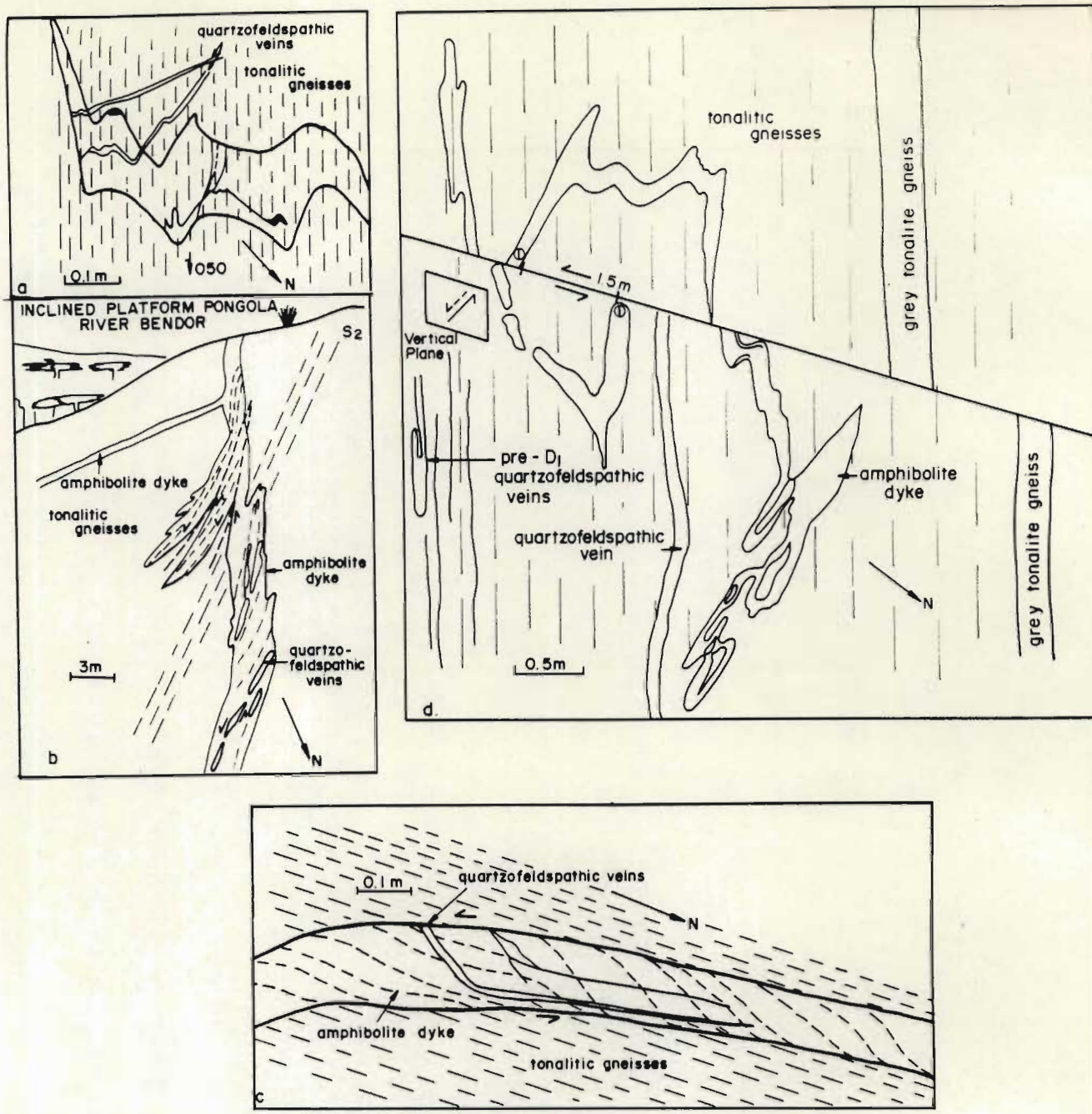

Fig. 8.26 a) - d) Sketches of deformed amphibolitic dykes in outcrops of the Layered Gneisses in the Pongola River on the farm Bendor 211 HT. Photographs of these dykes are shown in Fig. 8.27 a) - d) respectively. See text for discussion.

Fig. 8.27 Amphibolite dykes deformed as incompetent planar elements in Layered Gneisses, Pongola River, Bendor 211 HT. Sketches of these dykes are presented in Fig. 5.26.

Fig. 8.27a

Fig. 8.27b

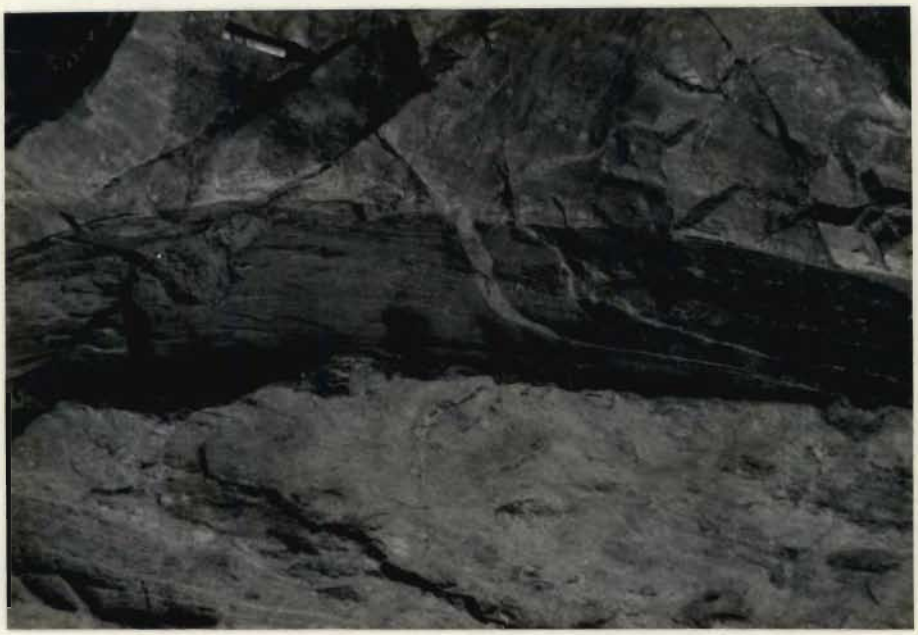

Fig. 8.27c

Fig. 8.27d

perpendicular to the enveloping surface. On the attenuated limbs however that closely parallel the flatttening plane, the foliation approaches parallelism with the margins and the sigmoidal pattern is poorly developed. Thin quartzofeldspathic veins deform competently and in the amphibolitic sheets deform at a faster rate than in the tonalitic gneisses due to the greater competency difference (Fig. 8.26a).

A large partially folded amphibolitic dyke (Fig. 8.26b) of which Fig. 8.26c is a portion displays a number of complex, related and interacting events. In these figures quartzofeldspathic veins in the mafic sheet are sigmoidal in shape and their symmetry and sense of rotation similar to that of the foliation. These observations are consistent with those reported by Talbot (1982) for mafic sheets from several deformed terranes. Fig. 8.26d is a superb example of a highly deformed amphibolite dyke which has cuspate margins in the fold closures and is boudinaged on the limbs. The shape is complicated by faulting about a steeply inclined northwesterly trending fault plane (Fig. 8.26d). Foliations in the amphibolite dyke (Fig. 8.26c) were used to determine the orientation and shape of the strain ellipsoid employing the method of Talbot (1982). As the sheet rotates shear stresses along the contacts with more competent host rocks induce antithetic rotation of internal features with respect to the sheet boundaries (Talbot, 1982). Antithetic layer parallel shears account not only for the oblique foliations within the sheets but also for the strains of any cross-cutting veins and the offsets of any irregularities in the contacts (Fig. 8.26b and 8.27b shears offsetting dyke) (Talbot, 1982). The sigmoidal foliations in incompetent sheets record different amounts of the same general strain in the same overall movement pattern (Talbot, 1982).

The theoretical considerations employed in this technique (Talbot, 1982) are similar to those for deformed competent planar elements (Talbot, 1970; Talbot, 1987). Poles of a straining planar body rotating towards X or XY will rotate towards Z or ZY of the strain ellipsoid (Talbot, 1982). These paths traced on a stereographic projection were called structural movement paths (Flinn, 1962) and trace parts of curves that extend from X or XY toward Z or ZY (Fig. 8.28), the length of the path depending on the original attitude of the plane and the amount of strain (Talbot, 1982). The apparent

structural movement paths (ASMP) converge on Z for oblate (flattened) ellipsoids. The ASMP for each sheet element can be defined by linking the poles of one of its contacts to as many poles to planar elements as practical. Talbot (1982) implies that three to four readings across sheets up to 80cm thick are adequate.

For the amphibolite dyke on Bendor 211 HT the ASMP in the equal area projection (Fig. 8.28) are shown as parts of great circles and interpreted to be due to a strain ellipsoid that is close to uniaxially oblate ($\nu = 1$) with the Z axis plunging 8 degrees towards 170. The exact shape of the ellipsoid is unclear as the structural movement paths closely parallel the XZ plane and are therefore insensitive to differences in the lode factor (ν), (see Talbot, 1982; Fig. 3). In Fig. 8.28 not all the ASMP focus on the same Z axis. One of the paths moves towards the ZX plane in which Z and X have rotated at least 16 degrees anticlockwise about Y which plunges at 58 degrees towards 277 and is marked by the intersection of the XY plane and the regional foliation. This suggests that different parts of the same sheet rotated by different amounts due to small inhomogeneities in the strain (Talbot, 1982). Although the pattern of data in Fig. 8.28 is not directly compatible with that in Talbot (1982) it can be concluded that the foliated amphibolites deformed as incompetent single layers and together with the tonalitic gneisses deformed by an almost homogeneous flattening that involved anticlockwise rotation (at least 16 degrees) about a steep Y axis.

Summary of strain data.

1. Pre-D_1 quartzofeldspathic veins, deformed as competent planar elements, reveal the shapes of the bulk (D_1 + D_2) minimum strain ellipsoids in the Layered Gneisses on Tafelberg 186 HT and Bendor 211 HT. Both strain ellipsoids reflect flattening strains, k = 0.48 and k = 0.78 respectively, that are consistent with field observations.

2. Field observations and bulk minimum strain ellipsoids reflect a more intense D_2 deformation in the Layered Gneisses on Tafelberg 186 HT.

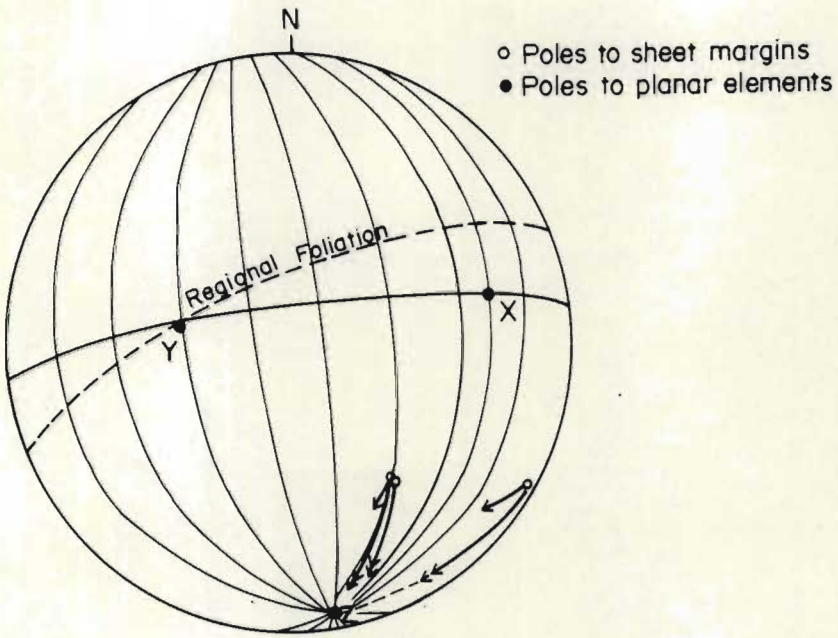

Fig. 8.28 Lower hemisphere equal area projection of apparent structural movement paths (ASMP) from foliations measured in the amphibolite dyke in Fig. 8.28b. Poles to sheet margins (o) are tied to the most angular foliation (.) within each sheet element by ASMP. The regional foliation is that in the host tonalitic gneisses.

3. Figure 8.29 shows diagramatically the shape and approximate orientation of the bulk minimum strain ellipsoids and the D_2 strain ellipsoid using incompetent amphibolitic dykes on Bendor 211 HT. A number of obvious differences between the strain ellipsoids are clearly demonstrated in this figure :

   a) The maximum extension direction, X plunges at 60 degrees to the southwest on Bendor 211 HT and that on Tafelberg 186 HT at 10 degrees in the same direction. If one assumes that the shape of the D_1 strain ellipsoids at both localities were similar, the differences in the orientations of the bulk strain ellipsoids are attributable to the orientation and shape of the D_2 strain ellipsoid.

   b) The axial ratios for the strain ellipsoid on Bendor 211 HT are unknown but presumably reflect a lower strain and percentage shortening than on Tafelberg 186 HT. This conclusion is consistent with field observations indicating a lower intensity D_2 deformation on Bendor 211 HT.

4. Amphibolite dykes deform as incompetent single layers in siliceous gneisses and develop sigmoidal internal foliations in response to a strain gradient across the layer. Foliations in deformed dykes allow one to limit the geometry of strain and shape (protate or oblate) of the bulk strain ellipsoid although the axial ratios and lengths cannot be quantitatively determined.

D_3

Shearing and faulting aligned northeastwards in the Commondale Supracrustals is interpreted on the basis of steeper lineations, to post date the mylonitic shearing along the Bazane trondhjemite-supracrustal contact (MAP 2). Faults in the supracrustals north and south of the Pongola River (MAP 2) are marked by 5 to 15m wide quartz veins. Subordinate en echelon quartz veins and strongly sheared talc-chlorite-magnesite and tremolite schists in a zone more than 100m wide mark the shear zone between the Commondale and Nederland synforms (MAP 2). In this area lineations, L_{SS}, defined by stretched quartz grains in vein quartz plunge at 70 degrees to the southwest (Fig. 8.30) reflecting a steeply inclined sinistral displacement or shear (MAP 1;

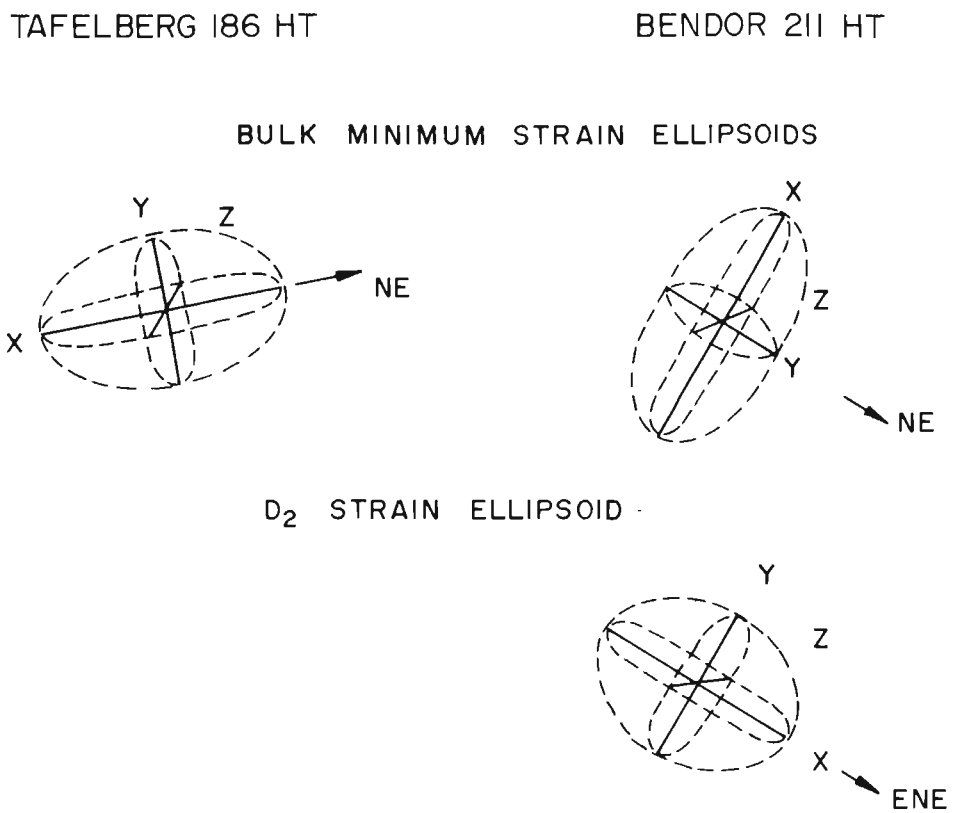

Fig. 8.29 Shapes and orientations of oblate ellipsoids. The bulk minimum strain ellipsoids are calculated from the axial ratios presented in Figure 8.22. The orientation of the axes of the D_2 strain ellipsoid on Bendor 211 HT are calculated from foliations in deformed amphibolite dykes, (Fig. 8.28) but the size of the ellipsoid is qualitative.

sense of displacement on Nederland 202 HT, and section looking down plunge of the Commondale synform).

Along the northern margin of the Matshempondo peridotites a strong penetrative fabric interpreted as S_1 obscures cumulate and spinifex textures. S_1 is intersected at an acute angle by shear zones up to several metres wide in which a strong east-northeasterly trending shear fabric is developed (Fig. 8.30). The small shear zones parallel the major D_3 displacement and their lineations plunge steeply to the northeast (Fig. 8.30).

D_4

Open to tight F_4 folds with steeply inclined axial surfaces trending northwest are recognized in the granitoids and supracrustals where they fold S_0, S_1 and S_2 (Fig. 8.31). The fold axes have a variety of plunges due to variations in the attitude of surfaces being folded by F_4 due to the earlier effects of D_1 and D_2. F_4 folds are recognized on a variety of scales ranging in size from 1cm to several kilometres (MAP 1). In the mafic and ultramafic schists S_1 is folded on a small scale by F_4 producing chevron folds with an amplitude of several centimetres to tens of centimetres. Layered Gneisses and the Bazane Porphyritic Trondhjemite Suite form the core of the large F_4 antiform that refolds the Commondale and Nederland synforms. The right hand limb of the Commondale synform is a refolded Type 3 interference structure in which F_1 and F_2 fold axes are rotated about F_4 axial surfaces (MAP 1 and MAP 2). In the Luneburg Tonalite Gneiss and Gneissic Leucotonalite (MAP 1 and MAP 3) F_4 produces Type 1 interference patterns by folding of the S_1 gneissosity (already folded by F_2). Because of the different interlimb angles between tight F_2 and other F_4 folds these Type 1 interference structures produce an open dome and basin arrangement with an arcuate elongation of domes and basins in a northeasterly direction.

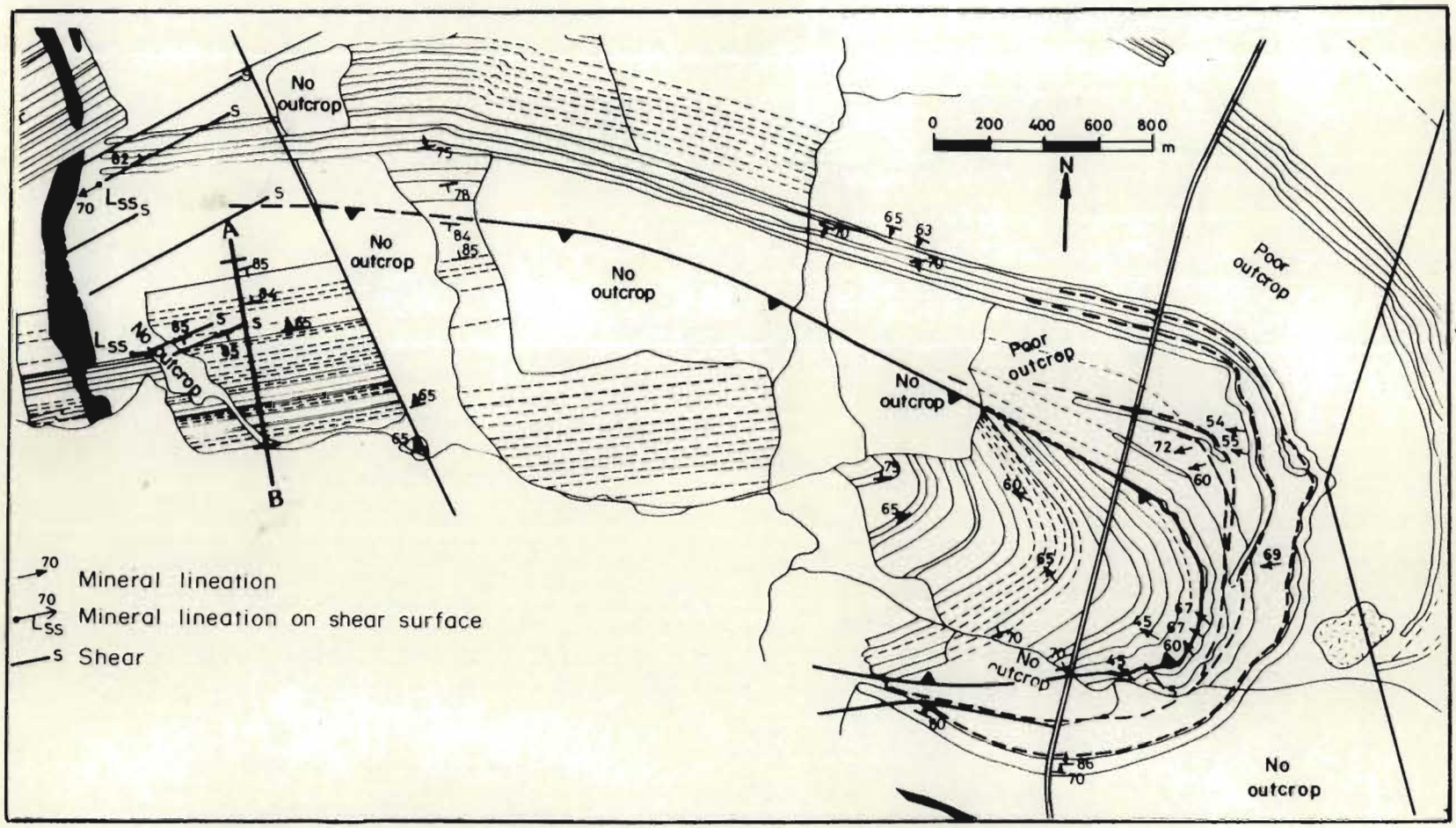

Fig. 8.30 Simplified map of the Commondale synform showing mineral lineations, the orientation of shears and lineations on shear surfaces and thrust faults.

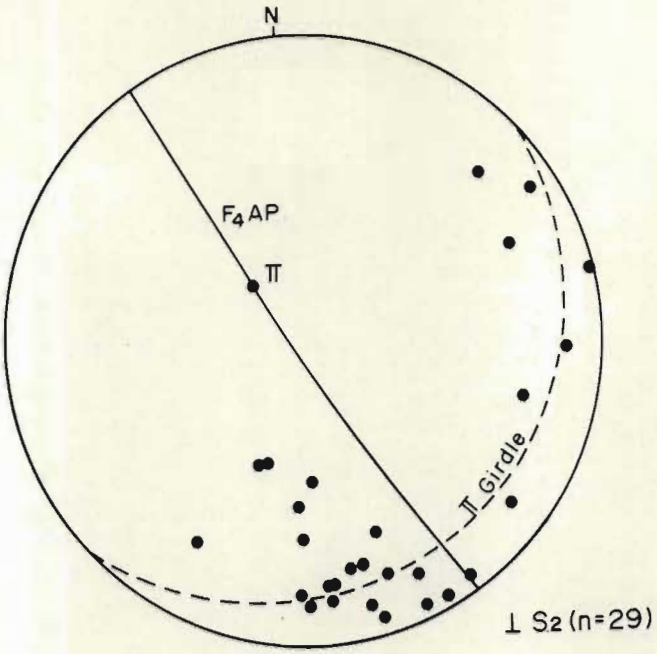

Fig. 8.31 a) Equal area projection of poles to S_2 in the Bazane Porphyritic Trondhjemite Suite south of the Commondale Supracrustal Suite. The spread of S_2 through 170 degrees confirms open F_4 folding about steeply inclined axial surfaces.

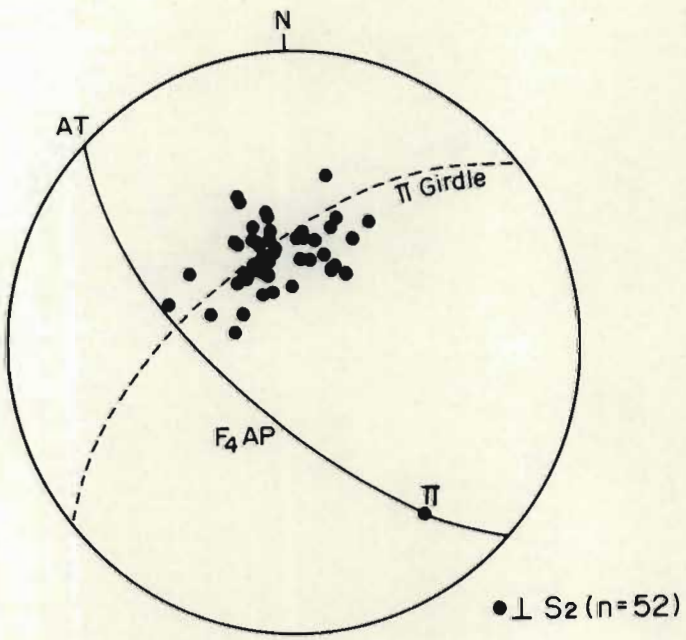

Fig.8.31 b) Equal area projection of poles to S_1 from open F_4 fold in the Luneburg Tonalite Gneiss (MAP 1). The S_1 fabric is folded about a northwesterly trending steeply dipping axial surface.

D_5 and later events.

These events involve deformation after deposition of the Pongola Sequence and are primarily recognized outside the study area (MAP 3).

These events may include : -

i) sinistral shearing and folding about northwesterly axial surfaces deforming the Pongola Sequence and imposing a second coaxial northwesterly deformation on the gneiss terrane

ii) the development of pull apart graben associated with a zone of northwesterly refoliation (D. R. Hunter, pers comm.)

iii) intrusion of the Usushwana Complex as a dyke like body into northwesterly trending graben.

Later events include west-northwest shearing and mylonitization along the contact between the pre-Pongola gneisses and Usushwana Complex. Detailed structural studies in the Pongola Sequence and granitoids east of Piet Retief are required to establish better control on the timing of these later deformational events.

CHAPTER 9

SUMMARY AND CONCLUSIONS

SUMMARY

The Archean granitoid rocks and spatially associated supracrustal suites of metavolcanic and metasedimentary rocks exposed in the map area reflect a sequence of extrusive and intrusive events that occurred during a period of approximately 500Ma from ~3.5Ga to ~3.0Ga. The various lithologies have been affected by a number of discrete deformational and metamorphic events during this time. Field relations, geochemistry and structural analysis suggest the following scenario for the evolution of the crust in this southeastern portion of the Kaapvaal Craton :

1) The bimodal Layered Gneisses characterized by trondhjemitic-tonalitic-granodioritic gneisses interlayered with subordinate amphibolites represent the earliest sialic crust. Trace element proportions and melting models are consistent with a two stage process for the generation of trondhjemitic-tonalitic magmas. Partial melting of the mantle initiated by a mantle plume (Condie and Hunter, 1976; Campbell and Jarvis, 1984) resulted in mafic and ultramafic volcanism. The second stage involves digestion of the volcanics back into the mantle through mantle sinks (Condie and Hunter, 1976) or by Archaean style subduction (Campbell and Jarvis, 1984) where partial melting of wet basaltic crust metamorphosed to amphibolite grade gave rise to trondhjemitic and tonalitic magmas.

2) The Luneburg Tonalite Gneiss is interpreted to be of similar age to the Layered Gneisses on the basis of their similar deformational histories.

3) The apparent concordance on a regional scale of the Luneburg gneiss with the Layered Gneisses could be the consequence of underplanting by a stratiform intrusion. High strains could also account for this relation, which remains equivocal because of the poor outcrop quality along the contacts.

4) The Layered Gneisses and the Luneburg Tonalite Gneiss represent the Gneiss Complex. This complex comprising predominantly siliceous rock-types provided a buoyant basement to the higher density volcanic rocks in the Commondale and adjacent supracrustal sequences.

5) The presence of pyritic metaquartzites, calc-silicate gneisses and layered amphibolites interlayered with Layered Gneisses, and medium-grained quartzites in the Commondale Supracrustal Suite suggests that thickening of this first sialic proto-crust (Gneiss Complex) by deformation and intrusion resulted in emergence of a continental fragment.

6) The Commondale Supracrustal Suite is characterized by a predominance of amphibolites and mafic to ultramafic schists (aluminum depleted peridotitic komatiites) interlayered with subordinate BIF and metaquartzites. CaO/Al_2O_3 and Al_2O_3/TiO_2 ratios and trace element proportions in the basaltic komatiites and peridotitic komatiites are consistent with their derivation by different amounts of partial melting of the same garnet peridotite source at depths between 200 and 400km (Ohtani, 1984). The supracrustal sequence may represent deposition and extrusion into an intracontinental basin that may have developed into a rift/graben by continued high heat flow (from a rising mantle plume) and the mass of the accumulating volcanic pile. It is possible that the appearance of BIF reflects an increase in hydrothermal circulation of iron-rich fluids related to the initial stages of rifting (Groves and Batt, 1984).

7) The Matshempondo Peridotite Suite (3337 $\pm$ 13 Ma, Wilson and Smith, in prep.) comprising a > 640m thick sequence of olivine cumulate and spinifex-textured peridotites heralds the end of observed ultramafic volcanism in the Commondale Supracrustal Suite. Sm-Nd data indicate sequential melting of depleted isotopically inhomogeneous mantle to produce the aluminum undepleted liquids from which the peridotites crystallized. This suite represents a volume of at least $10km^3$ of magma that is interpreted to have extruded, thermally eroded, ponded and crystallized in a lava lake. The high Al_2O_3/TiO_2 ratios reflect generation by partial melting of garnet peridotites at depths $\leq$

200km (Ohtani, 1984).

8) The generation of aluminum undepleted peridotitic komatiite liquids may reflect the continued rise of the mantle plume from ~400km to 200km, i.e. between 400 and 200km aluminum depleted liquids were generated and as these liquids and the plume continued to rise aluminum undepleted liquids were generated at $\leq$ 200km depth. The cessation of komatiitic volcanism may have been controlled by subsidence of the mantle plume, i.e. as the mantle plume subsided further melting in the lower mantle was inhibited.

9) The first deformational event recognized in both the Gneiss Complex and supracrustals is characterized by horizontal tectonism that may have been initiated by Archaean-style plate tectonics. D_1 thrusts and nappe structures are recognized in both the supracrustals and Gneiss Complex.

10) During this possible Archaean-style continental collision subduction of vast amounts of basaltic oceanic crust back into the mantle (Campbell and Jarvis, 1984) resulted in the generation of large volumes of trondhjemitic and tonalitic liquids that intruded as both sheets and diapirs crystallizing the :

a) Bazane Porphyritic Trondhjemite Suite (3230 $\pm$ 80Ma, Allsopp, unpublished data),
b) Leucotonalite Gneiss,
c) Braunschweig Tonalite Gneiss,
d) Hornblende Granodiorite Suite,
e) weakly foliated granitoids that intrude the Luneburg Tonalite Gneiss.

Ten to thirty percent batch melting of amphibolite of enriched Archaean tholeiite composition could produce liquids similar to those from which these granitoids crystallized.

11) The repetition of sodic granitoid underplating together with the earlier events of recumbent folding and thrusting resulted in considerable thickening of the crust.

12) The D_2 deformational event is characterized by upright folding about northeasterly trending vertical axial surfaces. On the basis of structural analysis and petrography this deformation is not the result of intrusion of sodic granitoids, but rather reflects a 'continental-scale' crustal shortening. The major deformation mechanism during D_2 was progressive simple shear that produced non-cylindrical folds. Orientations of fold-axes in the Commondale Supracrustal Suite suggest that it is preserved as a complex sheath-like structure in the gneiss terrane. This would infer that the supracrustals deformed more competently than the Layered Gneisses which are characterized by shallowly plunging folds. This suggestion is supported by the strong D_2 refoliation and ductile shearing of felsic layers in the Layered Gneisses.

13) Bulk minimum strain ellipsoids (D_1 + D_2) reflect crustal shortening of approximately 60 percent thereby indicating substantial vertical extension.

14) Late D_2 was characterized by mylonization along the Bazane trondhjemite-supracrustal contact and D_3 by sinistral faulting and shearing in the Commondale Supracrustal Suite.

15) Small volumes of leucocratic granite and quartz monzonite were intruded as sheets and diapirs respectively. Trace element characteristics and partial melting models are consistent with their derivation from magmas generated by melting of siliceous crust. Heat released i) by decay of radioactive elements in down-folded older siliceous gneisses and ii) by conduction in the lower crust from the mantle would be sufficient to initiate partial melting of the crust generating sodic granitic melts (Hunter and Wilson, in prep.).

16) D_4 is characterized by open to tight F_4 folding about northwesterly trending steeply inclined axial surfaces. Fold-axes have a variety of plunges due to the variations in attitudes of surfaces being folded due to the earlier effects of D_1 and D_2.

The tectonic and magmatic evolution recorded in the Commondale Supracrustal Suite and adjacent granitoid gneisses is broadly similar to that around the Assegaai, Mankayane and Barberton greenstone

remnants. An age of 3460 ± 80 Ma (Pb-Pb; Brèvart et al., 1986, quoted in Tegtmeyer and Kröner, 1987) for a cogenetic suite from the Komati Formation provides a maximum age for the Barberton greenstone belt, whereas the age of 3.3 Ga for the Moodies Group indicates greenstone evolution in the Barberton region over a period of at least 150Ma (Tegtmeyer and Kröner, 1987).

An age of 3337 ± 13Ma (Sm-Nd whole rock; Wilson and Smith, in prep.) for the Matshempondo Peridotite Suite provides a minimum age for the Commondale Supracrustal Suite. On the limited data available from the Commondale greenstone remnant it should not be concluded that the lower formations of the Barberton Sequence reflect an apparently earlier period of crustal evolution than the Commondale Supracrustal Suite.

The Bazane Porphyritic Trondhjemite Suite (Rb-Sr age of 3280 ± 80Ma; Allsopp, unpublished data) and the Anhalt leucotonalite were intruded at the interface between the Layered Gneisses and the Commondale and Assegaai supracrustal sequences respectively. These tabular intrusions contributed to the thickening and increasing stability of the early crust.

An age of 3229 ± 5 (U-Pb) for zircons from the Kaap Valley tonalite, has been interpreted as the age of a magmatic intrusion event (Tegtmeyer and Kröner, 1987). This tonalite intrudes the Onverwacht Group of the Barberton Sequence. The concordance of this age with that of the Bazane trondhjemite suggests the probability of widespread intrusion of tonalitic and trondhjemitic liquids at ~3.2Ga.

The major deformation events recorded within the Commondale Supracrustal Suite correspond closely to those recorded in the Barberton greenstone belt (De Wit, 1983) and to a greater extent the Assegaai supracrustal sequence west of Piet Retief (Talbot et al., 1987) and the Mankayane inlier in southwestern Swaziland (Jackson, 1984).

CONCLUSIONS

The aims of this research were to characterize geochemically and structurally the granitoids and greenstones in the study area and to relate the periods of granitoid emplacement to the deformational history and the development of the supracrustal sequences. The main conclusions are :

1. Inferences from field relations

The origin of conformable layers of amphibolite in the Layered Gneisses is enigmatic. The amphibolites could represent :

a) Mafic dykes intruded into the tonalitic-trondhjemitic suite and rotated to parallelism during early deformation events
b) basalts intruded by granite magmas
c) numerous sills intruded into the tonalitic-trondhjemitic suite that remained parallel to the lithological layering during deformation
d) intercalated basaltic flows in a felsic volcanic pile.

The intense deformation in the Layered Gneisses precludes evaluation of the above possibilities.

In the Layered Gneisses on Tafelberg 186HT a highly deformed sequence of metaquartzites, amphibolites, layered amphibolites and calc-silicate gneisses may represent the deep root of an older supracrustal sequence metamorphosed to a higher grade than the stratigraphically and structurally higher Commondale Supracrustal Suite. However, a number of other possibilities fundamental to a better understanding of the Layered Gneisses exist :

a) The layered amphibolites, calc-silicate gneisses and metaquartzites may be a deep highly deformed root of the Commondale Supracrustal Suite metamorphosed to a higher grade than the rest of the structurally higher supracrustals.

b) The Layered Gneisses may represent a felsic volcanic pile intercalated with basaltic flows or sheets, and minor arenaceous sediments. This would imply the existence of

siliceous basement older than the Layered Gneisses.

Whichever of these possibilities is correct, the presence of the metaquartzite points to a granitic basement having been in existence prior to the formation of the supracrustal sequences.

2. Granitoid geochemistry.

a) The similarity in the primordial mantle normalized LILE and HFSE patterns for the tonalitic, trondhjemitic and granodioritic gneisses suggest that these are crystallization products of liquids derived from broadly similar sources.

b) Ten to thirty percent batch melting of plagioclase amphibolite and amphibolite of enriched Archaean tholeiite composition could produce liquids similar to those from which the different tonalitic, trondhjemitic and granodioritic rock-types crystallized.

c) Phase diagram constraints and trace element distributions in the Bazane Porphyritic Trondhjemite Suite suggest that the components of this suite could represent the products of fractionation of a trondhjemitic liquid. Similarly the biotite and sodic granites that intrude the Luneburg Tonalite Gneiss may represent crystallization products from a fractionating leucotonalite magma.

d) The subordinate unfoliated granitoids (leucocratic granite and quartz monzonite, are derived by small degrees of partial melting of siliceous crustal rocks.

3. Matshempondo Peridotite Suite.

a) The Matshempondo Peridotite Suite is interpreted to have crystallized from ponded magma, possibly in a lava lake environment.

b) The microcyclic spinifex-cumulate layering observed in TYPE 3 cooling units has not been documented from komatiitic flows in other greenstone belts.

c) The Matshempondo peridotites are on the basis of Sm-Nd data and trace element characteristics interpreted to be derived from depleted, isotopically inhomogeneous mantle. The first stage melting events left residues in the mantle for between 33 and 112 Ma before the second melting event at 3337 Ma that produced the Matshempondo peridotitic liquids by sequential melting of these depleted residues.

d) Extremely high Al_2O_3/TiO_2 ratios between 60 and 90 that characterize the Matshempondo peridotites have not been documented before in aluminum undepleted peridotitic komatiites. These high ratios probably reflect mantle inhomogeneities created through extreme mantle differentiation and partial melting.

4. Structure and tectonics.

The structural analysis of the granitoid-supracrustal terrane has revealed a number of important features that also have a bearing on the interpretation of other similar Archaean terranes.

a) Horizontal tectonics dominated by thrusting and recumbent folding resulted in thickening and duplication of lithologies and layering in the supracrustals and Layered Gneisses respectively.

b) The timing (post D_1 - pre D_2) of underplating by significant volumes of sodic granitoids suggests that the mechanism by which the sodic granitoids were produced may be related to horizontal tectonics, i.e. Archaean-style subduction of significant volumes of primitive wet basaltic crust may be initiated during horizontal tectonism.

c) The significant crustal shortening and vertical extension during D_2 may have produced relatively deep-structures that are consistent with the interpretation that the Commondale Supracrustal Suite is preserved as a complex structural enclave in the gneisses.

REFERENCES

ABBEY, S. (1980). Studies in "Standard Samples" for use in general analysis of silicate rocks and minerals, Part 6 : 1979 edition of "Usable values". Geol. Surv. Can., Pap. 80-14, 30pp.

ANHAEUSSER, C.R. (1971). Cyclic volcanicity and sedimentation in the evolutionary development of Archaean greenstone belts of shield areas. Spec. Publ. geol. Soc. Aust., 3, 57-70.

ANHAEUSSER, C.R. (1973). The evolution of the early Precambrian crust of southern Africa. Phil. Trans. R. Soc. Lond., A 273, 359-388.

ANHAEUSSER, C.R. (1980). A geological investigation of the Archaean granite-greenstone terrane south of the Boesmanskop syenite pluton, Barberton Mountain Land. Trans. geol. Soc. S. Afr., 83, 73-106.

ANHAEUSSER, C.R. and ROBB, L.J. (1980). Regional and detailed field and geochemical studies of Archaean trondhjemite gneisses, migmitites and greenstone xenoliths in the southern part of the Barberton Mountain Land, South Africa. Precambrian Res., 11, 373-397.

ANNHAEUSSER, C.R. and ROBB, L.J. (1983). Chemical analyses of granitoid rocks from the Barberton Mountain Land. Spec. Publ. geol. Soc. S. Afr., 9, 189-219.

ARMSTRONG, N.V. (1980). The Geology and Geochemistry of the Nsuze Group in Northern Natal and Southeastern Transvaal. Unpub. Ph.D. thesis, Univ. of Natal, Pietermaritzburg. 386p.

AMSTRONG, N.V., HUNTER, D.R. and WILSON, A.H. (1982). Stratigraphy and Petrology of the Archaean Nsuze Group, Northern Natal and Southeastern Transvaal. South Africa. Precambrian Res., 19, 75-107.

ARNDT, N.T. (1977). Mineralogical and chemical variation in two thick, layered komatiitic lava flows. Carnegie Instn. Wash. Ybk 76, 494-502.

ARNDT, N.T. (1986a). Differentiation of komatiite flows. J. Petrology, 27, 279-301.

ARNDT, N.T. (1986b). Spinifex and swirling olivines in a komatiite lava lake, Munro Township, Canada. Precambrian Res., 34, 139-155.

ARNDT, N.T. and BROOKS, C. (1980). Penrose Conference Report, Komatiites. Geology 8, 155-156.

ARNDT, N.T.and NISBET, E.G. (1982). What is a komatiite? 19-27. IN Arndt, N.T. and Nisbet, E.G., Eds, Komatiites, Allen, London, 526pp.

ARNDT, N.T., FRANCIS, D. and HYNES, A.J. (1979). The field charactersitics and petrology of Archaean and Proterozoic komatiites. Can. Mineral., 17, 147-163.

ARNDT, N.T., NALDRETT, A.J. and PYKE, D.R. (1977). Komatiitic and iron-rich tholeiitic lavas of Munro Township, northeast Ontario. J. Petrology 18, 319-369.

ARTH, J.G. (1979). Some trace elements in Trondhjemites - their implications to magma genesis and paleotectonic setting, 123-132. IN Barker, F., Ed., Trondhjemites, Dacites and Related Rocks. Elsevier, Amsterdam, 659pp.

ARTH, J.G. and HANSON, G.N. (1975). Geochemistry and origin of the early Precambrian crust of northeastern Minnesota. Geochim. et. Cosmochim. Acta, 39, 325-362.

ARTH, J.G., BARKER, F., PETERMAN, Z.E. and FRIEDMAN, I. (1978). Geochemistry of the Gabbro - Diorite - Tonalite - Trondhjemite Suite of southwest Finland and its implications for the origin of Tonalitic and Trondhjemitic Magmas. J. Petrology, 19, 289-316.

AUVRAY, B., BLAIS, S., JAHN, B.-M. and PIQUET, D. (1982). Komatiites and komatiitic series in the Finnish greenstone belts, 131-146. IN Arndt, N.T. and Nisbet, E.G., Eds., Komatiites, Allen, London, 526pp.

BARKER, F. (1979). Trondhjemite : definition, environment and hypotheses of origin, 1-12. IN Barker, F., Ed., Trondhjemites, Dacites and Related Rocks. Elsevier, Amsterdam, 659pp.

BARKER, F. and ARTH, J.G. (1976). Generation of trondhjemitic-tonalitic liquids and Archaean bimodal trondhjemite-basalt suites. Geology, 4, 596-600.

BARKER, F., ARTH, J.G., PETERMAN, Z.E. and FRIEDMAN, I. (1976a). The 1.7 to 1.8 - b.y. - old trondhjemites of southwestern Colorado and northern New Mexico : Geochemistry and depth of genesis. Geol. Soc. America. Bull., 87, 189-198.

BARKER, F., FRIEDMAN, I., HUNTER, D.R. and GLEASON, J.D. (1976b). Oxygen istopes of some trondhjemites, siliceous gneisses and associated mafic rocks. Precambrian Res., 3, 547-557.

BARLEY, M.E. and BICKLE, M.J. (1982). Komatiites in the Pilbara Block, Western Australia, 105-115. IN Arndt, N.T. and Nisbet, E.G., Eds., Komatiites, Allen, London, 526pp.

BARNES, S-J. (1985). The petrography and geochemistry of komatiite flows from the Abitibi Greenstone Belt and a model for their formation. Lithos, 18, 241-270.

BARNES, S-J., GORTON, M.P. and NALDRETT, A.J. (1983). A comparative study of olivine and clinopyroxene spinifex flows from Alexo, Abitibi Greenstone Belt, Ontario, Canada. Contrib. Mineral. Petrol., 83, 293-308.

BARTON, Jr., J.M. (1983). Isotopic constraints on possible tectonic models for crustal evolution in the Barberton granite-greenstone terrane, southern Africa. Spec. Publ. geol. Soc. S. Afr. 9, 73-79.

BECKINSALE, R.D. (1979). Granite magmatism in the tin belt of south-east Asia, 34-44. IN Atherton, M.P. and Tarney, J., Eds. Origin of Granite Batholiths, Geochemical evidence. Shiva Publishing Limited, Orpington, Kent. 148pp.

BERTHè, D., CHOUKROUNE, P. and JEGOUZO, P. (1979). Othogneiss, mylonite and non coaxial deformation of granites : the example of the South American Shear Zone. J. Struct. Geol., 1, 31 - 42.

BESWICK, A.E. (1982). Some geochemical aspects of alteration and genetic relations in komatiite suites, 281-308. IN: Arndt, N.T. and Nisbet, E.G., Eds., komatiites. Allen, London, 526pp.

BESWICK, A.E. and SOUCIE, G. (1978). A correction procedure for metasomatism in an Archaean greenstone belt. Precambrian Res. 6, 235-248.

BICKLE, M.J. (1982). The magnesium content of komatiitic liquids, 479 - 494. IN Arndt, N.T. and Nisbet, E.G., Eds, Komatiites, Allen, London, 526pp.

BINNS, R.A., HALLBERG, J.A. and TAPLIN, J.H. (1982). Komatiites in the Yilgurn Block, Western Australia, 117 - 130. IN Arndt, N.T. and Nisbet, E.G. Eds, Komatiites, Allen, London, 526pp.

BROOKS, C. and HART, S.R. (1974). On the significance of komatiite. Geology, 1, 107-110.

CAMPBELL, I.H. and ARNDT, N.T. (1983). Pyroxene accumulation in spinifex-textured rocks. Geol. Mag., 119, 605 - 610.

CAMPBELL, I.H. and JARVIS, G.T. (1984). Mantle convection and early crustal evolution. Precambrian Res., 26, 15-56.

CARLSON, R.W., HUNTER, D.R. and BARKER, F. (1983). Sm-Nd age and isotopic systematics of the bimodal suite, ancient gneiss complex, Swaziland. Nature, 305, 701-704.

CARMICHAEL, I.S.E. (1963). The crystallization of feldspar in volcanic acid liquids (with discussion). Q. J. geol. Soc. London, 119, 95-131.

CARMICHAEL, I.S.E., TURNER, F.J. and VERHOOGEN, J. (1974). Igneous Petrology. McGraw-Hill Inc., New York, 739pp.

CHAYES, F. (1949). On ratio correlation in petrography. J. Geol., 57, 239 - 254.

COBBOLD, P.R. and QUINQUIS, H. (1980). Development of sheath folds in shear regimes. J. Struct. Geol., 2, 119 - 126.

COLLERSON, K.D. and BRIDGWATER, D. (1979). Metamorphic development of early Archaen tonalitic and trondhjemitic gneisses : Saglek area, Labrador, 205-273. IN : Barker, F. Ed. Trondhjemites, Dacites and Related Rocks. Elsevier, Amsterdam. 659pp.

CONDIE, K.C. (1973). Archaean magmatism and crustal thickening. Geol. Soc. America Bull., 84, 2981-2992.

CONDIE, K.C. (1981). Archean Greenstone Belts. Elsevier, Amsterdam, 433pp.

CONDIE, K.C. (1986). Origin and early growth rate of continents. Precambrian Res., 32, 261-278.

CONDIE, K.C. and HUNTER, D.R. (1976). Trace element geochemistry of Archean granitic rocks from the Barberton region, South Africa. Earth Planet. Sc. Lett., 29, 389-400.

COWARD, M.P. and POTTS, G.J. (1983). Complex strain patterns developed at the frontal and lateral tips to shear zones and thrust zones. J. Struct. Geol., 5, 383 - 399.

DE WIT, M. (1982). Gliding and overthrust nappe tectonics in the Barberton greenstone belt. J. Struct. Geol., 4, 117-136.

DE WIT, M.J., FRIPP, R.E.P. and STANISTREET, I.G. (1983). Tectonic and stratigraphic implications of new field observations along the southern part of the Barberton greenstone belt. Spec. Publ. geol. Soc. S. Afr., 9, 21-39.

DONALDSON, C.H. (1974). Olivine crystal types in harrisitic rocks of the Rhum pluton and in Archean spinifex rocks. Geol. Soc. America Bull., 85, 1721-1726.

DONALDSON, C.H. (1976). An experimental investigation of olivine morphology. Contr. Mineral. Petrol., 57, 187-213.

DONALDSON, C.H. (1982). Spinifex-textured komatiites : A review of textures, compositions and layering. 213-244. IN Arndt, N.T. and Nisbet, E.G., Eds., Komatiites, Allen, London, 526pp.

FAURE, G. (1986). Principles of Isotope Geology, 2nd. ed., Wiley, New York, 589pp.

FLINN, D. (1962). On folding during three-dimensional progressive deformation. Q. J. geol. Soc. London, 118, 385 - 433.

FLINN, D. (1978). Construction and computation of three dimensional deformations. J. geol. Soc. London, 135, 291 - 305.

GILL, R.C.O., BRIDGWATER, D. and ALLAART, J.H. (1981). The geochemistry of the earliest known metavolcanic rocks at Isua, West Greenland : a preliminary investigation, 313-325, IN Glover, J.E. and Groves, D.I., Eds., Archaean Geology, Spec. Publ. geol. Soc. Aust., 7, 515pp.

GLIKSON, A.Y. and SHERATON, J.W. (1972). Early Precambrian trondhjemitic suites in western Australia and northwestern Scotland, and the geochemical evolution of shields. Earth Planet. Sc. Lett., 17, 227-242.

GREEN, T.H. and RINGWOOD, A.E. (1968). Genesis of the calc-alkaline igneous rock suite. Contr. Mineral. Petrol., 18, 105-162.

GROVES, D.I. and BATT, W.D. (1984). Spatial and Temporal Variations of Archaean Metallogenic Associations in Terms of Evolution of Granitoid-Greenstone Terrains with Particular Emphasis on the Western Australian shield, 73 - 98. IN Kroner, A., Hanson, G.N. and Goodwin, A.M., Eds, Archaean Geochemistry. Springer-Verlag, Berlin, 286pp.

HAMMERBECK, E.C.I. (1977). The Usushwana Complex in southeastern Transvaal with special reference to its economic potential. D. Sc. thesis (unpubl.) Univ. Pretoria, 226pp.

HAMMERBECK, E.C.I. (1982). The Geology of the Usushwana Complex and associated formations - southeastern Transvaal. Geol. Surv. S. Africa., Memoir 70, 119pp.

HANSON, G.N. and GOLDICH, S.S. (1972). Early Precambrian rocks in the Saganaga Lake - Northern Light Lake Area, Minnesota - Ontario. Part II : Petrogenesis. Geol. Soc. America Mem., 135, 179-192.

HANSON, G.N. and LANGMUIR, C.H. (1978). Modelling of major elements in mantle-melt systems using trace element approaches. Geochim. et. Cosmochim. Acta, 42, 725-741.

HEGNER, E., KRONER, A. and HOFMANN, A.W. (1984). Age and isotopic geochemistry of the Archaean Pongola and Usushwana suites in Swaziland, southern Africa : a case for crustal contamination of mantle-derived magma. Earth Planet. Sc. Lett., 70, 267-279.

HEINRICH, E. Wm. (1965). Microscopic identification of minerals. McGraw-Hill, New York, 414pp.

HELZ, R.T. (1973). Phase relationships of basalts in their melting ranges at PH_20 = 5kb as a function of oxygen fugacity. Part I. Mafic phases. J. Petrology, 14, 249-302.

HELZ, R.T. (1976). Phase Relationships of Basalts in their Melting Ranges at PH_20 = 5kb. Part II. Melt Compositions. J. Petrology, 17, 139-193.

HOBBS, B.E., MEANS, N.D. and WILLIAMS, P.F. (1976). An Outline of Structural Geology, John Wiley and Sons, New York, 571pp.

HOLLOWAY, J.R. and BURNHAM, C.W. (1972). Melting relations of basalt with equilibrium water pressures less than total pressure. J. Petrology, 13, 1-29.

HUMPHREY, W.A. and KRIGE, L.J. (1931). The geology of the country south of Piet Retief. Explanation to sheet 68 (Piet Retief). Geol. Surv. S. Afr., 72pp.

HUNTER, D.R. (1968). The Precambrian terrane in Swaziland with particular reference to the granitic rocks. Ph.D. thesis (unpubl.), Univ. Witwatersrand, Johannesburg, 274pp.

HUNTER, D.R. (1969). An occurrence of the Dwyka Series in Southern Swaziland. Trans. geol. Soc. S. Afr., 72, 31-35.

HUNTER, D.R. (1970a). The Geology of the Usushwana Complex in Swaziland. IN Symposium on the Bushveld Igneous Complex and other Layered Intrusions Spec. Publ. geol. Soc. S. Afr., 1, 645-660.

HUNTER, D.R. (1970b). The Ancient Gneiss Complex in Swaziland. Trans. geol. Soc. S. Afr., 73, 107-150.

HUNTER, D.R. (1973). The granitic rocks of the Precambrian in Swaziland. Spec. Publ. geol. Soc. S. Afr., 3, 131-145.

HUNTER, D.R. (1974). Crustal development in the Kaapvaal Craton. Part I, The Archaean. Precambrian Res., 1, 259-294.

HUNTER, D.R. (1979). The role of tonalitic and trondhjemitic rocks in the crustal development of Swaziland and the eastern Transvaal, South Africa, 301-322. IN Barker, F., Ed. Trondhjemites, Dacites and Related Rocks. Elsevier, Amsterdam. 659pp.

HUNTER, D.R., ALLEN. A.R. and MILLAN, P. (1983). A Preliminary note on the Archaean supracrustal and granitoid rocks west of Piet Retief. Trans. geol. Soc. S. Afr. 86, 301-306.

HUNTER, D.R., BARKER, F. and MILLARD, Jr., H.T. (1978). The geochemical nature of the Archean Ancient Gneiss Complex and Granodiorite Suite, Swaziland : A Preliminary Study. Precambrian Res., 7, 105-127.

HUNTER, D.R., BARKER, F. and MILLARD, Jr., H.T. (1984). Geochemical investigation of Archaean Bimodal and Dwalile Metamorphic Suites, Ancient Gneiss Complex, Swaziland. Precambrian Res., 24, 131-155.

HUNTER, D.R., SMITH, R.G. and SLEIGH, D.W.W. (1986). Early Archaean evolution in northern Natal and southeastern Transvaal, 375-378. Geocongress 1986. Extended Abstracts, 7th - 11th July, 1986, Johannesburg, 1056pp.

HUPPERT, H.E., SPARKS, R.S.J., TURNER, J.S. and ARNDT, N.T. (1984). Emplacement and cooling of komatiitic lavas. Nature, 303, 19-22.

HUPPERT, H.E. and SPARKS, R.S.J. (1985). Komatiites I : Eruption and Flow. J. Petrology, 26, 694 - 725.

IRVINE, T.N. (1982). Terminology of Layered Intrusions. J. Petrology, 23, 127-162.

IRVINE, T.N. and BARAGAR, W.R.A. (1971). A guide to the chemical classification of common volcanic rocks. Can. J. Earth. Sci., 8, 523-548.

JACKSON, M.P.A. (1984). Archaen structural styles in the Ancient Gneiss Complex of Swaziland, southern Africa, 1-18. IN Kroner, A. and Greiling, R., Eds. Precambrian tectonics Illustrated. E E Schweizerbartsche Vertagsbuchandlung, Stuttgart. 1984.

JACKSON, M.P.A. and ROBERTSON, D.I. (1983). Regional implications of early Precambrian strains in the Onverwacht Group adjacent to the Lochiel granite, northwest Swaziland. Spec. Publ. geol. Soc. S. Afr., 9, 45-62.

JAHN, B., GRUAU, G. and GLIKSON, A.Y. (1982). Komatiites of the Onverwacht Group, S. Africa : REE Geochemistry, Sm/Nd Age and Mantle Evolution. Contrib. Mineral. Petrol., 80, 25 - 40.

JENSEN, L.S. (1976). A new cation plot for classifying subalkalic volcanic rocks. Ont. Dept. Mines, Misc. Pap. 66, 22pp.

KEAYS, RR. (1982). Palladium and iridium in komatiites and associated rocks : application to petrogenetic problems, 435-457. IN Arndt, N.T. and Nisbet, E.G., Eds., Komatiites, Allen, London, 526pp.

KINZLER, R.J. and GROVE, T.L. (1985). Crystallization and differentiation of Archean komatiitic lavas from northeastern Ontario : phase equilibrium and kinetic studies. Am. Miner., 70, 40 - 51.

LAJOIE, J. and GèLINAS, L. (1978). Emplacement of Archean peridotitic komatiites in La Motte Township, Quebec. Can. J. Earth Sci., 15, 672-677.

LEWIS, J.D. and WILLIAMS, I.R. (1973). The petrology of an ultramafic lava near Murphy Well, Eastern Goldfields, Western Australia. Report of the Geological Survey of Western Australia, 1972, 60 - 68.

LISTER, G.S. and SNOKE, A.W. (1984). S - C Mylonites. J. Struct. Geol., 6, 617 - 638.

LUDDEN, J.N. and GELINAS, L. (1982). Trace element characteristics of komatiites and komatiitic basalts from the Abitibi metavolcanic belt of Quebec, 331 - 346. In Arndt, N.T. and Nisbet, E.G., Eds., Komatiites, Allen, London, 526pp.

LUDDEN, J., GELINAS, L. and TRUDEL, P. (1983). Archean metavolcanics from the Rouyn district, Abitibi Greenstone Belt, Quebec, 2. Mobility of trace elements and petrogenetic constraints. Can. J. Earth Sci., 19, 2276 - 2287.

MATTHEWS, P.E., SHARRER, S.H. (1968). A graded unconformity at the base of the early Precambrian Pongola System. Trans. geol. Soc. S. Afr., 71, 251-271.

McBIRNEY, A.R. and NOYES, R.M. (1979). Crystallization and Layering of the Skaergaard Intrusion. J. Petrology, 20, 487 - 554.

McGREGOR, V.R. (1979). Archaean gray gneisses and the origin of the continental crust : Evidence, the Godthab region, west Greenland, 169-203. IN Barker, F., Ed., Trondhjemites, dacites and related rocks. Elsevier, Amsterdam. 659pp.

MOON, C.J. (1986). The Geochemistry of possible Proterozoic paleoregoliths in Southern Africa and implications for exploration, 847-850. Geocongress 1986 Extended Abstracts, 7th - 11th July, 1986, Johannesburg, 1056pp.

NALDRETT, A.J. and MASON, G.D. (1968). Contrasting Archaean ultramafic bodies in Dundonald and Clergue Townships, Ontario. Can. J. Earth Sci., 5, 111-143.

NESBITT, R.W. and SUN, S.-S. (1976). Geochemistry of Archaean spinifex-textured peridotites and magnesian and low-magnesian tholeiites. Earth. Planet. Sci. Lett., 31, 433 -453.

NESBITT, R.W., SUN, S.-S. and PURVIS, A.C. (1979). Komatiites : Geochemistry and Genesis. Canad. Mineral., 17, 165 - 186.

NISBET, E.G., BICKLE, M.J. and MARTIN, A. (1977). The Mafic and Ultramafic lavas of the Belingive Greenstone Belt, Rhodesia. J. Petrology, 18, 521 - 566.

NISBET, E.G., BICKLE, M.J., MARTIN, A., ORPEN, J.L. and WILSON, J.F. (1982). Komatiites in Zimbabwe, 97-104. IN Arndt, N.T. and Nisbet, E.G., Eds., Komatiites, Allen, London, 526pp.

NOCKOLDS, S.R. and ALLEN, R. (1953). The geochemistry of some igneous rock series. Geochim et. Cosmochim. Acta., 4, 105 - 142.

NORRISH, K. and HUTTON, J.T. (1969). An accurate X-ray spectrographic method for analysis of a wide range of geological samples. Geochim. Cosmochim. Acta, 33, 431 - 453.

O'CONNOR, J.T. (1965). A classification for quartz rich igneous rocks based on feldspar ratios. U.S. Geol. Surv. Prof. Pap., 525 - B, 79-84.

OHTANI, E. (1984). Generation of komatiitic magma and gravitational differentiation in the deep upper mantle. Earth. Planet. Sci. Lett., 67, 261 - 272.

O'NIONS, R.K. and PANKHURST, R.J. (1978). Early Archaean rocks and geochemical evolution of the earths crust. Earth Planet. Sci. Lett., 38, 211-236.

PASSCHIER, C.W. and SIMPSON, C. (1986). Porphyroclast Systems as Kinematic indicators. J. Struct. Geol., 8, 831 - 843.

PEARCE, J.A. and CANN, J.R. (1973). Tectonic setting of basic volcanic rocks determined using trace element analysis. Earth Planet. Sci. Lett., 19, 290 - 300.

PEARCE, J.A. and NORRY, M.J. (1979). Petrogenetic implications of Ti, Zr, Y and Nb variations in volcanic rocks. Contrib. Mineral. Petrol., 69, 33 - 47.

PEARCE, T.H. (1968). A Contribution to the theory of variation diagrams. Contr. Mineral. Petrol. 19, 142-157.

PETERMAN, Z.E. (1979). Strontium isotope geochemistry of late Archean to late Cretaceous tonalites and trondhjemites, 133-147. IN Barker, F., Ed., Trondhjemites, Dacites and Related Rocks. Elsevier, Amsterdam, 659pp.

PETERS, D.G., HAYES, J.M. and HIEFTJE, G.M. (1974). Chemical Separations and Measurements. W.B. Saunders Company, Philadelphia, 749pp.

PYKE, D.R., NALDRETT, A.J. and ECKSTRAND, O.R. (1973). Archean ultramafic flows in Munro Township, Ontario. Geol. Soc. America Bull. 84, 955-978.

RAMSAY, J.G. (1967). Folding and Fracturing of Rocks. McGraw-Hill, New York, 568pp.

RAMSAY, J.G. and HUBER, M.I. (1983). The Techniques of Modern Structural Geology, Vol. 1 : Strain Analysis. Academic Press, London, 307pp.

RIDLEY, J. (1986). Parallel stretching lineations and fold axes oblique to a shear displacement direction - a model and observations. J. Struct. Geol., 8, 647 - 653.

ROBB, L.G. and ANHAEUSSER, C.R. (1983). Chemical and Petrogenetic characteristics of Archaean tonalite - trondhjhemite gneiss plutons in the Barberton Mountain Land. Spec. Publ. geol. Soc. S. Afr., 9, 103-116.

ROBINS, B. (1973). Crescumulate layering in a gabbroic body on Seiland, northern Norway. Geol. Mag., 109. 533 - 542.

ROEDER, P.L. and EMSLIE, R.F. (1970). Olivine-Liquid Equilibrium. Contr. Mineral. Petrol., 29, 275 - 289.

ROLLINSON, H.R. and ROBERTS, C.R. (1986). Ratio Correlations and major element mobility in altered basalts and komatiites. Contrib. Mineral. Petrol., 93, 89 - 97.

SAGGERSON, E.P. and WILLIAMS, L.A. (1964). Ngurumanite from southern Kenya and its bearing on the origin of rocks in the northern Tanganyika alkaline district. J. Petrology, 5, 40-81.

SIMPSON, C. and SCHMID, S.M. (1983). An evaluation of criteria to deduce the sense of movement in sheared rocks. Geol. Soc. America Bull., 94, 1281 - 1288.

SMITH, H.S. and ERLANK, A.J. (1982). Geochemistry and petrogenesis of komatiites from the Barberton greenstone belt, South Africa, 347 - 396. IN Arndt, N.T. and Nisbet, E.G., Eds., Komatiites, Allen, London, 526pp.

SMITH, J.V. (1974). Feldspar Minerals. Vol. 2., Springer Verlag, Heidelberg, 690pp.

SMITH, R.G. (1983). The Geology of the Usushwana Complex southeast of Piet Retief. B.Sc. (Hons) thesis (unpubl.), Univ. of Natal, Pietermaritzburg, 71pp.

STREIKEISEN, A. (1976). To each plutonic rock its proper name. Earth Sci. Rev., 12, 1-33.

STRYDOM, D. and VISSER, J.N.J. (1986). Nappe structures in the highly deformed Proterozoic metasedimentary Aggeneys-Type Sequence of Western Bushmanland, South Africa. Precambrian Res., 33, 171-187

SUGDEN, T. (1987) Kinematic indicators : Structures that record the sense of movement in mountain chains. Geology Today, May - June, 93 - 99.

SUN, S.-S. and NESBITT, R.W. (1978). Petrogenesis of Archaean ultrabasic and basic volcanics : Evidence from rare earth elements. Contr. Mineral. Petrol., 65, 301 - 325.

SUN, S.-S., NESBITT, R.W. and SHARASKIN, A.Y. (1979). Geochemical characteristics of mid-ocean ridge basalts. Earth. Planet. Sci. Lett., 44, 119 - 138.

SYKES, L.R. (1978). Intraplate seismicity, reactivation of pre-existing zones of weakness, alkaline magmatism and other tectonism postdating continental fragmentation. Rev. Geophys. Space Phys., 16, 621-688.

TALBOT, C.J. (1970). The minimum strain ellipsoid using deformed quartz veins. Tectonophysics, 9, 47 - 76.

TALBOT, C.J. (1982). Obliquely foliated dykes as deformed incompetent single layers. Bull. geol. Soc. America, 93, 450 - 460.

TALBOT, C.J. (1987). Strains and vorticity beneath a tabular batholith in the Zambezi belt, northeastern Zimbabwe. Tectonophysics, 138, 121 - 158.

TALBOT, C.J., HUNTER, D.R. and ALLEN, A.R. (1987). Deformation of the Assegaai supracrustals and adjoining granitoids. Transvaal, South Africa. J. Struct. Geol., 9, 1 - 12.

TANKARD, A.J., JACKSON, M.P.A., ERIKSSON, K.A., HOBDAY, D.K., HUNTER, D.R. and MINTER, W.E.L. (1982). Crustal evolution of Southern Africa. Springer-Verlag, New York, 523pp.

TARNEY, J., WEAVER, B. and DRURY, S.A. (1979). Geochemistry of Archaean trondhjemitic and tonalitic gneisses from Scotland and East Greenland. 275-299. IN Barker, F., Ed., Trondhjemites, Dacites and Related Rocks. Elsevier, Amsterdam, 659pp.

TAYLOR, S.R. and McLENNAN, S.M. (1981). The composition and evolution of the continental crust : rare earth element evidence from sedimentary rocks. Phil. Trans. R. Soc. Lond., A301, 381 - 399.

TEGTMEYER, A.R. and KRÖNER, A. (1987). U-Pb zircon ages bearing on the nature of early Archaean greenstone belt evolution, Barberton Mountainland, Southern Africa. Precambrian Res., 36, 1 - 20.

TURNER, J.S., HUPPERT, H.E. and SPARKS, R.S. (1986). Komatiites II : Experimental and Theoretical Investigations of Post-emplacement Cooling and Crystallization. J. Petrology, 27, 397 - 437.

TUTTLE, O.F. and BOWEN, N.L. (1958). Origin of granite in the light of experimental studies in the system $NaAlSi_3O_8$-$KAlSi_3O_8$-SiO_2-H_2O. Geol. Soc. America Mem., 74, 153pp.

UPADHYAY, H.D. (1982). Ordovician komatiites and associated boninite-type magnesian lavas from Betts Cove, Newfoundland, 187 - 198. IN Arndt, N.T. and Nisbet, E.G., Eds. Komatiites, Allen, London, 526pp.

VILJOEN M.J. and VILJOEN, R.P. (1969a). A proposed new classification of the granitic rocks of the Barberton region. Spec. Publ. geol. Soc. S. Afr., 2, 152-180.

VILJOEN, M.J. and VILJOEN, R.P. (1969b). The geochemical evolution of the granitic rocks of the Barberton region. Spec. Publ. geol. Soc. S. Afr., 2, 189-218.

VILJOEN, M.J. and VILJOEN, R.P. (1969c). Evidence fro the existance of a mobile extrusive peridotitic magma from the Komatii Formation of the Onverwacht Group. Spec. Publ. geol. Soc., S. Afr., 2, 27 - 112.

VILJOEN, M.J., VILJOEN, R.P. and PEARTON, T.N. (1982). The nature and distribution of Archaean komatiite volcanics in South Africa, 53 - 79. IN Arndt, N.T. and Nisbet, E.G., Eds, Komatiites, Allen, London, 526pp.

VILJOEN, M.J., VILJOEN, R.P., SMITH, H.S. and ERLANK, A.J. (1983). Geological, textural and geochemical features of komatiitic flows from the Komati Formation. Spec. Publ. geol. Soc. S. Afr., 9, 1 - 20.

WADSWORTH, W.J. (1961). The layered ultrabasic rocks of southwestern Rhum, Inner Hebrides. Royal Soc. London Philos. Trans., ser. B, 244, 21 - 64.

WAGER, L.R. and BROWN, G.M. (1968). Layered Igneous Rocks. Oliver and Boyd, Edinburgh, 588pp.

WATCHORN, M.B. (1980). Fluvial and tidal sedimentation in the 3000 Ma Mozaan Basin, South Africa. Precambrian Res., 13, 27-42.

WATSON, E.B. (1982). Basalt Contamination by Continental Crust. Some Experiments and Models. Contrib. Mineral. Petrol., 80, 73-87.

WILSON, A.H. (1977). The Petrology and structure of the Hartley Complex of the Great 'Dyke', Rhodesia. Unpub. D. Phil. Thesis, University of Rhodesia.

WINKLER, H.G.F. (1979). Petrogenesis of Metamorphic Rocks, 5th. ed., Springer-Verlag, New York, 348pp.

WOOD, B.J. and FRASER, D.G. (1976). Elementary thermodynamics for geologists. Oxford University Press, Oxford, 303pp.

WOOD, D.A., JORON, J.L., TREUIL, M., NORRY, M. and TARNEY, J. (1979a). Elemental and Sr isotope variations in basic lavas from Iceland and the surrounding ocean floor. Contr. Mineral. Petrol., 70, 319-339.

WYLLIE, P.J. (1977). Crustal anatexis : An experimental review. Tectonophysics, 43, 41-71.

WYLLIE, P.J., HUANG, W.-L., STERN, C.R. and MAALØE, S. (1976). Granitic magmas : possible and impossible sources, water contents and crystallization sequences. Can. J. Earth Sci., 13, 1007-1019.

APPENDICES

APPENDIX 1

SAMPLE DESCRIPTIONS

Petrographic descriptions for the granitoids and associated rocks are summarized in TABLES 1 to 9. Descriptions for samples from the Matshempondo Peridotite Suite and Commondale Supracrustal Suite are summarized in TABLES 10 and 11 respectively. Many of the textures are similar for each rock-type and are discussed in the relevant chapters to avoid unnecessary repetition in the Appendix. The thin sections and samples are stored in the Department of Geology, University of Natal, Pietermaritzburg.

The following abbreviations are used in TABLES 1 to 9 :

PLAG : plagioclase
MICRO : microcline
QTZ : quartz
BIOT : biotite
MUSC : muscovite
ACC : accessory
GRUN : grunerite
HBL : hornblende
DIOP : diopside

The following abbreviations are used in TABLES 10 and 11 :

mg : medium-grained (1 - 2mm granular olivine)
fg : fine-grained (< 2cm olivine plates)
cg : coarse-grained (> 5cm olivine plates or orthopyroxene needles)
omc : olivine mesocumulate
ooc : olivine orthocumulate
ops : olivine plate spinifex
rops : random olivine plate spinifex
msc : mixed spinifex-cumulate
spx : spinifex
ol : olivine
opx : orthopyroxene
dvg : devitrified glass (altered)
sch : skeletal chromite
act : actinolite
diop : diopside
plag : plagioclase
trem : tremolite
chl : chlorite
serp : serpentine
mag : magnetite

APPENDIX 1

TABLE 1: MINERALOGY OF THE LAYERED GNEISSES

SAMPLE	PLAG	MICRO	QTZ	BIOT	MUSC	HBL	ACC
Leucotonalites and Tonalites							
WB1	38	-	37	20	-	-	5
WB3	38	-	38	17	-	-	7
WR2	35	5	35	20	-	-	5
WR4	40	6	35	15	-	-	4
WR5	44	6	34	14	-	-	2
WR7	40	5	36	14	-	-	10
WR9	42	5	35	16	-	-	2
WR10	30	7	33	25	-	-	5
B1	38	6	33	12	-	9	2
B3	37	4	34	14	-	10	2
B4	34	14	36	13	-	-	3
TG1	34	4	33	25	-	-	4
TG12	35	4	36	24	-	-	1
TG14	34	5	34	24	-	-	3
Trondhjemites							
WR6a	45	5	40	5	-	-	5
WR6c	44	6	41	6	-	-	3
WBS7	42	7	39	7	3	-	2
TG5	41	6	38	10	3	-	2
TG6	44	7	39	8	1	-	1
TG10	45	8	35	8	2	-	2
TG13	43	10	35	8	2	-	2
TG18	46	6	36	9	-	-	3
Granodiorites							
B2	40	22	26	10	-	-	2

SAMPLE	PLAG	MICRO	QTZ	BIOT	HBL	ACC
Amphibolites and Feldspathic amphibolites						
WTR4				-		
WR1	25	-	-	4	63	8
WR6d	40	-	4	-	50	6
TG8	12	-	1	-	84	3
TG9	20	-	1	-	78	1

Miscellaneous Rock-types

SAMPLE	PLAG	MICRO	QTZ	BIOT	HBL	DIOP	ACC	GRUN	PYRITE
Calc-Silicage gneiss									
TG11	20	53	-	-	-	25	2	(diop+plag layer)	
TG11	51	2	2	-	-	42	3	(diop+plag layer)	
Layered Amphibolite									
TG15	50	-	-	-	-	50	-	(diop+plag layer)	
TG15	40	-	-	-	60	-	-	(hbl+plag layer)	
Other Gneisses									
TG7	31	10	17	-	36	-	6		
TG17	39	19	30	-	11	-	1		
Metaquartzite									
TG16	-	-	70	-		-		25	5

TABLE 2: MINERALOGY OF THE LUNEBURG TONALITE GNEISS

SAMPLE	PLAG	MICRO	QTZ	BIOT	HBL	ACC
ZD1	53	3	20	19	3	2
KA1	50	5	22	8	13	2
KA2	50	4	15	12	18	1
KA4	56	6	15	6	15	2
LBE1	50	4	16	10	18	2
LBE2	55	4	17	12	10	2
KA6	55	7	20	10	5	3
DK3	55	5	20	10	9	1
JT1	52	4	22	14	6	2

TABLE 3: MINERALOGY OF THE LEUCOTONALITE GNEISS

SAMPLE	PLAG	MICRO	QTZ	BIOT	HBL	ACC
WG2	60	4	25	10	-	1
LLT1	48	5	24	14	6	3
LLT2	51	10	26	9	4	3
LLT3	52	7	24	8	7	2
WTR1	49	12	21	16	-	2
WTR5	51	11	22	14	-	2

TABLE 4: MINERALOGY OF THE BRAUNSCHWEIG TONALITE GNEISS

SAMPLE	PLAG	MICRO	QTZ	BIOT	HBL	ACC
VD2	45	5	20	10	20	1
VD1	43	5	20	11	21	1
FGT1	46	5	21	8	22	1

TABLE 5: MINERALOGY OF THE BAZANE PORPHYRITIC TRONDHJEMITE SUITE

This suite includes trondhjemitic, granodioritic, granitic and quartz monzonitic varieties.

SAMPLE	PLAG	MICRO	QTZ	BIOT	HBL	ACC	M,C,E	PS	MYRM	C-M-S
Trondhjemites										
TGU1	C	P	C	M		A	X	<3 cm	X	
PK1	C	P	C	M		Z	X	<2 cm		
VG3	C	P	C	M		Z	X	<1.5 cm	X	
WBS1	C	C	C	M		A,S	X	<4 cm	X	X
WBS6	A	P	C	M		Z	X	<4 cm	X	X
WBS5	A	M	C	M		Z,A,S	X	<10 cm	X	
VG1	A	P	C			Z,A	X	<8 cm		X
VG2	A	P	C	M		Z,A	X	<8 cm	X	
RT2	A	M	C	M		Z	X	<2.5 cm	X	
RT3	C	P	C	M		Z,A	X	<1 cm	X	
PD2	P		C	M			X	<3 cm	X	X
Granites										
NLD1	C	P	C	M		Al	X	<2.5 cm	X	
RT1	C	P	C	M		S	X	<1.5 cm	X	X
Granodiorites										
NLD2	P	P	C	M		Al	X	<2.5 cm	X	X
PD1	P	P	C	M		S	X	<3 cm	X	
ON1	P	P	C	M		S,A	X	<2 cm	X	X
Quartz Monzonites										
FGT2	C	C	P	M		A,S,Al	X	<3 cm	X	X
FGT3	C	C	P	M		Al	X	<7 cm	X	X
SKL1	C	C	P	M	~2%	Z,A	X	<4.5 cm	X	

ACC = Accessory where A = apatite
Al = allanite
Z = Zircon
S = sphene
PS = porphyroclast/megacryst size
M.C.E. = chlorite, magnetite epidote, where X = present
C-M-S = chlorite magnetite symplectite, where X = present
MYRM = Myrmekite, where X = present

A = >40%; C = <40-25%; P = 25-20%; M = 10-2%; ACC = <2%

TABLE 6: MINERALOGY OF THE HORNBLENDE GRANODIORITE SUITE

SAMPLE	PLAG	MICRO	QTZ	BIOT	HBL	ACC
Granodiorite						
LF1	40	5	15	69	25	6
LF3	40	6	12	9	28	5
MP1	50	15	18	10	6	1
GUT1	48	15	19	11	7	2
Tonalite						
MP9	45	-	16	15	25	1
MP10	50	-	20	15	13	1
Feldspathic Amphibolite						
MP5	50	-	8	12	29	1
MP7	40	-	3	13	42	2
MP8	40	-	4	14	40	2

TABLE 7: MINERALOGY OF WEAKLY FOLIATED GRANITOIDS INTRUSIVE INTO THE LUNEBURG TONALITE GNEISS

SAMPLE	PLAG	MICRO	QTZ	BIOT	ACC
Medium-grained Leucotonalite					
DK1	55	5	24	12	4
DK2	53	6	26	11	3
DK4	55	5	27	9	4
Biotite Granite					
LBE3	21	27	26	25	1
KA3	20	26	28	25	1
Sodic Granite					
RD1	32	28	26	9	5
RD2	40	30	21	14	5

TABLE 8: MINERALOGY OF THE LEUCOCRATIC GRANITE

SAMPLE	PLAG	MICRO	QTZ	BIOT	ACC*
WB2	32	36	24	4	4
WTR2	31	31	22	8	8
WTR3	30	36	22	7	5

* Includes chlorite, magnetite and epidote. Zircon and apatite are absent.

TABLE 9: MINERALOGY OF THE EQUIGRANULAR QUARTZ MONZONITE

SAMPLE	PLAG	MICRO	QTZ	BIOT	ACC
SKL2	31	34	17	16	2

TABLE 10 MINERALOGY OF THE MATSHEMPONDO PERIDOTITE SUITE

SAMPLE	TEXTURE AND NAME	APPROXIMATE MODAL PROPORTIONS ol	opx	dvg	sch	COMMENTS
ML1A	mg - omc	70	9	20	∿ 1	partial alteration ol-serp + talc, opx-chl+trem
ML1B	mg - ooc	36	41	23	< 1	as above
ML1C	mg - msc	30	39	30	∿ 1	as above
ML1D	mg - ooc	45	25	30	< 1	unaltered
ML2	cg - ops	∿ 30	∿ 45	∿ 25	∿ 2	no unaltered ol plates
ML2 random	fg - rops					altered to talc+serp+ trem+chl
ML3	mg - omc	80	10	10	-	as ML1A
ML4	mg - omc	75	10	15	-	as above
ML6	mg - ooc	52	20	28	< 1	as above
ML8A	mg - ooc	55	20	25	< 1	as above
ML8B	mg - ooc	62	15	23	< 1	as above
ML10	mg - ooc	55	15	30	< 1	as above
ML11	cg - ops	∿ 35	∿ 40	∿ 25	∿ 1	ol plates and opx needles
ML13	mg - ooc	50	15	35	< 1	as ML1A
ML14	mg - ooc	60	16	24	< 1	as above
ML15	mg - ooc	47	25	28	< 1	as above
ML16	mg - ooc	49	28	23	< 1	as above
ML19	mg - ooc	40	35	25	< 1	as above
ML20	mg - ooc	38	40	22	< 1	as above
ML21A	mg - ooc	35	40	25	< 1	as above
ML21B	mg - ooc	33	38	27	< 1	as above
ML24	mg - ooc	35	25	40	< 1	as above
ML25	cg - ops	∿ 40	∿ 28	30	∿ 2	ol plates and opx needles
ML26	mg - ooc	50	20	30	< 1	weakly foliated
ML28	mg - ooc	∿ 45	∿ 20	∿ 35	-	foliated and altered to talc+serp+trem+chl

SAMPLE	TEXTURE AND NAME	APPROXIMATE MODAL PROPORTIONS ol	opx	dvg	sch	COMMENTS
ML12/1	fg - ops	∿ 30	∿ 30	∿ 38	∿ 2	altered to trem+talc+ serp+chl
ML12/2	mg - ooc	55	10	35	< 1	
ML12/3	mg - ooc	60	5	40	< 1	
ML12/4	fg - ops	∿ 30	∿ 38	∿ 30	∿ 2	as ML12/1
ML12/5	mg - msc	∿ 35	∿ 35	∿ 30	< 1	
ML12/6	fg - ops	∿ 30	∿ 33	∿ 35	∿ 2	as ML12/1
ML12/7	mg - ooc	60	5	35	< 1	
ML12/8	fg - ops	∿ 30	∿ 33	∿ 35	∿ 2	as ML12/1
ML12/9	mg - ooc	58	10	32	< 1	
ML12/10	mg - ooc	65	12	23	< 1	
ML12/11	fg - ops	∿ 30	∿ 33	∿ 35	∿ 1	fresh ol plates rare. altered as ML12/1
ML12/2	mg - ooc	64	15	21	< 1	

CONSTITUENT MINERALS

C6, C7 C8	mg- cumulate	relict fractured ol, serp talc, chl, trem	strongly foliated but cumulate texture still recognizable
C9, C10 C11, C12, C13, C14, C15	mg- cumulate	opx, serp, talc, chl, ol trem+mag	cumulate textures recognized, dvg altered to isotropic chl and trem
ML2A	cg-opx blade spx	opx, cpx, trem, chl	dvg altered to chl, cpx to trem
79C	cg-opx needle spx (parallel growth variety)	opx, cpx, trem, chl,	opx alters to chl, cpx to trem+chl, dvg to chl
ML2B (Hopper)	cg-opx spx	opx, cpx, trem, chl (basal section, complex hopper opx intergrowths).	as above

TABLE 11 MINERALOGY OF SELECTED ROCKS FROM THE COMMONDALE SUPRACRUSTAL SUITE

SAMPLE	NAME	MINERAL CONSTITUENTS AND TEXTURE	COMMENTS
C2, C3, L5	serpentinite	Relict fractured ol, talc, serp, mag, chl, original cumulate textures recognized	C3 has foliation
C1	amphibolite	hbl (∿ 90%) plag (10%), accessory sphene	strong foliation, plag saussuritized
C5	amphibolite	hbl (85%) plag (15%)	intense foliation, plag saussuritized
SP2, SP4, SP6, SP8, SP12, SP14	amphibolite	hbl (85-90%), plag (10-13%) apatite, sphene, magnetite	foliation varies from moderate to strong
SP3, SP5, SP9, SP10, SP11	tremolite-actinolite schist	trem, act, chl, and accessory magnetite	as above
L1, L2, L3	calc-silicate	diop, plag, wollastonite, chl, mag, zircon	L1 contains abundant grains and granular aggregates of light emerald green grossularite

APPENDIX 2

SAMPLING AND ANALYTICAL TECHNIQUES

One hundred and fifty-six samples were analysed for major and trace elements. The sample localities are indicated on MAP 1. The major and trace element geochemistry for the 91 samples of granitoids and associated rock-types are given in Chapter 5. Analyses of 20 samples comprising calc-silicates and komatiites from the Commondale Supracrustal Suite are given in Chapter 6 and those for the 45 samples from the Matshempondo Peridotite Suite in Chapter 7. Further reduction of data including CIPW norm calculations are available from The Head, Department of Geology and Mineralogy, University of Natal, P O Box 375, Pietermaritzburg, 3200. These data reductions make use of a program developed by Wilson (pers. comm., 1981). All analyses done at the University of Natal, Pietermaritzburg were by X-ray fluorescence spectrometry. Sm and Nd isotope analyses were done using the mass spectrometer at the Carnegie Institution, Washington by Dr. A H Wilson of the University of Natal, Pietermaritzburg.

Sample Collection

Granitoid samples were collected from eleven lithological types throughout the study area in order to characterize geochemically the various types and the variations within them. The granitoids vary from medium-grained to coarse-grained and sample sizes of between 5 and 10kg can be considered representative of a particular sampling site for the medium-grained varieties. Samples of coarse-grained rocks such as the Bazane Porphyritic Trondhjemite Suite were between 20 and 30kg of fresh material which was considered adequate to avoid sampling error.

Sample suites from the Commondale Supracrustal Suite were collected at three localities. Sample sizes of about 10kg were considered as representative for the calc-silicates and about 3kg for the medium-grained amphibolites and fine-grained tremolite-actinolite schists.

Sample suites from the Matshempondo Peridotite Suite were collected at two localities. Sample sizes of the medium-grained cumulates and coarse-grained spinifex were about 4kg and 6kg respectively. For the

microcyclic unit sample sizes were constrained by the thickness of the slab and width of individual layers and varied between ±200g and 1kg.

Sample Preparation

Weathered material was removed from samples in the field. Any remaining excess material, joint planes and vein fillings were removed and samples were reduced to fragments 2 to 6cm in diameter by using a hydraulic sample splitter with hardened steel cutters. For samples from the Matshempondo Peridotite Suite a diamond rock saw was used to remove all fine joints and joint fillings and care was taken to avoid contamination from the saw blade.

For each of the samples the following procedure was undertaken :

1. Fragments were scrubbed under running water before being cleaned in an ultrasonic cleaner for 90 seconds.

2. Rinsed in distilled water and then dried at 100 degrees C for one to one and a half hours depending on sample size.

3. Samples were then crushed by a jaw crusher with hardened steel jaws to fragments < 1cm in diameter. Between each crush the jaw crusher was cleaned by brushing the jaw surfaces, vacuum cleaning and washing with acetone.

4. The crushed sample was reduced to 100g by the cone-and-quartering technique. For the large samples (20 - 30kg) the sample was reduced by cone-and-quartering, to 1kg, then milled in a swing mill for 5 seconds and, coned-and-quartered to a representative 100g sample. This was considered necessary to ensure a homogeneous mixture for the coarse-grained samples.

5. The 100g sample was milled to a fine powder in a swing mill. A tungsten carbide swing mill was used for the granitoids and a vidiasteel swing mill for the other rock types.

At the start of a sample run the jaw crusher was "washed" with a sample representative of the run. A run consisted of samples of similar compositions, e.g. tonalites, trondhjemites and granodiorites

were included in one run. After each sample run the steel jaws and housing were stripped and cleaned. The swing mill was cleaned in a similar way, but quartz was used first to clean the mill after samples with high serpentine, chlorite or tremolite contents 'caked' when milled.

Sample Preparation for X-ray Spectrometry

Major and minor elements were analysed using the lithium tetraborate fusion method of Norrish and Hutton (1969). All the trace elements were analysed using pressed powder pellets.

Preparation of Norrish fusion discs.

Silicia crucibles were cleaned in a dilute heated solution of HCl. Approximately 0.5g of sample was weighed into the silica crucibles and dried at 100 degrees C. These crucibles were placed in a furnace at 1000 degrees C for 4 hours, then removed and allowed to cool in a desiccator. The spectroflux used for the fusion discs was preheated in Pt crucibles at 1000 degrees C, and $\pm$ 0.4g of the ashed sample was added as close to the ratio weight sample/weight flux = 2.2 as possible. The samples, were fused at 1000 degrees C and the product cast in a brass dye maintained at 250 degrees C. Annealing occurred for approximately 3 hours on a heated asbestos plate and then fusion discs were allowed to cool gradually. The flux used was Johnson Mathie Spectroflux 105. Each new batch of flux was homogenized and a new set of standards made up. Fusion discs were stored separately in sealed plastic bags.

Pressed powder pellets

Approximately 8g of finely milled sample was mixed with 0.6 ml Mowiol and homogenized using an agate mortar and pestal. The sample was then placed in a metal die (position cylinder) and compressed to a pellet $\pm$ 5mm thick under a pressure of 8 tonnes for $\pm$ 10 seconds. The pellets were then hardened in an oven at 120 degrees C for between 3 and 4 hours. Ragged edges on the pellets were trimmed and contact was avoided with the surface to be irradiated. Pellets were stored in airtight plastic containers and separated from each other by cardboard discs.

X-Ray Fluorescence Spectrometry

Analyses by X-ray fluorescence spectrometry were done using a Philips PW 1410 spectrometer in the Department of Soil Science at the University of Natal, Pietermaritzburg. Instrument calibration was controlled with international standards and internal synthetic standards and blanks. International standards used were DTS-1, PCC-1, GSP-1, W-1, BCR-1, G-2, AGV, NIM G, NIM-N, NIM-P, NIM-D, NIM-S, NIM-L, BHVO and DRN. Internationally accepted standard values are from Abbey (1980). Dr. A H Wilson of the Department of Geology, University of Natal, Pietermaritzburg compiled the computer programs for reduction of count data and calculation of mass absorption coefficients.

Precision of XRF analyses

Precision of major and trace element analyses by X-ray fluorescence is below :

Major elements :

SiO_2 $\pm$0.3% at 50%
Al_2O_3, CaO, FeO $\pm$1% at 15%
MnO 0.03 at 0.5%
MgO $\pm$0.2% at 20%
Na_2O 0.15% at 4%
K_2O 0.05% at 4%
TiO_2 $\pm$0.01% at 1.5%
P_2O_5 0.03% at 0.5%

Trace elements

Nb, Y 0 - 200 ppm $\pm$5%
Zr 0 - 200 ppm $\pm$2%, 200 - 500 ppm $\pm$5%
Sr, Rb 0 - 500 ppm $\pm$5%
Cr, Ni 0 - 500 ppm $\pm$5%, 5000 - 2000 ppm $\pm$10%
Cu, Zn 0 - 200 ppm $\pm$50%
Sc 0 - 50 ppm $\pm$2%
V 0 - 300 ppm $\pm$5%
Ba 0 - 500 ppm $\pm$10%

Oxidation State of Iron

X-ray fluorescence analyses determine the total amount of iron in a rock. A standard ratio of fe^{2+}/fe^{3+} = 9 was used to compare the data from the different lithologies.

Sm - Nd analyses from the Matshempondo Peridotite Suite

Sm and Nd isotope analyses by mass spectrometry were performed by Dr. A H Wilson at the Department of Terrestrial Magnetism of the Carnegie Institution of Washington. Details of sample preparation and analytical techniques can be obtained from Dr. A H Wilson, Department of Geology, University of Natal,
P O Box 375, Pietermaritzburg, 3200.